

In vitro transgenic models to elucidate the molecular mechanisms of TDP-43 pathology in Amyotrophic Lateral Sclerosis

Ruxandra Mutihac

Christ Church College

University of Oxford

Thesis submitted for the degree of

Doctor of Philosophy

Trinity 2013

To my parents

Abstract

In vitro transgenic models to elucidate the molecular mechanisms of TDP-43 pathology in Amyotrophic lateral sclerosis

Ruxandra Mutihac, DPhil thesis, Christ Church College, Trinity term, 2013

Amyotrophic lateral sclerosis (ALS) is a rapidly progressing neurodegenerative disorder characterized by loss of upper and lower motor neurons. TDP-43 was identified as a major protein component of the characteristic neuronal inclusions and it has been detected in 90% of ALS cases. Furthermore, pathogenic mutations in the gene encoding TDP-43, *TARDBP*, were found in both sporadic and familial ALS cases.

The aim of this study is to investigate the molecular mechanisms of cellular dysfunction and ultimately death caused by TDP-43 mutations in human cells using established cell lines and human motor neurons derived from induced pluripotent stem cells (iPSCs). We generated a novel *in vitro* cellular model using a fluorescently tagged human genomic *TARDBP* locus carrying three ALS-specific mutations, A382T, M337V or Y374X. In site-specific bacterial artificial chromosome (BAC) human stable cell lines, TDP-M337V mislocalized to the cytoplasm more frequently than wild-type TDP-43 (TDP-Ypet) and TDP-A382T, an effect potentiated by oxidative stress. Cytoplasmic mislocalization was significantly higher in TDP-M337V cells compared to TDP-Ypet and correlated with cell death. Cells expressing the mislocalized TDP-M337V mutant spontaneously developed cytoplasmic punctae, while for TDP-A382T punctae were only revealed after endoplasmic reticulum (ER) stress induced by the calcium-modifying drug

thapsigargin (TG). Lowering Ca^{2+} concentration in the ER of TDP-Ypet cells partially recapitulated the effect of pathogenic mutations by increasing TDP-43 cytoplasmic mislocalization, suggesting Ca^{2+} dysregulation as a potential mediator of pathology. Ca^{2+} signaling from the ER was impaired in cells carrying TDP-43 mutations, with a 50% reduction in the levels of luminal ER Ca^{2+} stores content and delayed Ca^{2+} release induced by carbachol compared to TDP-Ypet cells. The deficits in Ca^{2+} release correlated with upregulation of Bcl-2 and siRNA-mediated knockdown of Bcl-2 restored amplitude of Ca^{2+} oscillations in TDP-M337V cells. These results suggest that TDP-43 pathogenic mutations elicit cytoplasmic mislocalization of TDP-43 through Bcl-2 regulation of ER Ca^{2+} signalling.

Preliminary work in iPSC-derived motor neurons transduced with genomic DNA expression TDP-43 vectors using Herpes Simplex Virus type 1 (HSV-1) amplicons showed cytoplasmic redistribution of TDP-43 under high oxidative stress, without significant differences between mutations and wild-type. TDP-43 mutations delivered by HSV-1 amplicons also did not affect survival of iPSC-derived motor neurons. In ALS patient-derived motor neurons carrying *C9orf72* expansions, TDP-43 pathology was not detected. However, preliminary data indicate that *C9orf72* MNs present ER Ca^{2+} dysregulation with significantly high intracellular Ca^{2+} concentration, which correlates with high protein levels of ER stress markers and low levels of Bcl-2.

This work highlights a potentially pathogenic role for TDP-43 mutations in the dysregulation of Ca^{2+} homeostasis and explores the use of iPS technology to investigate the effects of ALS-associated mutations in healthy and patient-derived motor neurons.

Declaration

Except where acknowledgment is made, all the work presented in this thesis was performed by the author in the Department of Physiology, Anatomy and Genetics, University of Oxford. The work reported in this thesis has not been submitted for any other degrees in this or any other University or Institute of learning.

Acknowledgments

This DPhil thesis has been made possible by the support and encouragement of many people along the way.

First of all, I would like to thank Richard and Kevin for offering me the opportunity to work in their labs and for providing me with their support throughout the entire process. I am especially grateful for their career guidance and for allowing me to develop and pursue my own interests within this project and for encouraging me every step of the way. I would also like to thank Javier for his patience and close supervision while I took my first steps in molecular cloning, for teaching me many techniques and for always finding time for discussions.

I would also like to thank the Motor Neuron Disease Association who have made this project possible by offering me the Lady Edith Wolfson Studentship to fund this work.

I have also benefited greatly from working alongside talented researchers in the Wade-Martins lab and I would like to thank all the members of the lab for making it an intellectually stimulating place to learn and work throughout the past 4 years. It has been a pleasure working with all of you. I am especially grateful to Michi for her advice and time dedicated to calcium signalling; to Liz and Hugo for their help with feeding my differentiating neurons when I was away and for the daily stem cell debates; to Anna for sharing her expertise on viral packaging and troubleshooting with me; to Brent for his time and advice on oxidative stress issues; to Ana and Milena for their friendship and for all the

fun evenings spent in Oxford. A big thank you goes to everyone else in ‘Office Awesome’, Tara, Lawrence, Harriet and Brian, who have made every working day stimulating and entertaining.

I would also like to thank Dr. Sally Cowley, Jane Vowles and Cathy Browne for generating iPSCs and providing me with cells anytime I needed them. Many thanks to David Gordon and Ben Davies for generating the TDP-43 mice and for all the useful advice and comments. Throughout my DPhil, I also found great support from the administrative offices of our Department. Specifically, I would like to thank Alex, Chantelle and Rita from the Financial Division and Colin from the Media Services for printing my posters on short notice.

I would also like to thank all my friends outside the lab in Oxford who have been a great support during my time here, especially Ravina, Sarina, Anca, Camille, Melanie, and the entire MSc in Neuroscience ’09, for being an amazing group of friends. Special thanks to Neil for being an inspiring dance teacher and friend, Rosa and Giles for introducing me to the salsa world and for being the best dance teachers, and to the entire Oxford University Salsa Team for the fun times spent together and performances.

Finally, I would like to express my deepest gratitude to my parents, Lucia and Radu, for all their unconditional love, support and encouragement, which have brought me to Oxford and made all this possible. Also, to my brother Radu-Cristian, to Oana, and my two lovely nephews, Eduard and Robert who have been a wonderful addition to our family since their arrival in this world. Last but not least, I would like to thank Alexandru for his love and support and for always being there for me throughout this journey, constantly reminding me there is a life outside the lab.

Publications and presentations arising from this work

Mutihac R, Alegre-Abarrategui J, Yamasaki-Mann M, Talbot K, Wade-Martins R (2013) '*TARDBP* pathogenic mutations increase cytoplasmic translocation of TDP-43 and cause Bcl-2 mediated reduction of endoplasmic reticulum Ca^{2+} signalling'. *Submitted.*

Mutihac R, Alegre-Abarrategui J, Yamasaki-Mann M, Cowley S, Vowles J, Talbot K, Wade-Martins R (2013) 'Functional effects of TDP-43 mutations in human motor neurons and genomic models'. Oral communication. *European Network for the Cure of ALS Meeting*, Sheffield, UK.

Gordon D, **Mutihac R**, Davies B, Ansorge O, Wade-Martins R, Talbot K (2013) 'A BAC model of TDP-43 associated MND as a tool to explore pathogenesis'. Poster presentation. *European Network for the Cure of ALS Meeting*, Sheffield, UK.

Mutihac R, Alegre-Abarrategui J, Yamasaki-Mann M, Cowley S, Vowles J, James W, Talbot K, Wade-Martins R (2012) 'Investigating the functional role of TDP-43 mutations in human induced pluripotent stem cells derived motor neurons. Poster presentation'. [Winner of the Sherrington Prize for Best Poster] *Oxford Neuroscience Symposium*, University of Oxford, UK.

Mutihac R, Alegre-Abarrategui J, Yamasaki-Mann M, Cowley S, Vowles J, James W, Talbot K, Wade-Martins R (2012) 'Investigating the functional role of TDP-43 mutations in human induced pluripotent stem cells derived motor neurons'. Poster presentation. *Society for Neuroscience Meeting*, New Orleans, USA.

Mutihac R, Alegre-Abarrategui J, Yamasaki-Mann M, Cowley S, James W, Talbot K, Wade-Martins R (2012) 'Investigation of TDP-43 pathology in human motor neurons'. Oral communication. *Oxford Stem Cell Institute Workshop*, Oxford University, UK.

Mutihac R, Alegre-Abarrategui J, Cowley S, Vargas-Caballero M, James W, Talbot K, Wade-Martins R (2012) 'Investigating the functional role of TDP-43 mutations in ALS pathology by delivery of full-length genomic constructs to human induced pluripotent stem cell derived motor neurons'. Poster presentation. *Oxford Neuroscience Symposium*, University of Oxford, UK.

Thomas M, **Mutihac R**, Alegre-Abarrategui J, Talbot K, Ansorge O, Wade-Martins R (2011) 'The role of TDP-43 and FUS in neurodegenerative disease.' Poster presentation. *Alzheimer's Research UK Annual Conference*, Leeds, UK.

Table of Contents

Abstract ..... **iii**

Declaration ..... **v**

Acknowledgments ..... **vi**

Publications and presentations arising from this work ..... **viii**

Table of Contents ..... **x**

List of Abbreviations ..... **xvii**

List of Figures ..... **xxii**

List of Tables ..... **xxvi**

Chapter 1: Introduction **1**

1.1. Amyotrophic lateral sclerosis **1**

1.1.1. Clinical features of ALS 2

1.1.2. Genetics of ALS 3

1.1.3. Pathological features of ALS 8

1.1.4. Current treatments 10

1.2. TDP-43 in ALS **10**

1.2.1. TDP-43 general characteristics and functions 10

1.2.2. TDP-43 in ALS pathology 13

1.2.3. TDP-43 models 16

1.3. C9orf72 in ALS **20**

1.3.1. C9orf72 pathology 20
1.3.2. TDP-43 in C9orf72 ALS pathology 22
1.4. Functional dysregulation in ALS 23
1.4.1. Calcium signalling in ALS 23
1.4.2. Endoplasmic reticulum stress in ALS 24
1.4.3. ER stress and Bcl-2 mediated Ca^{2+} regulation 24
1.5. Improved models of ALS 26
1.5.1. Whole genomic BAC loci 26
1.5.2. Human motor neurons derived from induced pluripotent stem cells (iPSCs) 27
1.5.2.1. Induced pluripotent stem cells 27
1.5.2.2. iPSC derived motor neurons as models of ALS 31
1.6. Aims of this thesis 35
Chapter 2: Materials and Methods 36
2.1. Cloning 36
2.1.1. Preparation of electrocompetent cells 36
2.1.2. Induction of Red/ET 37
2.1.3. Electroporation 37
2.2. DNA extraction 38
2.2.1. BAC plasmid mini prep 38
2.2.2. BAC Maxi preps 39
2.2.3. Restriction digests of plasmid DNA 40
2.2.4. DNA sequencing 40
2.3. Polymerase Chain Reaction 43
2.3.1. Colony PCR 46

2.3.2. Long range PCR 47

2.4. Site-directed mutagenesis 49

2.5. Cre/loxP recombination for retrofitting 50

2.6. Human Cell Culture 51

2.6.1. Reagents 51

2.6.2. Routine subculture 51

2.6.3. Long term storage and thawing 52

2.6.4. Cell counting 52

2.7. DNA delivery to human cell lines by lipofection 53

2.8. DNA delivery to human neurons by HSV-1 amplicons 53

2.8.1. Packaging of vectors in HSV-1 amplicons 53

2.8.2. HSV-1 amplicon concentration 55

2.8.3. Titration 55

2.8.4. X-Gal staining 56

2.8.5. Transduction 56

2.9. siRNA delivery to human cell lines 57

2.10. Generation of clonal HEK293 cell lines 58

2.11. Analysis of protein expression 59

2.11.1. Protein extraction 59

2.11.2. Subcellular compartmentalization 60

2.11.3. Western blotting 61

2.11.4. Imunofluorescence 62

2.12. Analysis of mRNA expression 64

2.12.1. RNA extraction 64

2.12.2. cDNA preparation 64
2.12.3. Reverse transcription PCR 66
2.13. Cell viability assay 66
2.13.1. MTT assay 66
2.13.2. MTS assay 66
2.14. Human iPSC differentiation to motor neurons 67
2.15. Live calcium imaging 68
2.15.1. Calcium-binding dye loading 68
2.15.2. ER Ca^{2+} release 69
2.15.3. ER Ca^{2+} content 69
2.15.4. Kainate and KCl stimulation 69
2.16. Data analysis 70
Chapter 3: Molecular cloning of *TARDBP* and disease-associated M337V, A382T and Y374 mutations 71
3.1. Subcloning the *TARDBP* genomic locus 74
3.2. Engineering a Ypet fluorescent tag into TDP-43 vectors by homologous recombination 77
3.3. Site-directed mutagenesis of A382T, M337V and Y374X in TDP-Ypet vectors ... 83
3.4. Expression analysis 89
3.5. Generation of site-specific PAC stable HEK293 cell lines carrying TDP-Ypet, TDP-A382T, TDP-M337V and TDP-Y374X 92
3.5.1. Retrofitting TDP-Ypet, TDP-A382T, TDP-M337V and TDP-Y374X with pH-FRT-Hy 93

3.5.2. Delivery of TDP-Ypet-FRT, TDP-A382T-FRT, TDP-M337V-FRT and TDP-Y374X-FRT PACs to HEK293 cells 94

3.6. Conclusions 100

Chapter 4: Functional effects of TDP-43 mutations on pathology and ER calcium signalling 103

4.1. M337V mutation increases cytoplasmic mislocalization of TDP-43 105

4.2. M337V mutation correlates with increased apoptosis 109

4.3. Oxidative stress potentiates pathology in M337V and A382T 112

4.3.1. Mild oxidative stress increases cell death in TDP-M337V cells 112

4.3.2. Mild oxidative stress increases M337V and A382T cytoplasmic mislocalization. 114

4.4. ER stress induces pathology in TDP-Ypet and TDP-A382T 117

4.4.1. Thapsigargin-induced ER stress induces cytoplasmic TDP-A382T punctae 117

4.4.2. ER stress induces cytoplasmic mislocalization in TDP-Ypet and TDP-A382T 121

4.5. M337V and A382T mutations alter ER Ca^{2+} signalling 122

4.5.1. M337V and A382T cause reduced ER Ca^{2+} release amplitude 122

4.5.2. M337V and A382T associate with low ER Ca^{2+} content 125

4.6. M337V and A382T do not associate with increased autophagy and ER stress induction 127

4.7. M337V and A382T associate with upregulation of Bcl-2 130

4.8. Bcl-2 knockdown restored ER Ca^{2+} release amplitude in TDP-M337V, but not in TDP-A382T 132

4.9. Conclusions 135

Chapter 5: Functional effects of ALS mutations in human induced pluripotent stem cell derived motor neurons 138

5.1. Optimization of motor neuron differentiation from human induced pluripotent stem cells 140

5.1.1. Generation of iPSCs from human dermal fibroblasts 140

5.1.2. Healthy iPSCs were successfully differentiated to motor neurons 141

5.2. Characterization of iPSC derived motor neurons 145

5.2.1. iPSC derived neurons express molecular markers of motor neurons 145

5.2.2. iPSC derived motor neurons are functionally active 151

5.3. Delivery of genomic TDP-43 loci to iPSC derived motor neurons by HSV-1 amplicons 153

5.3.1. Packaging of TDP-43 vectors into HSV-1 amplicons 153

5.3.2. Optimization of HSV-1 amplicons infectivity and retention in iPSC derived motor neurons 156

5.3.3. Genomic TDP-43 vectors were successfully expressed in iPSC derived motor neurons by HSV-1 amplicons 158

5.4. TDP-43 cytoplasmic mislocalization is detected in iPSC derived motor neurons following oxidative stress 162

5.4.1. High oxidative stress induces TDP-43 cytoplasmic mislocalization in healthy motor neurons 162

5.4.2. High oxidative stress induces TDP-43 cytoplasmic mislocalization in healthy motor neurons carrying TDP-43 mutations 163

5.5. M337V and A382T mutations do not affect neuronal survival 166

5.6. ALS patient iPSCs carrying C9orf72 expansions are successfully differentiated to motor neurons 168

5.6.1. Generation of iPSCs from ALS patients fibroblasts carrying the C9orf72 hexanucleotide repeats using the Sendai virus 168
5.6.2. C9orf72 iPSCs can be differentiated to motor neurons 168
5.7. Preliminary results suggest C9orf72 motor neurons display functional dysregulations 171
5.7.1. TDP-43 pathology is not present in the C9orf72 motor neurons 171
5.7.2. ER Ca^2 signalling is impaired in a C9orf72 patient line differentiated to motor neurons..... 174
5.7.3. Downregulation of Bcl-2 and upregulation of GRP78/BiP and p62 were detected in C9orf72 motor neurons..... 178
5.8. Conclusions..... 180
Chapter 6: General discussion and future directions..... 184
6.1. TDP-43 pathology in stable human cell lines 185
6.2. TDP-43 pathology in iPSC-derived motor neurons..... 191
6.3. C9orf72 iPSC-derived motor neurons 195
6.4. General iPSC discussion..... 197
6.5. Final conclusions..... 199
Bibliography..... 201

List of Abbreviations

AA	Ascorbic Acid
ALS	Amyotrophic Lateral Sclerosis
AD	Alzheimer's Disease
ANG	Angiogenin
ATG7	Autophagy-related protein 7
BAC	Bacterial Artificial Chromosome
BCA	Bicinchoninic acid
Bcl-2	B-cell CLL/lymphona 2
BDNF	Brain-derived neurotrophic factor
BFA	Benign focal atrophy
BSA	Bovine Serum Albumin
C9orf72	chromosome 9 open reading frame 72
CMV	Cytomegalovirus
cDNA	Complementary DNA
CNS	Central Nervous System
Ca^{2+}	Calcium
cAMP	Cyclic AMP
$CaCl_2$	Calcium chloride
CaMKII	Calcium calmodulin-dependent kinase II

CFTR	Cystic fibrosis transmembrane conductance regulator
DAPI	4,6-diamidino-2-phenylindole
Df19.9	Dermal fibroblasts line 19.9
DMEM	Dulbecco's Modified Eagle's Medium
DMEM/F12	Dulbecco's Modified Eagle Medium/F12 Supplement (1:1)
dNTP	deoxynucleotide triphosphates
EDTA	Ethylenediaminetetraacetic acid
ER	Endoplasmic reticulum
ERAD	Endoplasmic reticulum associated degradation
ES	Embryonic stem cells
fALS	Familial ALS
FBS	Foetal bovine serum
FTLD	Frontotemporal Lobar Dementia
FRT	Flp Recombination Target
FUS	Fused in sarcoma
GDNF	Glial-derived neurotrophic factor
GFP	Green Fluorescent Protein
GRP78/BiP	78 kDa glucose-regulated proteinImmunoglobulin heavy chain-binding protein
GWAS	Genome-wide association studies
H_2O_2	Hydrogen peroxide
HB9	Homeobox 9
HBSS	Hank's balanced salt solution
HDAC6	Histone deacetylase 6

HEK	Human embryonic kidney
hESC	Human embryonic stem cells
HFF1	Human foreskin fibroblast line 1
hnRNP	Heterogeneous nuclear ribonucleoprotein
HSV-1	Herpes Simplex Virus type 1
IGF1	Insulin-like growth factor
IP_3	Inositol triphosphate
IP_3R	IP_3 receptor
iPSC	Induced pluripotent stem cell
KA	Kainate
KCl	Potassium chloride
LC3	Microtubule-associated protein 1A/1B-light chain 3
LF	Lipofectamine
LF2000	Lipofectamine 2000
$MgCl_2$	Magnesium chloride
MND	Motor Neuron Disease
MEF	Mouse embryonic feeder
mRNA	Messenger RNA
miRNA	Micro interfering RNA
MN	Motor neuron
MOI	Multiplicity of infection
mPrp	Mouse prion promoter
NCI	Neuronal cytoplasmic inclusions
NEAA	Non-essential amino acids

NHDF 1, 2	Normal human dermal fibroblasts 1, 2
NSC34	Neuroblastoma x spinal cord clone 34
OPTN	Optineurin
PAC	P1-plasmid artificial chromosome
PBS	Phosphate Buffered Saline
PBP	Progressive bulbar palsy
PCR	Polymerase Chain Reaction
PFA	Paraformaldehyde
PLS	Primary lateral
PMA	Progressive muscular atrophy
PVDF	Polyvinylidene difluoride
RA	Retinoic Acid
RNA	Ribonucleic acid
RNAi	RNA interference
RRM	RNA recognition motif
TAE	Tris-acetate EDTA
TARDBP	Transactive response DNA binding protein
TBE	Tris-borate EDTA
TBS	Tris-Buffered Saline
TBST	TBS-Tween
TDP-43	TAR DNA binding protein 43
TE	Tris-EDTA
TG	Thapsigargin
sALS	Sporadic ALS

SD	Standard deviation
SDS	Sodium dodecyl sulfate
SDS-PAGE	SDS-polyacrylamide gel electrophoresis
SEM	Standard error of the mean
SERCA	Sarco/endoplasmic reticulum Ca^{2+}-ATPase
SHH	Sonic hedgehog
siRNA	Small interfering RNA
SMA	Spinal Muscular Atrophy
SNP	Single nucleotide polymorphisms
SOD1	Superoxide/Dismutase 1
UBQLN2	Ubiquilin 2
UPR	Unfolded protein response
UPS	Ubiquitin-proteasome system
UTR	Untranslated region
VAPB	Vesicle-associated membrane protein
VCP	Valosin-containing protein
XBP-1	X-box binding protein 1

List of Figures

1.1. TAR DNA-binding protein 43 (TDP-43) structure……..12

1.2. *C9orf72* transcripts produced by alternative splicing of the pre-mRNA……..……21

3.1. Overview of the cloning strategy used to generate full-length human genomic DNA TDP-43 vectors……..72

3.2. Subcloning the *TARDBP* genomic locus from a BAC to pCYPAC2……...74

3.3. Overview of the pRpsl-Chl homologous recombination strategy used for insertion of Ypet and M337V, A382T or Y374X mutations using the Red/ET recombination system……78

3.4. First round of homologous recombination for the insertion of Ypet before the stop codon of *TARDBP*……..79

3.5. Second round of homologous recombination for the insertion of Ypet before the stop codon of *TARDBP*……..80

3.6. Mutagenesis strategy used to engineer A382T, M337V and Y374X mutations in full-length genomic *TARDBP* vectors using site-directed mutagenesis……83

3.7. First round of homologous recombination for the insertion of pRpsl-Chl at each point mutation in exon 6 of *TARDBP* vectors……84

3.8. Second round of homologous recombination and confirmation of correct site-directed mutagenesis for A382T, M337V and Y374X into TDP-Ypet vectors……...85

3.9. Expression analysis by fluorescence in HEK293 and BE(2)-M17 cell lines after transient transfection of TDP-Ypet, TDP-M337V, TDP-A382T and TDP-Y374X vectors……..87

3.10. Expression analysis by immunoblotting for TDP-43 and GFP to confirm expression of the fusion TDP-Ypet from transiently transfected HEK293, BE(2)-M17 and NSC34 cells……....88

3.11. Schematic representation of the Flp-In system used for the generation of site-specific stable HEK293 lines expressing TDP-Ypet vectors…….92

3.12. Retrofitting by Cre/loxP of TDP-Ypet, TDP-A382T, TDP-M337V and TDP-Y374X with pH-FFRT-Hy plasmid……...93

3.13. Generation of site-specific PAC HEK293 stable cell lines expressing TDP-Ypet, TDP-A382T, TDP-M337V and TDP-Y374X……...94

3.14. Expression analysis of exogenous TDP-43 in HEK293 clones and selection of clones…….95

4.1. TDP-M337V mislocalized to the cytoplasm more frequently than TDP-Ypet in transiently transfected HEK293 cells……...…103

4.2. TDP-M337V mislocalized to the cytoplasm more frequently than TDP-Ypet in stable HEK293 cell lines……104

4.3. TDP-M337V associates with increased frequency of apoptosis……106

4.4. Oxidative stress increases apoptosis in TDP-M337V compared to TDP-Ypet……..109

4.5. Mild oxidative stress increases frequency of TDP-43 cytoplasmic relocalization in the presence of M337V and A382T mutations……..……111

4.6. Immunostaining showing cytoplasmic TDP-43 in TDP-Ypet cells and the formation of TDP-M337V and TDP-A382T punctae after thapsigargin-induced ER stress……114

4.7. M337V and A382T increase frequency of nuclear and cytoplasmic TDP-43 punctae……..…..115

4.8. TG-induced ER stress increases frequency of TDP-Ypet and TDP-A382T cytoplasmic mislocalization……..…..116

4.9. Low amplitude Ca^{2+} peaks are detected in M337V and A382T with high latency in M337V……..……..…119

4.10. Low TG-evoked ER Ca^{2+} content was detected in TDP-M337V and TDP-A382T…….....121

4.11. Autophagy and ER stress are not associated with TDP-43 mutations A382T and M337V…….……124

4.12. Upregulation of Bcl-2 is detected in TDP-M337V and TDP-A382T cells….……126

4.13. Bcl-2 knockdown in control, TDP-Ypet, TDP-M337V and TDP-A382T by RNAi……128

4.14. siRNA mediated Bcl-2 knockdown restores amplitude of ER Ca^{2+} release in TDP-M337V, but not in TDP-A382T……...129

5.1. Overview of the motor neuron differentiation protocol…….….139

5.2. Df19.9 and NHDF1 iPS cell lines differentiated to motor neurons are positive for motor neuron marker HB9 and the neuronal marker Tuj1……..…140

5.3. HFF1 iPS cell line is differentiated to motor neurons…….…...143

5.4. NHDF1, NHDF2 and HFF1 iPS differentiated motor neurons staining positive for motor neuron transcription factor Islet1 and Tuj1……....144

5.5. Motor neurons derived from iPSCs express choline acetyltransferase (ChAT)….…145

5.6. Glia are detected in the iPSC-derived motor neurons…….…146

5.7. Ca^{2+} signalling is detected in iPSC-derived motor neurons……148

5.8. TDP-43 vectors are packaged in infectious HSV-1 amplicons…….…….151

5.9. Optimization of HSV-1 transduction in iPSC-derived motor neurons…….…..153

5.10. HSV-1 amplicons carrying TDP-43 vectors are successfully transduced in iPSC-derived motor neurons……..155

5.11. TDP-43 vectors are expressed in iPSC-derived motor neurons after HSV-1 transduction……..156

5.12. Oxidative stress induces endogenous TDP-43 cytoplasmic mislocalization in iPSC-derived motor neurons……..159

5.13. TDP-Ypet, TDP-M337V and TDP-A382T form cytoplasmic punctae in iPSC-derived motor neurons in the presence of high oxidative stress……...160

5.14. TDP-43 mutations do not affect survival of iPSC-derived motor neurons……...…162

5.15. C9orf72 iPSCs can be differentiated to motor neurons……....165

5.16. C9orf72 iPSC-derived motor neurons express characteristic motor neuron markers…….166

5.17. C9orf72 iPSC-derived motor neurons do not show TDP-43 pathological cytoplasmic mislocalization…….168

5.18. High ER Ca^{2+} concentration and high intracellular Ca^{2+} are detected in motor neurons derived from C9_7245 iPSCs…….…172

5.19. C9_7245 motor neurons show downregulation of Bcl-2 and elevation of ER stress markers p62 and GRP78/BiP…….……..174

List of Tables

1.1. Overview of genetic loci and genes associated with familial ALS……..…..7

2.1. Oligos used for sequencing exon 6 in *TARDBP* ……..42

2.2. Oligos used for checking the presence of *TARDBP* exons and downstream regions……..44

2.3. Oligos used for RT-PCR on iPSC derived motor neurons……...45

2.4. Oligos used for the amplification of pCYPAC2 for subcloning the TARDBP genomic locus ……48

2.5. Oligos used for the amplification of pRpsl-Chl cassette for the insertion of mutations A382T, M337V and Y374X……48

2.6. Oligos used for site-directed mutagenesis……...50

2.7. Oligos sequences for checking integration of TDP-43 in HEK293 cells by FRT recombination…….…….59

2.8. Primary antibodies used for immunoblotting…….……..…...61

2.9. Primary antibodies used for immunostaining…….…….……63

CHAPTER 1

Introduction

1.1. Amyotrophic lateral sclerosis

Amyotrophic lateral sclerosis (ALS), also known in the USA as Lou Gehrig's disease, is the most common adult-onset motor neuron disorder, and has a rapidly progressive clinical course. It is characterized by death of upper motor neurons in the motor cortex and lower motor neurons in the brainstem and spinal cord. Weakness and atrophy occur as a result of muscle denervation following the loss of motor neurons in the anterior horn of the spinal cord. Progressive degeneration of the neuromuscular system ultimately results in death, usually due to respiratory failure, approximately 3-5 years after diagnosis (Brooks, 1994; Brooks et al, 2000). The incidence of ALS which represents the number of new cases, is approximately 2 in 100,000 individuals per year, and it is relatively uniform worldwide, with two high incidence foci of an ALS-like syndrome in the Kii peninsula and Guam (Ferraiuolo et al, 2011). The prevalence of ALS, which represents the number of existing cases, is 4-7 in 100,000, with no ethnic or racial predispositions (Abhinav et al, 2007).

1.1.1. Clinical features of ALS

Affected individuals generally present with asymmetric focal weakness of the extremities (poor handgrip or stumbling) or with bulbar findings (dysarthria, dysphagia). Muscle fasciculations and muscle cramps are also present. Most ALS patients develop limb weakness which then gradually progresses to generalized muscle atrophy and paralysis (Kiernan et al, 2011). The differences in the site of onset, pattern and speed of spread, as well as the degree of motor neuron dysfunction produces a remarkably variable clinical course for each individual. Two main types can be distinguished classified according to their site of onset: bulbar onset ALS and limb onset ALS.

Many patients show widespread involvement of the central nervous system (CNS) and, in addition to motor symptoms typical of ALS, often present symptoms of frontotemporal dementia (FTD). These cases are diagnosed with a mixed ALS-FTD syndrome (McKhann et al, 2001). In the past decades there has been increasing evidence suggesting that these two disorders occur together in the same patients and that ALS and FTD are part of the same clinicopathological spectrum of diseases (Gunnarsson et al, 1991; Lomen-Hoerth et al, 2002). Approximately 50% of ALS patients also present a form of cognitive impairment reminiscent of FTD, while 16% of FTD patients also show motor neuron disease symptoms, typically characterized by difficulty in swallowing and fasciculations (Hodges et al, 2004; Lomen-Hoerth et al, 2002). Oculomotor neurons are generally resistant to neurodegeneration in ALS.

1.1.2. Genetics of ALS

Even though it was initially classified as a sporadic disease with no genetic contribution, the increasing recognition of familial cases and developments in molecular biology techniques over recent decades has shown that genetics plays an important role in ALS. Approximately 90% of cases are indeed sporadic forms, without associations to known risk factors and no affected first degree relatives (Byrne et al, 2011). However, 5-10% of patients show an autosomal dominant pattern of inheritance (Sreedharan et al, 2008).

Since most neurodegenerative disorders are believed to be the result of multiple genetic variants interacting with age and environmental factors, genome-wide association studies (GWAS) have been performed to identify the genes involved in these disorders. GWAS make use of the abundant polymorphic genetic markers, such as single nucleotide polymorphisms (SNPs) and microsattellite markers and they have the potential for mapping sporadic ALS without making assumptions about the location of candidate genes (Lander et al, 2001). However, most GWA studies performed on ALS patients have mainly suffered from small sample size and therefore haven not provided enough power necessary for association analysis (Beleza-Meireles & Al-Chalabi, 2009).

Classical linkage analysis revealed in 1993 the presence of mutations in the superoxide dismutase (*SOD1*) in kindreds with ALS (Rosen et al, 1993). Since its discovery in 1993, 166 *SOD1* mutations have been reported to be associated with ALS and *SOD1* mutations were shown to account for approximately 20% of familial ALS (http://alsod.iop.kcl.ac.uk). Most of the mutations in *SOD1* associated with ALS are missense mutations, with a dominant pattern of inheritance, and have a variable effect on dismutase activity, suggesting that it is not a loss of the normal SOD1 function which is

central to pathogenesis. Through a yet unclear mechanism, the protein appears to gain a novel toxic function that leads to motor neuron death. SOD1 is a ubiquitous protein expressed in the cytosol, and in the presence of mutations is found in a misfolded form in the motor neurons and glial cells of the spinal cord (Nagai et al, 2007). SOD1 plays a major role in the protection of cells against oxidative damage by catalyzing the reduction of the superoxide anion to O_2 and H_2O_2 (Gurney et al, 1994). It has been associated with ALS pathology by affecting mitochondrial function, oxidative stress, excitotoxicity, axonopathy and endosomal trafficking (Beckman et al, 1993; Bosco et al, 2010; Wiedau-Pazos et al, 1996). Although there is marked variation, *SOD1* mutations are generally associated with rapid progression of ALS with no cognitive involvement.

In the last few years, other genes have been associated with classical ALS: *FUS* (Vance et al, 2009), *OPTN* (Maruyama et al, 2010), *ANG* (Greenway et al, 2006), *VCP* (Johnson et al, 2010), *UBQLN2* (Deng et al, 2011), *TARDBP* (Neumann et al, 2006) and *C9orf72* (DeJesus-Hernandez et al, 2011; Renton et al, 2011). A compiled list of genes currently associated with familial ALS is presented in Table 1.1. In 25% of familial cases the genetic cause is yet to be identified.

(1) Mutations in TDP-43 have been identified in 4-6% of familial ALS cases (Sreedharan et al, 2008) and in ~1% of apparently sporadic cases (Andersen & Al-Chalabi, 2011). The identification of mutations in patients with sporadic ALS suggests that rare variants can act as low penetrance dominant alleles (Talbot, 2009). The TDP-43 ALS cases are discussed in more detail in the next section (Chapter 1.2).

(2) Shortly after the discovery of TDP-43, C-terminal mutations in a functionally similar protein, 'fused in sarcoma' (*FUS*), were shown to segregate with the disease (Kwiatkowski et al, 2009). FUS is a ubiquitous nuclear protein involved in RNA processing

and under pathological conditions it is found translocated to the cytoplasm (Kwiatkowski et al, 2009). Mutations in the C-terminus, where its nuclear localization signal is located, appear to disrupt the ability of FUS to be imported into the nucleus and may explain its redistribution to the cytoplasm (Dormann et al, 2010). Post-mortem studies on ALS patients with FUS mutations revealed severe motor neuron loss in the spinal cord, but only moderate loss in the brain stem and motor cortex. Neuropathology also showed that globular cytoplasmic FUS inclusions were found in spinal motor neurons, with rare ubiquitin and p62 positive cytoplasmic inclusions and absence of TDP-43 positive inclusions (Kwiatkowski et al, 2009). Specific mutations in *FUS* cause a rapidly progressive juvenile form of ALS as well as rare cases of adult adult onset ALS (Baumer et al, 2010; Vance et al, 2009).

(3) Mutations in the proline-rich region of ubiquilin-2 (*UBQLN2*), which is an ubiquitin-like protein, have been identified in patients with ALS-FTD (Deng et al, 2011). The role of ubiquilin-2 in the cell is to degrade ubiquitinated proteins and it therefore plays a major role in autophagy and protein recycling. Ubiquitinated inclusions are found at post-mortem in the hippocampus, anterior horn of the spinal cord and frontal cortex of ALS-FTD patients, suggesting that dysfunctions in the protein degradation system may be an essential process for cell death in these cases (Deng et al, 2011). Furthermore, ubiquilin-2 positive skein-like inclusions have been detected in many ALS spinal cord samples and ubiquilin-2 immunoreactivity has been shown to co-localize with ubiquitin (Deng et al, 2011).

(4) Recessive and dominant mutations in the optineurin gene (*OPTN*) were identified as a cause of ALS (Maruyama et al, 2010). Neuropathology of the spinal cord of ALS patients carrying *OPTN* mutations shows loss of anterior horn cells and high levels of intracytoplasmic inclusions positive for OPTN (Maruyama et al, 2010). Inclusions positive

for TDP-43 or SOD1 were also immunostained by OPTN in the anterior horn motor neurons of ALS patients, while there was no OPTN immunoreactivity found in control cases.

(5) Angiogenin (ANG) was first associated with ALS in patients with an Irish or Scottish background (Greenway et al, 2006). Several missense mutations have been described in *ANG*, but only one of these segregates with ALS (van Es et al, 2009).

(6) Mutations in the valosin-containing protein (*VCP*) gene were identified by exome sequencing in an Italian family with autosomal dominantly inherited ALS (Johnson et al, 2010). VCP is an important protein involved in the maturation of autophagosomes and toxicity associated with VCP may be mediated by abnormalities in processing TDP-43 (Johnson et al, 2010).

(7) The discovery of an association between C9orf72 and ALS has come from linkage and GWA studies, which identified a significant locus on chromosome 9p21.2 linked to ALS (Vance et al, 2006). A hexanucleotide $(GGGGCC)_n$ repeat in a non-coding region of C9orf72 has been identified as the cause of 10% of sporadic ALS cases and up to 40% of familial ALS cases (DeJesus-Hernandez et al, 2011; Renton et al, 2011). The C9orf72 cases are discussed in more detail in Chapter 1.3.

A number of other genes, with varying degrees of evidence for involvement in ALS (eg; senataxin and the TAF proteins), have been identified and more await discovery. Taken together, these data indicate that the main proteins involved in the pathogenesis of ALS and FTD can be classified as either proteins associated with RNA processing or members of the protein degradation system.

Table 1.1. Overview of genetic loci and genes associated with familial ALS (adapted from Andersen & Al-Chalabi, 2011)

Location	Gene	Inheritance	Phenotypes	References
21q22.1	*SOD1*	Dominant	ALS PMA PBP (rare) BFA (rare)	(Rosen et al, 1993)
2q33.2	*ALS2*	Recessive	Juvenile PLS, juvenile ALS or infantile HSP	(Hadano et al, 2001)
18q21	Not identified	Dominant	ALS	(Hand et al, 2002)
9q34	*SETX*	Dominant	ALS	(Chen et al, 2004)
15q21.1	*SPG11*	Recessive	Juvenile ALS	(Orlacchio et al, 2010)
16q11.2	*FUS*	Dominant	ALS-FTD	(Vance et al, 2009); (Kwiatkowski et al, 2009)
20p13	Not identified	Dominant	ALS	(Sapp et al, 2003)
20q13.3	*VAPB*	Dominant	ALS, PBP or PMA	(Nishimura et al, 2004)
14q11.2	*ANG*	Dominant	ALS PBP or ALS-FTD	(Greenway et al, 2006); (van Es et al, 2009)
1p36.2	*TARDBP*	Dominant, Recessive (rare)	ALS ALS-FTD	(Gitcho et al, 2008); (Sreedharan et al, 2008); (Kabashi et al, 2008)
6q21	*FIG4*	Dominant	ALS PLS	(Chow et al, 2009)
10p15-p14	*OPTN*	Dominant	ALS	(Maruyama et al, 2010)
12q24	*ATXN2*	Dominant	ALS	(Elden et al, 2010)
9p21.2	*C9orf72*	Dominant	ALS	(DeJesus-Hernandez et al, 2011; Renton et al, 2011)

PBP: progressive bulbar palsy; PMA: progressive muscular atrophy; BFA: benign focal atrophy; PLS: primary lateral sclerosis.

1.1.3. Pathological features of ALS

ALS is a clinical syndrome with several different pathological signatures and pathology is generally indistinguishable between sporadic forms of ALS and most familial cases of ALS (Ravits et al, 2013).

All ALS cases, by definition, are characterized by loss of upper motor neurons and lower motor neurons in the brainstem and anterior horn of the spinal cord, with associated axonal degeneration in the projecting pathways from both upper motor neurons (the corticospinal tract) and lower motor neurons (projecting directly to muscle). Axonopathy is a basic pathological process observed in ALS and it is characterized by neurofilamentous accumulations in the axons (Julien et al, 1995). Tau positive punctate aggregates are also found in the amygdala and entorhinal cortex in post-mortem ALS tissue (Strong et al, 2006). Neuronal degeneration is accompanied by secondary changes such as astrogliosis and microglial activation (Nagai et al, 2007; Ravits et al, 2013). These processes have been gaining more attention recently as there is evidence that they may play a more central role in the degeneration of motor neurons (Nagai et al, 2007; Tong et al, 2013).

The pathological hallmark of ALS is the presence of characteristic ubiquitinated neuronal cytoplasmic inclusions(NCIs), with disease specific morphology (Leigh et al, 1991). Although ubiquitinated inclusions are a common finding in many age-related neurodegenerative disorders, the nature of these inclusions is still unclear, specifically whether they are harmful, protective or both at different stages during degeneration.

TDP-43 was identified in 2006 as the major component protein of NCIs in ALS and 50% of cases of the related neurodegenerative disorder FTLD, which has led to their re-classification as ‘TDP-43 proteinopathies’ (Neumann et al, 2006; Trojanowski & Lee, 2000).

The vast majority of sporadic forms of ALS and familial ALS without SOD1 or FUS-associated pathology present TDP-43 pathology. Regardless of clinical phenotype, these cases are characterized by nuclear depletion of TDP-43, which translocates to the cytoplasm and undergoes post-translational modifications such as ubiquitination and hyperphosphorylation (Neumann et al, 2006). TDP-43-positive cytoplasmic inclusions are not only found in the motor regions, but they are also widely present in the brain, specifically in the frontal and temporal cortices (Geser et al, 2008).

The cases without TDP-43 pathology can be subdivided into SOD1 and FUS-associated ALS, based on genetically defined neuropathology. SOD1 pathology is characterized by irregular, conglomerate NCIs which show variable immunoreactivity to ubiquitin (Mackenzie et al, 2007). Round inclusions that are positive for p62 and ubiquitin without TDP-43 are commonly found in the motor neurons of SOD1-associated ALS cases, along with a severe loss of the motor neurons in the anterior horn of the spinal cord (Mackenzie et al, 2007). FUS-associated ALS is characterized by the presence of cytoplasmic FUS positive inclusions with nuclear depletion of FUS (Kwiatkowski et al, 2009). There is severe loss of motor neurons in the spinal cord, with little cellular loss in the brainstem and showing few ubiquitin and p62 positive inclusions (Kwiatkowski et al, 2009).

It is now evident that multiple pathways converge on motor neuron degeneration in ALS, making it a complex syndrome with contributions from both neuronal degeneration and glial dysfunction.

1.1.4. Current treatments

Numerous clinical trials for ALS have been undertaken in the past decade, but so far the only drug currently used for treating patients with ALS is riluzole. Riluzole is a glutamate antagonist and is proposed to act as an anti-excitotoxicity agent. Its effects are only marginal though, prolonging the lifespan of patients by an average of 2-3 months (Miller et al, 2003). There are several important factors that contribute to lack of effective treatments to ALS patients: the disease has a high level of complexity, the basic biology behind ALS is not yet well understood, and there are no biomarkers available for ALS. In addition, a more timely diagnosis and improved drug delivery are future avenues that would bring more success to the treatment of ALS.

1.2. TDP-43 in ALS

1.2.1. TDP-43 general characteristics and functions

TDP-43 is a 414 amino acid nuclear protein which has 2 RNA recognition motifs (RRM) and a glycine-rich C-terminal domain (Figure 1.1) (Wang et al, 2008). It is a highly conserved, ubiquitously expressed nuclear protein involved in the regulation of pre-RNA processing, microRNA (miRNA) biogenesis and transcriptional repression (Ayala et al, 2008; Buratti et al, 2001).

TDP-43 was first identified as a novel cellular protein that binds to transactivator responsive DNA sequences within human immunodeficiency virus type I (HIV-1) and acts as a transcriptional repressor by inhibiting the promoter activity of this DNA element (Ou et al,

1995). Since its discovery, a multitude of studies have demonstrated the extensive involvement of TDP-43 in RNA processing.

The RNA recognition motif 1 (RRM1) plays an important role in binding to single stranded RNA (Ayala et al, 2005; Buratti & Baralle, 2001; Ou et al, 1995; Wang et al, 2004). Studies using high-throughput sequencing of RNA isolated by crosslinking immunoprecipitation showed that TDP-43 binds to over 6000 RNA species and that it preferentially localizes to intronic sequences, 3' untranslated regions and non-coding RNAs (Polymenidou et al, 2011; Tollervey et al, 2011). TDP-43 binding targets include a multitude of RNA transcripts involved in synaptic activity and neuronal development (Polymenidou et al, 2011; Tollervey et al, 2011). TDP-43 associates with members of the heterogeneous nuclear ribonucleoprotein (hnRNP) family of proteins and the interactions with these hnRNPs are based on its C-terminal glycine-rich region (Buratti et al, 2005; D'Ambrogio et al, 2009). As part of the hnRNP family of proteins, TDP-43 was shown to regulate the splicing of human cystic fibrosis transmembrane conductance regulator (Buratti et al, 2001), apolipoprotein A2 (Mercado et al, 2005) and survival of motor neuron (Bose et al, 2008). In addition, many other splicing events on other transcripts are believed to be mediated by TDP-43 as recently evidenced by transcriptome-wide analysis (Polymenidou et al, 2011).

TDP-43 has also been described as a component of the Drosha complex where it is involved in miRNA biogenesis (Buratti et al, 2010). TDP-43 associates with the Drosha complex in the perichromatin, which is the main site of miRNA biogenesis. The levels of several miRNAs was shown to be altered upon knockdown of TDP-43 (Ling et al, 2010). By expression profiling, TDP-43 silencing in HEK293 and SH-SY5Y cells was shown to trigger the downregulation of histone deacetylase 6 (HDAC6), which might have widespread effects on gene expression (Fiesel et al, 2009).

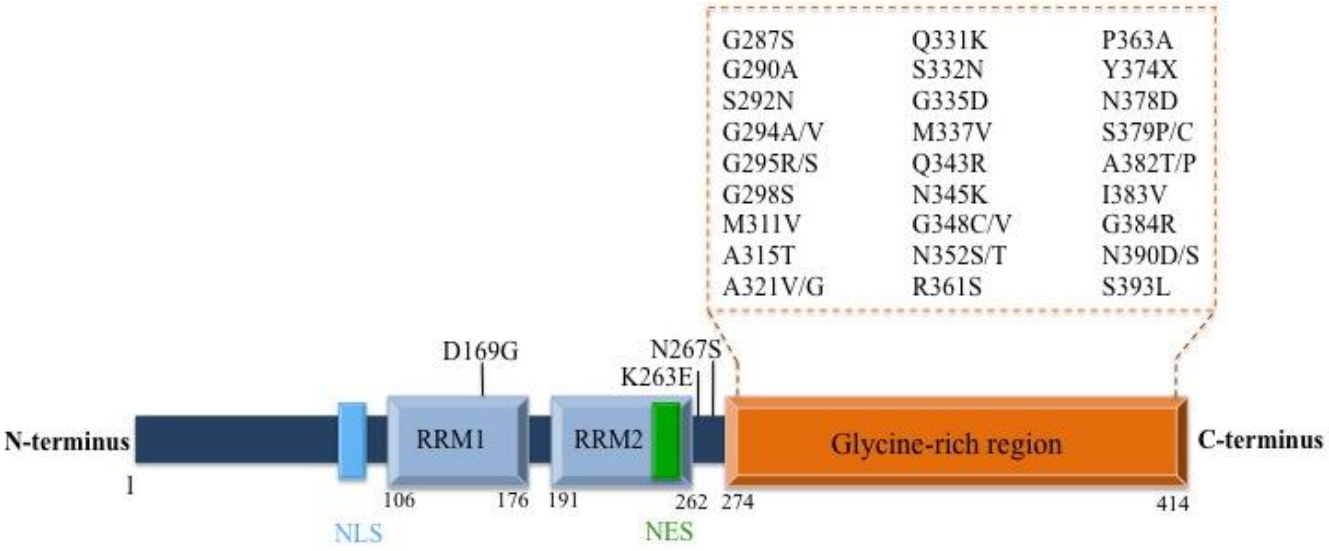


Figure 1.1. **TAR DNA-binding protein 43 (TDP-43) structure.** TDP-43 contains two RNA-recognition motifs (RRM1 and RRM2), a carboxy-terminal glycine rich region, a nuclear localization signal (NLS) and a nuclear export signal (NES). The mutations identified in TDP-43 that associated with familial ALS or FTLD are clustered in the glycine-rich domain,or in its vicinity. One mutation is located within RRM1 (exon 4). Adapted from Lee et al, 2012.

1.2.2. TDP-43 in ALS pathology

Cytoplasmic redistribution of TDP-43 is a hallmark feature of ALS (Neumann et al, 2006) and, even though extensively studied, the functional contribution of its relocalization to disease is still unclear. In addition to representing a marker of ALS pathology, TDP-43 positive inclusions have been identified in Parkinson's disease (Lin & Dickson, 2008), Alzheimer's disease (Amador-Ortiz et al, 2007) and Huntington's disease (Schwab et al, 2008).

Pathological TDP-43 undergoes several post-translational modifications and in cytoplasmic inclusions is ubiquitinated and hyperphosphorylated (Neumann et al, 2006), but it is unclear whether these modifications lead to aggregate formation or they are merely a consequence of the presence of intracellular aggregates. Cytoplasmic translocation of TDP-43 can be increased by oxidative stress which induces association of TDP-43 with stress granules in motor neuronal cell models (Colombrita et al, 2009), suggesting it may play a role in physiological response to injury and in the stabilization of mRNAs.

Ubiquitination was shown to be a late event in neurodegeneration, as some groups reported TDP-43 positive cytoplasmic pre-inclusions that were not positive for ubiquitin (Strong et al, 2007). Ubiquitin tagging is essential for targeting proteins to the ubiquitin-proteasome system (UPS) and the disruption of this system was demonstrated to lead to increased levels of cytoplasmic TDP-43 aggregates in a cellular model (Winton et al, 2008). In support of the hypothesis that the UPS plays a major role in the turnover of TDP-43, mutations in *UBQLN2* were shown to lead to TDP-43-mediated neurodegeneration.

Phosphorylated TDP-43 was detected in all TDP-43 positive inclusions and C-terminal cleaved fragments, indicating that phosphorylation is an early disease

phenomenon that precedes ubiquitination (Hasegawa et al, 2008). The phosphorylated TDP-43 fragments are believed to contribute to aggregate formation by inhibiting UPS degradation (Zhang et al, 2010).

In vivo studies have shown that TDP-43 aggregation is not a necessary event to induce neurodegeneration, although the sole presence of TDP-43 aggregates may be sufficient to induce motor neuron death (Gitler & Shorter, 2011). TDP-43 was shown *in vitro* to spontaneously form aggregates bearing structural similarities to TDP-43 inclusions seen in degenerating neurons in ALS and FTLD (Johnson et al, 2009). The propensity for its toxic aggregation was potentiated by the presence of ALS-associated mutations in the C-terminal domain (Johnson et al, 2009). Interestingly, the sequence of the TDP-43 C-terminal region shows striking similarity to prion proteins and the C-terminal glycine-rich domain is necessary, though not sufficient, for aggregation and toxicity (Gitler & Shorter, 2011). Despite several *in vitro* and *in vivo* studies focusing on TDP-43 toxicity, the effect of TDP-43 aggregation on neuronal death remains unclear.

Another feature of TDP-43 positive inclusions is the detection of low molecular weight species of 25 kDa or 35 kDa in sarkosyl-insoluble brain extracts, representing truncated fragments of TDP-43 (Arai et al, 2006; Neumann et al, 2006). Truncated TDP-43 products were mainly detected in the brains and not in the spinal cord of ALS and FTLD-TDP patients (Igaz et al, 2008). It is as yet unclear whether these C-terminal fragments are toxic due to a gain or loss of function. It has been previously reported that TDP-43 truncated species impair neurite growth in a cell culture model, which was rescued by full-length TDP-43 (Yang et al, 2010). In contrast, the opposite effect was observed in a different model. In *Drososphila melanogaster* expression of C-terminal fragments did not induce toxicity, while overexpression of full-length TDP-43 was neurotoxic (Voigt et al, 2010). Furthermore, the

presence of truncated TDP-43 did not seem to correlate with disease in the *D. melanogaster* model.

Mutations in *TARDBP* have been identified in approximately 4-6% of fALS patients and in a minority of sALS, suggesting it has a direct role in the pathogenesis of ALS (Daoud et al, 2009; Gitcho et al, 2008). The majority of mutations are concentrated in the C-terminal glycine-rich domain (Pesiridis et al, 2009), and are predicted to result in abnormal RNA-protein or protein-protein interactions. The mechanism by which these mutations influence neurodegeneration and alter protein function remains poorly understood. Recent studies aimed at elucidating the role of TDP-43 and the effects of mutations *in vitro* and *in vivo* suggest that *TARDBP* mutations confer neurotoxic properties to the TDP-43 protein, which are specific to primary motor neurons (Fiesel et al, 2009; Kabashi et al, 2009). The location of ALS-associated mutations in *TARDBP* is presented in Figure 1.1.

There are currently three potential hypotheses to explain TDP-43 toxicity: (a) loss of nuclear function and RNA splicing defects resulting from its relocalization to the cytoplasm; (b) toxic gain of function in the cytoplasm or (c) toxicity due to aggregates. It is highly likely that these mechanisms are not mutually exclusive and TDP-43 toxicity may be the result of aberrant translocation to the cytoplasm where it binds to RNAs and gains a toxic function, while losing its normal nuclear function of RNA processing (Voigt et al, 2010).

1.2.3. TDP-43 models

A multitude of animal models have been developed in the attempt to recapitulate TDP-43 pathology associated with ALS and to elucidate the molecular mechanisms underlying TDP-43 proteinopathies.

Three groups reported mouse lines generated using transgenic expression of human *TARDBP* cDNA from the mouse prion promoter (mPrp), which drives high expression preferentially in neurons and glia in the brain and spinal cord (Stallings et al, 2010; Tsai et al, 2010; Wegorzewska et al, 2009). Wegorzewska et al reported that mice expressing human TDP-43 carrying the A315T mutation under the mPrp promoter showed progressive gait abnormality, weight loss and death by 5 months of age (Wegorzewska et al, 2009). However, due to the lack of viable litters expressing wild-type TDP-43 the results must be interpreted with caution as a direct comparison between mice expressing mutant TDP-43 and wild-type TDP-43 could not be made. A different study also reported that founder mice expressing high levels of wild-type, A315T and M337V TDP-43 could not be propagated due to early death (Stallings et al, 2010). One line expressing A315T TDP-43 developed ALS-like motor phenotypes, showing muscle denervation, ubiquitin-positive inclusions and gliosis in the ventral horn, while the control line expressing wild-type TDP-43 did not show a phenotype (Stallings et al, 2010). A study performed on a mouse line expressing homozygous human wild-type TDP-43 under the mPrp promoter showed a severe early onset motor phenotype, weight loss, progressive gait disorder and death by 2 months (Xu et al, 2010). Neuropathologically, these mice showed axonal degeneration, microglial activation, cleaved TDP-43 fragments and some phospho-TDP-43 positive inclusions. The mice that were hemizygous for wild-type TDP-43 did not develop a phenotype (Xu et al, 2010). The same

group found that overexpression of human TDP-43 carrying the M337V mutation in mice causes gait abnormalities and early death, accompanied by neuropathological modifications such as widespread ubiquitination, abnormal mitochondrial aggregates and high levels of cleaved TDP-43 products of 25 kDa and 35 kDa (Xu et al, 2011).

Several other mouse and rat models were developed using different promoters to drive expression of *TARDBP* in the attempt to circumvent toxic effects found by overexpressing TDP-43 under the mPrp promoter. Post-natal transgenic expression was obtained in mice under Thy-1.2 and CaMKII promoters or under an inducible tetracycline (tet) system in rats.

The Thy-1.2 promoter was used by two other groups to drive expression of human *TARDBP* cDNA constructs in mice (Shan et al, 2010; Wils et al, 2010). This promoter was engineered to drive expression of the transgene solely from neuronal cells. In homozygous mice overexpressing human wild-type TDP-43 under the Thy-1.2, gait abnormalities developed at 2 weeks of age and survival was less than 1 month, while the hemizygous mice did not show a phenotype (Wils et al, 2010). Similar results were reported by a second group who developed a Thy-1.2 driven wild-type TDP-43 mouse model (Shan et al, 2010). One of the lines expressing high levels of human wild-type TDP-43 showed early gait abnormalities followed by death within 3 weeks. Despite showing no motor neuron loss and normal survival, neuropathological examination of the lower expressing lines revealed morphological abnormalities of the axonal mitochondria and neuromuscular junctions (Shan et al, 2010).

The only transgenic line expressing mouse wild-type TDP-43 was developed in 2010 under the calcium calmodulin-dependent kinase II promoter (CaMKII) (Tsai et al, 2010). This promoter drives expression predominantly in the neurons of the neocortex, hippocampus, amygdala and basal ganglia. In this mouse model, behavioural and motor

abnormalities were reported as well as brain atrophy with ~24% cortical neuron loss, indicating symptoms reminiscent of FTLD-ALS (Tsai et al, 2010).

Two transgenic rat lines expressing either TDP-43 minigene or TDP-43 cDNA were also generated (Zhou et al, 2010). For the generation of these rats, a human wild-type TDP-43 minigene was used, which contained sequences of the endogenous promoter region in addition to intronic and exonic sequences. The wild-type TDP-43 expressing rats showed normal development, while the M337V TDP-43 expressing rats developed progressive paralysis, indicating this is a highly pathogenic mutation and is sufficient to induce neurotoxicity (Zhou et al, 2010). Using a tetracycline-inducible promoter and cDNA carrying the M337V mutation in TDP-43, the same group found that induction of the mutant form of TDP-43 after birth leads to neurodegeneration and gait disorder (Zhou et al, 2010).

In two invertebrate models, *Drosophila melanogaster* and *C.elegans,* overexpression of human TDP-43 was sufficient to cause neurodegeneration even in the absence of mutations (Ritson et al, 2010). However, when the M337V pathogenic mutation was overexpressed, neuronal cell death was more severe than when wild-type TDP-43 was overexpressed in *Drosophila melanogaster* (Ritson et al, 2010).

Overexpression of mutant human *TARDBP* (A315T, G348C and A382T) in zebrafish embryos caused premature and excessive branching of motor neurons, accompanied by shorter axons (Kabashi et al, 2009). Interestingly, knockdown of the *TARDBP* orthologue in zebrafish, showed a similar deficit in motor development (Kabashi et al, 2009).

The studies undertaken in rodent models of TDP-43 highlight some important aspects: overexpression of wild-type TDP-43 appears to consistently induce motor phenotypes similar to the ones triggered by mutant TDP-43; mutant forms of TDP-43 overexpressed in mice

appear to be more toxic than wild-type TDP-43 and neurodegeneration is induced by mutant TDP-43 in a dose-dependent manner.

1.3. C9orf72 in ALS

1.3.1. C9orf72 pathology

The recently discovered hexanucleotide intronic GGGGCC expansion in chromosome 9 open reading frame 72 (*C9orf72*) accounts for approximately 40% of fALS cases, 5% of sporadic ALS, 40% of FTLD cases and establishes a firm genetic link between ALS and FTLD (DeJesus-Hernandez et al, 2011; Majounie et al, 2012; Renton et al, 2011).

The expansion is located in an intronic or promoter region upstream of the *C9orf72* coding region and the number of GGGGCC hexanucleotide repeats is estimated to be around 700 and 1600 repeats in patients compared to a maximum of 27 in healthy controls (Figure 1.2) (DeJesus-Hernandez et al, 2011; Renton et al, 2011; van der Zee et al, 2013).

The function of the *C9orf72* gene and its pathogenic mechanisms are currently unknown. Three pathomechanisms have been recently proposed: i) a toxic gain of function as the result of an accummulation of RNA transcripts containing the GGGGCC repeat within nuclear foci observed in the frontal cortex and spinal cord of patients, ii) haploinsufficiency, a potential loss of function due to reduced mRNA levels of one C9orf72 transcript (DeJesus-Hernandez et al, 2011; Gijselinck et al, 2012), and iii) repeat-associated non-ATG translation that occurs in the absence of an initiating ATG codon over the GGGGCC repeat expansion and produces homopolymeric proteins of polyglutamine, polyserine or polyalanine prone to aggregation (Ash et al, 2013; Mori et al, 2013).

Clinically, carriers of the *C9orf72* hexanucleotide expansion have an earlier age of disease onset, a more rapid progression, and show significantly greater rate of cognitive decline compared to unselected ALS patients (Irwin et al, 2012).

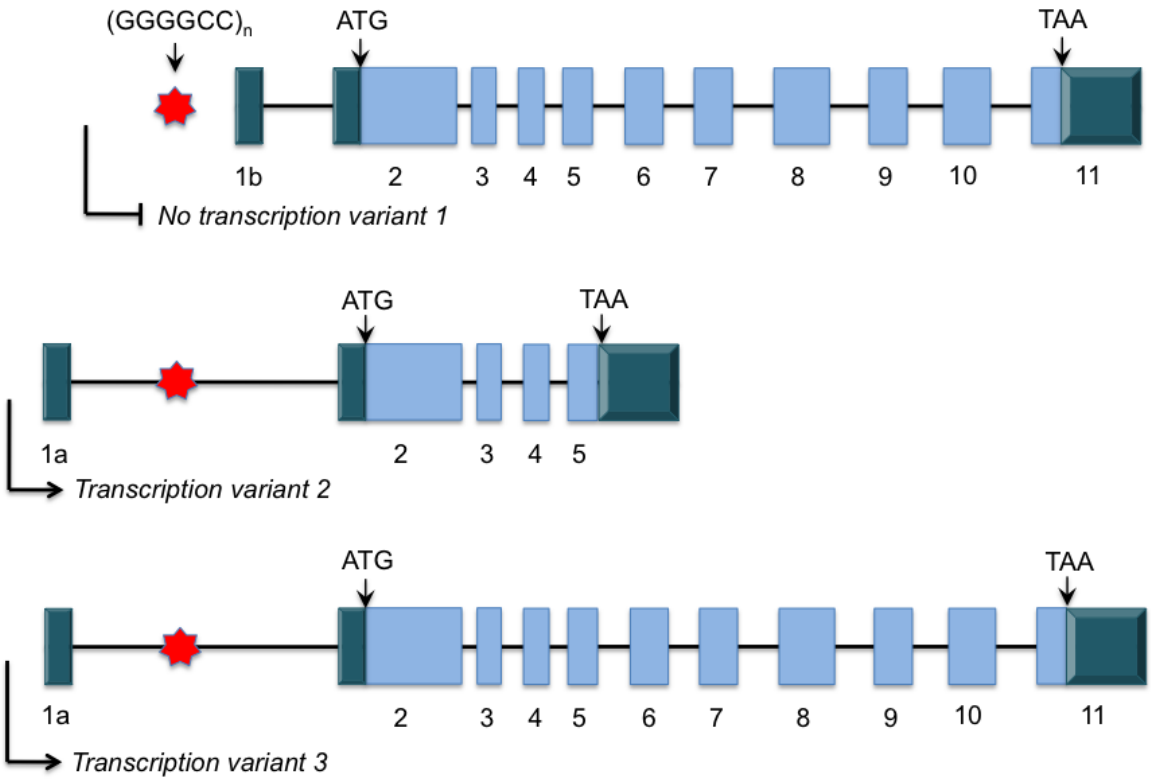


Figure 1.2. ***C9orf72*** **transcripts produced by alternative splicing of the pre-mRNA.** The light blue boxes represent coding exons and the dark blue boxes represent noncoding exons. The arrows indicate the position of the start codon (ATG) and stop codon (TAA) for each transcript. The $(GGGGCC)_n$ repeat is indicated with a red star. Adapted from DeJesus-Hernandez, 2011.

1.3.2. TDP-43 in C9orf72 ALS pathology

Neuropathological analysis showed that TDP-43 aggregation remains the core feature of *C9orf72* cases of ALS. TDP-43-positive neuronal cytoplasmic inclusions reminiscent of TDP-43 proteinopathies have been identified in spinal motor neurons as well as in extra-motor regions of *C9orf72* cases such as the frontal and temporal lobe (Cooper-Knock et al, 2012; King et al, 2012). All *C9orf72* ALS cases from a study in Northern England showed classical amyotrophic lateral sclerosis pathology with TDP-43 inclusions in spinal motor neurons (Cooper-Knock et al, 2012).

In addition to TDP-43 positive neuronal and glial inclusions, *C9orf72*-associated cases exhibit distinctive cerebral pathology characterized by abundant cytoplasmic and intranuclear inclusions immunopositive for ubiquitin and sequestosome-1/p62, suggesting disrupted protein degradation (Bieniek et al, 2012; Cooper-Knock et al, 2012; Troakes et al, 2012). Interestingly, cytoplasmic inclusions were detected in the pyramidal layer of the hippocampus and the cerebellar granular and molecular layers of *C9orf72* ALS patients (Al-Sarraj et al, 2011). These NCIs were abundantly immunopositive for p62 but negative for TDP-43.

The interplay between *C9orf72* expansions and TDP-43 is currently unknown, but understanding the pathological and functional overlap of these proteins consistently associated with ALS and FTD will provide important insights into the mechanism of disease.

1.4. Functional dysregulation in ALS

1.4.1. Calcium signalling in ALS

Calcium (Ca^{2+}) dysregulation plays a central role in the pathophysiology of ALS. It has recently been established that a combination of Ca^{2+} influx during neurotransmission and low cytosolic Ca^{2+} buffering contributes to the preferential vulnerability of motor neurons in ALS.

A large number of physiological processes are mediated by Ca^{2+} oscillations, with information being encoded by the frequency as well as the amplitude of Ca^{2+} spikes. The cytoplasmic Ca^{2+} elevation functions as a second messenger to regulate many processes, and the complex patterns of Ca^{2+} oscillations or waves are transmitted to downstream effectors such as Ca^{2+}-sensitive phosphatases and kinases involved in the regulation of apoptosis. Even though increases in cytosolic Ca^{2+} have commonly been associated with the apoptotic signal transduction pathway, depletion of the ER Ca^{2+} pool can also contribute to cell death (Lam et al, 1994).

Several recent studies in *SOD1* ALS models have suggested that dysregulation of calcium homeostasis plays an important role in the toxicity of cellular models, promoting early protein aggregation into inclusions (Tradewell et al, 2011; Tradewell & Durham, 2010).

A recent study implementing genome-wide RNAi screening to identify regulators of the nucleocytoplasmic shuttling of TDP-43 has indicated that TDP-43 expression and localization are under genetic control by calcium and reduction in ER calcium fluxes promotes nuclear exclusion and degradation of TDP-43 (Kim et al, 2012).

1.4.2. Endoplasmic reticulum stress in ALS

The ER plays a vital role in many cellular processes and one of them is storage of Ca^{2+} and release. The ER is a multifunctional organelle that is able to detect and integrate incoming signals, modulate its own luminal dynamics and generate output signals in response to environmental changes (Corbett & Michalak, 2000).

The ER is involved in cellular signalling and organelle communication, which includes ER stress-dependent activation of transcriptional processes, Ca^{2+} signalling communication to the plasma membrane Ca^{2+} channels and ER-associated degradation (ERAD). Recent studies on autopsied ALS patients and ALS models have indicated that ER stress markers are up-regulated in ALS motor neurons suggesting that ER stress may affect ALS pathogenesis (Atkin et al, 2008; Ilieva et al, 2007). Furthermore, ER stress is predicted to disrupt ER-mitochondria calcium exchange and contribute to dysregulation of intracellular Ca^{2+} buffering capacity of motor neurons in models of ALS (Grosskreutz et al, 2010).

1.4.3. ER stress and Bcl-2 mediated Ca^{2+} regulation

Motor neuron cell death is believed to occur in ALS through the activation of apoptosis and caspases, and damage to the ER-mitochondria functions are likely to contribute to this process. There is currently convincing evidence that unrestricted release of Ca^{2+} from the ER is an important signal for the activation of the apoptotic process (Annis et al, 2004; Hajnoczky et al, 2003; Orrenius et al, 2003; Zhu et al, 2000).

The anti-apoptotic protein Bcl-2 is involved in the regulation of ER calcium release by several different mechanisms. Bcl-2 can decrease Ca^{2+} concentration in the lumen of the ER, resulting in less Ca^{2+} available for release (Foyouzi-Youssefi et al, 2000; Palmer et al, 2004;

Pinton et al, 2000). It has been hypothesised that luminal ER Ca^{2+} concentration is modulated by the ratio of antiapoptotic Bcl-2 and proapoptotic Bcl-2 family members. This was proposed following the observation that cells deficient in Bax and Bak, two proapoptotic family members of the Bcl-2 family, showed increased leakage of ER Ca^{2+} and led to a consequent decrease in steady-state ER Ca^{2+} levels (Scorrano et al, 2003). Another potential mechanism by which Bcl-2 may reduce ER Ca^{2+} concentration is by reducing the levels of the sarco/endoplasmic reticulum Ca^{2+}-ATPase (SERCA) pumps on the ER membrane (Michaelis et al, 2004). The SERCA pumps play an essential role in the re-uptake of free cytosolic Ca^{2+} ions into the ER to maintain high luminal ER Ca^{2+} levels. Depletion of SERCA pumps can lead to a decrease in the Ca^{2+} sequestering capacity of the ER. The third proposed mechanism is that Bcl-2 may form an ion-transmitting pore in the ER membrane that would allow leakage of ER Ca^{2+} ions down a concentration gradient into the cytosol (Foyouzi-Youssefi et al, 2000). A different hypothesis is that Bcl-2 may limit the release of Ca^{2+} from the ER by binding to the IP_3 receptor (IP_3R) (Rong et al, 2008).

There are therefore a variety of mechanisms proposed for the action of Bcl-2 on regulating ER Ca^{2+} homeostasis: Bcl-2 can downregulate the ER Ca^{2+} pool by both downregulating the capacitative Ca^{2+} influx (Pinton et al, 2000) and by increasing ER Ca^{2+} leakage (Foyouzi-Youssefi et al, 2000; Pinton et al, 2000), or by interacting with the IP_3 receptor and restricting cytosolic release of ER Ca^{2+} (Rong et al, 2008). These hypotheses are not necessarily mutually exclusive and there is a possibility that Bcl-2 has evolved several mechanisms to control Ca^{2+} homeostasis.

1.5. Improved models of ALS

1.5.1. Whole genomic BAC loci

The models currently available to study ALS have relied on cDNA constructs, which are driven by strong heterologous promoter and result in protein overexpression unrelated to physiological levels. This has been a significant obstacle in studying the function of TDP-43 as non-physiologically regulated high expression of wild-type TDP-43 was shown to be toxic in a multitude of *in vitro* and *in vivo* models (Ritson et al, 2010; Shan et al, 2010; Wils et al, 2010). Since overexpression of TDP-43 is not detected in patients and expression of TDP-43 is tightly self-regulated, it is not physiologically relevant to investigate functional effects of TDP-43 in overexpressing systems.

To overcome this obstacle, it is advantageous to use bacterial artificial chromosomes (BACs). BACs are vectors derived from the F factor of *E.coli* that are maintained as low copy replicons. They have a large cloning capacity, being capable of accommodating sequences up to 300 kilo basepairs, which can incorporate almost any element responsible for the expression of a gene of interest. For this reason, they are considered complete expression units.

BACs can carry complete genomic loci including exonic and intronic sequences, as well as the native promoter elements. Under the control of its endogenous promoter, expression of a gene of interest is physiologically regulated (Senior & Wade-Martins, 2005). The Wade-Martins laboratory has previously shown that BAC-mediated gene delivery can successfully generate physiologically regulated expression of whole genomic loci *in vitro* in several different cellular models (Alegre-Abarrategui et al, 2009; Peruzzi et al, 2009; Wade-Martins et al, 2003).

1.5.2. Human motor neurons derived from induced pluripotent stem cells (iPSCs)

1.5.2.1. Induced pluripotent stem cells

In the past decades, the process of reprogramming somatic cells to a pluripotent state has been studied extensively. In 1962, Dr. John Gurdon's pioneering work demonstrated for the first time that the specialisation of cells is reversible showing that frog somatic cell nuclei can be reprogrammed after transfer into enucleated oocytes and they can develop into tadpoles (Gurdon, 1962). Later, reprogramming was proved to be possible in vertebrates when sheep (Wilmut et al, 1997) and mice (Wakayama et al, 1998) were successfully cloned. These were the first indications that terminally differentiated cells can be reverted to a pluripotent state in response to external stimulation.

During development, cells in the embryo undergo a unidirectional transition from totipotent zygote to pluripotent inner cell mass and epiblast cells and then to more restricted, fully differentiated cells. This transition process takes place under the regulation of cell-cell interactions and results in specific epigenetic modifications (Jaenisch & Young, 2008). However, when cultured *in vitro* the regulation of this process can be artificially obtained by addition or withdrawal of specific growth factors from the culture medium to direct the fate of the cell to the desired cell type.

In 2006, a breakthrough study by Kazutoshi Takahashi and Shinya Yamanaka established for the first time murine ES-like cell lines from mouse embryonic fibroblasts and skin fibroblasts by expressing four transcription factor genes encoding *Oct4*, *Sox2*, *Klf4* and

c-Myc (Takahashi & Yamanaka, 2006). The cells obtained by induction of these four transcription factors, termed induced pluripotent stem cells (iPSCs), acquire properties similar to those of ES cells. The iPSCs present morphology, proliferation and gene expression remarkably similar to ES cells.

The breakthrough discovery was followed shortly by a study from the same group which showed that using the same four transcription factors, human fibroblasts could also be reprogrammed to a pluripotent state (Takahashi et al, 2007a). A parallel study showed the same reprogramming capacity of somatic cells to pluripotent stem cells by replacing two of the Yamanaka transcription factors, *c-Myc* and *Klf4*, with *Nanog* and *Lin28* (Yu et al, 2007b). Furthermore, subsequent studies have shown that successful reprogramming of human tissue to iPSCs can be obtained from a variety of tissues in addition to skin fibroblasts (Takahashi et al, 2007b), such as keratinocytes (Aasen et al, 2008) and blood cells (Loh et al, 2009).

The four transcription factors used by Yamanaka et al for successful reprogramming of somatic cells to a pluripotent state are *Oct4*, *Sox2*, *Klf4* and *c-Myc*. *Oct4* is implicated in regulating expression of several genes involved in embryonic development and it is exclusively expressed in pluripotent stem cells. *Oct4* has been consistently present in all cocktails used for reprogramming. *Sox2* is a transcription factor that forms a complex with Oct4 and the family of Sox2 genes are tightly associated with Oct4 in maintaining pluripotency. Sox2 is not absolutely necessary for iPSC induction from neural progenitors where endogenous Sox2 expression already exists. *Klf4* contains three zinc-finger domains and acts as both an activator and repressor of transcription. This transcription factor was later shown not to be essential to the induction of pluripotency (Yu et al, 2007b), but its presence could increase the efficiency by one thousand fold (Huangfu et al, 2008). *C-Myc* is an oncogene which was part of the original Yamanaka cocktail of transcription factors and it

significantly enhances the reprogramming efficiency, but it was also later shown to be non-essential to the generation of iPSCs (Takahashi et al, 2007b). Alternatively, *Nanog* and *Lin28* are two other transcription factors that were used by Thomson et al. to generate iPSCs where they were used to replace *c-Myc* and *Klf4* (Yu et al, 2007a). *Nanog* is involved in ES cell proliferation and self-renewal by working co-ordinately with *Oct4* and *Sox2* in regulating pluripotency. *Lin28* is an mRNA binding protein expressed in embryonic stem cells.

Several methods of delivery have been developed in the attempt to enhance iPSC efficiency and differentiation propensity to specific germ lines. Transcription factors have been successfully delivered to somatic cells by retroviruses, lentiviruses, adenoviruses, plasmid transfections, protein transductions, chemical treatment and, more recently, by the Sendai virus. The initial method used by Yamanaka and Thomson was retroviral-mediated delivery of the transcription factors, each packaged individually in a retrovirus (Takahashi et al, 2007b; Yu et al, 2007a). This has lead to concerns due to genomic integration of the virus into the host genome leading to malignant transformations or altered differentiation potential. These problems were overcome by direct protein transductions and chemical induction of pluripotency, but due to low reproducibility and high variability these methods do not represent the primary choices for reprogramming (Muller et al, 2009).

The replication-defective and persistent Sendai virus (SeVdp) vector was recently developed as an alternative for safer and efficient cellular reprogramming (Nishimura et al, 2011). The SeVdp vector can carry the four transgenes (*Oct4/Sox2/Klf4/c-Myc*), deliver them efficiently to human somatic cells and stably express the exogenous genes. This system presents a major advantage over previous reprogramming strategies. As a non-integrating virus, the RNA of SeVdp can be quickly and thoroughly removed from the target cells using siRNAs, which is a significant advantage allowing the generation of homogenous vector-free

iPSCs. When there is incomplete suppression of the exogenous genes, their effects can greatly affect the characteristics of iPSCs.

For reprogramming somatic cells the expression of the exogenous genes is necessary for 10-20 days (Jaenisch & Young, 2008). Ideally, once reprogrammed, these factors should be replaced with their endogenous homologs for the cells to acquire self-regulated pluripotency (Jaenisch & Young, 2008). While this can be partially accomplished with retroviral and lentiviral methods, these integrating viruses can be easily reactivated and since their silencing is not well controlled, they can affect the safety and differentiation potency of iPSCs and can lead to malignant cell transformations.

There is significant variability in the differentiation efficiency of each iPS line to certain lineages (Hu et al, 2010). Hu et al. have investigated the efficiency of six iPSC lines to differentiate to neuroectoderm and found high variability independent of transgene integration. When compared to the differentiation propensity of hESCs, the iPSCs generated by retroviral delivery of the transcription factors exhibited highly variable efficiencies (~15% compared to ~79% in hESCs). Similarly low variable differentiation rates were identified in iPSCs obtained by lentiviral reprogramming. Although transgene integration was suspected to be the reason for low differentiation efficiency, the hypothesis was dismissed when iPSCs obtained by non-integrating methods (Yu, 2009) exhibited similarly low neural differentiation efficiencies.

Though extremely promising as a technique for advancing cell replacement therapy in regenerative medicine, there are a series of obstacles that will need to be resolved before one can take full advantage of iPSCs for therapeutic purposes. One challenge is the incomplete reprogramming process of the fibroblasts to iPSCs that occurs in some of the clones. Such incomplete reprogramming may impair the differentiation propensity of iPSCs to certain cell

types. Another aspect that could delay the use of iPSCs for clinical purposes is the presence of the transgenes in reprogrammed cells and in differentiated cells. The transcription factors are typically delivered to somatic cells by genome-integrating viruses. Although they are generally silenced during the differentiation process, their reactivation can lead to tumorigenesis (Okita et al, 2007) and it can inhibit the propensity of final differentiation to the desired cell type. The newly developed techniques for delivery of transgenes could significantly improve the safety of iPSCs for clinical purposes.

1.5.2.2. iPSC derived motor neurons as models of ALS

Currently, one of the goals of iPSC technology is to use these cells and differentiated lineages for drug screening and for elucidating disease mechanisms in the affected cell types derived from patient iPSCs. This technique allows access to previously unavailable pools of cells, which otherwise could not be obtained from living human subjects.

Induced pluripotent stem cells provide tremendous opportunities because they can be derived from accessible tissues such as peripheral blood and skin fibroblasts and then, by directed differentiation *in vitro*, they can be used to generate neuronal cells. When derived from patient tissue, the differentiated neurons carry the disease-specific genetic background which renders neurons vulnerable to disease and they can provide new insights into disease pathogenesis which were previously unattainable.

Fibroblasts from patients carrying *SOD1* mutations and *TARDBP* mutations have recently been reprogrammed to iPSCs and differentiated to motor neurons for the investigation of molecular mechanisms of pathogenesis (Dimos et al, 2008; Egawa et al, 2012). Such models have provided interesting new insights into ALS pathology. The first

study describing the successful generation of iPSC-derived motor neurons from ALS patients came in 2008 from Dimos et al. They produced iPSCs from an 82-year old patient diagnosed with familial ALS carrying a *SOD1* dominant mutation, proving that cells from elderly patients can be successfully reprogrammed to a pluripotent state and differentiated to motor neurons.

Two recent studies have reported the successful generation of iPSC-derived motor neurons from ALS patients carrying TDP-43 mutations (Bilican et al, 2012; Egawa et al, 2012). Both studies reported that TDP-43 mutations did not affect the motor neuron differentiation process and described disease-specific phenotypes in the adult motor neurons. Motor neurons carrying the M337V mutation in TDP-43 showed elevated levels of soluble and insoluble TDP-43 and decreased survival in longitudinal studies (Bilican et al, 2012). In the second study, Egawa et al. obtained motor neurons from several ALS patients carrying TDP-43 mutations for performing a drug screen (Egawa et al, 2012). While the mutations in TDP-43 (M337V, Q343R or G298S) did not affect the efficiency of motor neuron differentiation, they found that patient derived motor neurons recapitulated key aspects of the disease previously detected in postmortem tissue of ALS patients. Specifically, TDP-43 in ALS iPSC-derived motor neurons was distributed in both nucleus and cytoplasm forming pre-inclusion-like aggregates, while healthy control iPSC-derived motor neurons showed exclusively nuclear TDP-43 localization (Egawa et al, 2012). Furthermore, susceptibility to cell death was significantly increased in ALS iPSC-derived motor neurons in the presence of arsenite-induced oxidative stress and this phenotype could be reversed by anacardic acid, which was identified through drug screening.

In a recent study, a different perspective was explored by the same groups who shifted their attention from investigating neuronal pathology in ALS iPSC-derived motor neurons to

exploring the contribution of ALS iPSC-derived glia to disease pathology (Serio et al, 2013). Astrocytes differentiated from ALS iPSCs obtained from the same M337V TDP-43 patients exhibited increased levels of soluble TDP-43 and cytoplasmic mislocalization, but without nuclear depletion of TDP-43. Astrocytes carrying the M337V mutation were also more susceptible to cell death under basal conditions, which was not seen in neuronal culture. In contrast with *SOD1* experiments (Di Giorgio et al, 2007), M337V astrocytes did not affect the survival of healthy iPSC-derived motor neurons in co-culture (Serio et al, 2013).

Where aging is not a key part of disease pathogenesis, modelling using iPSCs may be straightforward. Motor neurons differentiated from iPSCs derived from an SMA patient revealed functional deficits reminiscent of disease when compared to motor neurons differentiated from a healthy person (Ebert et al, 2009). This was the first study to report a clear phenotype in patient iPSC derived neurons, showing a reduced number and size of motor neurons when compared to control motor neurons derived from the fibroblasts of the patient's unaffected mother (Ebert et al, 2009). Establishing a clear phenotype is more challenging when the disease under investigation is associated with the aging process or is a genetically inherited disease with low genetic penetrance. Patients survive with certain genetic mutations for decades and a convergence of several unidentified factors may trigger disease onset. Aging is clearly a factor in ALS, but this remains a challenge to model in iPSC-derived motor neurons.

Another important consideration is that current protocols for motor neuron differentiation do not clearly define the subtype identity of motor neurons produced, making functional and disease modelling difficult to interpret.

The potential for iPS technology is enormous and it is currently only at the beginning. Stem cell technology harbours the potential to generate a limitless source of patient-iPSCs for both regenerative medicine and basic research into the molecular pathogenesis of neurodegenerative diseases.

1.6. Aims of this thesis

There are currently many challenges in understanding TDP-43 proteinopathies, mainly due to the high complexity of TDP-43 function and shortage of disease relevant models. The purpose of this thesis is to investigate the functional effects of three ALS-associated mutations in TDP-43 *in vitro* in cellular models and in human motor neurons derived from iPSCs reprogrammed from fibroblasts of healthy volunteers and *C9orf72* ALS patients. The work has been organized under three main aims:

1. Construction of vectors carrying the full-length *TARDBP* genomic locus, engineering of a fluorescent Ypet tag to the C-terminus and insertion of 3 disease specific mutations A382T, M337V or Y374X (Chapter 3)
2. Investigation of functional phenotypes associated with TDP-43 mutations in site-specific BAC HEK293 clonal cell line by analysis of subcellular localization, relocalisation in response to oxidative and ER stress and calcium imaging assays for the investigation of ER Ca^{2+} release and contents (Chapter 4)
3. Investigation of functional phenotypes associated with ALS mutations in healthy and ALS iPSC derived motor neurons (Chapter 5)**.**

CHAPTER 2

Materials and Methods

2.1. Cloning

2.1.1. Preparation of electrocompetent cells

Highly electrocompetent *E.coli* bacterial cells (ElectroMAX DH10B) containing the BACs were made by inoculating the bacteria in 1.5 mL of Luria Bertani (LB) medium with the appropriate antibiotic (chloramphenicol for BACs and kanamycin for PACs) and incubated overnight at 37^{o}C with shaking at 225 rpm. After 12 hours, the culture was tipped in a 1 L flask with 100 mL of LB and the appropriate antibiotics. The culture was grown at 37^{o}C with shaking for 1.5 hours and the optical density checked at 600 nm using a cell density meter (WPA) until it reached 0.35-0.36. The bacteria were then transferred to 250 mL centrifuge flask and allowed to chill on ice for 15 minutes. The bacteria were pelleted by centrifugation in an Avanti J-E centrifuge at 6000 rpm, 4^{o}C. The supernatant was discarded and the pellets were washed with 10% glycerol three times at 6500 RPM, 7000 RPM and 7500 RPM

respectively at 4^{o}C. After the last wash, the bacteria were aliquoted in 50 µL and stored at -80^{o}C.

2.1.2. Induction of Red/ET

The electrocompetent cells containing the PACs and Red/ET were prepared as described above, with a few changes. The cultures were grown at 30^{o}C with shaking for 1.5 hours until the optical density reached 0.1-0.13. The Red/ET was induced by addition of 1.5 ml of fresh 10% L-arabinose per culture. The cultures were grown at 37^{o}C for another 40 minutes until the optical density reached 0.30-0.35. The cells were then pelleted and washed as previously described.

2.1.3. Electroporation

The bacterial DNA electroporations were carried out using a Gene Pulser system (Bio-Rad). 50 µL of electrocompetent bacterial cells were electroporated according to the manufacturer's instructions in 0.1 cm cuvettes. 1 ng of Red/ET expressing plasmid was electroporated into electrocompetent cells containing the TDP-43 vectors. For homologous recombinations, 8 µL of the purified template DNA (pCYPAC2, Ypet) were electroporated into electrocompenet cells carrying the vectors and Red/ET. The parameters used were the following: potential difference 1800 V, capacitance 25 µF and internal resistance 200 Ω. Following electroporation, the bacteria were incubated in 450 µL SOC medium or 550 µL LB (for homologous recombinations) at either 30^{o}C (when containing the Red/ET plasmid) or 37^{o}C with shaking for 1 hour or 1 hour and 15 minutes (for homologous recombinations). 2 µL and

100 µL were then plated on LB agar Petri dishes containing the correct antibiotics and incubated overnight at 30°C or 37°C.

Transformation efficiency was carried out in parallel by electroporating 50 µL of electrocompetent bacterial cells with 1 µL of pUC19 plasmid DNA (10 pg/µL; Invitrogen). 20 µl of bacteria were plated on LB agar Petri dishes containing ampicillin and they were grown overnight at 37°C. The next day transfection efficiency was evaluated by counting the number of colonies and calculating the number of colony forming units (CFU) per µg DNA:

2.2. DNA extraction

2.2.1. BAC plasmid mini prep

The following buffers were used for BAC plasmid DNA extraction: STET buffer (8% sucrose, 5% Triton X-100, 50 mM EDTA, 50 mM TrisCl pH 8), bacterial alkaline lysis buffer (1% SDS, 0.2 M NaOH) and neutralisation buffer (7.5 M ammonium acetate). A single bacterial colony was seeded in 1.5 mL LB culture containing the appropriate antibiotic and grown overnight at 37°C with shaking. To pellet the cells, the culture was centrifuged at 5000 rpm for 10 minutes and the supernatant was aspirated. The pellet was resuspended in 70 µL STET buffer and 200 µL alkaline SDS solution were added to lyse the bacterial cells. 150 µL of 7.5 M ammonium acetate were then added and after 5 minutes on ice, the samples were centrifuged at 13,000 rpm, 4°C for 20 minutes. The supernatant was transferred into a fresh tube and 250 µL isopropanol were added and mixed by inversion. To pellet the DNA, the samples were again centrifuged at 10,000 rpm for 8 minutes. The supernatant was aspirated

and the pellet was washed with 200 µL of 70% ethanol. The samples were centrifuged at 10,000 rpm, for 8 minutes. The ethanol was aspirated and the pellet air dried for 5-10 minutes. The DNA was resuspended in 50 µL of Tris-EDTA containing 5 µg/mL RNase A.

2.2.2. BAC Maxi preps

Large quantities of high quality plasmid DNA were obtained using a plasmid Maxi Kit (Qiagen). A fresh BAC streak was made on an LB plate with chloramphenicol 15 µg/mL. An individual colony was picked and grown in 1.5 mL LB with chloramphenicol for 8 hours. Then the culture was tipped into 250 mL of LB with chloramphenicol overnight. The next day, the samples were transferred to new bottles and centrifuged for 15 minutes at 4^{o}C and 6,000 rpm. The supernatant was discarded and 15 ml of P1 buffer with RNase A was used for resuspension. The bottle was then placed back in the incubator at 37^{o}C for 10 minutes. 15 ml of P2 were added and 5 minutes were allowed for lysis. Afterwards, 15 ml of chilled P3 were added, mixed by inversion and incubated on ice for 20 minutes. The bacterial lysate was then spun down at 9000 rpm in a J 10.5 rotor in Beckmann J2 centrifuge for 35 minutes at 4^{o}C. The Qiagen column was equilibrated with 15 ml of QBT, and the supernatant was filtered through a Kimwipe tissue followed by 2 washes with 30 ml QC. The DNA was eluted into Oakridge tubes using 15 ml of QF warmed up to 55^{o}C. 10.5 ml of isopropanol were added and the samples centrifuged at 4^{o}C for 30 minutes at 14,000 rpm in J-17 rotor Beckmann J2 centrifuge. The supernatant was discarded and 3.5 ml of 70% ethanol were added, followed by another centrifugation at 4^{o}C for 30 minutes, at 14,000 rpm in J-17 rotor. The pellet was left to air dry for 15 minutes and resuspended in 250 µl TE overnight. The next day, the samples were centrifuged.

2.2.3. Restriction digests of plasmid DNA

The restriction enzymes, buffers and bovine serum albumin (BSA) were purchased from New England Biolabs (NEB). Restriction digests were prepared by adding the following components:

Components	Volume/amount
DNA maxi prep	200 ng
10x Restriction buffer	1.5 µL
20x BSA	0.75 µL
Restriction enzyme	0.3 µL
MilliQ H_2O	up to 15 µL

When miniprep DNA was used, 10 µl of miniprep DNA were digested with 5 µl digestion mix. The digestion mix with DNA were incubated at 37^{o}C for 2 hours and the results were analysed by agarose gel electrophoresis (for small plasmids) or by pulsed-field gel electrophoresis (for BACs and PACs).

2.2.4. DNA sequencing

The region of interest to be sequenced was amplified via PCR using standard PCR conditions and the quality of the amplified DNA was checked by agarose gel electrophoresis. An ExoSAP reaction was carried out in order to remove PCR buffers, salts and dNTPs by using exonuclease 1 (NEB) and shrimp alkaline phosphatise (Promega). The reaction consisted of the following components:

Components	Per reaction
PCR product	25 µL
10x SAP buffer	1 µL
SAP (500 U/ul)	1 µL
Exonuclease I (20 U/ul)	0.1 µL
Milli-Q H_2O	0.9 µL

The samples were incubated at 37°C for 1 hour and 80°C for 20 minutes.

The DNA sequencing reactions were performed according to BigDye Terminator v3.1 Cycle Sequencing protocol (Applied Biosystems). The reaction mix consisted of the following:

Components	Per reaction
BigDye	0.5 µl
5x Sequencing buffer	1.75 µl
Primer (10 µM)	1 µl
DNA template	5 µl
MilliQ H_2O	1.75 µl

The following PCR program was used:

96° for 1 minute

96° for 10 seconds
50°C for 5 seconds
60°C for 4 minutes
} x30 cycles

The samples were spun down and purified after the sequencing reaction. 4 µl of EDTA/NaAC were added to each well followed by 50 µl of 100% ethanol and mixed well. The plate was spun at 3000 x *g* at 4^{o}C for 30 minutes followed by a brief 10 seconds spin at 185x *g* inverted. 70 µl of 70% ethanol were added to each well and the plate was spun at 1650 x g at 4^{o}C for 15 minutes. The caps were removed, the plate was inverted and spun for another 1 minute at 185 x *g*. The samples were left to dry and taken to the sequencing facility.

Table 2.1 : Oligos used for sequencing exon 6 in *TARDBP* (Chapter 3.4)

Name	**Oligo sequence**
Seq_mutations_exon_6_S	CATGCCCAGCCTATGTCTTT
Seq_mutations_exon_6_A	AGCAGCTTCAGGGTCAGCTT

2.3. Polymerase Chain Reaction

PCR reactions were carried out using AmpliTaq Gold DNA polymerase (Applied Biosystems) in 96-well plates (Starlab) on a PCR Peltier Thermocycler (PTC-225, MJ Research) with the following components:

Components	Per reaction
DNA template	30 ng
10x Buffer	1.5 µL
$MgCl_2$ 25 mM	1.5 µL
dNTPs 8 mM	0.75 µL
Primer Forward 1 µM	0.75 µL
Primer Reverse 1 µM	0.75 µL
Taq Gold 5 U/ µl	0.2 µL
Milli-Q H_2O	Up to 15 µL

The following conditions were used:

95°C for 10 minutes

95°C for 20 seconds
58°C for 20 seconds } x30 cycles
72°C for 3 minutes

72°C for 5 minutes

Table 2.2: Oligos used for checking the presence of *TARDBP* exons and downstream region (Chapter 3.3)

Name	Oligo sequence
Seq_exon_1_S	GAGGGCATGAACGAGCTCTA
Seq_exon_1_A	TCACAGCCTTGCGTTCATAG
Seq_exon_2_S	TCCGCTACTCTTTATTTCATGG
Seq_exon_2_A	ATGAAAGTTCCATCTCAAAGG
Seq_exon_3_S	CAGCCCTGAATGCAAAGAAT
Seq_exon_3_A	GAAAATGAGCTCAACTCTCACAGA
Seq_exon_4_S	CAAAACTCACACTCTCACAATGC
Seq_exon_4_A	TCGTGTTTTTCCAGTAAGACTCC
Seq_exon_5_S	ACTATTTGGCAAAGATTTGTTTTT
Seq_exon_5_A	GCAATTCCAATGCTAAGAATTTA
Seq_exon_6_S	TGTGGAAATGCCATGTTTTG
Seq_exon_6_A	AATGCCTGTGAAGACCTTGG
TDP43_down_1_S	TTCAAATGTTTATGGAACAAGCAC
TDP43_down_1_A	TTCATAGCGTTGATACGACTCC
TDP43_down_2_S	AGGTGGGGGAATGTGGTAAC
TDP43_down_2_A	GGGCATTAGGTAAACTACCAACAC

Table 2.3: Oligos used for RT-PCR on iPSC derived motor neurons

Name	Oligo sequence
Olig2 S	GGACAAGCTAGGAGGCAGTG
Olig 2 A	ATGGCGATGTTGAGGTCGTG
Pax6 S	ATGTGTGAGTAAAATTCTGGGCA
Pax6 A	GCTTACAACTTCTGGAGTCGCTA
Nkx6.1 S	CACACGAGACCCACTTTTTCC
Nkx6.1 A	CCCAACGAATAGGCCAAACG
HPRT S	AATTATGGACAGGACTGAACGTCTTGCT
HPRT A	TCCAGCAGGTCAGCAAAGAATTTATAGC
ChAT S	CGTGGACAACATCAGATCG
ChAT A	ATGGCCATGACTGTGTATGC

2.3.1. Colony PCR

Colony PCR was used to quickly identify the clones where homologous recombination had taken place. Individual clones were picked from the Petri-dishes into 10 µl of MilliQ-H_2O in a 96-well plate. PCR reactions were performed using AmpliTaq Gold :

Components	**Per reaction**
Colony template	2.5 µL
10x Buffer	1.5 µL
$MgCl_2$ 25 mM	1.5 µL
dNTPs 8 mM	0.75 µL
Primer Forward 1 µM	0.75 µL
Primer Reverse 1 µM	0.75 µL
Taq Gold 5 U / µl	0.2 µL
Milli-Q H_2O	Up to 15 µL

The following PCR program was used:

95°C for 10 minutes
95°C for 20 seconds
50°C for 30 seconds } x30 cycles
72°C for 3 minutes
72°C for 5 minutes

2.3.2. Long range PCR

Long range PCR was performed for the amplification of fragments longer than 1 kb using Extend Long Template PCR (Roche). One reaction consisted of the following:

Components	Per reaction
DNA template	40 ng
10x Buffer 3	2.9 µL
dNTPS (8 mM)	5.8 µL
Primer Forward (10 uM)	2.9 uL
Primer Reverse (10 uM)	2.9 uL
Enzyme mix (Extend long range PCR)	0.43 µL
MilliQ-H	Up to 25 µL

The following PCR program was used:

95^{o}C for 10 minutes

95^{oC} for 30 seconds

52-68^{o}C for 30 seconds } x35 cycles

68^{o}C for 12 minutes

68^{o}C for 8 minutes

Table 2.4: Oligos used for the amplification of pCYPAC2 for subcloning the *TARDBP* genomic locus (Chapter 3.2)

Name	Oligo sequence
pCYPAC2-TDP43 sense	AGAACAAGTTTAAAAACAAAGAGCATGGACAGGCAGTTT ACAGAAATGCCAACAGCCAGTATGAAAAGAGACTGGATT GACCCGGAACCCTTAATATAAC
pCYPAC2-TDP43 antisense	AGCGTGACTGTTCCTCCGGTGAACCTCAGTTTCTTAGCTT CTTTCCTTCCTTGGGCACAGAGACAGGCTTCTCCCAAAAT CATTTAATTGGTGGTGCTGC

Table 2.5: Oligos used for the amplification of pRpsl-Chl cassette for the insertion of mutations A382T, M337V and Y374X (Chapter 3.4)

Oligos	Sequence
pRpslChl_for_A382T_S	AAACCAGGCCTTCGGTTCTGGAAATAACTCTTATAGTGGC TCTAATTCTGGTGCAGGCCTGGTGATGATGGCGGGATC
pRpslChl_for_A382T_A	CCTCCATTAAAACCACTGCCCGACCCTGCATTGGATGCTG ATCCCCAACCAATTGGCTGCTAGCTTACGCCCCGCCC
pRpslChl_for_M337V_S	TAATCCAGCCATGATGGCTGCCGCCCAGGCAGCACTACA GAGCAGTTGCCCTATGGGCCTGGTGATGATGGCGGGATC
pRpslChl_for_M337V_A	TTTTGGTTATTACCCGATGGGCCTGACTGGTTCTGCTGGCT GGCTAACATGCCCAGCTGCTAGCTTACGCCCCGCCC
pRpslChl_for_Y374X_S	AAGGCAACATGCAGAGGGAGCCAAACCAGGCCTTCGGTT CTGGAAATAACTCTTAGGCCTGGTGATGATGGCGGGATC
pRpslChl_for_Y374X_A	CCCTGCATTGGATGCTGATCCCCAACCAATTGCTGCACCA GAATTAGAGCCACTAGCTGCTAGCTTACGCCCCGCCC

2.4. Site-directed mutagenesis

Site-directed mutagenesis was done by PCR using the Stratagene Pfu Turbo polymerase using the following conditions:

Components	**Per reaction**
10x buffer	5 µL
Forward primer (125 ng/ul)	1 µL
Reverse primer (125 ng/ul)	1 µL
dNTP mix (10 mM)	1 µL
DNA (10ng/ul)	2.5 µL
H_2O	38.5 µL
***Pfu Turbo* polymerase (2.5 U/ul)**	1 µL

The following program was used:

95^{o}C for 1 minute

95^{o}C for 30 seconds

55^{o}C for 1 minute

68^{o}C for 10 minutes

After amplification, 1 µL of DpnI restriction enzyme was added to the reactions and incubated for 1 hour at 37^{o}C. To check the PCR production of mutated plasmids, 5 µL of each PCR mix were separated on a 1% agarose gel.

Table 2.6: Oligos used for site-directed mutagenesis (Chapter 3.4)

Oligos	Sequence
A382T_mutagenesis_S	GTGGCTCTAATTCTGGTGCAACAATTGCTTGGGGATCAGCA
A382T_mutagenesis_A	TGCTGATCCCCAACCAATTGTTGCACCAGAATTAGAGCCAC
M337V_mutagenesis_S	TACAGAGCAGTTGGGGTATGGTGGGCATGTTAGGCAGCCAG
M337V_mutagenesis_A	CTGGCTGGCTAACATGCCCACCATACCCCAACTGCTCTGTA
Y374X_mutagenesis_S	GGTTCTGGAAATAACTCTTAATAGTGGCTCTAATTCTGGTG
Y374X_mutagenesis_A	CACCAGAATTAGAGCCACTATTAAGAGTTATTTCCAGAACC

2.5. Cre/loxP recombination for retrofitting

Cre-mediated loxP recombination was used in order to introduce an FRT element into the TDP-Ypet, TDP-A382T, TDP-M337V and TDP-Y374X PAC constructs. Two reaction mixtures were prepared:

Components	Reaction 1	Reaction 2
Each PAC	1 µg	1 µg
pH-FRT-Hy plasmid	1.5 µg	100 µg
10x Cre buffer	1 µL	1 µL
Cre recombinase (NEB)	1 µL	1 µL
Milli-Q-H_2O	Up to 10 µL	Up to 10 µL

The mixtures were incubated at 37^{o}C for 1 hour followed by inactivation of the enzyme at 70^{o}C for 5 minutes. The samples were left at room temperature for 10 minutes and drop-dyalised against 50 mL of Milli-Q-H_2O for 1.5 hours, using 0.25 µm membrane filters (Millipore). The samples were then electroporated into ElectroMAX DH-10B competent cells and plated on 15 cm agar dishes containing kanamycin and ampicillin. Successful recombinants were identified by restriction digests and pulsed-field gel electrophoresis.

2.6. Human Cell Culture

All cell culture was carried out under aseptic conditions in a Class II tissue culture cabinet. The cells were grown in saturated humidity incubators at 37^{o}C with 5% CO_2.

2.6.1. Reagents

The reagents used in the experiments were purchased from the following companies: Dulbecco's modified Eagle's medium high glucose (DMEM), DMEM/F12 (1:1), Hank's Balanced Salt Solution (HBSS), were purchased from PAA; L-glutamine, phosphate buffered saline (PBS), trypsin-EDTA, 100U/mL penicillin and 0.1 mg/mL streptomycin (P/S) and dimethyl sulfoxide (DMSO) were purchased from Sigma.; Opti-MEM (OM), foetal bovine serum (FBS), sodium pyruvate and non-essential amino acids (NEAA) were purchased from Invitrogen.

2.6.2. Routine subculture

Every 3-5 days, HEK293 cells were passaged. The old medium was removed and the cells were washed with 10 mL PBS. Cells were trypsinized with 2 mL trypsin-EDTA at 37^{O}C for 5 minutes and the reaction was neutralised by the addition of 7 mL of normal growth medium.

Between 1 and 4 mL of the cell suspension were transferred to a new 75 cm^2 flask with 12 mL of fresh growth medium.

2.6.3. Long term storage and thawing

For long-term storage, cells were transferred to a liquid nitrogen tank. Briefly, a confluent T75 flask was trypsinized and cells were centrifuged at 1000g for 5 minutes, at room temperature. The cell pellet was resuspended in 3 mL of normal growth and 3 mL of freezing mix (90% FBS, 10% DMSO). After mixing, the cells were equally distributed to 3 cryovials, which were allowed to freeze overnight at -80^oC before transferring to the liquid nitrogen tank. For thawing, a cryovial was rapidly warmed up in a 37^oC water bath and the medium containing the cells was transferred to a 15 mL falcon tube containing 10 mL of normal growth medium. The cells were centrifuged at 900 x *g* for 10 minutes and the supernatant was discarded. The cell pellets were resuspended in 3 mL of normal growth medium and distributed in two 25 cm^2 culture flasks in different ratios.

2.6.4. Cell counting

Cell counting was performed using a haemocytometer. Briefly, cells were trypsinized and transferred to a 15 mL falcon tube. 10 µl of cell suspension were loaded onto a haemocytometer and cells were counted in four 4x4 mm squares. The number of cells per mL was calculated by multiplying the average number of cells by 10,000.

2.7. DNA delivery to human cell lines by lipofection

For delivery of BAC DNA to human cells, lipofection was used according to the manufacturer's instructions (Invitrogen). Briefly, a 6 cm dish was seeded with $1x10^6$ cells in DMEM supplemented with 10% FBS, 1% Pen/Strep and 1% L-Glutamine and allowed to grow overnight. 2 tubes were prepared the next day, Tube A containing 250 µL of OptiMEM, 4 µg of BAC DNA, and 10 µL of Plus reagent (Invitrogen) and Tube B with 250 µL OptiMEM and 16 µL Lipofectamine. After 10 minutes, Tube B was added to Tube A and allowed to form complexes for 40 minutes. The cells were washed twice with OptiMEM and 1 mL of OptiMEM was left in the dish after the second wash. 500 µl of the mixture were added to each sample and allowed to transfect for 4 hours. Afterwards the cells were washed 3 times with OptiMEM and 3.5 mL of media were added. 24 hours later, the medium was changed and the cells were allowed to grow for 3 further days.

2.8. DNA delivery to human neurons by HSV-1 amplicons

2.8.1. Packaging of vectors in HSV-1 amplicons

The following plasmids were used for packaging of TDP-43 vectors into HSV-1 amplicons: fHSVΔpacΔ27, which lacks the essential HSV-1 packaging/cleavage sites, and pEBHICP27. The pEBHIPC27 encodes ICP27, that was deleted from the HSV-1 genome and was supplied *in trans* from this plasmid and from the Vero 2–2 cell line, a clonal cell line expressing ICP27 (Lufino et al, 2011).

The Vero 2-2 cells were grown until confluent in normal growth medium (DMEM, 10% FBS, 1% P/S, 1% L-G, 500 µg/mL G418) and seeded in 6 cm dishes at a cell density of $1x10^6$ in seeding medium (DMEM, 10% FBS, 1% P/S, 1% L-Glutamine). After 24 hours, when cells were 80-90% confluent, the following components were co-transfected:

Tubes	Components	Reaction
Tube A	fHSVΔpacΔ27	2 µg
	pECHICP27	0.2 µg
	TDP-43 BAC	2 µg
	OptiMEM	250 µL
	Plus reagent	10 µL
Tube B	OptiMEM	250 µL
	Lipofectamine	23 µL

The components were mixed in Tube A in the order described above and incubated for 10 minutes at room temperature. Tube B was then added to Tube A dropwise and complexes were allowed to form for 30-40 minutes. After 30 minutes, OptiMEM was added to reach a volume of 1.5 mL per dish. The Vero 2-2 cells were washed twice with 2.5 mL of OptiMEM and the transfection mix was added to the plates (1.5 mL/dish). The transfection mix was left for 4 hours at 37^OC. After 4 hours, the mix was removed and the cells were washed 3 times with 2.5 mL OptiMEM and 3.5 mL of packaging medium was added to the cells (DMEM, 6%

FBS, 1% P/S, 1% L-G, 25 mM HEPES). Packaging was allowed to take place for 60 hrs at 37^{O}C.

After 60 hrs, the cells from 3-6 dishes were harvested in a 50 mL Falcon tube and snap frozen on dry-ice with ethanol for 30 minutes before proceeding with the concentration protocol.

2.8.2. HSV-1 amplicon concentration

The harvested Vero 2-2 cells were thawed in a 30^{O}C waterbath and the cells were broken open using a sonicator (Fisher Scientific Sonic Dismembrator Model 500) set for 50% amplitude for 30 seconds at 4^{O}C. Cellular debris was spun down by centrifugation at 1200 x *g* for 10 minutes at 4^{O}C. The supernatant was filtered using a 0.42 µm filter unit and loaded onto a 30% sucrose cushion in ultracentrifuge tubes. The tubes were balanced and placed in an ultracentrifuge (Beckman ultracentrifuge L70) to spin at 22,000 rpm on SW32Ti rotor at 4^{O}C for 3 hours. After centrifugation, the supernatant was carefully removed and 250 µL DMEM complete medium was added to resuspend the viral pellet by pippetting. The amplicons were then aliquoted in 50 µL aliquots and stored at -80^{O}C.

2.8.3. HSV-1 amplicon titration

The amplicon vectors carry a reporter expression cassette designed for titration of the viral stocks. The ß-galactosidase reporter is under the transcriptional control of the immediate HSV-1 promoter pIE4/5. To titrate the amplicon stocks, G16.9 cells were used. The G16.9 cells stably express the HSV-1 protein VP16, which enhances the expression of the pIE4/5 promoter and therefore enhances the reporter gene expression. G16.9 cells were grown in normal growth medium (DMEM, 10% FBS, 1% P/S, 1% L-G, and 200 µg/mL Hygromycin

B). The cells were seeded in triplicate for each vector in a 24-well plate at a density of 4 x 10^5 cells/well in seeding medium (DMEM, 10% FBS, 1% P/S, 1% L-G) and allowed to adhere to the plate overnight. The next day, one amplicon stock per condition was defrosted and dilutions were prepared in 250 µL titration medium (DMEM, 2% FBS, 1% L-G and 25 mM HEPES). The seeding medium was then aspirated from the G16.9 cells and each well was transduced with either 5 µL, 2 µL or 1 µL of the viral stock. After 24 hours, ß-galactosidase assay was performed.

2.8.4. X-Gal staining

The transduction medium was removed and the cells were washed once with PBS. The cells were then fixed in fixative solution for 10 minutes at room temperature (DPBS, without $CaCl_2$ and $MgCl_2$, 2% formaldehyde, 0.05% glutaraldehyde). The cells were washed twice with PBS and 300 µL of staining solution (DPBS, 5 mM potassium fericyanide, 5 mM potassium ferrocyanide and 2 mM $MgCl_2$) were added containing X-gal (5-bromo-4-chloro-3-indolyl-ß-D-galactoryranoside) at 1 mg/mL. The assay was left overnight at 37^OC and the blue cells were counted under an inverted microscope.

2.8.5. HSV-1 amplicon transduction

Several multiplicities of infectivity (MOIs – viral particles/cell) were assessed in iPSC-derived motor neurons using a GFP-expressing plasmid packaged in HSV-1 amplicon. Following titration, the MOI was calculated and amplicons stocks were diluted in normal growth medium for human motor neurons and added to the cells. The transduction was

allowed to proceed for 24 hours and the medium containing the viral amplicons was changed with fresh normal growth medium. The transduction efficiency was assessed by immunostaining or by live fluorescence.

2.9. siRNA delivery to human cell lines

HEK293 cells were seeded 20 hours before transfection at a density of 12 x 10^4 cells per well in a 12 well plate and allowed to adhere in DMEM High glucose+10%FBS+10%L-glutamine media. After 20 hrs, the cells were washed 2 times with Opti-MEM (OM, Life Technologies) and 1 ml of Opti-MEM was left to cover the cells. For each well to be transfected, 2 μL of Lipofectamine 2000 (Life Technologies) transfection reagent was resuspended in 100 μL OM and incubated at room temperature for 10 minutes. Each pre-validated Silencer® Select siRNA (Life Technologies) was reconstituted at a stock concentration of 50 μM and 2.4 μL of siRNA stock were resuspended in 100 μL OM. After 10 minutes, the Lipofectamine2000 mixture was gently added to the siRNA mix and complexes were allowed to form for 20 minutes. After 20 minutes incubation, 200 μL of siRNA:Lipofectamine2000 mix was added to each well. After 6 hours, 600 μL of 30% FBS in OM were added to each well and after 24 hours, the media was replaced with DMEM High glucose+1%L-glutamine+1%penicillin/streptomycin. The siRNAs used in this experiment were the following: Bcl-2 siRNA (s194310) and control siRNA (AM4635). Calcium homeostasis analysis and western blotting were performed on cells 48 hours after transfection.

2.10. Generation of clonal HEK293 cell lines

HEK293-FRT cells were previously developed and described in our lab (Alegre-Abarrategui et al, 2009). Briefly, the HEK293-FRT cells were obtained by transfecting HEK293 cells with the pFRT/*lac*Zeo plasmid (Invitrogen) using Lipofectamine (Life Technologies), following the manufacturer's instructions. Selection was performed for clones resistant to 100 µg/mL of zeocin (Invitrogen). HEK293 clonal cell lines expressing full-length TDP-Ypet, TDP-M337V, TDP-A382T and TDP-Y374X vectors were obtained by co-transfecting HEK293-FRT cell lines with pOGG plasmid (Life Technologies), which expresses *Flp* recombinase, and TDP-Ypet-FRT, TDP-M337V-FRT, TDP-A382T-FRT and TDP-Y374X-FRT retrofitted with pH-FRT-Hy. As controls, HEK293-FRT cells were transfected with either pH-FRT-Hy and pOG44 (positive control) or pH-FRT-Hy only (negative control). The following mixes were prepared for transfection of a 6 cm dish:

Tubes	Components	Experiment	Positive Control	Negative Control
Tube A	TDP-FRT	3200 ng	-	-
	pH-FRT-Hy	-	730 ng	730 ng
	pOG44	800 ng	800 ng	-
	OM	250 µL	250 µL	250 µL
	Plus reagent	10 µL	10 µL	10 µL
Tube B	OM	250 µL	250 µL	250 µL
	Lipofectamine	16 µL	16 µL	16 µL

The transfection was allowed to take place for 48 hours and then cells from each 6 cm dish were split in two 10 cm dishes. After 24 hours, the selection antibiotic was added to the medium at a concentration of 250 µg/µL hygromycin B (Invitrogen). Cells were allowed to grow for 3 weeks and fresh medium was provided every 2 days. Individual clones were picked in 96-well plates and expanded to T25 cm^2 flasks. At that point, each clone was screened for insertion of the constructs in the FRT site using PCR.

Table 2.7 : Oligos sequences for checking integration of TDP-43 in HEK293 cells by FRT recombination

Name	Oligo sequence
pSV40_S	CCAGTTCCGCCCATTCTC
LacZ_A	GGCGATTAAGTTGGGTAACG
Hygro_A	CAGCTATTTACCCGCAGGAC

2.11. Analysis of protein expression

2.11.1. Protein extraction

Cells were lysed 4 days following transfection in RIPA buffer (0.5% sodium deoxycholate, 0.1% SDS, 1% NP-40 and 1% protease inhibitor cocktail). The cells were washed and scraped in PBS followed by centrifugation at 1700 x *g* for 2 minutes and lysed in 50 µL of RIPA buffer. They were incubated on ice for 30 minutes and sonicated. The lysate was left for 30 minutes on ice and centrifuged at 1,200 x *g* for 10 minutes. The supernatant was

retained and stored at -80^{o}C. Protein content was quantified by BCA assay according to the manufacturer's instructions (Sigma).

2.11.2. Subcellular compartmentalization

Nuclear and cytoplasmic fractions were extracted according to the manufacturer's instructions using the NE-PER nuclear/cytoplasmic extraction kit (Pierce Fischer, cat. 78833). The kit was composed of Cytoplasmic Extraction Reagents I and II (CER I and II) and a Nuclear Extraction Reagent (NER). Before proceeding with the extraction, protease inhibitors (Roche) were added to CER I and NER (1/100). Cells were washed once with PBS and harvested in PBS. The cell suspensions were centrifuged for 3 minutes at 500 x *g*, at 4^{O}C. The supernatant was discarded and the cell pellet was resuspended in 200 µL ice-cold CER I. The tube was thoroughly vortexed to resuspend the cell pellet and the cells were incubated on ice for 10 minutes. After 10 minutes, ice-cold CER II was added to the suspension and mixed by vortexing. After 1 minute incubation on ice, the suspension was vortexed and centrifuged for 5 minutes at 16,000 x *g*. The supernatant containing the cytoplasmic fraction was immediately transferred to a clean pre-chilled tube and placed on ice.

The insoluble fraction formed after centrifugation was resuspended in NER buffer. The suspension was thoroughly mixed by vortexing for 15 seconds every 10 minutes for a total of 40 minutes. After 40 minutes, the tube was centrifuged at maximum speed (~16,000 x *g*) at 4^{O}C for 10 minutes and the supernatant was immediately transferred to a pre-chilled clean tube. The samples were stored at -80^{O}C until further use.

2.11.3. Western blotting

10 µg of protein were heated at 65°C in 1x Laemelli buffer for 10 minutes and then separated on a 10% SDS-polyacrylamide gel electrophoresis (SDS-PAGE in 1x running buffer at 200V). The protein was then transferred to a polyvinylidene difluoride (PVDF membrane, Millipore) in 1x transfer buffer at 100V for 70 minutes. Membranes were blocked in blocking buffer (Tris buffered saline, 0.1% Tween-20, 5% milk) overnight. The next day, the blots were probed using primary antibodies for 3 hours at room temperature: rabbit-anti-TARDBP (ProteinTech, 1:1000), mouse-anti-GFP (Invitrogen, 1:500), mouse-anti-GAPDH (Abcam, 1:500) and mouse-anti-Histone H1 (Abcam, 1:500). The membranes were washed 3 times for 10 minutes in TBS 0.1% Tween-20 and the appropriate horse radish peroxidase-conjugated secondary antibodies (BioRad) were applied for 1 hour. After washing, chemiluminescence was done using an ECL$^+$ kit (Amersham). Image J was used for protein quantification and normalization.

Table 2.8.: Primary antibodies used for immunoblotting

Antigen	Host	Type	Manufacturer	Catalogue number	Dilution
ATG7	rabbit	monoclonal	Millipore	04-1055	1:1000
B-actin	rabbit	monoclonal	Abcam	ab8227	1:5000
Bcl-2	mouse	monoclonal	DAKO	M0887	1:500
Bcl-$X_{S/L}$	rabbit	polyclonal	Santa Cruz Biotechnology	sc-7195	1:200
Calreticulin	rabbit	polyclonal	ProteinTech	10292-1-AP	1:200
ChAT	goat	polyclonal	Millipore	AB143	1:500
Histone H1	mouse	monoclonal	Abcam	ab11079	1:500
GAPDH	mouse	monoclonal	Abcam	mAb9484	1:1000

GFP	rabbit	polyclonal	Invitrogen	A-11122	1:1000
GFP	mouse	monoclonal	Invitrogen	A-11120	1:500
GRP78/BiP	rabbit	polyclonal	Abcam	ab-21685	1:200
LC3B	mouse	monoclonal	Sigma	L7543	1:200
TARDBP	rabbit	polyclonal	ProteinTech	10782-2-AP	1:500
TARDBP	mouse	monoclonal	ProteinTech	60019-2-Ig	1:500
SQST1/p62	mouse	monoclonal	Abcam	ab56416	1:1000

2.11.4. Imunofluorescence

For immunofluorescence, the cells in a 24 well plate were fixed in 500 µL of 4% paraformaldehyde for 30 minutes. The samples were washed with DPBS three times and then blocked for 1 hour in IF blocking buffer (0.01%TritonX-100/TBS with 10% normal goat serum). The cells were washed once with IF wash buffer (0.01% Triton X-100, TBS) and incubated in 300 µL of primary antibody, HB9 (DSHB, 81.5c10, 1:100), Choline acetyltransferase (Millipore, AB144P), β-III tubulin (Covance, MRB-435P), with the following secondary antibodies: Alexa Fluor 488 and Alexa Fluor 568 (Invitrogen, 1:500). The primary antibodies were incubated overnight at 4^{o}C, and the samples were washed 3x10 minutes the next day with 0.01% TritonX-100/TBS. The cells were then incubated in the appropriate secondary antibodies for 1 hour and washed 3x10 minutes with wash buffer. DAPI was added to one of the washes 1:2000 for nuclear staining. The coverslips were then mounted in FluorSave (Calbiochem) and ready for visualization.

Table 2.9.: Primary antibodies used for immunostaining

Antigen	Host	Type	Manufacturer	Catalogue number	Dilution
ChAT	goat	polyclonal	Millipore	AB143	1:100
Hb9/MNR2	mouse	monoclonal	DSHB	81.5C10	1:50
Islet-1	mouse	monoclonal	DSHB	40.3A4	1:100
TARDBP	rabbit	polyclonal	ProteinTech	10782-2-AP	1:500
Tuj1 (β-III tubulin)	rabbit	monoclonal	Covance	MRB-435P	1:1000

2.12. Analysis of mRNA expression

2.12.1. RNA extraction

RNA was extracted from cultures cells using the RNeasy Mini kit (Qiagen), according to the manufacturer's instructions. Briefly, the cells were washed with PBS and harvested in 1 mL of PBS. The cells were centrifuged at 2000 x *g* for 5 minutes and the pellet was resuspended in 350 µL of Buffer RLT. The cells were homogenized by thorough vortexing. An equal amount of 70% ethanol was added to the lysate. The sample was then transferred to an RNeasy spin column placed in a 2 mL collection tube and the sample was centrifuged for 15 s at 8000 x *g*. The flow-through was discarded. 700 µL of Buffer RW1 was then added to the RNeasy spin column and the samples were centrifuged for 15 s at 8000 x *g* to wash the spin column membrane and the flow-through was discarded. 500 µL of Buffer RPE were added to the RNeasy spin column and centrifuged for 15 s at 8000 x *g* to wash the spin column membrane. The flow-through was discarded. The last step was repeated once again with a 2 minute centrifugation for the final wash of the membrane and the flow-through was discarded. The column was placed in a new 1.5 mL collection tube and 30 µL of diethylpyrocarbonate (DEPC)-treated water were added directly to the column (Life Technologies). The sample was centrifuged for 1 minute at full speed and RNA was eluted. The RNA was stored at -80^{O}C until further use.

2.12.2. cDNA preparation

Complementary deoxyribonucleic acid (cDNA) was prepared by reverse transcription of the RNA obtained in step 2.11.1 using a SuperScript Reverse Transcriptase kit (Life Technologies).

The following components were mixed in a microfuge tube:

Components	Per reaction
RNA	500 ng
Random primers	1 µL
dNTPs (10 mM)	1 µL
DEPC H_2O	Up to 13 µL

This mixture was heated for 5 minutes at 65^{O}C and the following components were added:

Components	Per reaction
First strand buffer (5x)	500 ng
DTT (0.1 M)	1 µL
RNase Out	1 µL
Superscript RT III	1 µL

After addition of these components, the tubes were placed in a thermocycler and the following program was run:

25^{O}C for 5 min

55^{O}C for 60 min

70^{O}C for 15 min

2.12.3. Reverse transcription PCR

PCR for the amplification of cDNA was done as previously described in section 2.3. using 1 μL of cDNA.

2.13. Cell viability assay

2.13.1. MTT assay

One of the methods used for determining cell viability was MTT assay (Sigma). This assay measures the activity of living cells by mitochondrial dehydrogenase reduction of the 3-(4,5-dimethylthiazol-2-yl)-2,5-diphenyl tetrazolium bromide (MTT) tetrazolium ring. The reduction results in the formation of insoluble purple MTT formazan crystals that can be dissolved in acidified isopropanol and measured by spectrophotometry. Cells were grown in 24-well plates and washed once with PBS. MTT was added to each well at a concentration of 0.5 mg/mL in 250 μL OM and incubated at 37^{O}C for 3 hours. After 3 hours, the purple crystals were dissolved in 250 μL of MTT solvent (0.1 N HCl in anhydrous isopropanol) and the absorbance was read at 570 nm on a Synergy HT (BioTek) spectrophotometer.

2.13.2. MTS assay

Cell viability was determined using the CellTiter Aqueous Non-Radioactive Cell Proliferation Assay, according to manufacturer's instructions (MTS assay, Promega). Briefly, HEK293 cells were plated on 24 well plates at a density of $12x10^4$ cells/well and treated with 10 μM H_2O_2, 50 μM H_2O_2 or 100 nM thapsigargin for 24 hours at 37^{o}C. Phenazine methosulfate

(provided by the manufacturer) was added to the MTS solution ([3-(4,5-dimethylthiazol-2-yl)-5-(3-carboxymethoxyphenyl)-2-(4-sulfophenyl)-2H-tetrazolium) and 100 µL of the mix were added to each well for 4 hours at 37^{o}C. The absorbance of the formazan product was measured at 490 nm using Synergy HT (BioTek) spectrophotometer.

2.14. Human iPSC differentiation to motor neurons

The reagents used for human iPSC differentiation to motor neurons were purchased from the following companies: ascorbic acid (Sigma, cat. no. A4403), B27 without vitamin A 50x (Gibco-BRL, cat.no. 12587-010), brain-derived neurotrophic factor (BDNF) (PeproTech, cat.no. 450-02), glia-derived neurotrophic factor (GDNF) (PeproTech, cat.no. 450-10), IGF1 (PeproTech, cat.no. 100-11), cyclic AMP (Sigma, cat.no. D-0260), bovine serum albumin (BSA) (Sigma, cat.no. A-7906), N2 supplement 100x (Gibco-BRL, cat.no. 17502-048), retinoic acid (RA) (Sigma, cat.no. R2625), sonic hedgehog (SHH) (R&D, cat.no. 1845-SH), Heparin (Sigma, cat.no. H3149), ROCK inhibitor (Y-27632) (Calbiochem, cat.no. 688000) Geltrex hESC qualified (Invitrogen, cat.no. A1048002).

The iPS cells were obtained as embryoid bodies (EBs) from the Oxford Stem Cell Institute and the EBs were kept in suspension for 3 days in DMEM/F12 (1:1) supplemented with N2, non-essential amino acids and 2 µg/mL heparin. Fresh media was prepared and changed every 48 hours. After 4 days in suspension, the EBs were plated on Geltrex coated wells and allowed to expand for 48 hours. The old medium was then replaced with fresh neural differentiation medium containing 0.1 µM retinoic acid (RA) and the cells were allowed to differentiate for 5 days. The differentiating cells were evaluated under the microscope for the formation of neural rosettes and neural-tube-like structures and the

colonies presenting these features were lifted and grown in suspension in the presence of 0.1 µM RA and 100 ng/mL sonic hedgehog (SHH) for ventralization, supplemented with B27 and ROCK inhibitor (10 µM). After 5 days the neurospheres larger than 300 µM were dissociated by accutase treatment or pipetting and allowed to grow for 8 days. The spheres were then plated on Geltrex coated coverslips in neural differentiation medium supplemented with BDNF, GDNF, IGF (10 ng/ml), cAMP (1 µM) and ascorbic acid (200 ng/ml) while the RA and SHH concentrations were reduced to 50 nM and 50 ng/ml respectively. After 7 days the cells were immunostained for Hb9, Islet1 and βIII-tubulin. After 14 days in neuronal differentiation medium, the cells were immunostained for Hb9, TujI and synaptophysin for the formation of synapses.

2.15. Live calcium imaging

2.15.1. Calcium-binding dye loading

HEK293 cell lines carrying wt-TDP, TDP-A382T and TDP-M337V were loaded with 10 µM Fluo 4-AM dissolved in 0.2 dimethyl sulfoxide (Sigma-Aldrich) in Dulbecco's Modified Eagle Medium High Glucose (DMEM, PAA) for 20 mins at 25^{o}C. To image Ca^{2+} signals, we used wide-field fluorescence microscopy using a Nikon TE 2000 inverted microscope equipped with a 40 x oil-immersion objective and EMCCD camera (Evolve 128, Photometrics) for imaging fluorescence emission (510-600 nm) at a frame rate of 300 s^{-1}. Fluorescence was imaged at 37^{o}C from a 12 x 12 µm (128 x 128 pixel) region within 18 mm cover slips, on which HEK293 cells were cultured.

2.15.2. ER Ca^{2+} release

For ER Ca^{2+} release, carbamoylcholine chloride (Sigma) was applied at a final concentration of 10 μM in Hank's Balanced Salts Solution (HBSS), depleted of $CaCl_2$ and $MgCl_2$ (Life Technologies), under continuous superfusion for 5 minutes at a flow rate of 511 μL/min. Increases in fluorescence were recorded on a Nikon microscope using MetaMorph software and analyzed, as described next.

2.15.3. ER Ca^{2+} content

For HEK293 cells, ER Ca^{2+} contents were assessed by fluorescence measurements upon application of 1 μM thapsigargin (Life Technologies) in HBSS depleted of $CaCl_2$ and $MgCl_2$. For iPSC-derived motor neurons, ER Ca^{2+} contents were assessed by application of 10 μM thapsigargin. Fluorescence measurements are expressed as a ratio ($\Delta F/F_o$) of the mean change in fluorescence (ΔF) at a pixel relative to the resting fluorescence at that pixel before stimulation (F_o). Image analysis was performed using MetaMorph and ImageJ software.

2.15.4. Kainate and KCl stimulation

The motor neurons derived from iPSCs were loaded with 1 μM Fluo 4-AM dissolved in 0.2% DMSO in DMEM High Glucose, supplemented with 0.04% Pluronic acid for 30 mins at 25^{o}C. Spontaneous Ca^{2+} transients were detected and recorded for 5-10 minutes. Stimulation of voltage-gated Ca^{2+} channels was done by application of 100 μM kainate or 50 mM KCl in $CaCl_2$ depleted HBSS medium under continuous superfusion at 37^{O}C.

2.16. Data analysis

All quantitative data was analysed using GraphPad Prism. Student's *t* tests were performed on samples and groups of 3 or more samples were subject to One-Way ANOVA analysis, with Holm-Sidak *post hoc* comparisons. Alpha was set at 0.05 for all ANOVAs and *post hoc* tests.

CHAPTER 3

Molecular cloning of *TARDBP* and disease-associated M337V, A382T and Y374 mutations

In the first part of this project, I developed an improved expression model of TDP-43 to study the effects of ALS-specific mutations in a physiologically relevant human cell model using bacterial artificial chromosome (BAC) constructs. The BAC carrying the entire genomic locus of *TARDBP* with upstream and downstream regulatory sequences was subcloned to a P1-derived artificial chromosome (PAC), a Ypet tag was engineered upstream of the stop codon and one of three disease-associated mutations (A382T, M337V and Y374X) were inserted in exon 6 by site-directed mutagenesis (Figure 3.1). The integrity of the constructs was verified by sequencing, restriction digests and PCR amplification, and expression was confirmed by transient transfections in several cell models, such as HEK293, BE(2)-M17 (neuronal model) and NSC34 (motor neuron model). In order to generate site-specific PAC stable cell lines, the vectors were retrofitted with a plasmid carrying a Flp recombinase target (FRT) site which allowed transfection in HEK293 cells and generation of stable clones expressing TDP-Ypet, TDP-M337V, TDP-A382T and TDP-Y374X that were used for functional analyses in the following chapters.

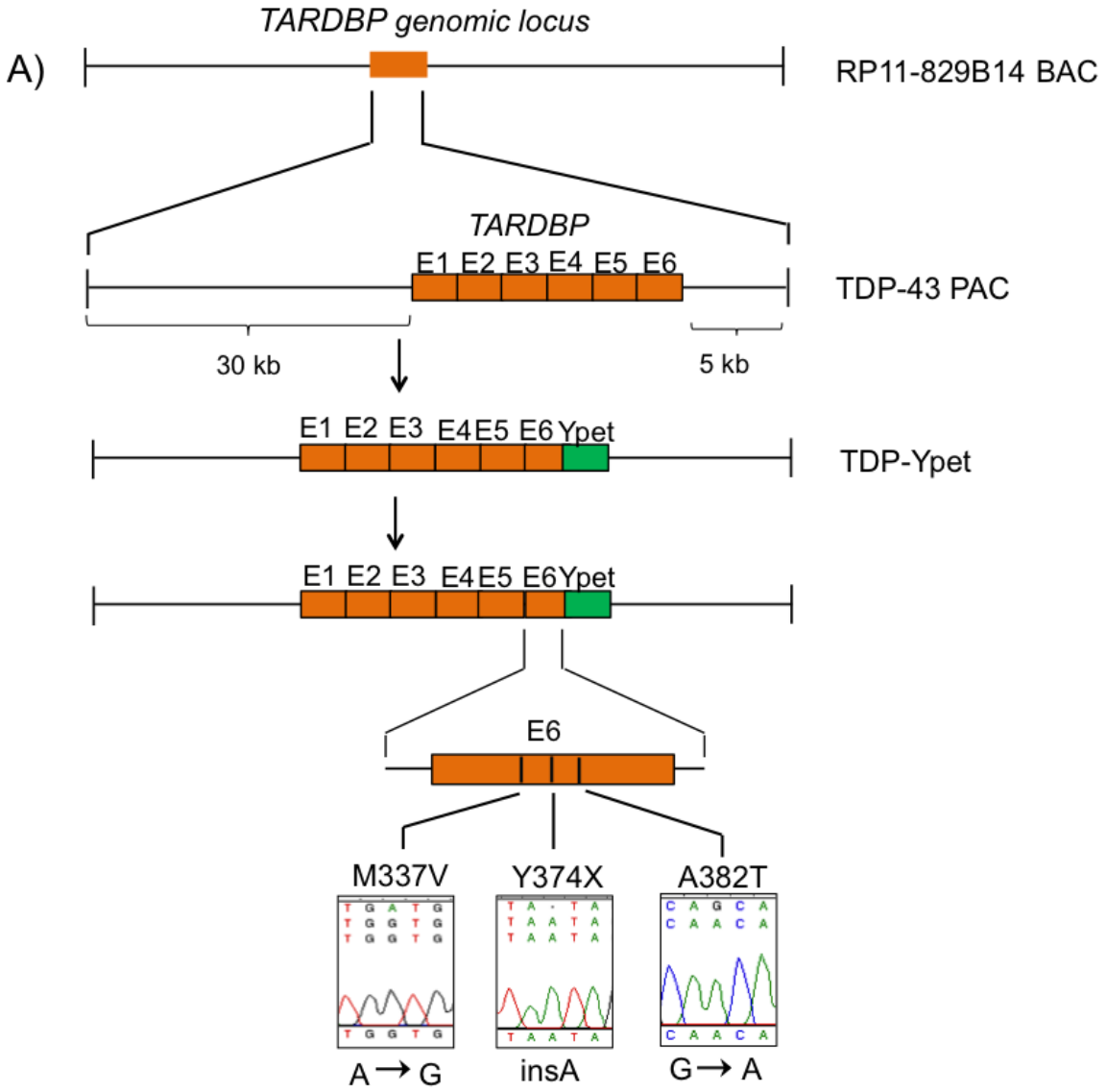
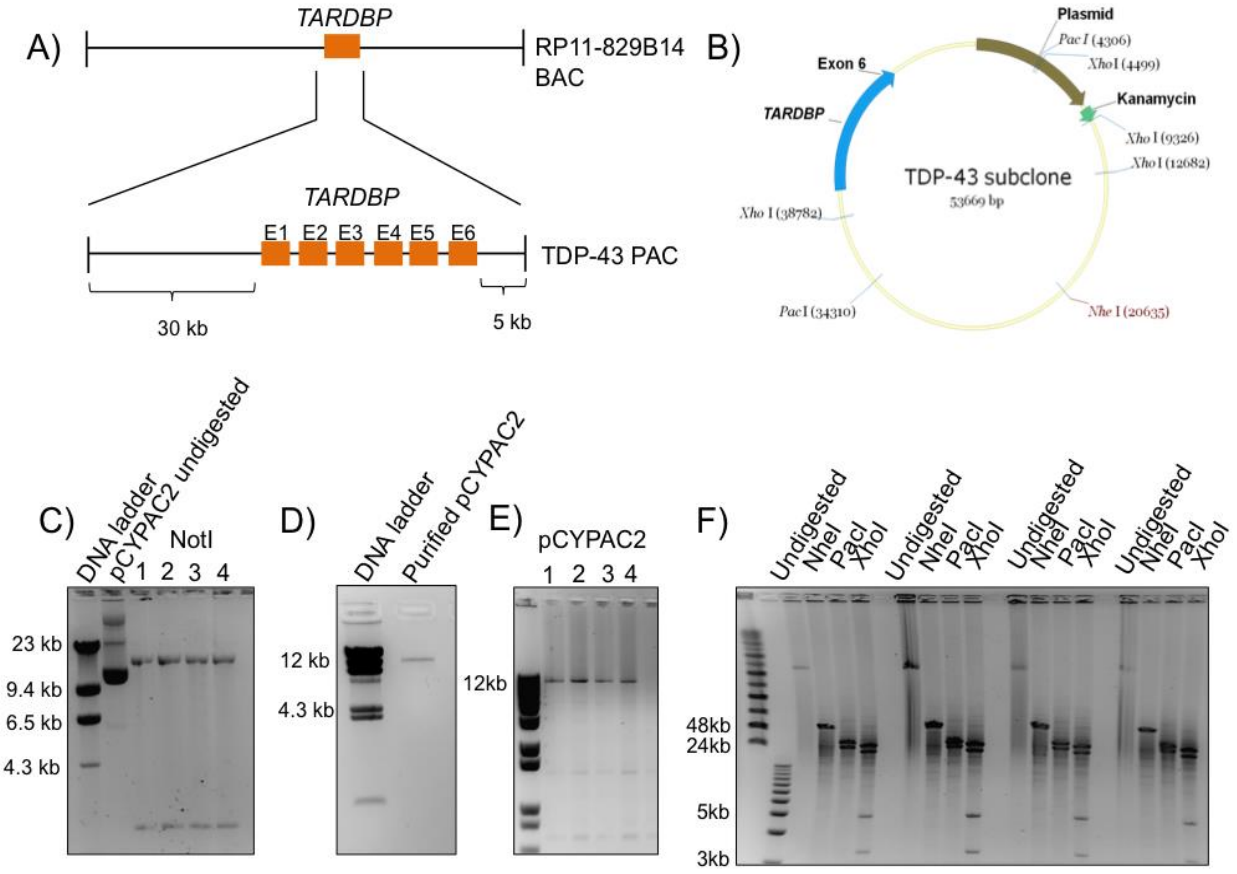


Figure 3.1: Overview of the cloning strategy used to generate full-length human genomic DNA TDP-43 vectors. The RP11-829B14 BAC was subcloned to a PAC with 30 kb upstream and 5 kb downstream sequences. A 714 bp Ypet sequence was cloned immediately before the stop codon of exon 6 and three disease-related mutations were engineered in exon 6, M337V, Y374X and A382T, each in a separate vector.

3.1. Subcloning the *TARDBP* genomic locus

We obtained the pBACe3.6 plasmid RP11-829B14 containing the human *TARDBP* full-length genomic locus of 47.5 kilobasepairs (kb) from the BACPAC Resources Centre at Children's Hospital Oakland Research Institute, Oakland, CA. In order to exclude from our construct other genes present on the genomic locus carried by the BAC, the *TARDBP* genomic locus containing 12 kb exonic and intronic sequences was subcloned into a purified pCYPAC2 plasmid with 30 kb upstream and 5 kb downstream regions of the gene, as illustrated in Figure 3.2.A.

Subcloning was performed using homologous recombination in *E.coli* and the Red/ET system. The Red/ET system is a technique for genomic DNA manipulation that is precise and independent of the size of the DNA to be altered as well as independent of the presence of restriction sites, overcoming the problems previously encountered by traditional DNA engineering techniques. Recombination by Red/ET is based on homology regions, which are regions of DNA sequences shared by the two molecules that recombine. Since the sequences can be chosen freely, any position on a target can be modified allowing precise and specific exchange of genetic material between two DNA molecules (Zhang et al, 2000).



First, the pCYPAC2 plasmid was linearised using *NotI* restriction digest (Figure 3.2.C). The linearised pCYPAC2 product was purified to ensure elimination of undigested circular template DNA (Figure 3.2.D). Before transformation in bacteria carrying the TDP-43 BAC, the purified and linearised pCYPAC2 was amplified by PCR with primers containing homology arms flanking the upstream and downstream regions of interest in the genomic locus of *TARDBP* (Figure 3.2.E). Long homology arms of 110 bp were used in order to increase efficiency of the recombination process.

Figure 3.2: **Subcloning the *TARDBP* genomic locus from a BAC to pCYPAC2.** A) The strategy used for subcloning TDP-43 from the RP11-829B14 BAC (202.4 kb) to a P1-derived artificial chromosome (PAC) with 30 kb upstream and 5 kb downstream of the gene and B) the vector map of the subcloned product with the restriction sites used for confirmation of correct subcloning. C) The pCYPAC2 was linearized by a *NotI* digest and D) the product purified following gel extraction. E) The purified pCYPAC2 plasmid was amplified with 4 primers for the addition of ~110 bp homology to the region of interest for subcloning. F) The homologous recombination was achieved by a helper plasmid carrying a recombinase (Red/ET) and the correct colonies were confirmed by restriction digests. Expected sizes: *NheI* - 53 kb; *PacI* – 30 kb and 23 kb; *Xho*I – 26 kb, 19 kb, 5 kb and 3.3 kb.

In parallel, the electrocompetent bacterial cells carrying the *TARDBP* BAC were electroporated with 1 ng of pSC101-BAD-gbaA plasmid expressing the Red/ET recombinase enzyme. After checking the presence of both *TARDBP* BAC and pSC101-BAD-gbaA plasmid, the cells were made electrocompetent and electroporated with the amplified pCYPAC2 and homologous recombination was allowed to take place. Cells that correctly incorporated the selected *TARDBP* genomic locus on pCYPAC2 backbone would be resistant to kanamycin, as opposed to the chloramphenicol resistance on the BAC backbone. Kanamycin was therefore used as a selection antibiotic and the colonies growing on kanamycin were screened first by colony PCR for successful recombination events and by restriction digests with *NheI*, *PacI* and *XhoI*. The correct products were re-electroporated to ensure elimination of contamination by co-existing plasmids (Figure 3.2.F). The final subclone pCYPAC2 plasmid carrying the *TARDBP* genomic locus was therefore reduced to 55 kb, which exclusively contained 12.5 kb *TARDBP* intronic and exonic sequences, 30 kb upstream promoter region of *TARDBP* and 5 kb downstream sequence, in addition to the pCYPAC2 backbone (Figure 3.2.B)

3.2. Engineering a Ypet fluorescent tag into TDP-43 vectors by homologous recombination

In order to deliver the PACs carrying full-length human genomic loci of *TARDBP* in a human cell line, it was necessary to insert a tag that could be used to distinguish between

endogenous TDP-43 expression and PAC driven expression of TDP-43. Moreover, since subcellular localization of TDP-43 is a key indicator to its pathogenic behaviour, a fluorescent label was necessary to allow detection of TDP-43 in live cells.

The green fluorescent protein (GFP) is a commonly used reporter of expression that exhibits bright green fluorescence when exposed to blue light. Ypet is a 714 bp variant of the green fluorescent protein and it was engineered upstream to the stop codon of *TARDBP*. The C-terminus of TDP-43 was the choice of location for the fluorescent tag because we aimed to ensure detection of the C-terminal region of TDP-43 as this region is known to be prone to aggregation and commonly identified in pathological inclusions in motor neurons from spinal cord of ALS patients.

A Ypet tag was inserted by two rounds of homologous recombination using the Red/ET recombination system, as previously described in section 3.1. The recombination involved a two-step process based on the dual resistance/sensitivity cassette pRpsl-Chl (Figure 3.3).

The first round of homologous recombination involved the amplification of pRpsl-Chl plasmid with homology sequences of 80 bp to allow specific targeting of the site of interest in the immediate downstream region of *TARDBP* exon 6 (Figure 3.4.A). In order to increase recombination efficiency for the next step, four long primers were used for amplification and they were designed to also carry 15-20 bp homology to Ypet in addition to homology arms flanking exon 6 and downstream region of *TARDBP*. The plasmid carrying pRpsl-Chl was amplified by PCR and purified before electroporation into electrocompetent cells carrying the TDP-43 PAC (Figure 3.4.B). Correct colonies containing both the pRpsl-Chl cassette (which confers resistance to chloramphenicol) and the PAC construct (which confers resistance to kanamycin) were initially screened by restriction digests and junction PCR (Figure 3.4.C-D).

The DNA from the correct colonies was then re-electroporated into empty cells to eliminate contamination from co-existing plasmids (Figure 3.4.E).

In the second round of homologous recombination, the pRpsl-Chl cassette was replaced with the Ypet tag (Figure 3.5.A). In the first instance, the plasmid carrying Ypet sequence was amplified by PCR with 4 primers designed to add homology arms flanking 110 bp of exon 6 and 110 bp downstream region of *TARDBP*, in order to improve efficiency of recombination events in the second round (Figure 3.5.B). The 934 bp PCR product containing the Ypet sequence and 220 bp homology to *TARDBP* was purified and electroporated into electrocompetent cells carrying the *TARDBP* PAC with pRpsl-Chl cassette and homologous recombination was allowed to occur in the presence of Red/ET plasmid. Selection of colonies was performed on kanamycin and streptomycin, based on counterselection of pRpsl-Chl. The successful recombination events were screened by junction PCR flanking the Ypet sequence inserted at the end of exon 6 of *TARDBP*, exon PCR and restriction digests (Figure 3.5.C-E). The correct insertion of Ypet sequence before the stop codon of *TARDBP* and loss of pRpsl-Chl was therefore confirmed (Figure 3.5.F).

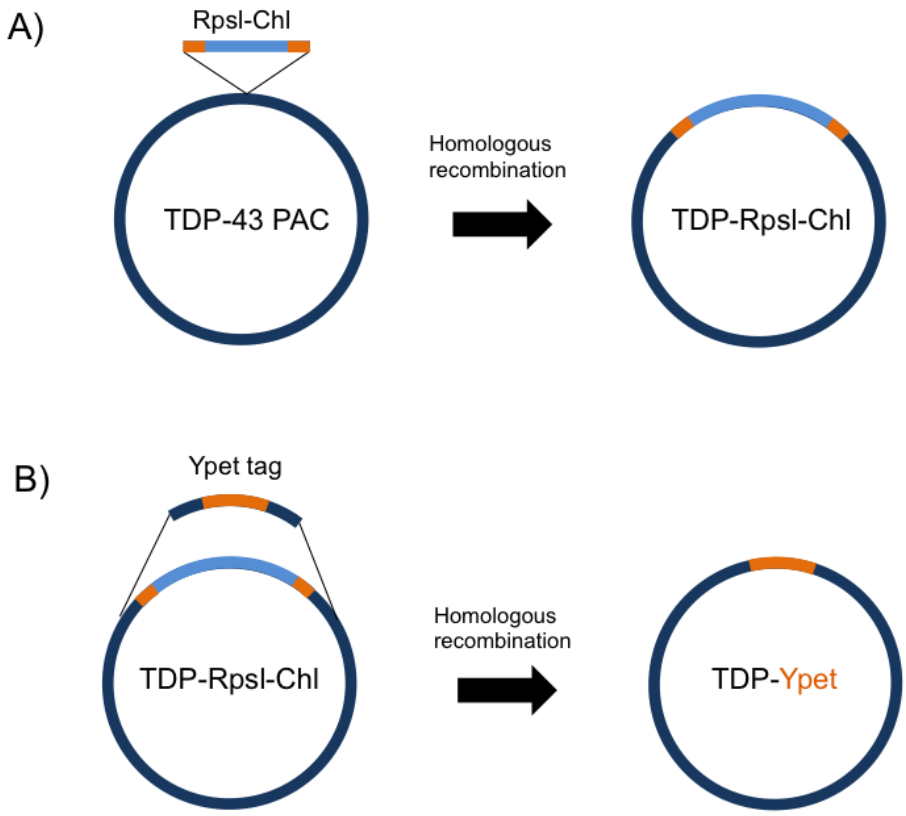


Figure 3.3: **Overview of the pRpsl-Chl homologous recombination strategy used for insertion of Ypet using the Red/ET recombination system**. A) First round of homologous recombination in *E.coli* involves cloning the pRpsl-Chl at the site of interest in the TDP-43 PAC after PCR amplification with primers containing homology arms to the immediate upstream and downstream sequences of the region of interest. Homologous recombination takes place in the presence of recombinases from the Red/ET system. B) Second round of homologous recombination involves the amplification of Ypet by PCR with primers containing homology arms to the upstream and downstream sequences of the region of interest in TDP-pRpsl-Chl. Homologous recombination takes place in the presence of Red/ET system.

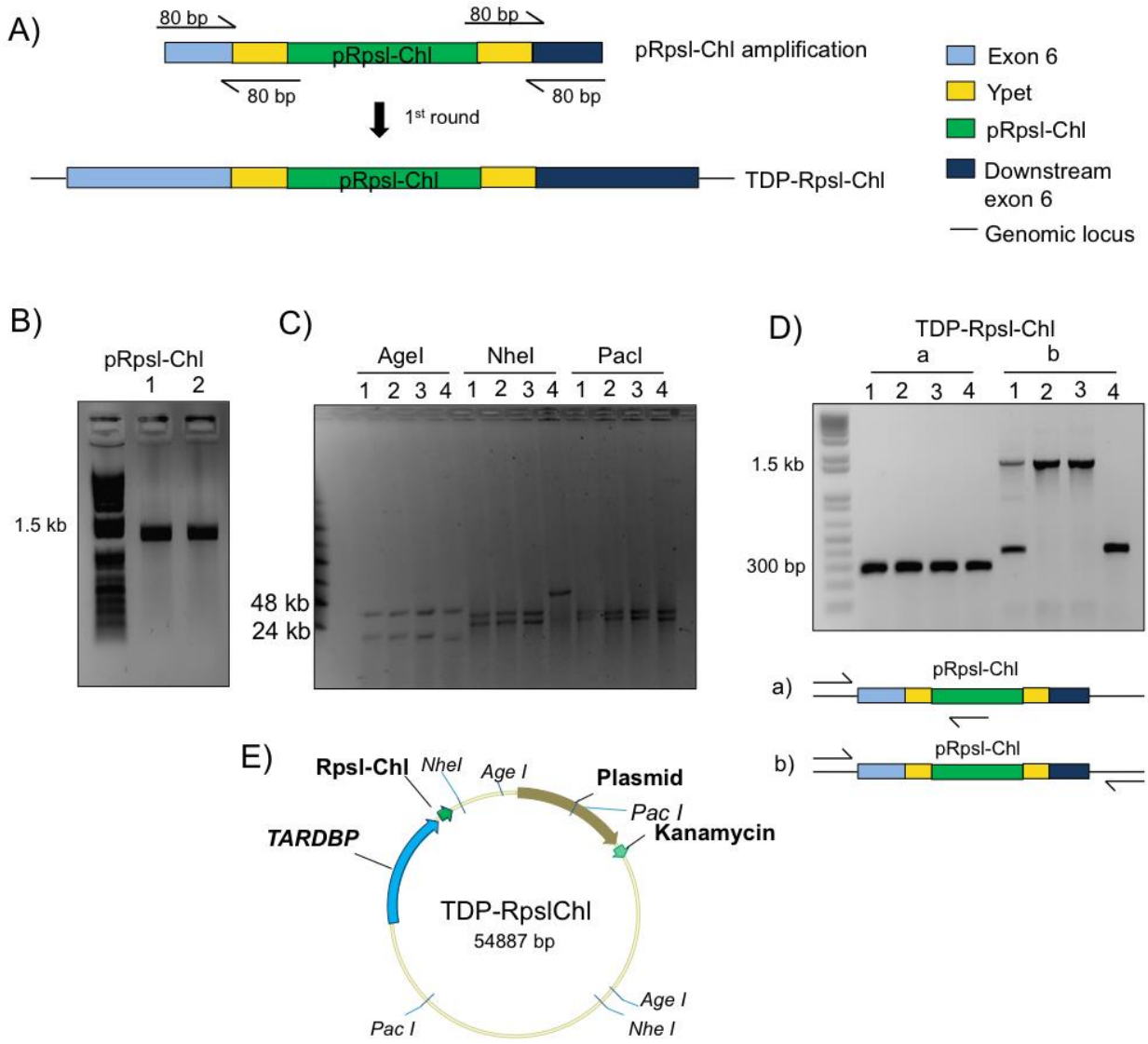


Figure 3.4: First round of homologous recombination for the insertion of Ypet before the stop codon of *TARDBP*. A) Schematic illustration of the first round of the recombination process. Four 80 bp primers are used to amplify the pRpsl-Chl with exon 6 homology regions and an additional 20 bp of Ypet sequence (yellow). B) The PCR product following the amplification and purification of pRpsl-Chl. C) Confirmation of pRpsl-Chl correct integration in the TDP-43 vector by restriction digests (*NheI* : 30 kb + 25 kb; *PacI* : 30 kb + 25 kb, *AgeI*: 37 kb + 17 kb + 1.7 kb). Colony 4 shows an unsuccessful recombination event (*NheI*: 52 kb). D) PCR amplifications of the upstream junction pRpsl-Chl – TDP-43 and the entire pRpsl-Chl cassette inserted in the vector (junction: 290 bp; cassette: 1.5 kb). E) Schematic illustration of the product of the first round of homologous recombination, TDP-pRpsl-Chl vector.

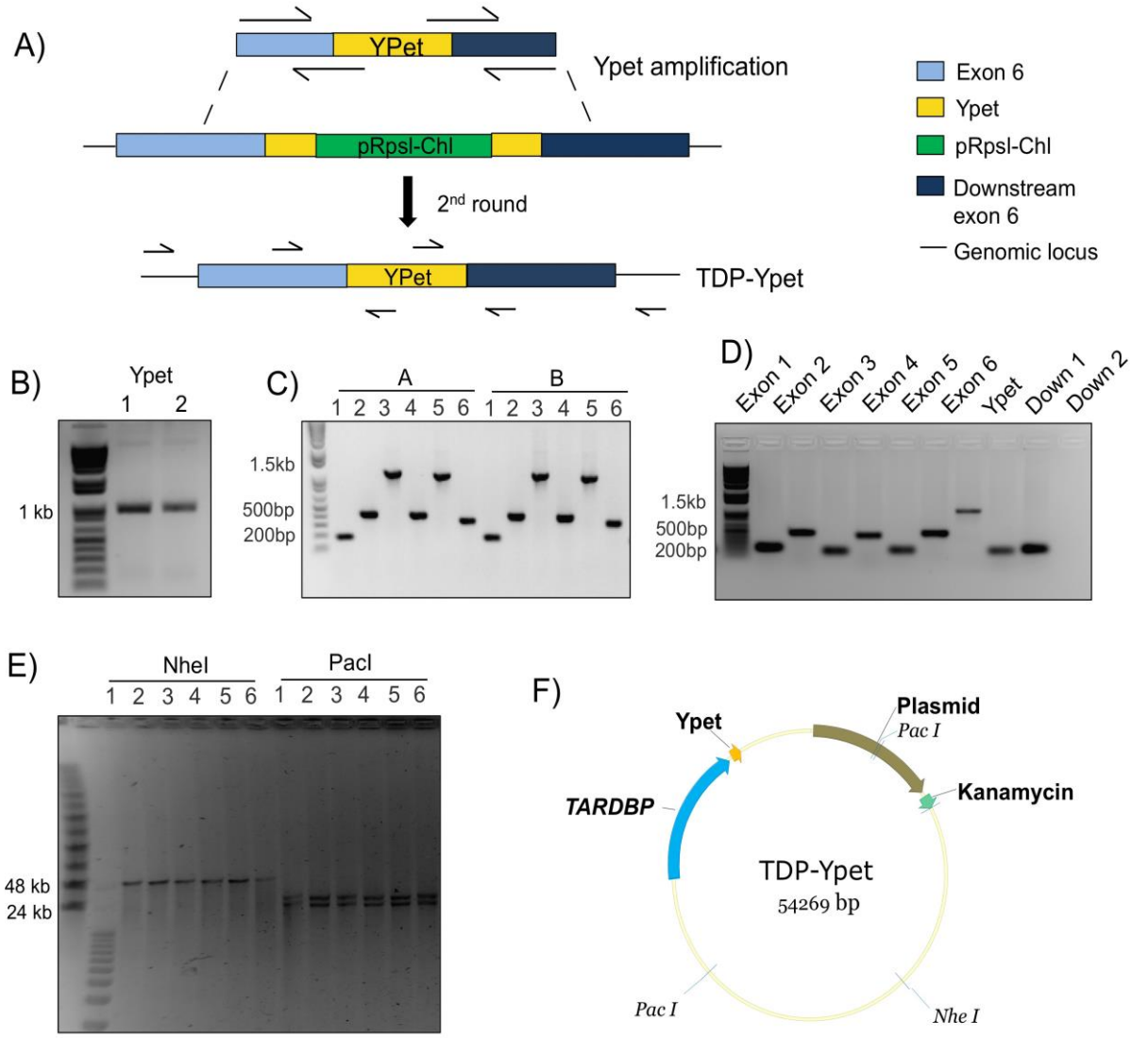


Figure 3.5: Second round of homologous recombination for the insertion of Ypet before the stop codon of *TARDBP*. A) Schematic representation of the second round of homologous recombination where the Ypet sequence is amplified with four primers and electroporated into the cells containing TDP-Rpsl-Chl for homologous recombination to take place (legend on the right) B) Amplification of Ypet with four primers. C) PCR amplification of the junctions of Ypet in TDP-43 vector from 2 different positive colonies, labelled A and B (1 - short upstream junction 190 bp; 2 - long downstream junction 421 bp; 3 - entire Ypet 1199 bp; 4 - long upstream junction 405 bp; 5 - entire Ypet 1129 bp; 6 - short downstream junction 355 bp). D) PCR amplification of each exon of TDP-43, the Ypet reporter gene region and 2 kb downstream. E) *NheI* and *PacI* restriction digests confirming the correct exchange between pRpslChl and Ypet in the vectors (*NheI*: 52 kb; *PacI*: 30 kb and 22 kb) F) Vector map of TDP-Ypet illustrating the restriction sites.

3.3. Site-directed mutagenesis of A382T, M337V and Y374X in TDP-Ypet vectors

The identification of *TARDBP* gene mutations in both familial and sporadic cases of ALS has recently placed TDP-43 at the center of ALS pathogenesis (Pesiridis et al, 2009). Up to date, over 40 missense mutations have been identified in *TARDBP* and one frameshift mutation, all but one (D169G) residing in the C-terminal glycine rich domain encoded by exon 6 of *TARDBP* (Daoud et al, 2009; Pesiridis et al, 2009). From the list of mutations associated with ALS, I have chosen to engineer three mutations that present different levels of pathogenicity and potentially different mechanisms of action.

The first mutation (A382T) is the most common missense mutation identified in *TARDBP*, frequently encountered in both sporadic and familial forms of ALS (Pesiridis et al, 2009). The second missense mutation chosen is M337V, which is the most pathogenic mutation identified so far and resides in a strongly phylogenetically conserved region of TDP-43 (Sreedharan et al, 2008). The third mutation Y374X is a frame-shift mutation resulting in the creation of a premature stop codon and consequently, in the truncation of TDP-43 (Daoud et al, 2009).

The strategy used for the generation of the mutations in exon 6 of *TARDBP* is outlined in Figure 3.6. Briefly, the pRpsl-Chl cassette was used as previously described to determine the location of each mutation within exon 6 of the *TARDBP* PAC. In parallel, the three mutations were each engineered in separate plasmids carrying the cDNA of *TARDBP* using site-directed mutagenesis and PCR amplified after confirmation by sequencing (Figure 3.6.B). Finally, the pRpsl-Chl on *TARDBP* PAC was exchanged by homologous recombination with exon 6 from the cDNA construct carrying the correct mutation.

The first round of homologous recombination for the insertion of ALS-specific mutations consisted of PCR amplification of pRpsl-Chl with homology arms flanking the upstream and downstream region of exon 6 for each mutation (Figure 3.7.A). Using the Red/ET system as previously described, the cells carrying TDP-Ypet were made electrocompetent and electroporated with the amplified pRpsl-Chl. Successful homologous recombination events were screened by restriction digests by *NheI* (which generated 2 fragments in the presence of the correct integration of pRpsl-Chl into TDP-Ypet) and junction PCR (Figure 3.7.B-D). Colonies showing correct integration of pRpsl-Chl cassette into exon 6 of TDP-Ypet were used for the second round of homologous recombination.

In the second round of homologous recombination, exon 6 carrying A382T, M337V or Y374X was exchanged with the pRpsl-Chl in TDP-Ypet PAC. Mutations were inserted in exon 6 by site-directed mutagenesis and, in the absence of the specific generation of a restriction site when mutations were inserted, the entire exon 6 was sequenced to ensure correct exchange of bases and absence of other mutations in exon 6. The A382T mutation consisted of a base pair change from G → A, the M337V mutation consisted of a base pair change from A → G while the Y374X was an insertion of A (Figure 3.1.A). Each mutation was inserted independently in a different vector. The entire exon 6 containing each mutation was amplified and recombined with exon 6 of the TDP-Ypet PAC and the resulting vectors were confirmed by restriction digests and sequencing (Figure 3.8.B,C).

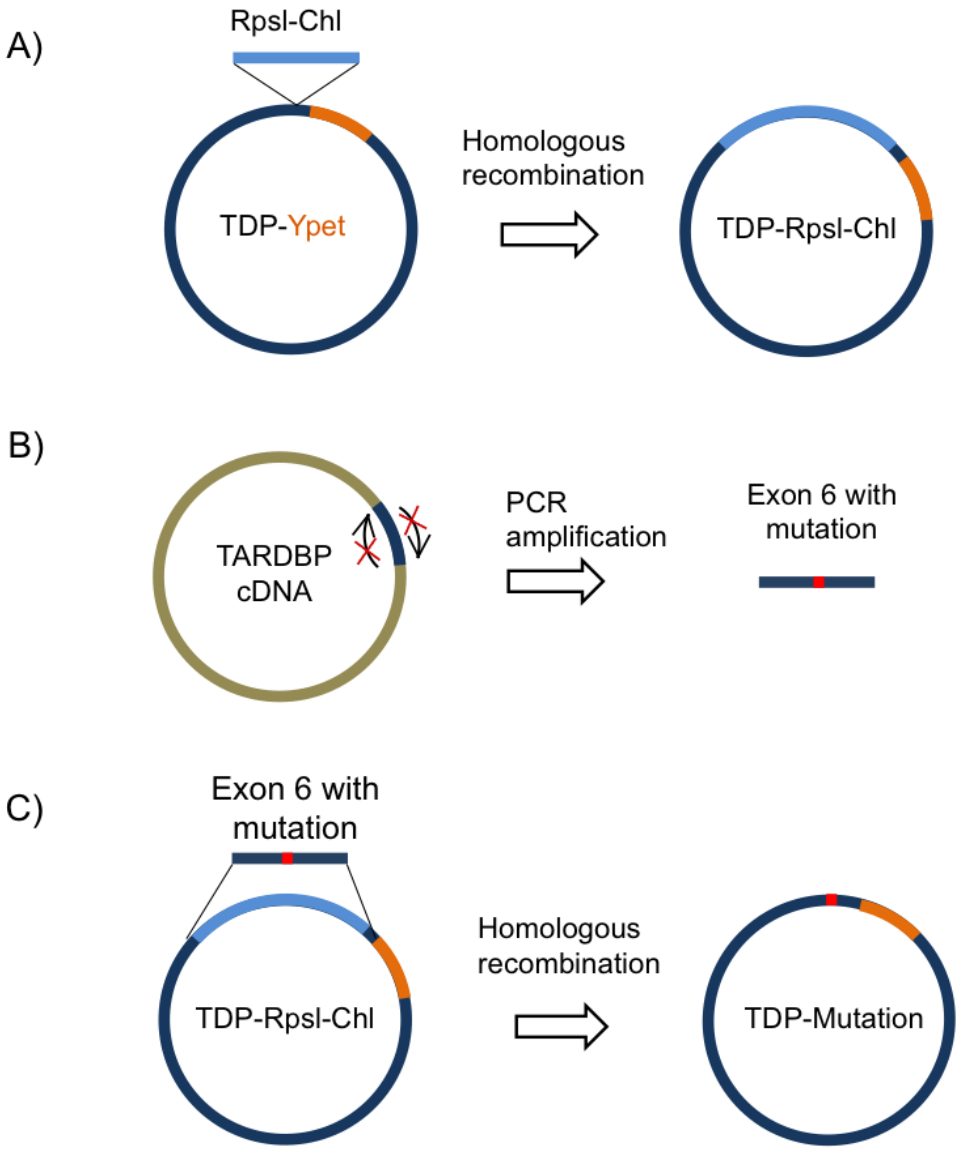


Figure 3.6: **Mutagenesis strategy used to engineer A382T, M337V and Y374X mutations in full-length genomic *TARDBP* vectors using site-directed mutagenesis.** A) The first round of homologous recombination consisting of the insertion of pRpsl-Chl in the site of the mutation in exon 6. B) The site-directed mutagenesis performed on a cDNA plasmid of *TARDBP* by amplification with 2 primers that contain the mutation (red cross). C) Exon 6 carrying the mutations is recombined with the TDP-Y-Rpsl-Chl where pRpsl-Chl is exchanged with the mutation.

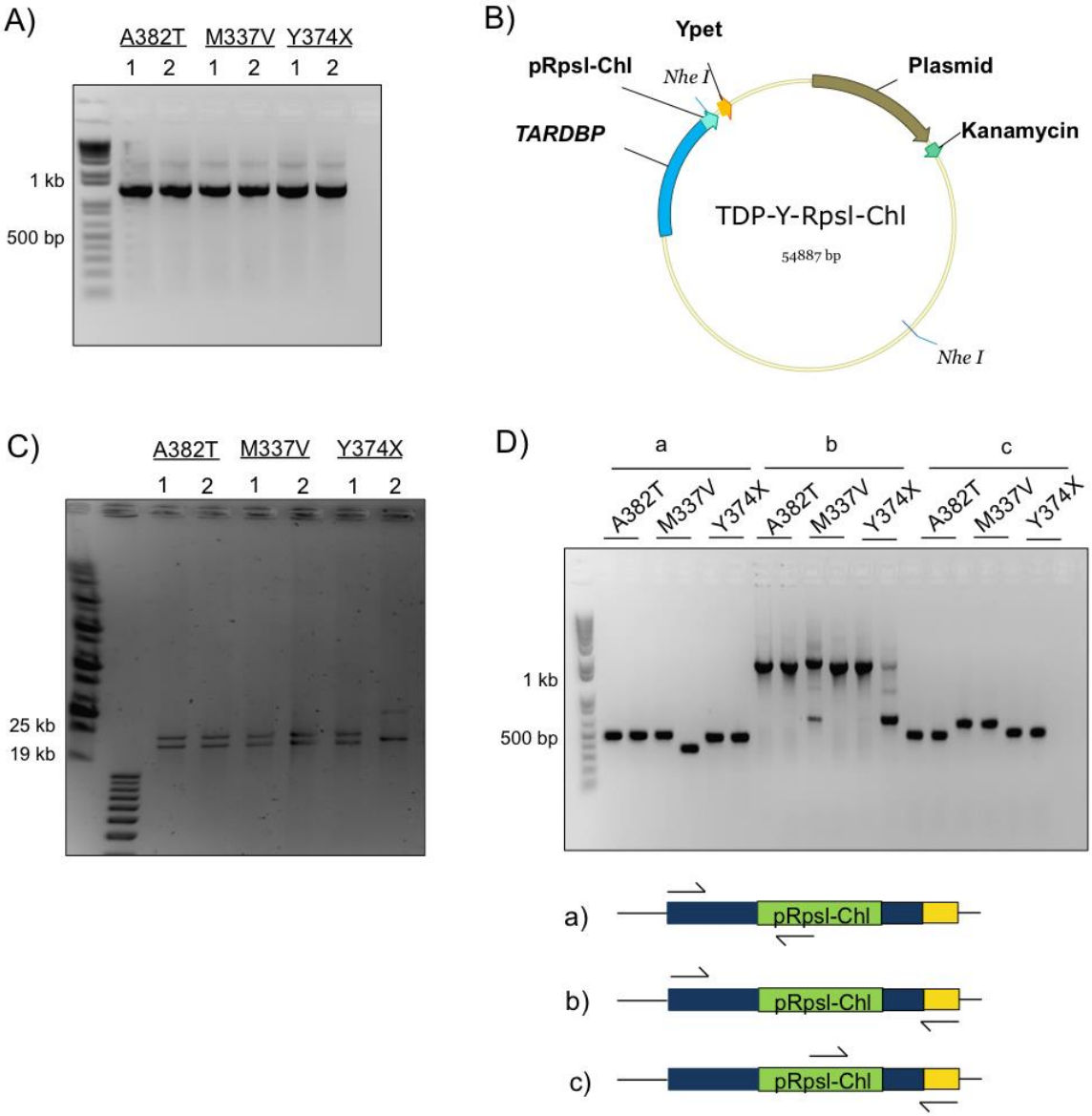

A)
A382T M337V Y374X
1 2 1 2 1 2
1 kb
500 bp
B)
Ypet
pRpsl-Chl
Nhe I
Plasmid
TARDBP
Kanamycin
TDP-Y-Rpsl-Chl
54887 bp
Nhe I
C)
A382T M337V Y374X
1 2 1 2 1 2
25 kb
19 kb
D)
a
b
c
A382T M337V Y374X A382T M337V Y374X A382T M337V Y374X
1 kb
500 bp
a)
pRpsl-Chl
b)
pRpsl-Chl
c)
pRpsl-Chl

Figure 3.7: First round of homologous recombination for the insertion of pRpsl-Chl at each point mutation in exon 6 of *TARDBP* vectors. A) Amplification of Rpsl-Chl with homologous sequences to the adjacent regions of each mutation in *TARDBP* exon 6. B) Vector map of the first round of homologous recombination product and C) confirmation of the correct integration of pRpsl-Chl in the vectors by restriction digests with *NheI* (expected bands: 30 kb and 25 kb) and D) by PCR amplification of the upstream junction (a), entire pRpsl-Chl cassette (b) and downstream junction (c).

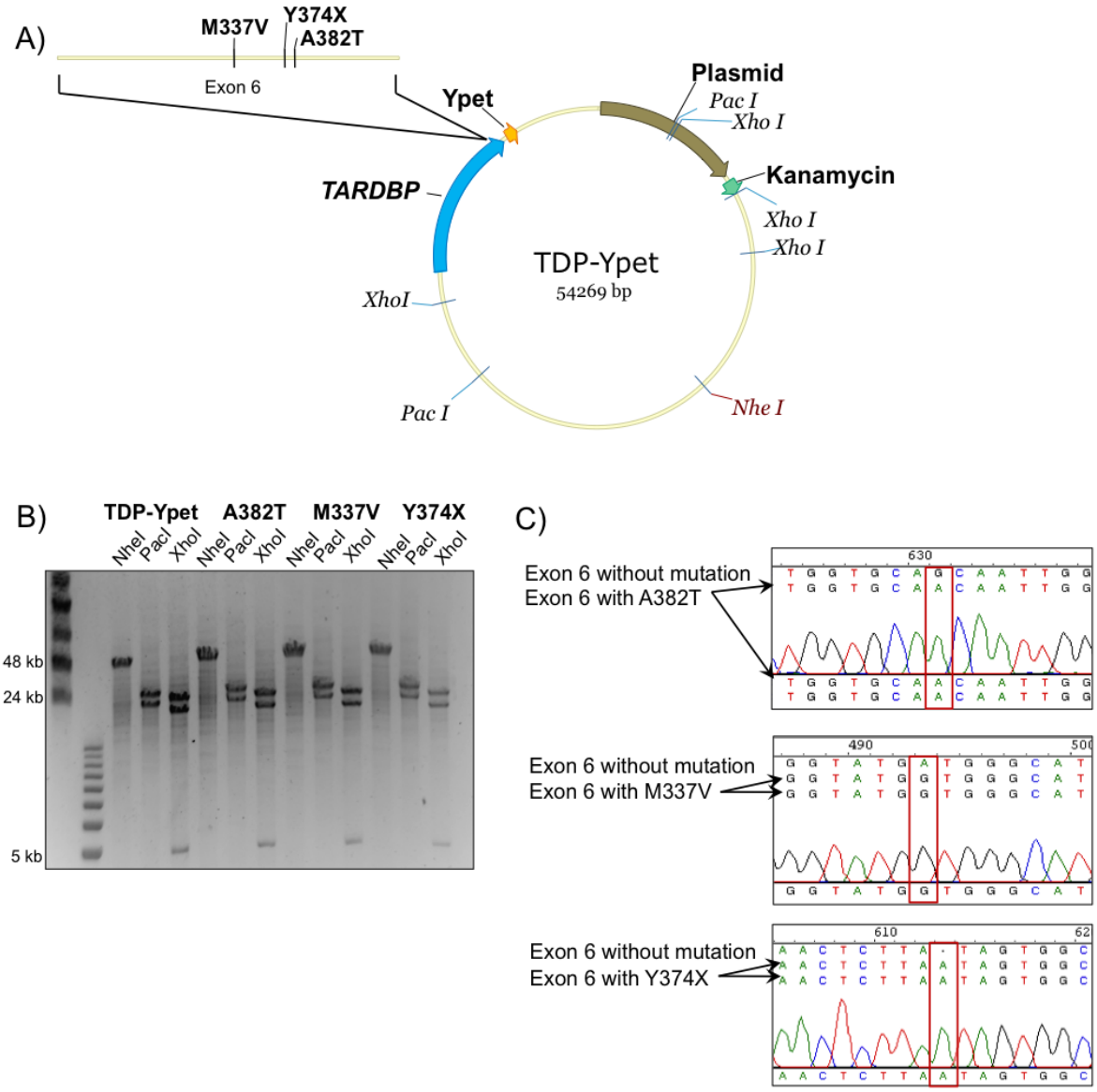


Figure 3.8: Second round of homologus recombination and confirmation of correct site-directed mutagenesis for A382T, M337V and Y374X into TDP-Ypet vectors. A) Vector map of the TDP-Ypet vector with the location of each mutation and restriction sites which were used to confirm the integrity of the vectors (B). C) Sequencing results of the vectors confirming the correct insertion of the mutations A382T (exchange bases G->A), M337V (exchange bases A->G) and Y374X (insertion of A). The first row represents a region of exon 6 sequence without the mutation and the next two rows represent exon 6 with each respective mutation, highlighted in the sequence by the red boxes.

3.4. Expression analysis

The TDP-Ypet, TDP-A382T, TDP-M337V and TDP-Y374X vectors were validated by transient transfections in three different cell lines and expression was assessed by fluorescence and western blotting. Transient transfections in immortalized human cell lines, HEK293 and neuronal BE(2)-M17, showed successful fluorescence expression of exogenous TDP-43 from the vectors 3 days following transfection (Figure 3.9.A,B). As expected, no fluorescence was detected in cells transfected with TDP-Y374X, which is a truncated form of TDP-43 and therefore does not express the C-terminus of TDP-43 where the fluorescent tag Ypet has been engineered. Immunoblotting analysis confirmed successful expression of exogenous TDP-43 from TDP-Ypet, TDP-A382T, TDP-M337V and TDP-Y374X transfected HEK293 and BE(2)-M17 cell lines as well as in a mouse immortalized motor neuronal cell line, NSC34 (Figure 3.10.A-C). Various transfection efficiencies were achieved in HEK293, BE(2)-M17 and NSC34 cell lines, with 15%, 8% and 5% transfection efficiency, respectively.

Due to the low transfection efficiency of delivering full-length genomic PAC constructs to human cells, for functional investigation of the mutations we proceeded by generating site-specific PAC stable HEK293 cell lines carrying TDP-Ypet, TDP-A382T, TDP-M337V and TDP-Y374X. Clonal cell lines have several advantages providing stable expression of the vectors by genome integration of the exogenous construct in a specific site, eliminating confounding functional effects derived from overexpression of a specific gene. Furthermore, it allows improved comparison of functional effects between different genotypes, which could otherwise be attributed to differential protein expression levels.

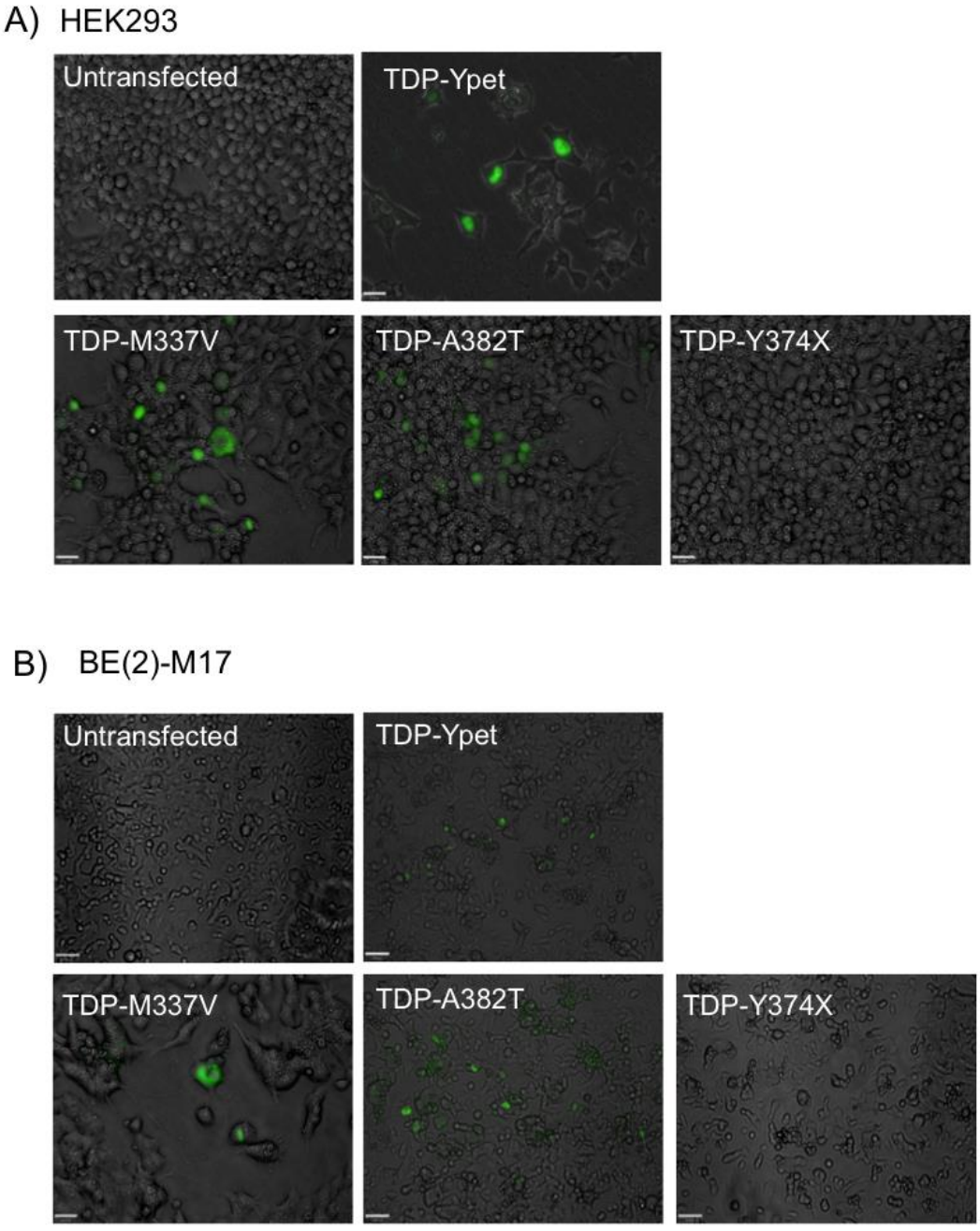


Figure 3.9: Expression analysis by fluorescence in HEK293 cells and BE(2)-M17 cell lines after transient transfection of TDP-Ypet, TDP-M337V, TDP-A382T and TDP-Y374X vectors. Vectors expression in A) HEK293 and B) BE(2)-M17 cell lines. Fluorescence was detected 3 days after transfection and confirmed physiological expression of TDP-Ypet in the nucleus. TDP-A382T and TDP-M337V vectors localized in both nucleus and cytoplasm while the TDP-Y374X showed no specific fluorescence. Transfection efficiency was higher in HEK293 cells (~15%) than in BE(2)-M17 (~10%). HEK293 cells exhibited better survival and maintenance of normal cellular morphology. Scale bar = 70 μm.

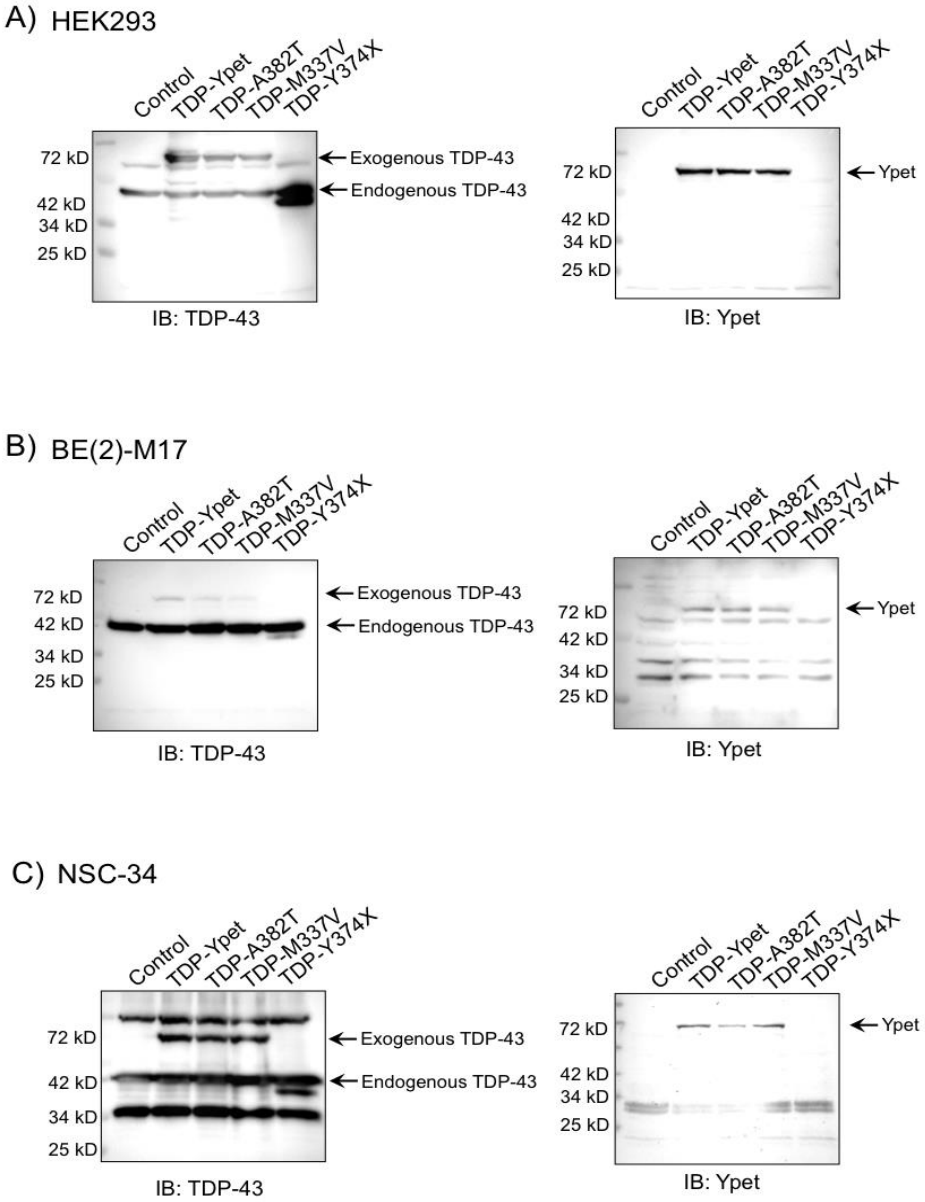


Figure 3.10: Expression analysis by immunoblotting for TDP-43 and GFP to confirm expression of the fusion TDP-43-Ypet from transiently transfected HEK293, BE(2)-M17 and NSC34 cell lines. Immunostaining of transfected A) HEK293 , B) BE(2)-M17 and C) NSC-34 cells for TDP-43 and GFP to confirm expression of TDP-Ypet, TDP-A382T, TDP-M337V and TDP-Y374X vectors in each cell line. Endogenous TDP-43 was detected in all cell lines (~42 kDa) and the fusion proteins were also successfully expressed (~72 kDa). GFP staining confirms the presence of Ypet tagged TDP-43 expressed by TDP-Ypet, TDP-A382T and TDP-M337V vectors, while no GFP staining is detected in the TDP-Y374X transfected cells, which express the truncated TDP-Y374X protein at ~40 kDa.

3.5. Generation of site-specific PAC stable HEK293 cell lines carrying TDP-Ypet, TDP-A382T, TDP-M337V and TDP-Y374X

In order to generate clonal HEK293 cell lines with TDP-43 vectors, we used a version of the Flp-In system, which has the advantage of allowing integration and expression of the vectors at a specific genomic location. The Flp-In system streamlines the generation of stable mammalian expression cell lines using a *Saccharomyces cerevisiae*-derived DNA recombination system. Briefly, this method of DNA manipulation relies on a recombinase (Flp) derived from *S.cerevisiae* and site-specific recombination into a specific Flp Recombination Target (FRT) site in the genome of the host cell line. The first step of this system involves the generation of a Flp-In host line by transfection of HEK293 cells with pFRT/lacZeo target site vector, which contains a *lacZ-Zeocin* fusion gene under the SV40 promoter and has an FRT site inserted just downstream of the ATG initiation codon of the *lacZ-Zeocin* fusion gene. HEK293 successfully incorporating a unique FRT site and *lacZ-Zeocin* fusion gene were selected for zeocin resistance. The generation of the HEK293-FRT cell line had been previously performed and described by the lab and this host cell line was used in this study (Alegre-Abarrategui et al, 2009). The second component of the Flp-In system is a pH-FRT-Hy plasmid, which is used to retrofit the vectors to embed an FRT site, a hygromycin resistance gene lacking a promoter and the ATG start codon (Figure 3.11). The final component of the Flp-In system is the pOG44 plasmid, which expresses the Flp recombinase under the control of the CMV promoter and is used for co-transfection with the retrofitted vectors in the host line.

3.5.1. Retrofitting TDP-Ypet, TDP-A382T, TDP-M337V and TDP-Y374X with pH-FRT-Hy

In order to add the FRT elements to the TDP-Ypet vectors we used Cre-*lox* recombination taking advantage of the presence of a *loxP* site on the PAC backbone. The Cre-*lox* mechanism is a recombination strategy developed as a technology for genome manipulation and successfully used in mammalian cells, yeasts, plants, mice and other organisms. The recombination requires only two elements: (1) the Cre recombinase – an enzyme which catalyzes the recombination between two *loxP* sites; (2) *loxP* sites: specific 34 bp sequences with a core sequence of 8bp where recombination occurs (Sternberg & Hamilton, 1981).

The plasmid pH-FRT-Hy, which was used for retrofitting, contains an FRT site, hygromycin resistance gene, lacZ gene and lacks a promoter and the start codon. This plasmid was recombined with the TDP-Ypet, TDP-A382T, TDP-M337V and TDP-Y374X vectors by Cre-*lox* recombination (Figure 3.12.A). The correct colonies were identified by restriction digests using *AfeI* (Figure 3.12.B). Following retrofitting, the vectors TDP-Ypet-FRT, TDP-A382T-FRT, TDP-M337V-FRT and TDP-Y374X-FRT were transfected in HEK293 cells for confirmation that fluorescent expression has been maintained (Figure 3.12.C).

3.5.2. Delivery of TDP-Ypet-FRT, TDP-A382T-FRT, TDP-M337V-FRT and TDP-Y374X-FRT PACs to HEK293 cells

HEK293 TDP-43 stable cell lines were generated using the Flp-FRT recombination technology, as previously described (Figure 3.13.A). The retrofitted TDP-43 PACs were delivered to HEK293-FRT host line by lipofection and efficiency of transfection was assessed by X-gal staining (data not shown). Selection of positive clones was performed in the presence of hygromycin and clone generation was validated using both positive and negative controls. As positive control, cells transfected with pH-FRT-Hy and pOG44 were used, and as negative control, we used cells transfected with pH-FRT-Hy or TDP-Ypet-FRT only. Following 3 weeks in culture, approximately 20 positive clones for each genotype were picked and expanded. Genomic DNA and protein were extracted for analysis of integration and protein expression. Correct integration was assessed by amplification of the junction between SV40 promoter and hygromycin cassette in several clones for each genotype, as shown in Figure 3.13.A. Results showed integration of the plasmid in all picked clones and from these, three clones for each genotype were selected for further characterization (Figure 3.13.B). The presence of concatemers was assessed by PCR to exclude clones which had several copies of the pH-FRT-HY plasmid integrated into the TDP-Ypet vectors (Figure 3.13.C).

Exogenous TDP-Ypet expression was assessed by immunofluorescence in TDP-Ypet, TDP-A382T, TDP-M337V HEK293 clonal cell lines and it was confirmed in all clones (Figure 3.14.A). As expected, immunofluorescence was not detected in HEK293 clonal cell lines carrying the truncated version of TDP-43, TDP-Y374X. Protein expression was assessed in all selected clones by immunoblotting with TDP-43 and Ypet (Figure 3.14.B,C),

and one of each genotype was selected which showed similar expression levels of exogenous TDP-43 as assessed by protein quantification (Figure 3.14.D).

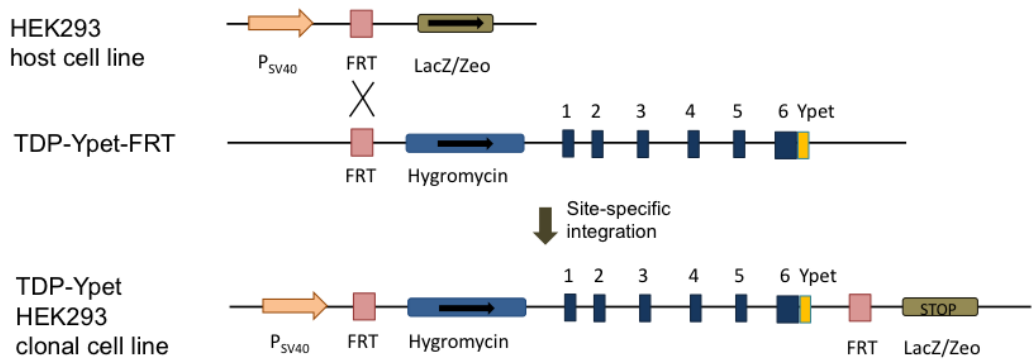


Figure 3.11: Schematic representation of the Flp-In system used for the generation of site-specific stable HEK293 lines expressing TDP-Ypet vectors. A HEK293-FRT host cell line was generated which contains an integrated FRT site, lacZ and SV40 early promoter. The TDP-Ypet vectors were retrofitted with a plasmid containing an FRT site, and a hygromycin resistance gene lacking a promoter and a start codon. Upon co-transfection of the retrofitted TDP-Ypet vectors and a plasmid encoding the *flippase* recombinase, site-specific integration was achieved in HEK293-FRT host cell line.

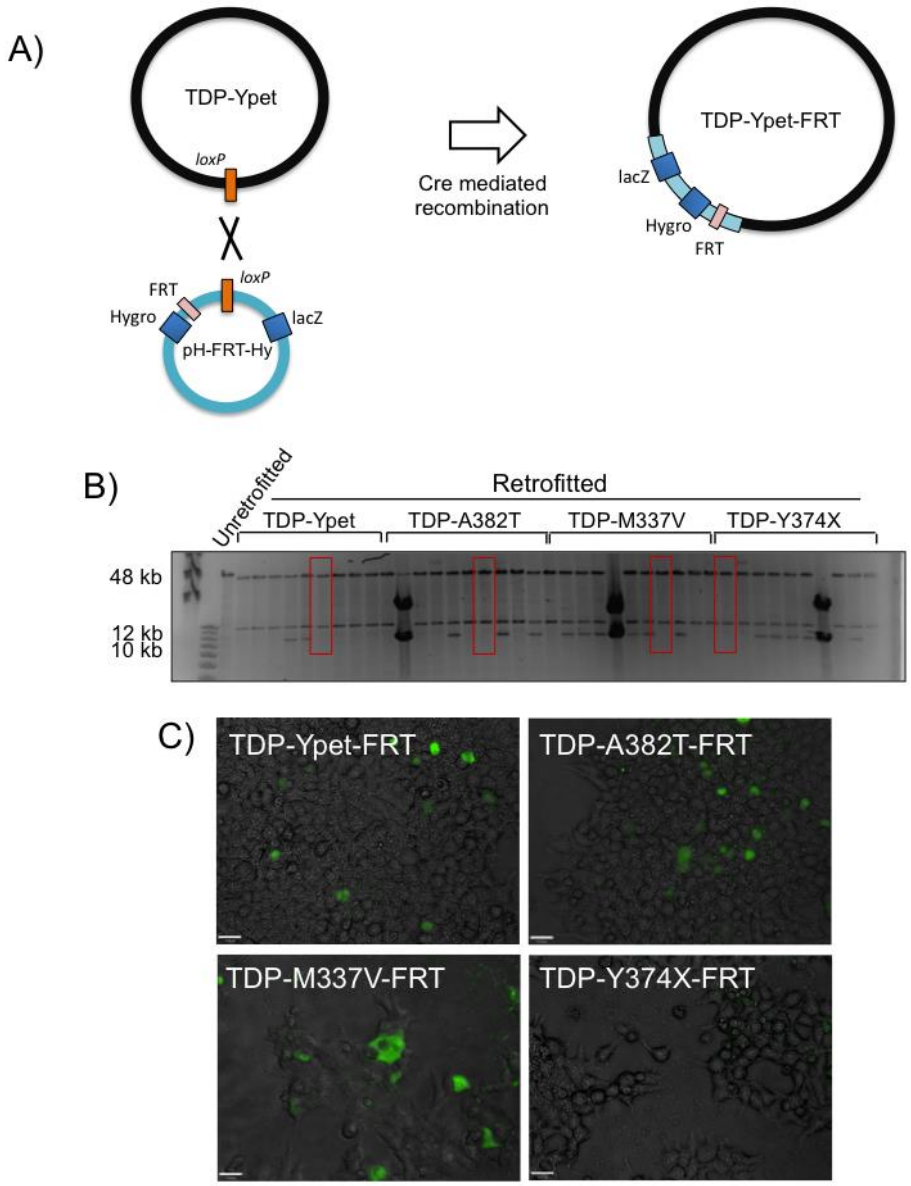


Figure 3.12: Retrofitting by Cre/lox of TDP-Ypet, TDP-A382T, TDP-M337V and TDP-Y374X with pH-FRT-Hy plasmid. A) Schematic representation of the retrofitting strategy between the loxP sites of TDP-Ypet and pH-FRT-Hy. B) Confirmation of successful retrofitting events in vectors carrying each mutation by restriction digests with *AfeI* (expected bands: 52 kb and 12 kb). C) Vector expression confirmed after retrofitting by transient transfection into HEK293 cells.

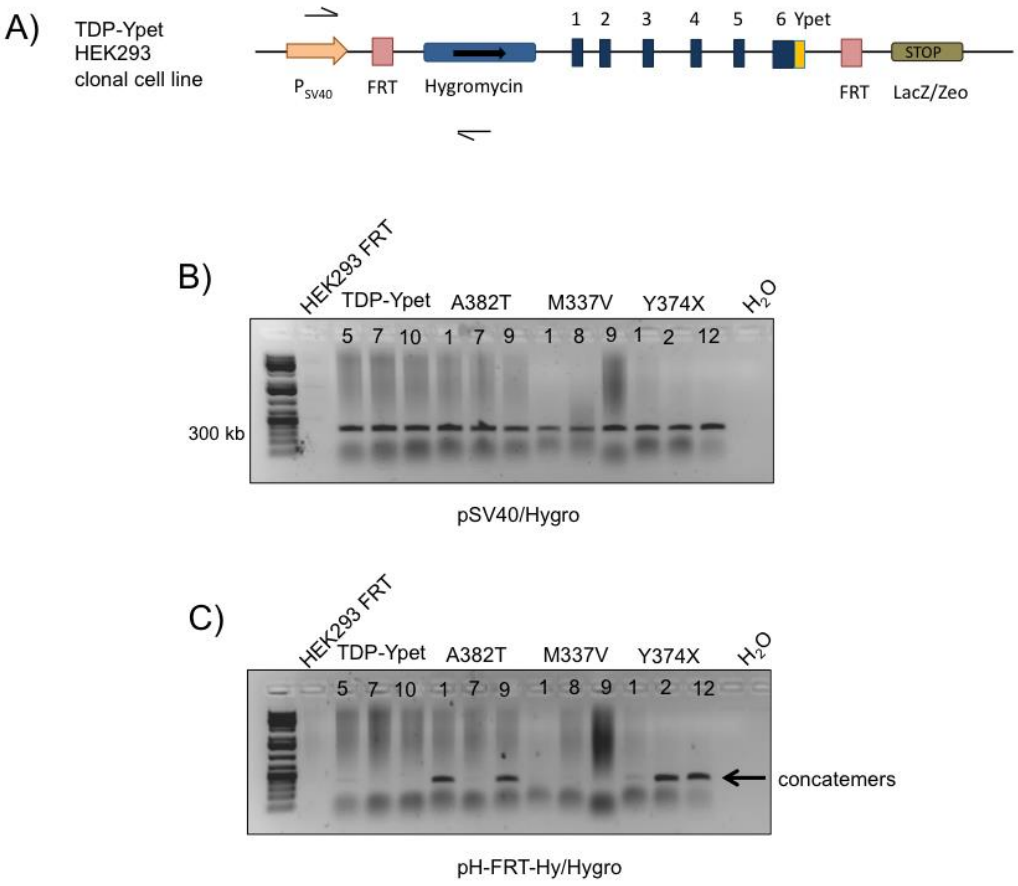

A)
TDP-Ypet
HEK293
clonal cell line
1 2 3 4 5 6 Ypet
STOP
P SV40
FRT
Hygromycin
FRT
LacZ/Zeo
B)
HEK293 FRT
TDP-Ypet
A382T
M337V
Y374X
H2O
5 7 10 1 7 9 1 8 9 1 2 12
300 kb
pSV40/Hygro
C)
HEK293 FRT
TDP-Ypet
A382T
M337V
Y374X
H2O
5 7 10 1 7 9 1 8 9 1 2 12
concatemers
pH-FRT-Hy/Hygro

Figure 3.13: Generation of site-specific PAC HEK293 stable cell lines expressing TDP-Ypet, TDP-A382T, TDP-M337V and TDP-Y374X. A) Illustration of the location of the PCR primers used for confirmation of correct integration of TDP-Ypet-FRT vectors in HEK293-FRT genome. B) PCR for confirmation of integration of TDP-Ypet-FRT in the host cell lines for each genotype and C) PCR showing clonal lines with only one integration and several integrations (arrows show presence of concatemers).

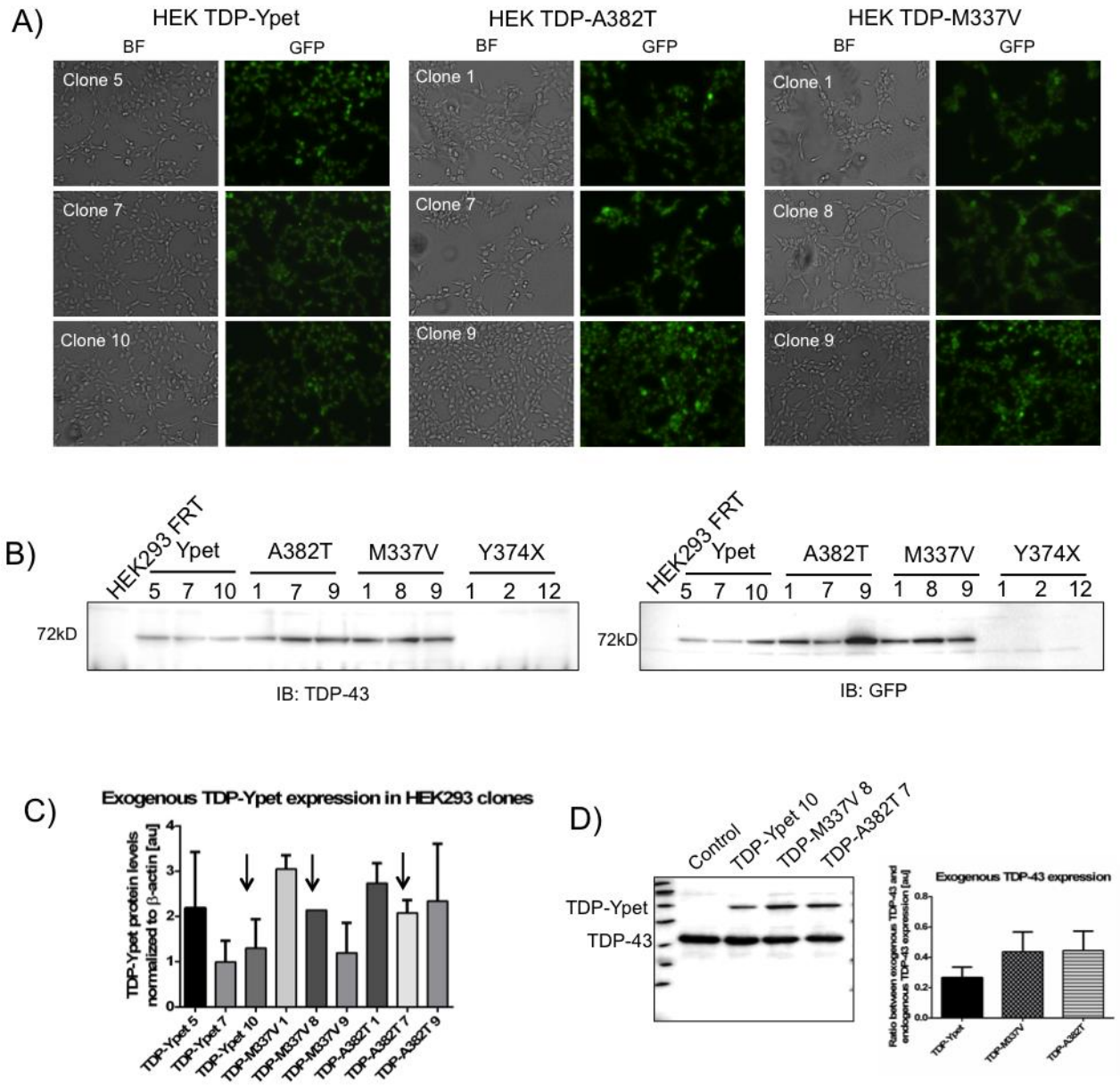


Figure 3.14: Expression analysis of exogenous TDP-43 in HEK293 clones and selection of clones. A) Immunofluorescence using GFP antibodies showing successful expression of TDP-Ypet, TDP-A382T and TDP-M337V in the generated HEK293 clonal cell lines. The clonal cell line expressing TDP-Y374X did not show fluorescence, due to the truncating mutation. B) Confirmation of exogenous TDP-Ypet, TDP-A382T, TDP-M337V expression by immunoblotting with TDP-43 and GFP antibodies and C) quantification of expression levels in all genotypes. D) Selection of one clone from each genotype with similar expression levels of exogenous TDP-43.

3.6. Conclusions

This chapter describes the generation of novel full-length genomic locus *TARDBP* PACs, the cloning steps undertaken for the development of a fusion protein TDP-Ypet and the engineering of disease-associated mutations. Since the main aim of this thesis is understanding the molecular mechanisms of TDP-43 proteinopathies in a relevant cell model, we developed improved site-specific PAC stable HEK293 cell lines, using a technology previously described in the laboratory (Alegre-Abarrategui et al, 2009).

There are several advantages to full-length genomic DNA BAC technology compared to traditional cDNA overexpression models. The BAC technology enables cloning of an entire genomic locus that encompasses all the regulatory elements for a specific gene, including introns, promoters, upstream and downstream sequences, which are known to encode essential regulatory information for protein function and expression (Venter et al, 2001). Traditional cDNA constructs drive expression of the gene of interest from a strong heterologous promoter, leading to non-physiological protein overexpression and impeding reliable functional experiments. Such cellular and transgenic models of TDP-43 overexpression have previously been established and the non-physiological increase in wild-type TDP-43 correlated with high toxicity and cell death, even in the absence of mutations or cellular stress (Barmada et al, 2010; Lagier-Tourenne et al, 2010; Wegorzewska & Baloh, 2011). Therefore, in order to study functional effects of TDP-43 and its mutations we developed PAC vectors carrying the entire human *TARDBP* genomic locus under the control of its endogenous promoter sequence to provide physiological regulation of gene expression.

From approximately 44 mutations identified in TDP-43 and associated with ALS/FTLD, I chose to engineer A382T, M337V and Y374X in the PAC vectors, which

encompass a variety of pathogenicity levels and potential mechanisms of action. The A382T mutation is the most commonly encountered TDP-43 mutation in families with ALS and FTLD, and it has also been recently identified in Parkinson's disease patients (Borghero et al, 2011; Cannas et al, 2013; Mosca et al, 2012). Patients carrying the A382T mutation, either in homozygous or heterozygous state, present with a variety of clinical conditions, ranging from neurological diseases to non-neurological diseases (Mosca et al, 2012). Investigation into its mechanism of action could reveal important overlapping mechanisms between ALS, FTLD, PD and other related parkinsonisms in which it is involved. The M337V was the second mutation engineered into the TDP-43 PACs. The M337V was chosen as it was previously identified as the most pathogenic mutation associated with ALS and FTLD (Sreedharan et al, 2008). Exogenous expression of TDP-43-M337V in chick embryos resulted in a dramatic reduction in maturation and development of normal limb buds, as well as increased cell death, suggesting a toxic gain of function for the M337V mutation (Sreedharan et al, 2008). The Y374X was the third mutation engineered into the TDP-43 PACs and it is a frame-shift mutation that creates a premature stop codon leading to the expression of truncated TDP-43 (Daoud et al, 2009).

Expression of TDP-Ypet, TDP-A382T, TDP-M337V and TDP-Y374X was evaluated in three different cell lines in order to identify the best suitable cell line available for generating a stable cell line. HEK293 cells were chosen as they were easily transfectable and a widely used cellular model; BE(2)-M17 were chosen due to their neuronal properties as a human neuroblastoma cell line; NSC34 is a hybrid cell line generated by fusion of motor neuron enriched, embryonic mouse spinal cord cells with mouse neuroblastoma and this line was chosen as a motor neuron-like model. Due to low transfection efficiencies observed in BE(2)-M17 and NSC34, as well as reduced cell survival in these cell lines following

transfection, HEK293 cell lines were chosen to develop a site-specific PAC stable cell line. Furthermore, the HEK293 FRT host line had been previously engineered and validated in the laboratory (Alegre-Abarrategui et al, 2009).

The four vectors carrying *TARDBP* genomic locus and mutations were successfully delivered to the HEK293 host cell line and stably expressed the fusion proteins TDP-Ypet, TDP-A382T, TDP-M337V and TDP-Y374X. The detected expression levels of the fusion proteins were significantly lower than endogenous TDP-43 expression, which could be the result of self-regulation. TDP-43 was recently shown to autoregulate its expression in a negative feedback loop by acting as a splicing regulator to reduce its expression levels through binding to the 3' UTR of its own pre-mRNA (Ayala et al, 2011; Polymenidou et al, 2011). In order to dissociate between the effect of mild overexpression and mutation-associated phenotype, we screened the clones and carried on with three lines of each genotype, which expressed the fusion protein at comparable levels for functional analyses.

Using the novel TDP-43 vectors, we investigated the functional effects of TDP-43 and its disease-related mutations on its subcellular localization under normal and oxidative stress conditions, as well as its effects on cellular physiology, specifically looking at its involvement in calcium signalling regulation from the endoplasmic reticulum (ER).

CHAPTER 4

Functional effects of TDP-43 mutations on pathology and ER calcium signalling

TDP-43 is a ubiquitously expressed and highly conserved nuclear protein which plays a major role in the regulation of gene expression by modulating transcription, splicing, micro-RNA biogenesis, RNA transport and stress response (Buratti & Baralle, 2001; Buratti et al, 2001; Freibaum et al, 2010; Mercado et al, 2005; Ou et al, 1995; Wang et al, 2008). Although predominantly nuclear, TDP-43 is believed to shuttle between the nucleus and cytoplasm as several studies have detected the presence of diffuse cytoplasmic TDP-43 in normal cells (Ayala et al, 2005; Ayala et al, 2008; Wang et al, 2004; Winton et al, 2008).

In ALS and FTLD-U, TDP-43 is fragmented and depleted from the nucleus and accumulates in ubiquitinated cytoplasmic inclusions (Neumann et al, 2006). The mechanism

underlying TDP-43 redistribution from the nuclear to the cytoplasmic compartment as well as the functional consequences of this redistribution remain to be elucidated.

To study the physiological effects of TDP-43 disease associated mutations, we developed a TDP-43 cellular model using the full-length genomic *TARDBP* locus and engineered A382T, M337V and Y374X mutations, tagged with the green fluorescent protein (GFP) variant, Ypet, as described in the previous chapter. For functional studies, the cells carrying TDP-Y374X mutation were not included because the truncating mutation resulted in a cleaved product of TDP-43, which lacks the C-terminus where the Ypet reporter was cloned. Therefore, due to difficulties in detecting this construct reliably in cultures we did not include it in the functional assays presented in this Chapter.

Cells stably expressing TDP-Ypet, TDP-A382T and TDP-M337V constructs were analyzed before and after exposure to oxidative and ER stress conditions to identify whether TDP-43 mutations render cells more susceptible to typical ALS pathology and cell death. In addition, cellular physiology was investigated by analyzing calcium homeostasis and a novel role is proposed for TDP-43 on the regulation of ER Ca^{2+} signalling.

4.1. M337V mutation increases cytoplasmic mislocalization of TDP-43

Under normal physiological conditions, TDP-43 is located mainly in the nucleus. However, under pathological conditions, aberrant aggregates of TDP-43 form typical cytoplasmic inclusions that are associated with ALS and FTLD (Neumann et al, 2006). We investigated the subcellular localization of TDP-43 in order to determine whether the presence of the engineered mutations trigger localization differences that are reminiscent of ALS pathology.

To analyze localization of TDP-43, HEK293 cells were transiently transfected with TDP-Ypet, TDP-M337V, TDP-A382T and TDP-Y374X vectors and the subcellular localization of the fluorescent proteins was analyzed four days following transfection. Even though the majority of the cells expressed the fusion protein in the nucleus, we detected nuclear depletion of TDP-43 in some of the cells carrying TDP-M337V, which was accompanied by exclusively cytoplasmic mislocalization of TDP-43 (Figure 4.1.A). Cell counting in transiently transfected cells demonstrated significantly increased frequency of cytoplasmic mislocalization of TDP-M337V compared to TDP-Ypet, with 8.5% of cells showing cytoplasmic re-localization in TDP-M337V compared to only 1.2% in TDP-Ypet ($p<0.05$, Student's *t* test) (Figure 4.1.B). Cellular fractionation was performed to analyze the levels of nuclear and cytoplasmic TDP-43 in the three clonal cell lines and illustrative immunoblots suggest higher levels of cytoplasmic TDP-43 in the cells carrying the M337V mutation compared to A382T and wild-type TDP-Ypet (Figure 4.1.C).

To further confirm this is a mutation-specific phenotype and unrelated to different levels of expression between the vectors after transient transfections, the subcellular localization analysis was replicated in the site-specific BAC stable HEK293 lines, described

in Chapter 3. Due to low expression of the vectors in the clonal HEK293 cell lines, TDP-Ypet fluorescence in live cells could not be detected. Consequently, the cells were fixed and subcellular localization was analysed by immunofluorescence with antibodies against GFP (Figure 4.2.A).

In the clonal HEK293 cell lines, TDP-M337V was detected exclusively in the cytoplasm in 2.7% of cells compared to only 0.7% cytoplasmic mislocalization in TDP-Ypet (p<0.001, ANOVA) (Figure 4.2.B). A trend towards cytoplasmic mislocalization was observed in the less pathogenic mutation, A382T, which induced cytoplasmic mislocalization in 1.4% of the cells (Figure 4.2.B).

Many cell culture models have previously shown that cytoplasmic TDP-43 is toxic, while some models have yielded mixed results and the mechanistic relevance of cytoplasmic versus nuclear TDP-43 is yet unknown. To address this issue in our model, we next investigated whether cytoplasmic redistribution of TDP-43 in the mutations bearing cells associates with cell death.

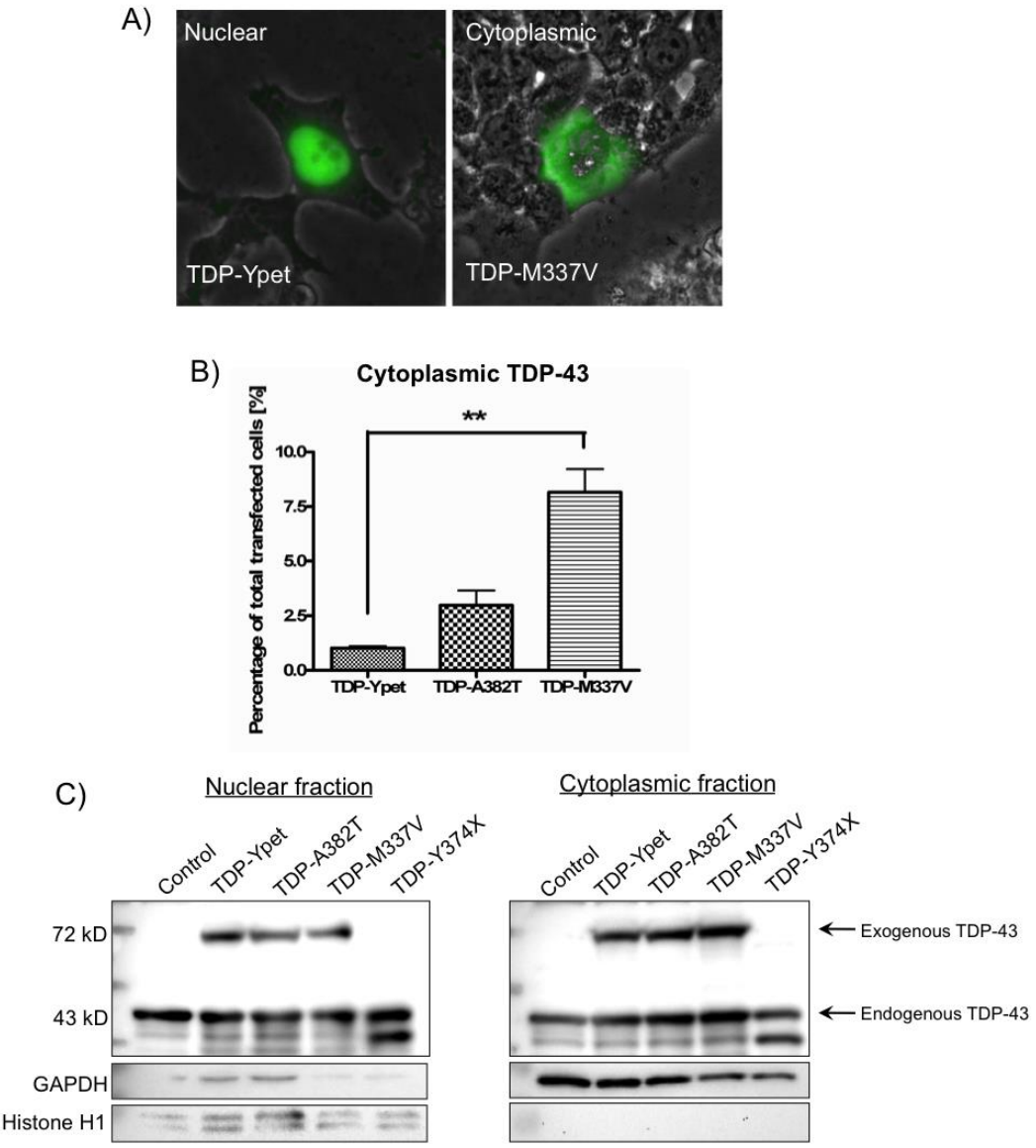


Figure 4.1: TDP-M337V mislocalizes to the cytoplasm more frequently than TDP-Ypet in transiently transfected HEK293 cells. A) Physiological expression of TDP-Ypet was detected primarily in the nucleus in transiently transfected HEK293 cells, while TDP-M337V showed exclusively cytoplasmic mislocalization in some cells; B) Cell counts showed 1% of TDP-Ypet cells with cytoplasmic mislocalization, 2.7% of TDP-A382T cells with cytoplasmic mislocalization and 8% of the cells transfected with TDP-M337V exclusive re-localization of TDP-43 from the nucleus to the cytoplasm (**p<0.05, ANOVA); C) Immunoblotting showed detection of exogenous TDP-43 in both cytoplasmic and nuclear fractions.

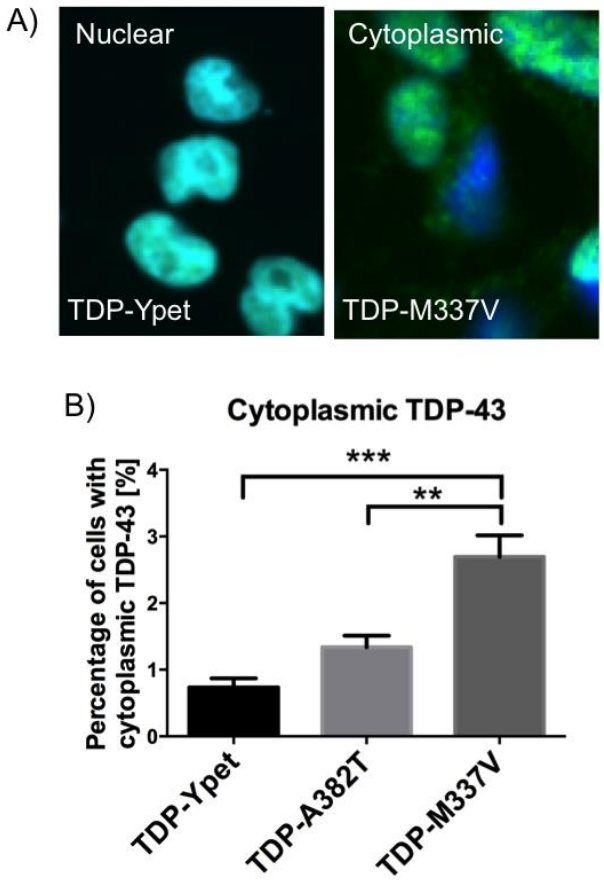


Figure 4.2: TDP-M337V mislocalizes to the cytoplasm more frequently than TDP-Ypet in stable HEK293 clonal cell lines. A) Immunostaining for GFP in HEK293 clonal cell lines stably expressing TDP-Ypet, TDP-A382T and TDP-M337V; B) Cell counts showed exclusively cytoplasmic mislocalization in 2.7% of cells carrying TDP-M337V compared to re-localization in only 0.7% of TDP-Ypet cells (***p<0.001, ANOVA). Data are representative of cell counts from 20 different fields of view, each containing ~20 cells. Scale bar: 20 μm.

4.2. M337V mutation correlates with increased apoptosis

To investigate susceptibility to cell death in the cells carrying M337V and A382T mutations, levels of cleaved caspase-3 were analyzed in clonal HEK293 cell lines. Caspases (cysteine-aspartic acid proteases) are a family of structurally-related cysteine proteases that are synthesized as inactive pro-enzymes and are processed to their active form in cells undergoing apoptosis. The activation requires proteolytic processing at conserved aspartic residues to produce two subunits, large and small, that dimerize to form the active enzyme. Caspases function in a proteolytic cascade where they proteolytically cleave and activate other caspases, as well as other relevant targets in the cells. Upon activation of apoptosis, proteolytic cleavage of procaspase 3 generates an active 18 kDa caspase-3 fragment which targets key modulators of the apoptotic pathway downstream.

Immunostaining with cleaved caspase-3 showed a high percentage of apoptotic TDP-M337V cells (23.5%) compared to TDP-Ypet (5.1%) ($p<0.001$, ANOVA) (Figure 4.3.A,B). Furthermore, significant cytoplasmic co-localization was identified between TDP-M337V and cleaved caspase-3, with 6.3% of cells carrying TDP-M337V showing cytoplasmic co-localization of TDP-43 and cleaved caspase-3, compared to only 2% of cells carrying TDP-Ypet ($p<0.05$, ANOVA) (Figure 4.3.C). In line with these findings, using an MTS cell proliferation assay I detected significantly decreased cell proliferation in the TDP-M337V cells compared to TDP-Ypet cells ($p<0.01$, ANOVA) (Figure 4.3.D).

These results suggest a correlation between TDP-43 cytoplasmic mislocalization and increased frequency of apoptosis in the presence of the M337V mutation.

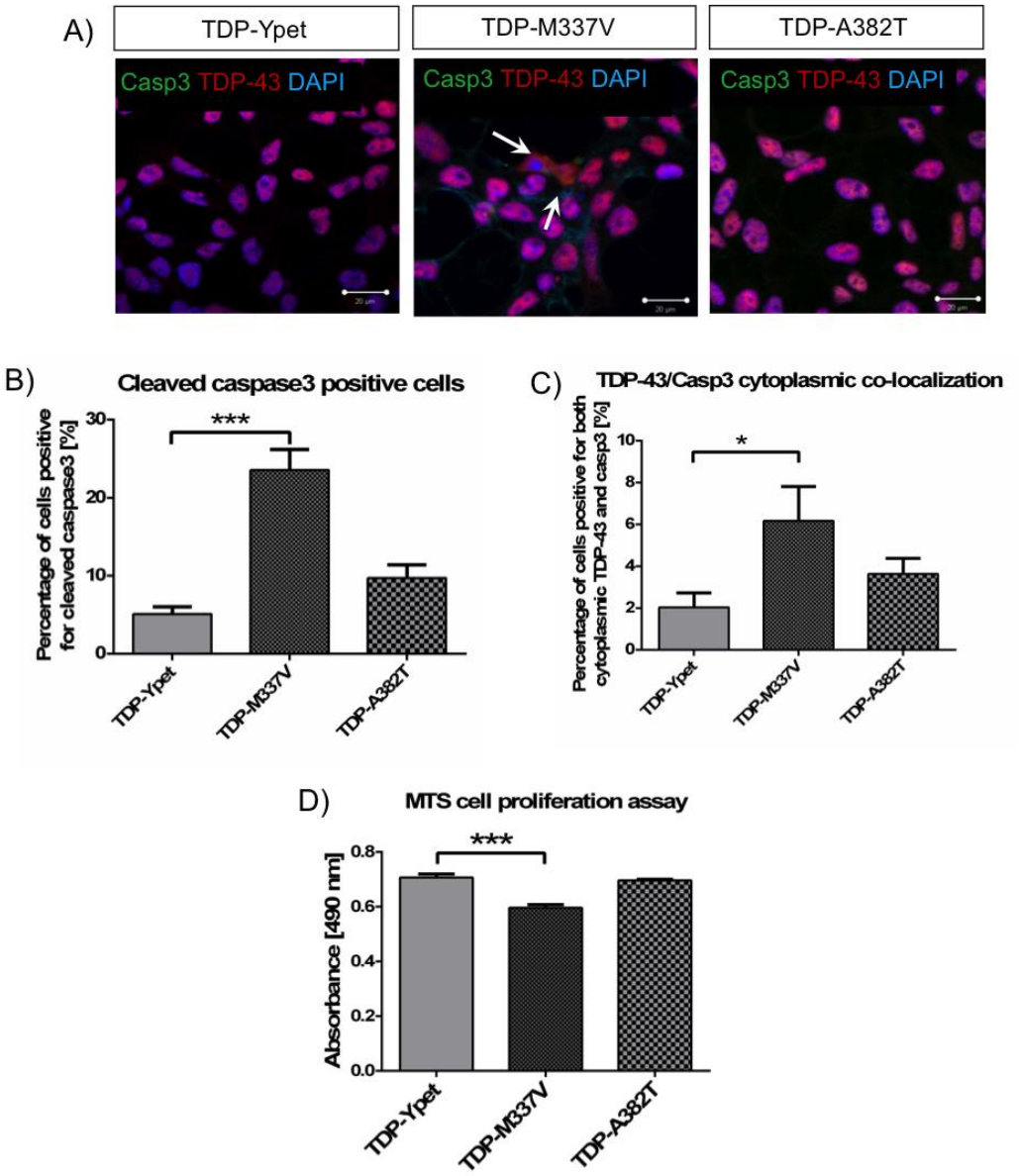


Figure 4.3: **TDP-M337V associates with increased frequency of apoptosis.** A) Immunostaining against cleaved caspase-3 and TDP-43 shows that cytoplasmic TDP-43 co-localizes with caspase-3 in the TDP-M337V cells (indicated by the arrows). B) Cell counting shows 20% of cells carrying TDP-M337V are positive for cleaved caspase-3 compared to 8% of cells carrying TDP-Ypet (**p<0.01, ANOVA); C) TDP-43 and caspase-3 cytoplasmic co-localization was identified in 6% of TDP-M337V cells compared to 2% of TDP-Ypet (*p<0.05, ANOVA). D) MTS cell proliferation assay revealed decreased cell proliferation in TDP-M337V cells (***p<0.01, ANOVA) (n=3 independent experiments). Data are representative of cell counting from 10 different fields of view, each containing ~20 cells. Scale bar: 20 μm.

4.3. Oxidative stress potentiates pathology in M337V and A382T

4.3.1. Mild oxidative stress increases cell death in TDP-M337V cells

There is substantial evidence implicating oxidative stress as a central mechanism promoting motor neuron death in ALS, including elevated markers of oxidative damage in ALS patient spinal cord and cerebrospinal fluid (Ferrante et al, 1997; Shaw et al, 1995). Furthermore, in addition to genetic determinants, a variety of cellular stressors were shown to increase cytoplasmic TDP-43 and its colocalization with stress granules (Colombrita et al, 2009; Dewey et al, 2011; Freibaum et al, 2010; Nishimoto et al, 2010).

To investigate whether oxidative stress enhances the potential pathogenic roles of TDP-M337V and TDP-A382T, we used hydrogen peroxide (H_2O_2). Hydrogen peroxide is a mild oxidant which can pass through cell membranes (Waldron & Rozengurt, 2000) and that is also continuously produced intracellularly by the mitochondrial respiration and the membrane-associated NADPH oxidase complex (Vignais, 2002). It is also the most stable and long-lived reactive oxygen species (ROS) (Kress et al, 1995; Li & Jackson, 2002) and has been widely used as a stressor in cell culture for the study of ALS related pathology.

To determine the minimum amount of H_2O_2 necessary to induce cellular stress we used increasing concentrations of H_2O_2 that were applied to untransfected HEK293 cells. Cells were incubated with 10 μM, 25 μM, 50 μM, 100 μM, 200 μM, 500 μM and 1000 μM H_2O_2 for 6 hours and 24 hours and survival was determined by an MTT assay (Figure 4.4.A). Since we aimed to determine the lowest concentration of H_2O_2 sufficient to induce mild oxidative stress without initiating cell death, the chosen concentrations for the experiments were 10 μM and 50 μM H_2O_2.

Using the determined concentrations, the clonal HEK293 cells expressing TDP-Ypet, TDP-M337V and TDP-A382T were incubated in media containing H_2O_2 for 24 hours and survival was assessed to determine whether the presence of M337V or A382T increased susceptibility to cell death. Reduced survival was seen in HEK293 cells carrying TDP-M337V compared to TDP-Ypet under normal conditions ($p<0.01$, ANOVA) and also following oxidative stress induced by 50 μM H_2O_2 ($p<0.05$, ANOVA) (Figure 4.4.B). These results demonstrate that the M337V mutation renders cells more susceptible to cell death both under basal and oxidative stress conditions.

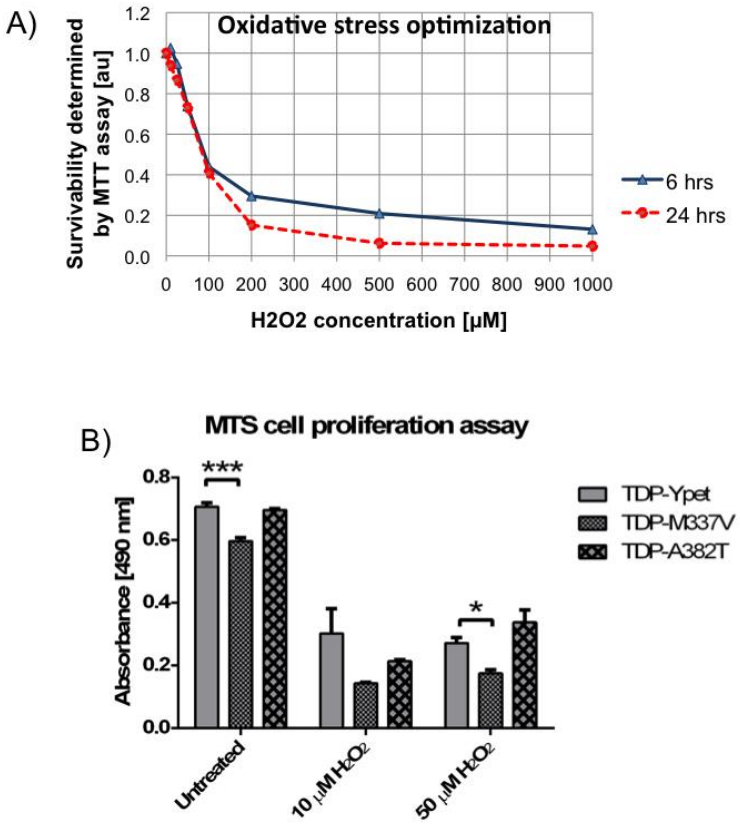


Figure 4.4: Oxidative stress increases apoptosis in TDP-M337V compared to TDP-Ypet. A) Optimization of H_2O_2 concentrations was performed on untransfected HEK293 cells which were exposed to 0 µM, 10 µM, 25 µM, 50 µM, 100 µM, 200 µM, 500 µM and 1 mM H_2O_2 followed by an MTT assay to determine cell death associated with each condition. Optimal concentrations were determined to be 0 µM, 10 µM and 50 µM H_2O_2. B) MTS survival assay shows significantly increased cell death TDP-M337V cells compared to HEK TDP-Ypet under normal conditions (**p<0.01, ANOVA) and after treatment with 50 µM H_2O_2 (*p<0.05, ANOVA) and no significant differences between genotypes after treatment with 10 µM H_2O_2 (n=3 independent experiments, each performed in triplicate).

4.3.2. Mild oxidative stress increases M337V and A382T cytoplasmic mislocalization

To investigate the mechanism underlying the increased cell death of TDP-M337V cells following oxidative stress, I evaluated the subcellular localization of TDP-43 under oxidative

stress conditions, using the predetermined concentrations. Immunofluorescence studies revealed dose-dependent cytoplasmic mislocalization of exogenous TDP-M337V after treatment with 10 μM and 50 μM H_2O_2 in HEK293 clonal cell lines (Figure 4.5.A,B). In the presence of 10 μM H_2O_2, TDP-M337V mislocalized to the cytoplasm in 12.8% of the cells, compared to only 3.6% for TDP-Ypet ($p<0.05$, Student's *t* test), while TDP-A382T did not significantly mislocalize to the cytoplasm at this concentration. In the presence of 50 μM H_2O_2 exogenous TDP-M337V was found in the cytoplasm in 25.2% of the cells compared to only 8.5% of the cells carrying TDP-Ypet ($p<0.001$, ANOVA). After treatment with 50 μM H_2O_2 significant cytoplasmic mislocalization was observed in TDP-A382T cells also, which showed TDP-43 cytoplasmic mislocalization in 21.3% of the cells ($p<0.001$, ANOVA).

These results suggest that mutation-induced cytoplasmic mislocalization of TDP-M337V is associated with increased susceptibility to cell death, which is enhanced in the presence of increasing levels of oxidative stress.

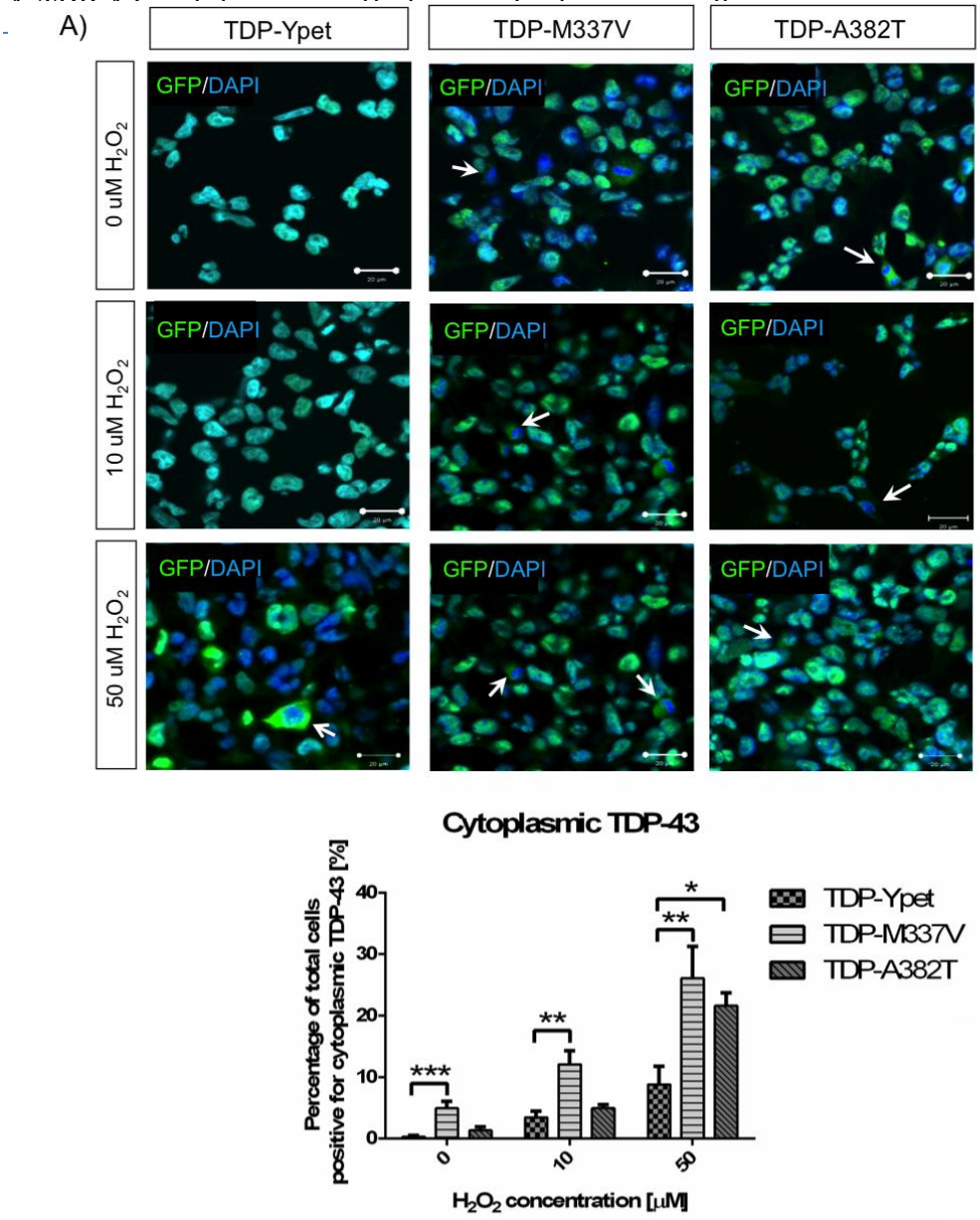


Figure 4.5: Mild oxidative stress increases frequency of TDP-43 cytoplasmic re-localization in the presence of M337V and A382T mutations. A) Immunofluorescence shows characteristic subcellular localization of GFP tagged TDP-43 after treatment with 0 µM, 10 µM and 50 µM H_2O_2, with TDP-A382T and TDP-M337V showing increased frequency of cytoplasmic exogenous TDP-43 at 10 µM and 50 µM (indicated by the arrows). B) Quantification of cell counting cytoplasmic versus nuclear localized exogenous TDP-43 confirming cytoplasmic redistribution of TDP-M337V in 12.8% of the cells after treatment with 10 µM H_2O_2 and in 25.2% of the cells after treatment with 50 µM H_2O_2, while TDP-A382T showed cytoplasmic re-localization in 21.3% of the cells at 50 µM H_2O_2 (***p<0.001, ANOVA). Data are representative of cell counts from 20 different fields of view, each containing ~30 cells. Scale bar: 20 µm.

4.4. ER stress induces pathology in TDP-Ypet and TDP-A382T

4.4.1. Thapsigargin-induced ER stress induces cytoplasmic TDP-A382T punctae

The ER is responsible for protein folding, post-translational modification and trafficking of many transmembrane and secretory proteins (Schröder, 2008). Prevention of protein misfolding is vital to maintain cellular homeostasis and the accumulation of misfolded proteins initiates ER stress. The first response of the ER to deal with ER stress is through the unfolded protein response (UPR), which results in an overall decrease of protein translation and upregulation of specific target genes encoding ER chaperones (Ron & Walter, 2007). If homeostasis is not restored, cell death is initiated by apoptotic signals. Recently, ER stress has been shown to play a key role in the early stages of neurodegeneration in ALS (Atkin et al, 2008; Saxena et al, 2009; Wang et al, 2011).

To investigate the effects of ER stress, clonal HEK293 cells expressing TDP-43 mutations were treated with 100 nM thapsigargin (TG) for 24 hours (Figure 4.6.A). TG is a widely used ER stressor that acts as a potent selective inhibitor of the sarcoplasmic endoplasmic reticulum Ca^{2+} ATPase (SERCA) pump located on the ER membrane. The main function of the SERCA pump is to maintain high luminal Ca^{2+} in the ER and TG blocks its Ca^{2+} reuptake mechanism leading to low ER Ca^{2+} concentration and initiation of ER stress.

We found that TG-induced ER stress increased the number of cells with cytoplasmic TDP-A382T punctae, which are typical of protein aggregations ($p<0.05$, ANOVA) (Figure 4.7.A). Even under normal conditions, TDP-43 mutations M337V and A382T were found to have an effect on nuclear punctae, as higher levels of nuclear TDP-43 punctae were found in M337V and A382T mutations bearing cells compared to TDP-Ypet ($p<0.05$, $p<0.001$,

respectively, ANOVA) (Figure 4.7.B). Susceptibility to cell death in the presence of ER stress was also investigated in TDP-Ypet, TDP-M337V and TDP-A382T cells by an MTS cell proliferation assay. We found a clear effect of reduced survival with the severe mutation M337V under basal conditions, but survival did not appear to be affected by TG treatment in any of the genotypes (Figure 4.7.C).

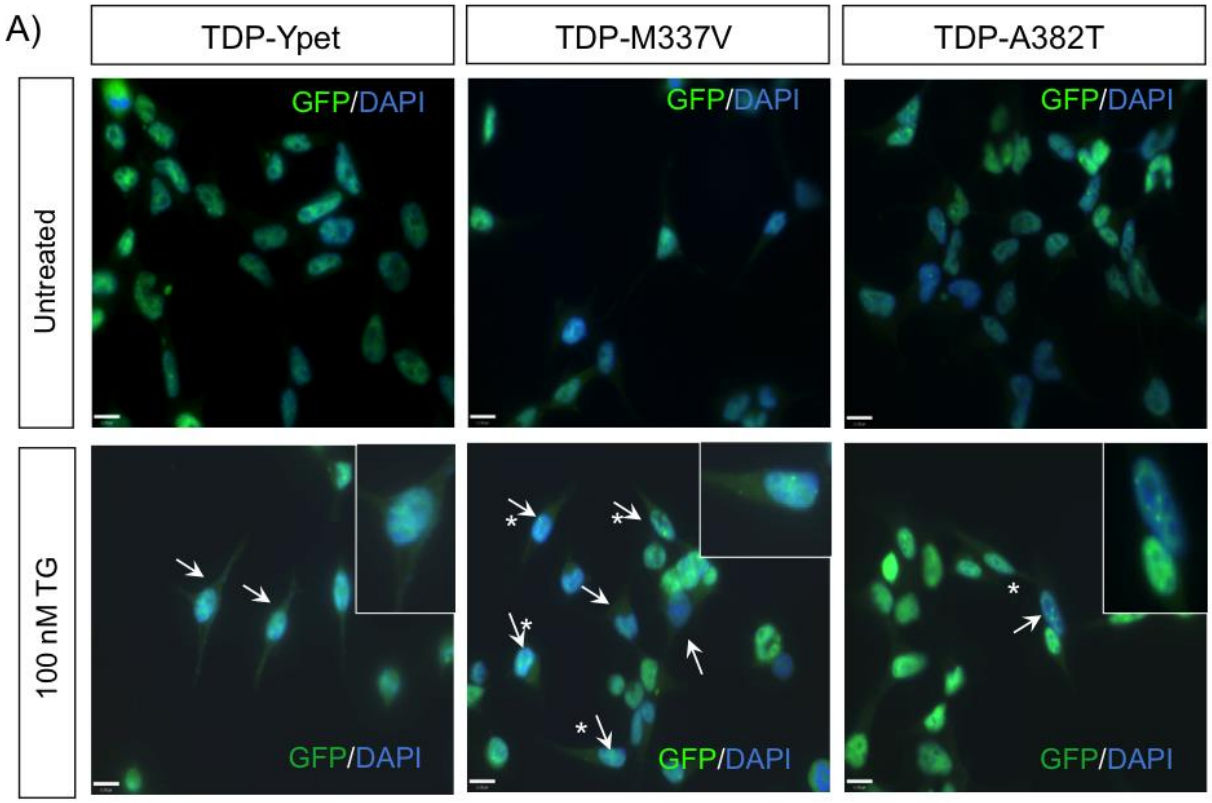


Figure 4.6: Immunostaining showing cytoplasmic TDP-43 in TDP-Ypet cells and the formation of TDP-M337V and TDP-A382T punctae after TG-induced ER stress. Immunofluorescence showing exogenous TDP-43 (GFP) under normal conditions (upper panels) and after treatment with 100 nM TG for 24 hours (lower panels), with arrows highlighting cytoplasmic TDP-43 and starred arrows highlighting nuclear or cytoplasmic punctae.

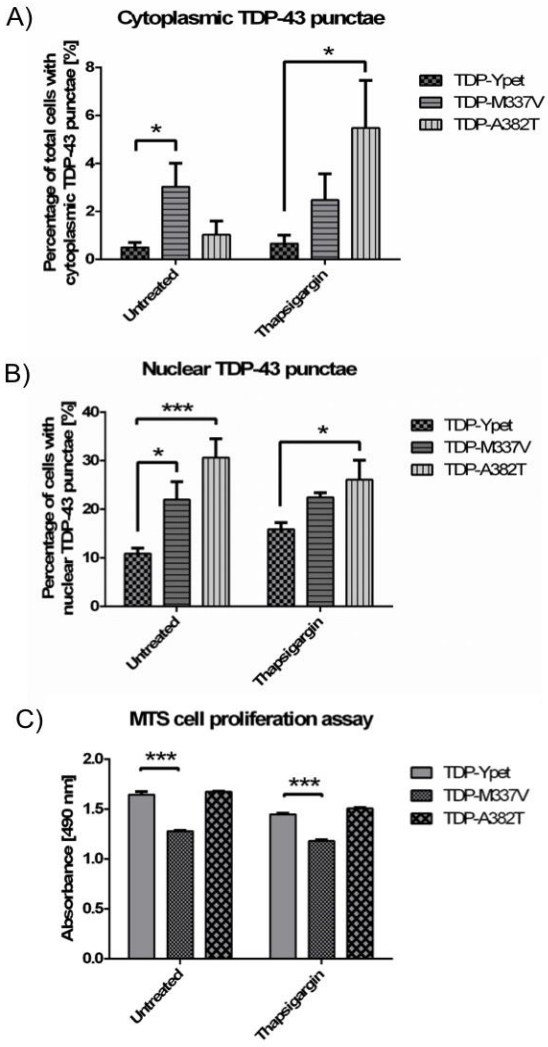


Figure 4.7: M337V and A382T increase frequency of nuclear and cytoplasmic TDP-43 punctae. A) Quantification of the frequency of cytoplasmic punctae observed in untreated TDP-Ypet, TDP-M337V and TDP-A382T cells, with 0.3% of TDP-Ypet cells positive for cytoplasmic punctae, and 3% of TDP-M337V (*p<0.05, ANOVA), and TG-treated cells with 0.4% TDP-Ypet cells positive for cytoplasmic punctae compared to 5.7% of TDP-A382T (*p<0.05, ANOVA). B) Quantification of the frequency of nuclear punctae identified in untreated TDP-Ypet, TDP-M337V and TDP-A382T, with 10.8% of TDP-Ypet nuclear inclusions compared to 21.9% TDP-M337V and 30.6% TDP-A382T (*p<0.05, ***p<0.001, respectively) and TG-treated TDP-Ypet, TDP-M337V and TDP-A382T, with 26% of TDP-A382T cells positive for nuclear punctae compared to 15.6% of TDP-Ypet cells (*p<0.05, ANOVA). D) MTS cell proliferation assay showing decreased survival of TDP-M337V cells compared to TDP-Ypet cells under normal conditions (***p<0.01, ANOVA) and after 24 hrs treatment with 100 nM thapsigargin (*p<0.05). Data are representative of cell counts from 20 different fields of view, each containing ~30 cells. Scale bar: 20 μm.

4.4.2. ER stress induces cytoplasmic mislocalization in TDP-Ypet and TDP-A382T

Next, we investigated whether ER stress induces cytoplasmic mislocalization similar to the mislocalization observed by H_2O_2 oxidative stress. Using 100 nM TG for 24 hours, cytoplasmic TDP-43 mislocalization was induced in TDP-Ypet and TDP-A382T ($p<0.05$, Student's *t* test), while cytoplasmic TDP-M337V levels were already significantly elevated before treatment and remained at a high level after TG treatment (Figure 4.8).

These results show that TG-induced ER stress triggers cytoplasmic mislocalization in TDP-Ypet and TDP-A382T, which partially mimicks the mislocalization observed in M337V. As TG induces ER stress by lowering luminal Ca^{2+} content, we investigated the hypothesis that TDP-43 mutations may alter ER Ca^{2+} dynamics.

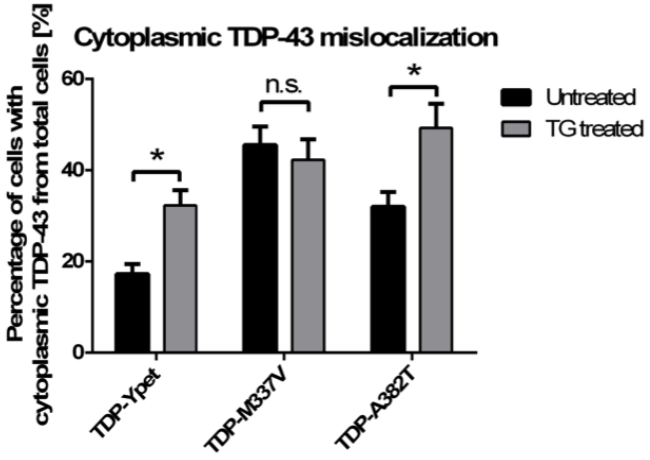


Figure 4.8: TG-induced ER stress increases frequency of TDP-Ypet and TDP-A382T cytoplasmic mislocalization. Cell counts to identify cells positive for both nuclear and cytoplasmic localization of TDP-43 showed that TG-induced ER stress increased frequency of cytoplasmic mislocalization in 32.2% of TDP-Ypet cells, compared to 18% before treatment (*$p<0.05$, Student's *t* test). Similarly, TDP-A382T cytoplasmic localization increased to 49.7% of cells compared to 36% of cells before treatment, in the absence of complete nuclear TDP-43 exclusion (*$p<0.05$, Student's *t* test).

4.5. M337V and A382T mutations alter ER Ca^{2+} signalling

4.5.1. M337V and A382T cause reduced ER Ca^{2+} release amplitude

Since one of the main actions of TG is to alter Ca^{2+} dynamics in the ER, and TG alone partially mimicked the effects of the mutations, we sought to investigate whether the mutations themselves induce an alteration in Ca^{2+} signalling.

Cells carrying TDP-Ypet, TDP-A382T and TDP-M337V mutations were exposed to 10 μM carbachol for 5 minutes under continuous perfusion. Exposure to carbachol stimulates Ca^{2+} release from ER stores through the production of IP_3 whose subsequent binding to the IP_3 receptor (IP_3R) on the ER membrane transiently opens channels releasing Ca^{2+} from the ER lumen. The release of ER Ca^{2+} produces rapid elevations in cytosolic Ca^{2+} concentration, which form characteristic fluorescence spikes and waves. Cytosolic Ca^{2+} released from the ER was detected using a fluo-4 AM Ca^{2+} binding dye. Different patterns of oscillations were observed between the untransfected HEK293, TDP-Ypet, TDP-A382T and TDP-M337V cells in cytosolic Ca^{2+} content upon continuous exposure to carbachol (Figure 4.9.A,B). Results represent the average values of recordings performed in 2 different clones for each genotype. A response to carbachol was detected in 50% of the cells in all cell lines (n=40 cells).

The amplitude and latency of the highest Ca^{2+} peak were measured and cells carrying TDP-M337V and TDP-A382T mutations showed reduced amplitude of Ca^{2+} peaks compared to untransfected (control) and TDP-Ypet (Figure 4.9.C). The recorded cells carrying TDP-M337V showed a mean amplitude of $\Delta F/F_0$=0.31±0.04 (mean±SEM), and TDP-A382T had a mean amplitude of $\Delta F/F_0$=0.48±0.04, while untransfected cells showed a mean amplitude of

$\Delta F/F_0$=0.69±0.04 and TDP-Ypet had a mean amplitude of $\Delta F/F_0$=0.66±0.04 (p<0.01, ANOVA).

Cells carrying TDP-M337V also showed delayed Ca^{2+} release with an average of 76.33±9 seconds (mean±SEM) compared to untransfected cells (53.4±8 seconds) and TDP-Ypet cells (52.5±8 seconds) (p<0.05, ANOVA), while TDP-A382T showed a delay of 65.5±8 seconds, not significantly different from the controls (Figure 4.9.D).

Therefore, the mutations A382T and M337V were associated with low ER Ca^{2+} release peaks and M337V was also associated with delayed onset of carbachol-evoked Ca^{2+} release from the ER.

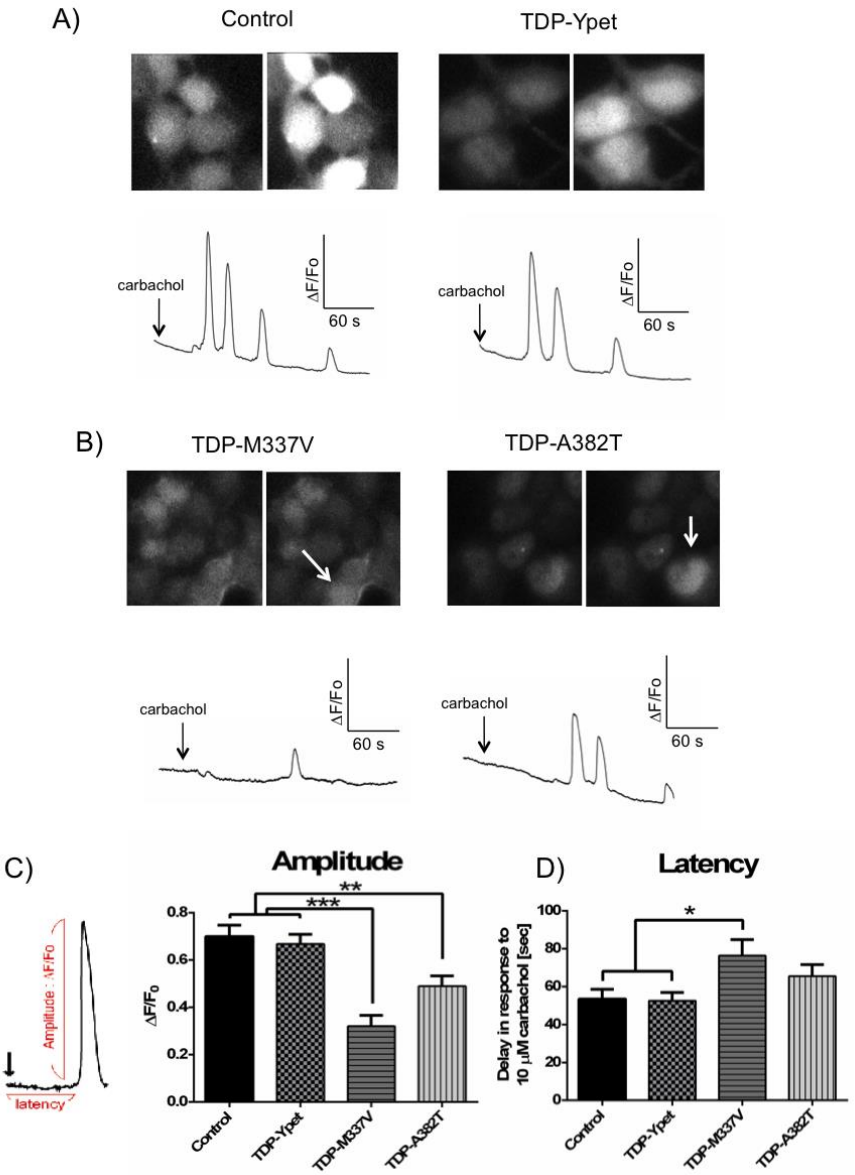


Figure 4.9: Low amplitude calcium peaks are detected in M337V and A382T cells with high latency in M337V. A) Representative fluorescent traces detected on stimulation with 10 μM carbachol for 5 minutes in untransfected cells (control), TDP-Ypet, and B) TDP-A382T and TDP-M337V after loading with Fluo-4 AM calcium binding dye and perfused with Ca^{2+}-free HBSS medium. C) Amplitude of the first calcium peak elicited measured after background subtraction and normalization using ImageJ software showing average values for control=0.69±0.04 (mean±SEM) , TDP-Ypet=0.66±0.04; TDP-M337V=0.31±0.04, TDP-A382T=0.48±0.04, with significantly lower amplitude peaks in TDP-M337V compared to control and TDP-Ypet (***p<0.001; ANOVA) and TDP-A382T (*p<0.01, ANOVA). D) The delay of the first calcium peak in response to 10 μM carbachol was recorded, with mean values control=53.46±5.15 (mean±SEM), TDP-Ypet=52.58±4.39, TDP-M337V=76.33±8.45 and TDP-A382T=65.60±6.05, with significant delay observed in TDP-M337V compared to control and TDP-Ypet (*p<0.05, ANOVA).

4.5.2. M337V and A382T are associated with low ER Ca^{2+} content

Thapsigargin is a potent selective inhibitor of the SERCA pump located on the ER membrane. The SERCA pump maintains high luminal calcium concentration, which is essential for a number of vital cellular processes, such as protein synthesis (Brostrom & Brostrom, 1990) and protein processing (Sambrook, 1990). Upon inhibition of the SERCA pump by TG, calcium fluxes from the ER lumen along a steep concentration gradient into the cytoplasm, which leads to an increase in the cytoplasmic calcium concentration. The elevation of cytosolic Ca^{2+} in response to TG and the subsequent increase in fluorescence are an indirect measure of the total Ca^{2+} within the ER lumen.

Upon the application of 1 μM TG we detected a representative change in fluorescence and the height of the resulting peak was measured to determine ER Ca^{2+} content (Figure 4.10.A). Ionomycin was also applied to the cells after recovery to induce Ca^{2+} release from all cellular organelles and it was used as a control experiment to discriminate between live cells and dead cells. The increase in fluorescence detected is indicative of cytoplasmic Ca^{2+} elevation that is dependent on the total intracellular Ca^{2+} levels (Purkiss & Willars, 1996). Cells that did not respond to application of 1 μM ionomycin were not included in the analysis. Within seconds after addition of 1 μM TG, I detected significantly lower levels of Ca^{2+} in the TDP-M337V ($\Delta F/F_0$=0.64±0.07) and TDP-A382T ($\Delta F/F_0$=0.23±0.01) cells compared to untransfected ($\Delta F/F_0$=0.90±0.08) and TDP-Ypet ($\Delta F/F_0$=1.12±0.09), which had two fold higher calcium levels (p<0.001, ANOVA) (Figure 4.10.A,B).

To determine the molecular mechanisms underlying the association between TDP-M337V and low ER Ca^{2+} stores, I investigated the role of TDP-43 on regulators of Ca^{2+} homeostasis.

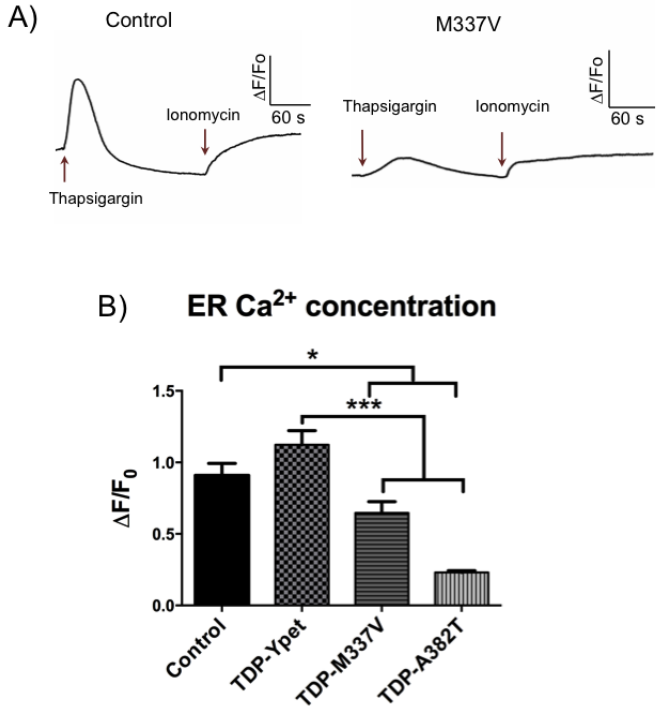


Figure 4.10: Low TG-evoked ER Ca^{2+} content was detected in TDP-M337V and TDP-A382T. A) Representative traces show TG-evoked Ca^{2+} peaks in control cells and TDP-M337V, in response to application of 1 µM TG. B) ER Ca^{2+} content measurement upon application of 1 µM TG, shows significantly reduced levels of Ca^{2+} in A382T and M337V carrying cells compared to control (*p<0.05, ANOVA) and TDP-Ypet (***p<0.001, ANOVA).

4.6. M337V and A382T do not associate with increased autophagy and ER stress induction

Calcium homeostasis in the ER is a complex process regulated by multiple factors. Apart from the SERCA pumps and IP_3 receptors, luminal calcium binding proteins also contribute to the retention of calcium within the ER such as calreticulin, GRP78/BiP and GRP94. These proteins also act as ER chaperones and are involved in protein processing, synthesis and under ER stress conditions, they mediate the unfolded protein response (UPR). Proteins that are involved in the UPR are physiologically bound to the ER resident protein GRP78/BiP, but when ER stress occurs, BiP preferentially binds to misfolded protein, thereby releasing the UPR sensor proteins (IRE1, PERK, ATF6) (Bertolotti et al, 2000; Paschen & Mengesdorf, 2005; Shen et al, 2002).

In order to further investigate the susceptibility of TDP-M337V cells to ER stress at the molecular level, the cells were treated with 100 nM TG for 24 hours and I compared differences in the expression of ER proteins involved in calcium homeostasis and stress response. As expected, when exposed to thapsigargin for 24 hours I found elevations in GRP78/BiP in all three cell lines, without significant differences between the genotypes (Figure 4.11.A,B). Levels of p62, a marker of the UPR pathway, were detected at similar levels between genotypes (Figure 4.11.C). Induction of the autophagic pathway was assessed by measuring the ratio between LC3-II/LC3-I. I did not detect impairments in the activation of autophagy associated with M337V or A382T when compared to TDP-Ypet or control (Figure 4.11.D). Upregulation of Bcl-X_S, associated with apoptosis, was detected in cells carrying the M337V mutation, both under normal and stress conditions ($p<0.05$, ANOVA).

Finally, RNA was extracted from the clonal HEK293 cells and cDNA was analyzed for splicing of XBP-1. The alternative splicing of XBP-1 mRNA by IRE1 is one of the main downstream effects of ER stress (Calfon et al, 2002; Yoshida et al, 2001). No differences were observed in splicing of XBP-1, suggesting ER stress is not involved in the phenotype observed in M337V and A382T mutations and the Ca^{2+} signaling dysregulation is an effect of the mutations in the absence of ER stress (Figure 4.11.G).

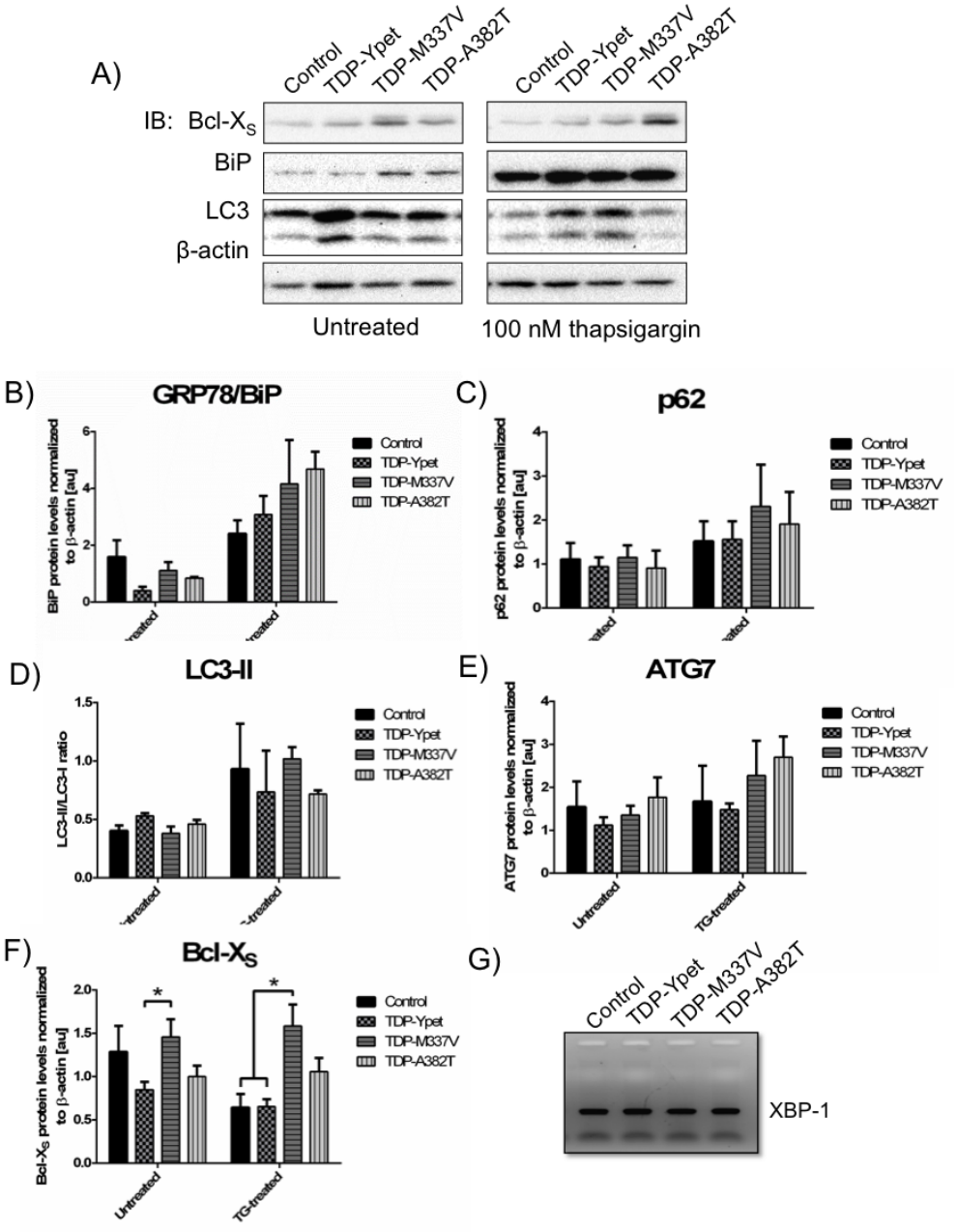


Figure 4.11: Autophagy and ER stress are not associated with TDP-43 mutations A382T and M337V. A) Immunoblotting for Bcl-X_S, BiP, LC3-II in untreated cells and after treatment with 100 nM TG for 24 hours. Quantification of protein expression shows no differences between TDP-Ypet, TDP-M337V and TDP-A382T in levels of B) GRP78/BiP, C) p62, D) LC3 and E) ATG7. F) High levels of Bcl-X_S are detected in TDP-M337V (*p<0.05, ANOVA). G) No alternative splicing is detected in TDP-M337V or TDP-A382T compared to TDP-Ypet and control cells. N=3.

4.7. M337V and A382T associate with upregulation of Bcl-2

An essential player in the modulation of ER Ca^{2+} fluxes is Bcl-2. Bcl-2 is a 26-kDa protein localized in the mitochondrial and ER membranes where it has an important role in modulating Ca^{2+} release events (Oakes et al, 2003; Scorrano et al, 2003). Bcl-2 was shown to interact with IP_3R on the ER membrane where it inhibits the activity of this Ca^{2+} channel, interfering with Ca^{2+} oscillations (Rong et al, 2008). Overexpression of Bcl-2 models have shown reduced ER Ca^{2+} oscillations and increased leakage of Ca^{2+} from the ER (Lam et al, 1994).

We detected significantly elevated levels of Bcl-2 in the TDP-M337V and TDP-A382T cells compared to TDP-Ypet and control HEK293 cells ($p<0.05$, ANOVA) (Figure 4.12.A,B).

To explore whether elevation of Bcl-2 levels mediates the dysregulation we observed in ER Ca^{2+} signaling, we used RNA interference to lower intracellular levels of Bcl-2 and analyzed whether knockdown of Bcl-2 restores Ca^{2+} signalling.

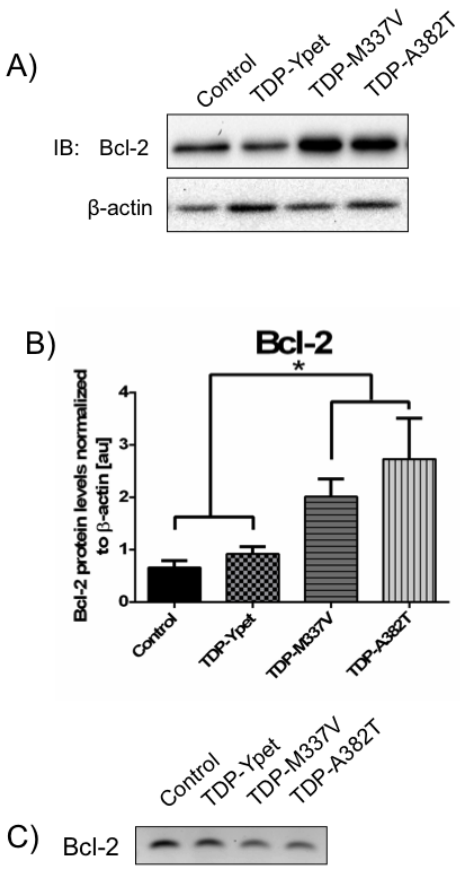


Figure 4.12: Upregulation of Bcl-2 is detected in TDP-M337V and TDP-A382T cells. A) Immunoblot showing increased expression of Bcl-2 protein levels in TDP-M337V and TDP-A382T compared to both untransfected HEK293 cells and TDP-Ypet and B) quantification of immunoblotting confirming higher levels of Bcl-2 in M337V and A382T (*p<0.05, ANOVA). C) RT-PCR showing similar levels of Bcl-2 gene expression in TDP-Ypet, TDP-M337V and TDP-A382T.

4.8. Bcl-2 knockdown restored ER Ca^{2+} release amplitude in TDP-M337V, but not in TDP-A382T

In order to investigate the relation between increased Bcl-2 levels and Ca^{2+} dysregulation, I used RNA interference to knockdown Bcl-2 and investigate Ca^{2+} signaling. Knockdown of Bcl-2 was performed using 100 nM siRNA, which achieved up to 70% knockdown in the four cell lines (Figure 4.12.A,B). As expected, reduced levels of Bcl-2 increased amplitude of Ca^{2+} release from the ER upon carbachol stimulation in TDP-Ypet, compared to cells transfected with scrambled siRNA (Figure 4.13.A,B). Latency was not affected by Bcl-2 knockdown in the wild-type TDP-Ypet (Figure 4.13.B). Following siRNA knockdown of Bcl-2, ER Ca^{2+} release amplitude in TDP-M337V cells increased from $\Delta F/F_0=0.78\pm0.1$ (mean±SEM) to $\Delta F/F_0=1.41\pm0.3$, which reached similar levels to the amplitude of Ca^{2+} oscillations in TDP-Ypet cells after Bcl-2 knockdown ($\Delta F/F_0=1.81\pm0.2$). Amplitude of carbachol-evoked ER Ca^{2+} release in TDP-A382T was not increased following Bcl-2 knockdown and remained lower than TDP-Ypet, showing an amplitude of $\Delta F/F_0=0.79\pm0.09$ when transfected with scrambled siRNA and $\Delta F/F_0=0.74\pm0.09$ after siRNA mediated Bcl-2 knockdown. These results suggest that knockdown of Bcl-2 substantially restores the regulation of Ca^{2+} signaling in TDP-M337V, while additional factors may be contributing to the Ca^{2+} signaling dysregulation observed in TDP-A382T (Figure 4.13.C).

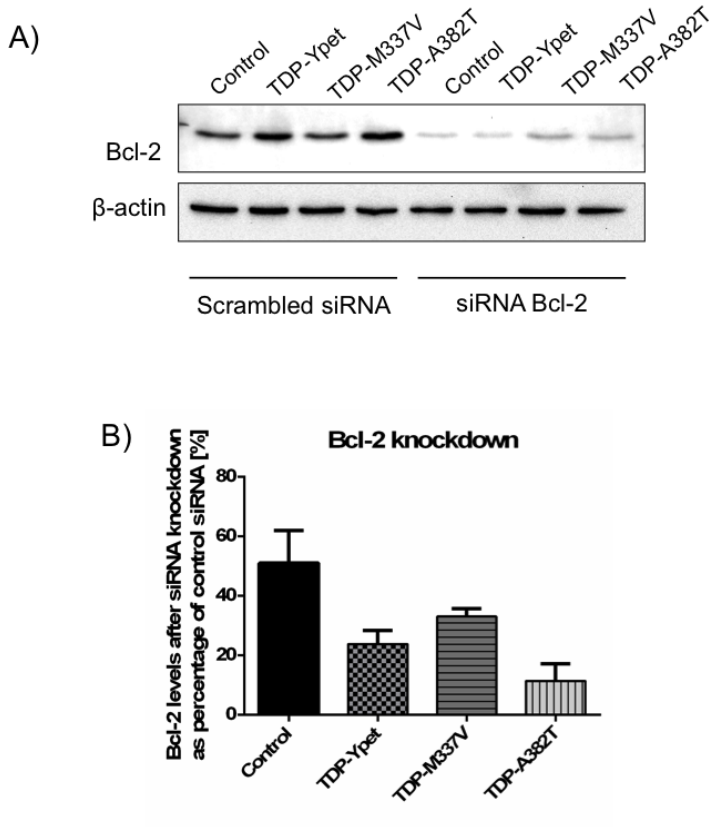


Figure 4.13: Bcl-2 knockdown in control, TDP-Ypet, TDP-M337V and TDP-A382T by RNA interference. A) Immunoblotting showed successful knockdown of Bcl-2 in all four cell lines and B) quantification showed up to 80% knockdown in TDP-Ypet. 90% knockdown in TDP-A382T, and 70% knockdown in TDP-M337V.

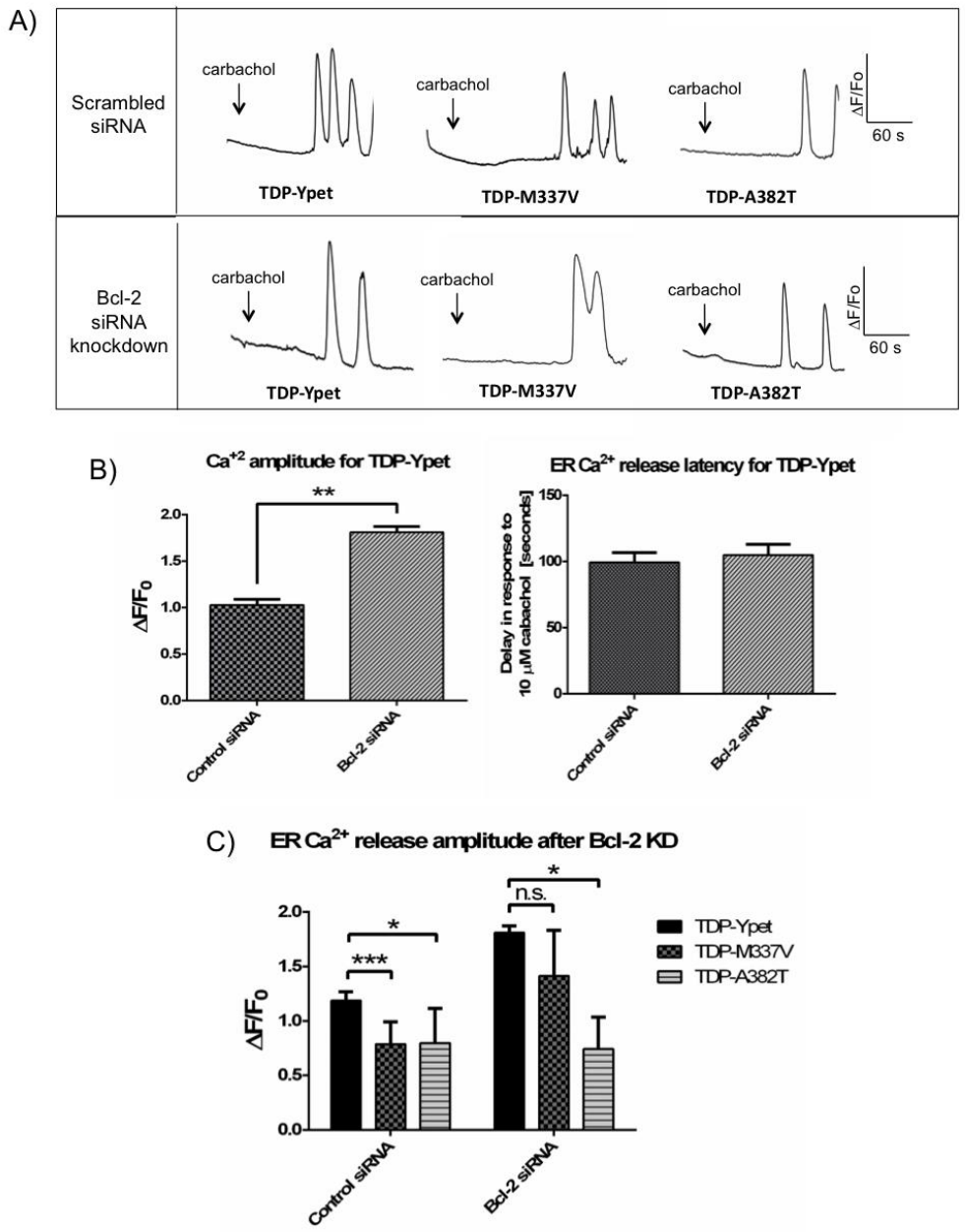


Figure 4.14: SiRNA mediated Bcl-2 knockdown restores amplitude of ER Ca^{2+} release in TDP-M337V, but not in TDP-A382T. A) Traces of ER Ca^{2+} release during the application of 10 μM carbachol in clonal cell lines transfected with either scrambled siRNA (top panel) or Bcl-2 siRNA (bottom panel). B) Effects of Bcl-2 knockdown on ER Ca^{2+} dynamics in HEK293 TDP-Ypet cells, showing increased amplitude upon carbachol induced ER Ca^{2+} release, with average values of $\Delta F/F_0$=1.188±0.2(mean±SEM) when transfected with scrambled siRNA, and $\Delta F/F_0$=1.81±0.2(SEM) after Bcl-2 knockdown (**p<0.01, ANOVA). ER Ca^{2+} release delay was not affected by Bcl-2 knockdown, with averages of t=99.2±21.6 secs when transfected with scrambled siRNA control, and t=104.8±21 secs (*n.s.*). Data represent average values and SEM. C) Amplitude of ER Ca^{2+} release in TDP-Ypet, TDP-M337V and TDP-A382T cells following Bcl-2 knockdown, showing increased levels of Ca^{2+} oscillations in TDP-M337V which reach similar values to TDP-Ypet Ca^{2+} oscillations after Bcl-2 knockdown (mean±SD).

4.9. Conclusions

In this chapter, I show that mutations in a physiological construct of genomic *TARDBP* induce *in vitro* cytoplasmic redistribution of TDP-43, which is associated with increased levels of apoptosis and ER Ca^{2+} dysregulation.

Cells carrying the most pathogenic mutation in TDP-43, M337V, showed significantly higher cytoplasmic translocation of TDP-43 than TDP-Ypet and TDP-A382T. The frequency of aberrant translocation was potentiated by H_2O_2-induced oxidative stress. Our *in vitro* model recapitulates the phenotype observed in the affected neurons of patients with ALS or FTLD, which show a striking redistribution of nuclear TDP-43 to the cytoplasm and display the presence of TDP-43 inclusions in the nucleus, processes or cytoplasm (Arai et al, 2006; Neumann et al, 2006). The most pathogenic mutation, M337V, was previously shown to delay development in chick embryo and cause neuronal apoptosis *in vivo* (Sreedharan et al, 2008). However, the mechanistic relevance of TDP-43 cytoplasmic redistribution to neurodegeneration, and whether it has a causative role or is a consequence, is still unclear.

In addition to cytoplasmic redistribution, I showed that the M337V mutation had a clear effect on increasing the number of cytoplasmic TDP-43 punctae, even in the absence of external cellular stressors, while the A382T mutation required ER stress induction to elevate levels of cytoplasmic punctae.

Furthermore, TG-induced ER stress significantly increased cytoplasmic mislocalization of TDP-Ypet, which partially recapitulated the phenotype observed in TDP-M337V. Similarly, TG treatment increased cytoplasmic mislocalization of the less pathogenic mutation, TDP-A382T, to similar levels seen with TDP-M337V. Since TG acts by inhibition

of the Ca^{2+}-ATPase pump on the ER, I hypothesized that ER Ca^{2+} signalling may mediate the pathological effects observed in TDP-M337V. To test this hypothesis, I investigated differences in ER Ca^{2+} dynamics using pharmacological stimulation.

The Ca^{2+} signalling experiments showed that TDP-43 mutations cause ER Ca^{2+} dysregulation. On stimulation with carbachol, decreased Ca^{2+} release from the ER was detected in cells carrying TDP-M337V and TDP-A382T, along with delayed Ca^{2+} release in TDP-M337V cells. The levels of ER Ca^{2+} content were investigated by stimulation with high concentrations of TG and I found that TDP-M337V and TDP-A382T had significantly lower ER Ca^{2+} stores when compared to TDP-Ypet.

Significant upregulation of Bcl-2 protein was detected in cells carrying TDP-43 mutations. It has previously been shown that overexpression of Bcl-2 in cell culture reduces thapsigargin-induced efflux of ER Ca^{2+}, interfering with Ca^{2+} signaling (Lam et al, 1994).

RNAi mediated knockdown of Bcl-2 was sufficient to restore the amplitude of ER Ca^{2+} release in cells carrying the M337V mutation. Cells carrying the less pathogenic mutation, A382T, did not show an increase in Ca^{2+} amplitude following Bcl-2 knockdown, suggesting there may be additional compensatory mechanisms, which render this mutation also less severe. Our functional results confirm that the M337V mutation is more pathogenic than A382T as M337V shows increased cytoplasmic punctae and cytoplasmic redistribution of TDP-43 in the absence of stress, while A382T shows pathological effects only under oxidative or ER stress conditions.

These results support the hypothesis that TDP-43 mutations disrupt ER Ca^{2+} dynamics and that their effects are modulated by Bcl-2. A gain-of-function disease mechanism may be proposed for TDP-43 mutations M337V and A382T in which the

disruption of ER Ca^{2+} signalling is induced by TDP-43 mutations and associates with aberrant TDP-43 translocation to the cytoplasm.

CHAPTER 5

Functional effects of ALS mutations in human induced pluripotent stem cell derived motor neurons

Successful reprogramming of differentiated human somatic cells to pluripotent cells has recently been a major breakthrough which offers a multitude of opportunities for regenerative medicine and basic research on human diseases (Takahashi et al, 2007b). Differentiated somatic cells can be reprogrammed to an embryonic-like state by overexpressing a combination of only four transcription factors, *OCT4, SOX2,* and either *KLF4* and *c-MYC* (Takahashi et al, 2007b) or *Lin28* and *NANOG* (Yu et al, 2007b). Following this landmark discovery, there has been much hope invested in patient-specific stem cells based on the assumption that they can be differentiated into disease-specific cell types and used to model diseases *in vitro* to elucidate the molecular mechanisms underlying pathology.

In this chapter, we used induced pluripotent stem cell (iPSC) technology to investigate the role of ALS mutations in healthy human motor neurons and in ALS patients' motor neurons. First, healthy and ALS iPSCs were generated by Dr. Sally Cowley and colleagues in the Oxford Stem Cell Facility. Then, a protocol was adapted and optimized (Hu & Zhang,

2009) for the differentiation of human motor neurons from iPSCs. The fully differentiated healthy and ALS motor neurons underwent a thorough characterization by analysis of gene expression, neuronal marker expression and functional assays. Calcium signalling was used to assess functionality of the motor neurons. To specifically study the effects of TDP-43 mutations, the vectors described in Chapter 3 were packaged into viral particles of Herpes Simplex Virus type 1 (HSV-1) amplicons and delivered to healthy differentiated motor neurons. HSV-1 has the advantages of high neurotropism and high transgene capacity, allowing packaging of BACs (Wade-Martins et al, 2001). Following delivery of TDP-43 vectors to the healthy motor neurons, cytoplasmic mislocalization and cell death were investigated under basal conditions and oxidative stress conditions.

In the final part of this chapter, we differentiated and analyzed calcium signalling from the ER in motor neurons derived from ALS iPSCs carrying C9orf72 expansions (DeJesus-Hernandez et al, 2011; Renton et al, 2011). Expansions of the GGGGCC hexanucleotide repeat in intron 1 upstream of the coding region of C9orf72 have been recently identified as the most common cause of familial FTLD and ALS (DeJesus-Hernandez et al, 2011). One iPS line from two different ALS patients, one presenting with cognitive impairments (C9_Turke) and one presenting with typical motor ALS motor symptoms (C9_7245) were generated at the Oxford Stem Cell Facility by Sendai virus reprogramming. Preliminary studies in C9orf72 iPSCs derived motor neurons suggest altered Ca^{2+} signalling in the C9_7245 patient line, accompanied by reduced levels of Bcl-2 protein and elevated levels of GRP78/BiP and p62, in the absence of TDP-43 pathology.

5.1. Optimization of motor neuron differentiation from human induced pluripotent stem cells

5.1.1. Generation of iPSCs from human dermal fibroblasts

The healthy human iPSC lines used in this study were HFF1, Df19.9 and NHDF1 and NHDF2. The HFF1 iPS had been previously obtained from the American Tissue Culture Collection (CRL-2429) and induction of pluripotency had been previously performed by lentiviral delivery of transcription factors *SOX2, OCT4, LIN28* and *NANOG*.

NHDF-1 and NHDF-2 iPS lines were derived at the Oxford Stem Cell Facility by Dr. Sally Cowley and Jane Vowles. Briefly, NHDF1 and NHDF2 iPS lines were derived from normal human dermal fibroblasts obtained from Lonza (NHDF CC-2511). Pluripotency was induced using retroviruses encoding for the original reprogramming genes used by Takahashi and Yamanaka (*KLF4, SOX2, OCT4, c-Myc* and *NANOG*) (Takahashi et al, 2007b). The fibroblasts were infected on day 0 and day 1 with equal amounts of each retroviral supernatant and 5 µg/ml polybrene. The cells were then transferred onto outbred mouse embryonic feeder cells (MEFs) on 0.1% gelatin coated plates on day 4 and from day 5 onwards they were grown in KnockOut Serum Replacement medium supplemented with 50 µg/ml ascorbic acid and 0.5 µM Valproic acid. This medium was substituted with MEF-conditioned medium from day 10 onwards.

On day 28, the colonies displaying iPSC morphology were picked and passaged on MEFs every 5-7 days. Before differentiation, iPSCs were adapted to feeder-free culture conditions by three passages of enzymatic dissociation onto Matrigel-coated plates in mTeSR^{TM}1 supplemented with 10 µM Rock inhibitor. Morphological assessments, passageability and immunocytochemistry for pluripotency markers were used as initial

indicators of pluripotency. Genome integrity was analysed by Illumina Human CytoSNP-12v2.1 beadchip array and the subsequent analysis was done using KaryoStudio. Pluripotency was assessed using the PluriTest online (www.pluritest.org), which was performed after Illumina HT 12v4 transcriptome array analysis.

After three passages of feeder-free cultures, the iPSCs were dissociated and plated on Aggrewell plates in mTeSR-1 medium supplemented with 10 μM Rock inhibitor at a density to achieve 10,000 cells per EB. The EBs were fed daily 75% with mTeSR-1 and harvested after 4 days for differentiation.

5.1.2. Healthy iPSCs were successfully differentiated to motor neurons

In vitro cell differentiation protocols recapitulate signalling that occurs during embryogenesis. The differentiation of iPSCs to spinal motor neurons is a three-stage process that involves neuralization, caudalization and ventralization. I differentiated the reprogrammed iPSC lines into motor neurons by optimizing a previously published protocol (Hu & Zhang, 2009).

The differentiation process and media components are outlined in Figure 5.1.A. Briefly, the motor neuron differentiation protocol started with neural induction of EBs and was followed by neural progenitor stages and neural maturation. After 4 days in neural induction medium, the EBs were plated onto Geltrex-coated plates and caudalization of the neural progenitors was obtained by addition of retinoic acid (RA) to the neural differentiation medium at a concentration of 0.1 μM. After 10 days, the colonies displaying neural rosette structures were isolated and expanded in suspension in the form of neurospheres in the presence of the ventralizing growth factor, sonic hedgehog (SHH) at a concentration of 100

ng/mL. The protocol was modified at this step to enhance cell survival by addition of Rock inhibitor Y27632, which prevents cell detachment and is a widely used supplement in stem cell cultures (Koyanagi et al, 2008; Zhang et al, 2011).

After two weeks of culture as neurospheres, the cells were plated on Geltrex-coated coverslips and terminal differentiation was induced by addition of brain derived neurotrophic factor (BDNF), glial-derived neurotrophic factor (GDNF), insulin-like growth factor (IGF-1), cyclic AMP (cAMP) and ascorbic acid. The differentiating motor neurons were cultured for another 3-4 weeks before functional assays were performed.

Following differentiation, a reliable method to determine cell identity was necessary to assess the efficacy of the protocol. Two iPS lines were used for the optimization of the protocol, Df19.9 and NHDF1. Cellular morphology was analyzed throughout the differentiation process to ensure correct formation of EBs on day 4, formation of neural rosettes and neural tube-like structures on days 13 and 14, identification of neurospheres on day 15 and final attachment of neurons to Geltrex on day 28 followed by the extension of axonal and dendritic structures from day 32 onwards (Figure 5.1.B).

The differentiated motor neurons were first identified by immunostaining with the motoneuron markers HB9 and neuronal marker β-III tubulin (TujI). HB9 is a motor neuron specific transcription factor from the homeobox domain protein family widely used as a marker for the differentiation of motor neurons in stem-cell derived cultures (Wichterle et al, 2002). Co-expression of HB9 and Tuj1 was detected in Df19.9 and NHDF1 cell lines, suggesting that successful differentiation of iPSCs to motor neurons was achieved and the protocol could be reliably used for further experiments (Figure 5.2). The fully differentiated motor neurons were next characterized to assess their functionality and maturation.

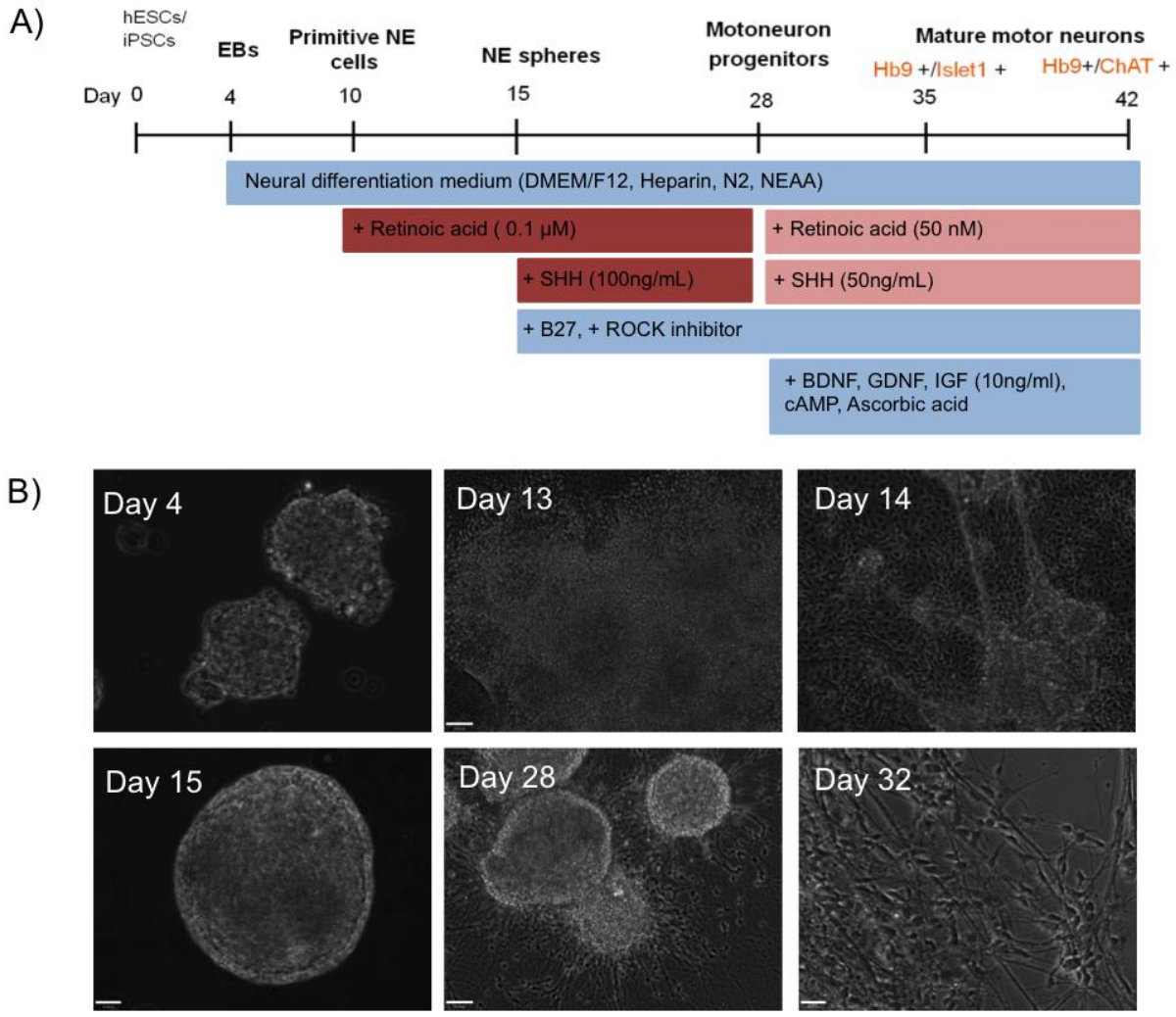


Figure 5.1. **Overview of the motor neuron differentiation protocol.** A) Schematic representation of the timeline of the protocol and B) the morphology of the cells during the differentiation process. After 4 days in neural differentiation medium, the cells are held in suspension and plated on Geltrex-coated plates where they form neural rosettes and neural-tube-like structures (day 13,14) in the presence of 0.1 µM RA. The neurospheres are obtained by lifting the rosette structures on day 15 and allowing the cells to form neurospheres in the presence of RA and SHH. On day 28 the spheres are plated on Geltrex-coated plates where they extend axonal projections and they are allowed to mature for two to four weeks. Scale bars: 70 µm (days 4, 13, 15, 28), 20 µm (days 14 and 32).

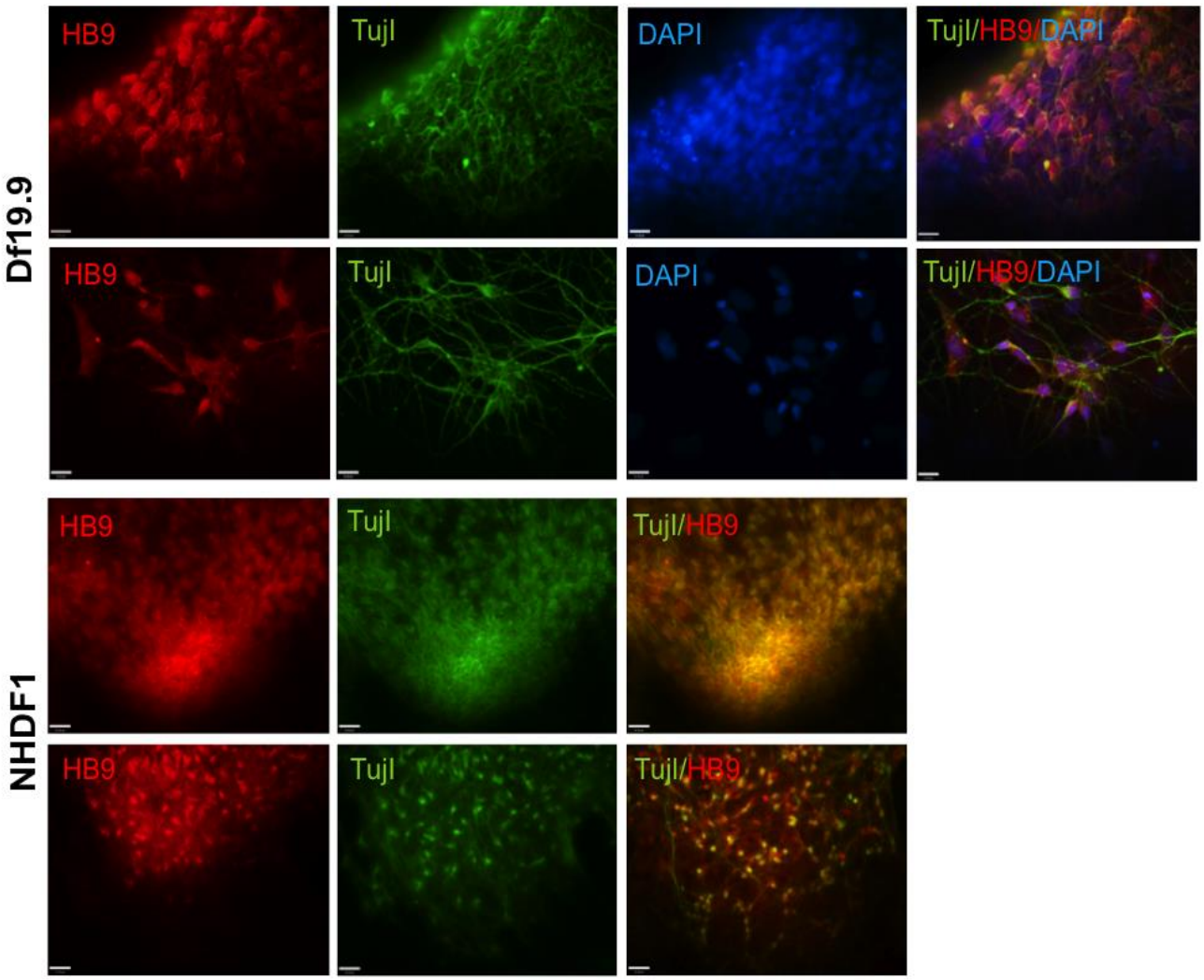


Figure 5.2. **Df19.9 and NHDF1 iPS cell lines differentiated to motor neurons are positive for the motor neuron marker HB9 and the neuronal marker ß-III tubulin (TujI).** Scale bars : 20 µm (top panels), 70 µm (bottom panels).

5.2. Characterization of iPSC-derived motor neurons

5.2.1. iPSC-derived neurons express molecular markers of motor neurons

In addition to NHDF1 and Df19.9, which were used as preliminary cell lines to assess efficacy of the differentiation protocol, iPSCs derived from the HFF1 cell line were also successfully differentiated to motor neurons, as shown by HB9 and Tuj1 immunostaining (Figure 5.3.A). In these iPSC-derived motor neurons we also detected expression of synaptophysin, which is a synaptic vesicle protein essential for the formation of synapses (Figure 5.3.B).

To assess differentiation efficiency, Islet-1 immunostaining was used as a second motor neuron marker in HFF1, NHDF1 and NHDF2 cell lines (Figure 5.4.A). Islet-1 has been previously established as the earliest marker of developing motor neurons, before other motor neuron properties are detectable (Ericson et al, 1992). Differentiation efficiency was assessed by counting cells which co-expressed Islet-1 and Tuj1 in the cell population obtained after 8 weeks of culture. Eight different fields of view from two independent differentiations were assessed. From 1648 DAPI stained nuclei, 169 cells were expressing Tuj1, indicating that 12.3% of cells expressed this neuronal marker (Figure 5.4.B). Moreover, approximately 80% of the Tuj1 positive cells also expressed Islet-1, showing that although neuronal differentiation has a low yield, the majority of iPSCs differentiating to the neural lineage are specifically motor neurons (Figure 5.4.C).

The presence of choline acetyltransferase (ChAT) in these cells also demonstrates an advanced degree of cholinergic neuron maturation, which was identified by immunostaining and immunoblotting (Figure 5.5.A,B). Choline acetyltransferase is the enzyme responsible

for the synthesis of acetylcholine, which is a specific indicator of the functional state of a cholinergic neuron in the central and peripheral nervous systems. ChAT is generally present at the synaptic endings of a cholinergic neuron where it mediates the reaction involving the transfer of an acetyl group from acetyl coenzyme A to choline (Oda, 1999).

The specific activation of gene expression typical for motor neurons during the differentiation process was assessed by reverse transcriptase (RT)-PCR. RNA was extracted from the iPSCs throughout the differentiation process at three different stages: an early stage before neural induction (iPS), intermediate stage of neural stem cells (NSCs) and after the final differentiation (MN). It has previously been established that spinal MN progenitors express Pax6, Nkx6.1 and Olig2 and differentiated MNs express HB9, Islet-1 and ChAT (Wichterle et al, 2002). Activation of Nkx6, Pax6 and Olig2 was detected in the NSCs along with weak expression of ChAT (Figure 5.5.C). ChAT expression was significantly increased later during the differentiation process (Figure 5.5.C).

To assess the identity of the remaining cells in our culture, which were not positive for motor neuron progenitor markers or fully differentiated motor neurons, I used immunostaining for the glial fibrillary acidic protein (GFAP) to test for the presence of reactive astrocytes (Figure 5.6). Spontaneous glial differentiation from iPSCs was previously reported in neural populations which were cultured for extended periods of time (>90 days) and frequently dissociated (Krencik & Zhang, 2011). Next, we investigated the functionality of the motor neurons obtained by the differentiation of iPSCs.

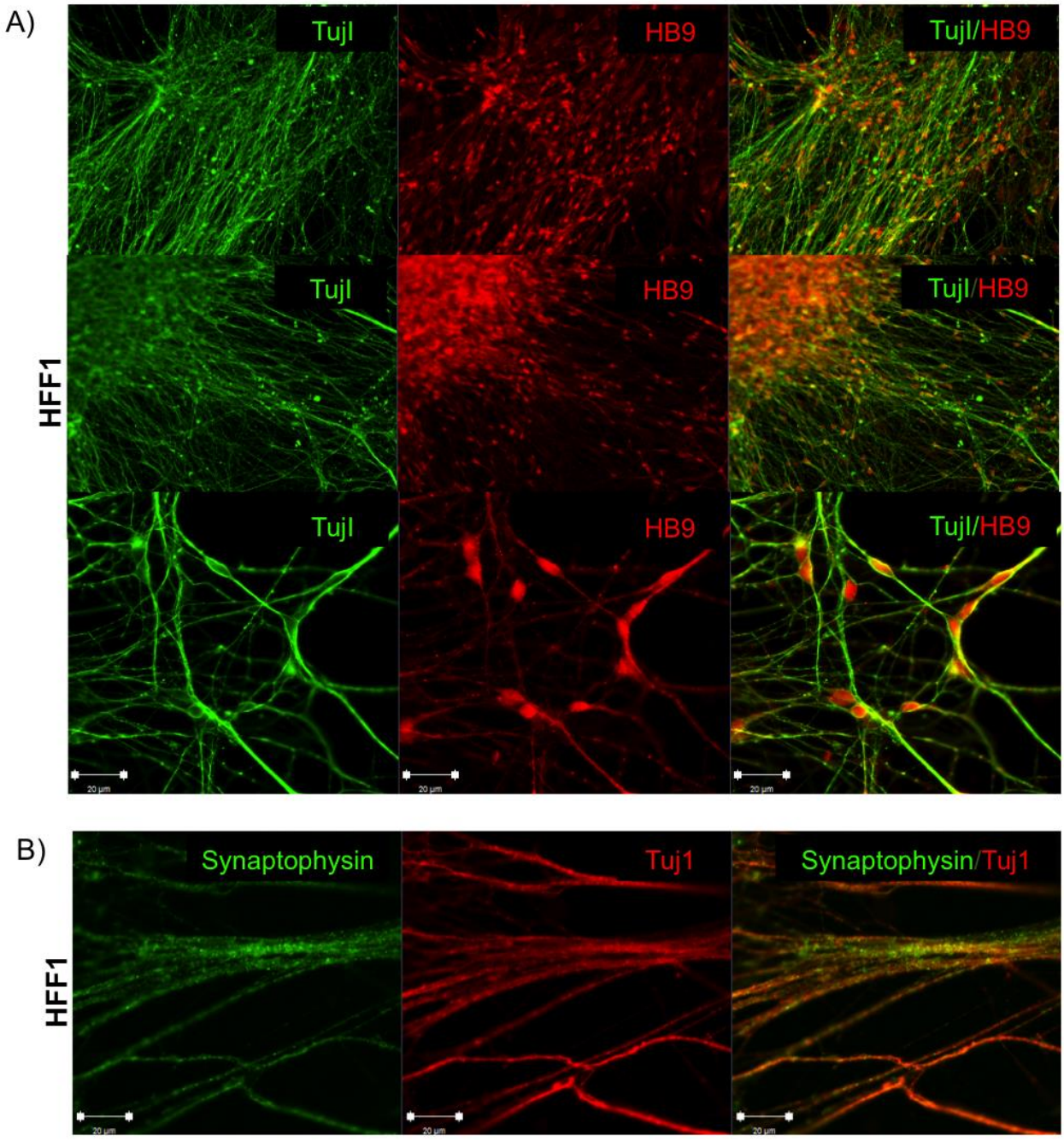


Figure 5.3. **HFF1 iPS cell line is differentiated to motor neurons**. A) Immunostaining shows cells positive for HB9 and TujI, and B) expression of synaptic marker synaptophysin on Tuj1 positive neurons. Scale bar: 20 µm.

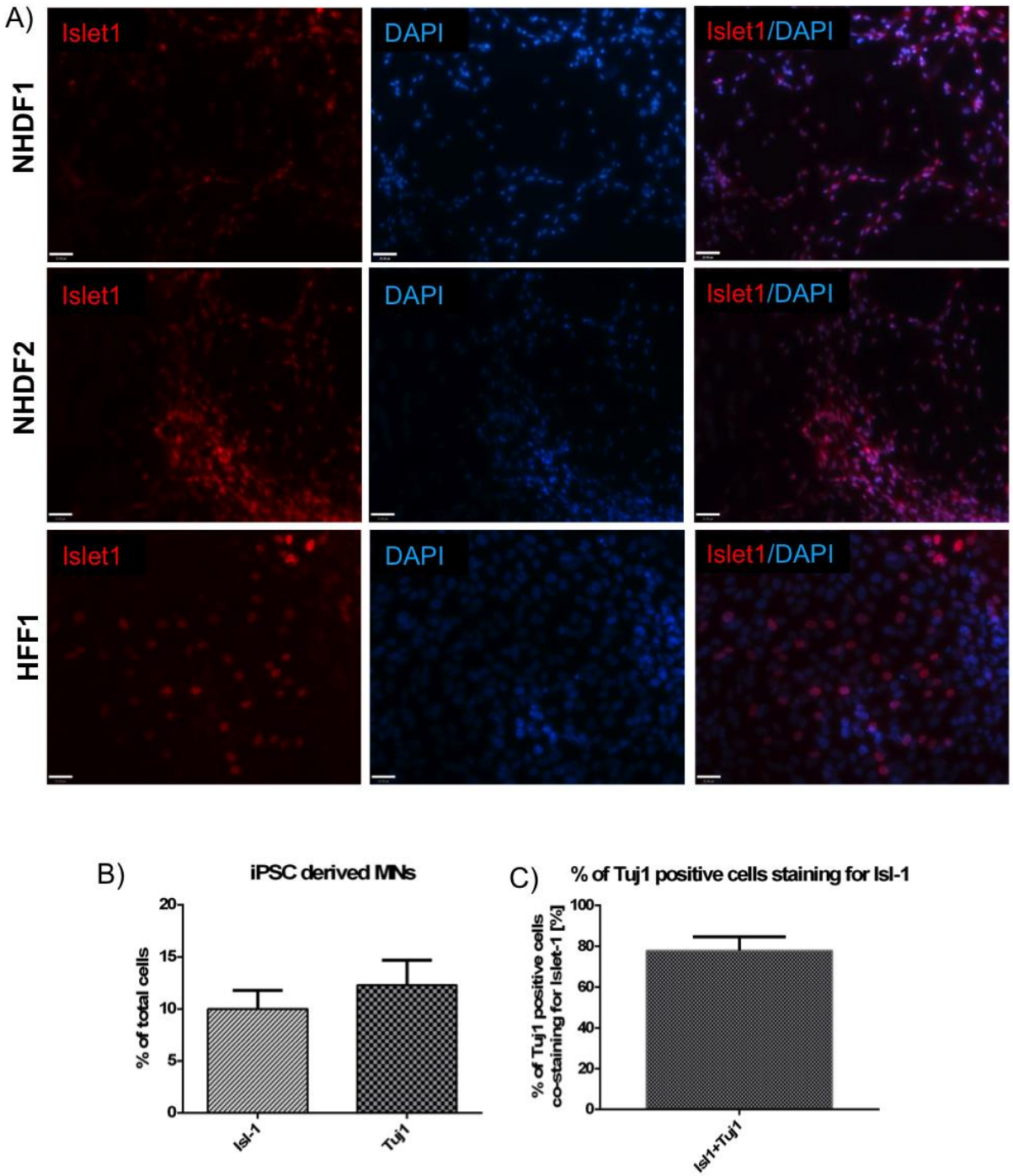


Figure 5.4. NHDF1, NHDF2 and HFF1 iPSC-derived motor neurons staining positive for motor neuron transcription factor Islet1 and neuronal marker Tuj1. A) HB9 immunostaining of NHDF1, NHDF2 and HFF1 cells on day 32 of differentiation B) Quantification of iPSCs derived neurons immunopositive for Islet1 from 8 different cultures of 2 independent differentiations shows 10% cells positive for Islet-1 and 12% cells positive for Tuj1. C) Cell counts show that 80% of the Tuj1 positive cells co-express Islet-1. Scale bar = 70 µm.

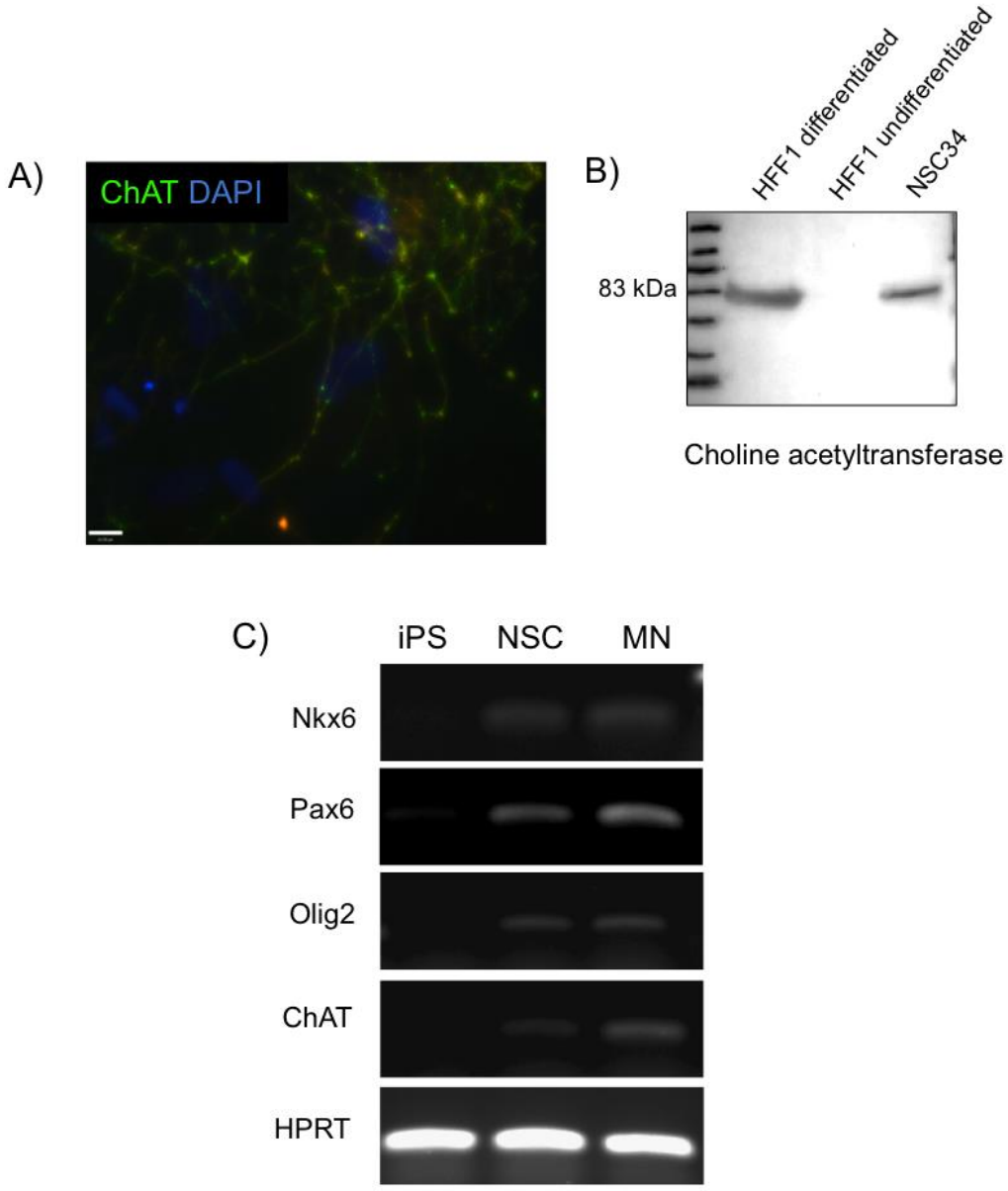


Figure 5.5. Motor neurons derived from iPSCs express choline acetyltransferase (ChAT). A) Immunostaining and B) immunoblotting shows expression of ChAT in iPSC-derived motor neurons on day 52 of differentiation. C) Reverse-transcriptase PCR shows expression of Nkx6, Pax6, Olig2 and ChAT at the stage of neural stem cells (NSC) during the differentiation process and at the final motor neuron (MN) stage. None of these genes are expressed in the precursor iPS cells. HPRT was used as a house-keeping gene and it is stably expressed in all stages of differentiation. Scale bar : 20 µm.

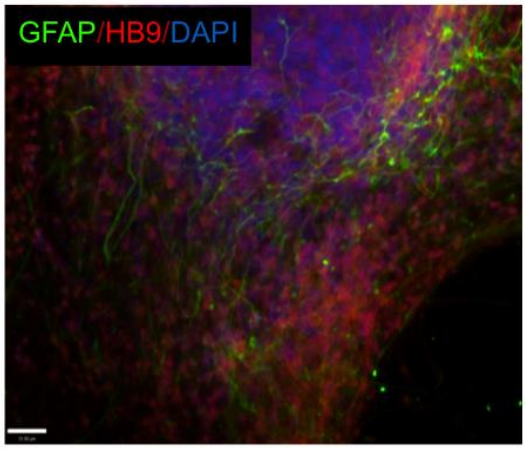


Figure 5.6. Glia are detected in the iPSC derived neuronal culture. Immunostaining shows GFAP positive cells are present in the neuronal culture, particularly present at the edges of the neurospheres. Scale bar: 70 µm.

5.2.2. iPSC-derived motor neurons are functionally active

To establish the phenotypic maturation of human iPSC-derived motor neurons, we studied their physiological properties.

First, we monitored intracellular Ca^{2+} dynamics in the absence of external pharmacological stimulation to detect spontaneous activity. The fully differentiated motor neurons were loaded with the Ca^{2+} sensitive dye Fluo-4AM and activity was recorded (Figure 5.7.A). Spontaneous calcium transients were visible in the cell bodies and processes of the recorded cells, even without treatment (n=10) (Figure 5.7.A).

Next, exogenous pharmacological stimulation was applied to the cells to determine specificity of the motor neurons. KCl was applied to depolarize the membrane and open voltage-gated Ca^{2+} channels. A representative response obtained following the application of KCl is shown in Figure 5.7.A and Figure 5.7.B. Kainate (KA) was applied to the cells to activate ionotropic glutamate receptors and an influx of Ca^{2+} was observed upon addition of KA to the cells (Figure 5.7.C). Immunostaining confirmed that cells responding to KA and KCl in these mixed cultures were Islet-1 positive (Figure 5.7.A, right image).

These results demonstrate that iPSCs can be successfully differentiated to motor neurons that are capable of eliciting action potentials and that display spontaneous Ca^{2+} activity, demonstrating they are functionally active and can be used reliably as models for functional assays.

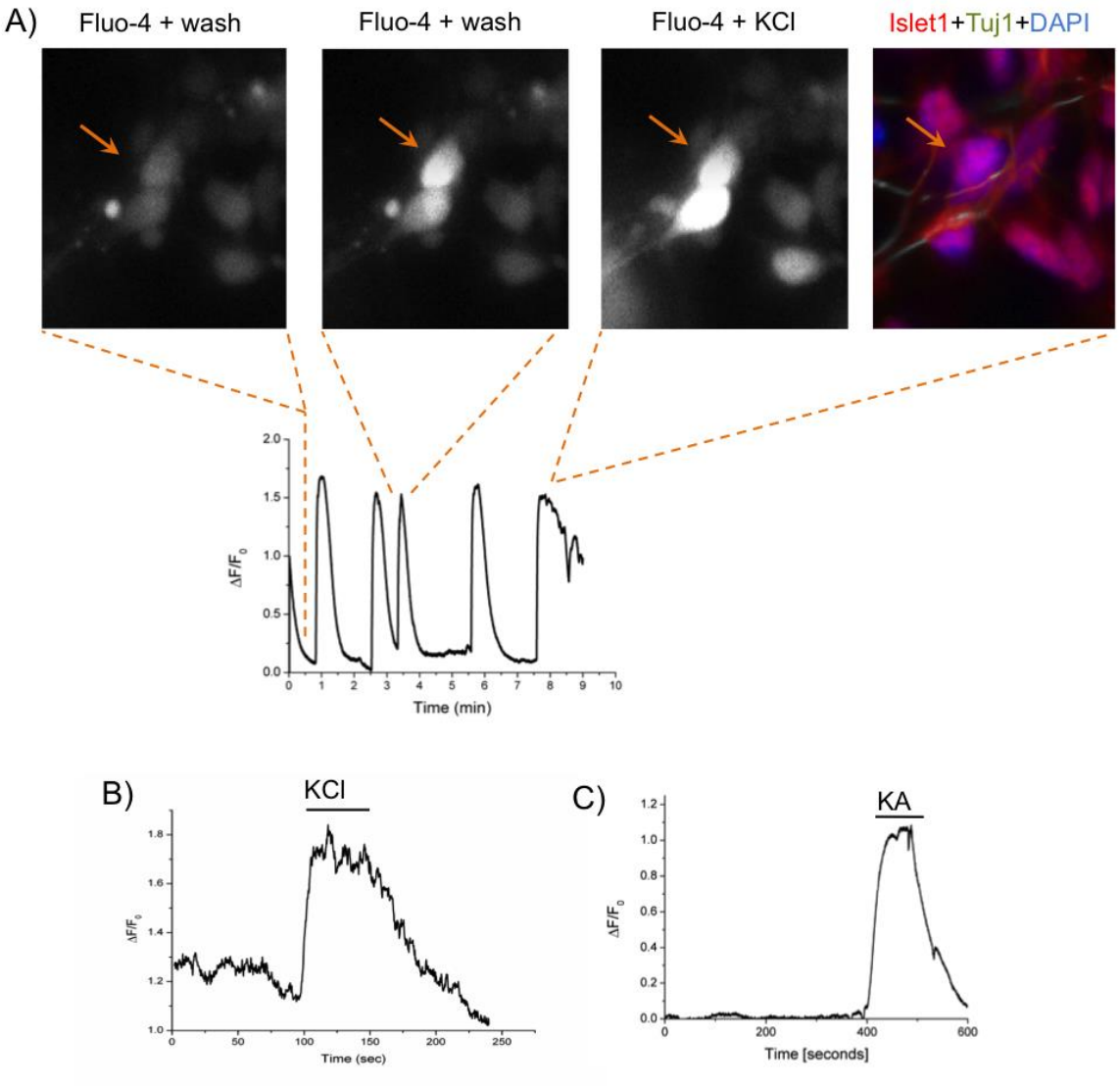

A)
Fluo-4 + wash
Fluo-4 + wash
Fluo-4 + KCl
Islet1+Tuj1+DAPI
ΔF/F0
Time (min)
B)
KCl
Time (sec)
C)
KA
Time [seconds]

Figure 5.7. Calcium signalling is detected in iPSC-derived motor neurons. A) Spontaneous Ca^{2+} transients are recorded from the motor neurons in 2 independent differentiations (n=10). Application of 50 mM KCl elicits a sustained Ca^{2+} response in Islet-1 positive motor neurons. B) Representative response of iPSC derived motor neurons upon application of 50 mM KCl and C) 100 µM kainate (KA).

5.3. Delivery of genomic TDP-43 loci to iPSC-derived motor neurons by HSV-1 amplicons

5.3.1. Packaging of TDP-43 vectors into HSV-1 amplicons

A wide range of viral gene transfer technologies is currently available for gene therapy and for functional genetic purposes. The available systems vary in their range of infectivity, stability of expression and transgene capacity. This is an important limitation when using whole genomic DNA loci models. To address this issue, we used a Herpes Simplex Virus type-1 based vector (HSV-1) that is the leading technology capable of infectious delivery and expression of complete genomic loci (Senior & Wade-Martins, 2005; Wade-Martins et al, 2001). HSV-1 amplicons have a very high transgene capacity (~152 kb), which allows the delivery of large genomic DNA loci. Other advantages of HSV-1 amplicons include episomal replication and retention, overcoming host gene disruption or insertional mutagenesis. They are also capable of transducing both dividing and nondividing cells.

To deliver TDP-Ypet, TDP-M337V and TDP-A382T vectors to iPSC-derived motor neurons by HSV-1, we first retrofitted the vectors with pH-FRT-Hy plasmid (FRT) as described in Chapter 3 and illustrated in Figure 5.8.A. In addition to the FRT, lacZ and hygromycin cassettes, the pH-FRT-Hy plasmid also carries the necessary elements for HSV-1 amplicon packaging and expression, which are HSV-1 *oriS* and HSV-1 pac (Figure 5.8.A,B).

The retrofitted vectors carrying HSV-1 elements were packaged into HSV-1 viral particles in Vero 2-2 cells, using a previously described protocol routinely used in the Wade-

Martins laboratory (Lufino et al, 2011). The HSV-1 amplicons are made by an improved helper-virus free system using a helper HSV-1 genome cloned into a BAC (fHSVΔpacΔ27) (Saeki et al, 2001). The HSV helper virus genome within the BAC plasmid is lacking the essential viral gene ICP27. The Vero 2-2 cells have been previously engineered to express ICP27 and more ICP27 is supplied *in trans* during the transfection process from the plasmid pEBHICP27.

The retrofitted TDP-Ypet, TDP-M337V and TDP-A382T were co-transfected with fHSVΔpacΔ27 and pEBHICP27 in Vero 2-2 cells and the packaging reaction was allowed to proceed for 60 hours. Once packaging was complete, the Vero 2-2 cells were lysed and the viral particles were extracted and concentrated on a 30% sucrose cushion to eliminate potential toxicity from cellular debris contaminating the amplicon preparation. Titration of the TDP-43 HSV-1 amplicon viral stocks was performed using the β-galactosidase assay in G16.9 cells, a cell line that was engineered to express the HSV-1 protein VP16 that enhances reporter gene expression from the IE4/5 promoter.

Following titration, equal amounts of viral particles were delivered to the iPSC-derived motor neurons and expression was assessed (Figure 5.8.C). Before delivery of TDP-43 vectors to the terminally differentiated motor neurons, infectivity and viral retention was assessed in iPSC derived motor neurons using HSV-1 amplicons carrying a GFP-expressing plasmid.

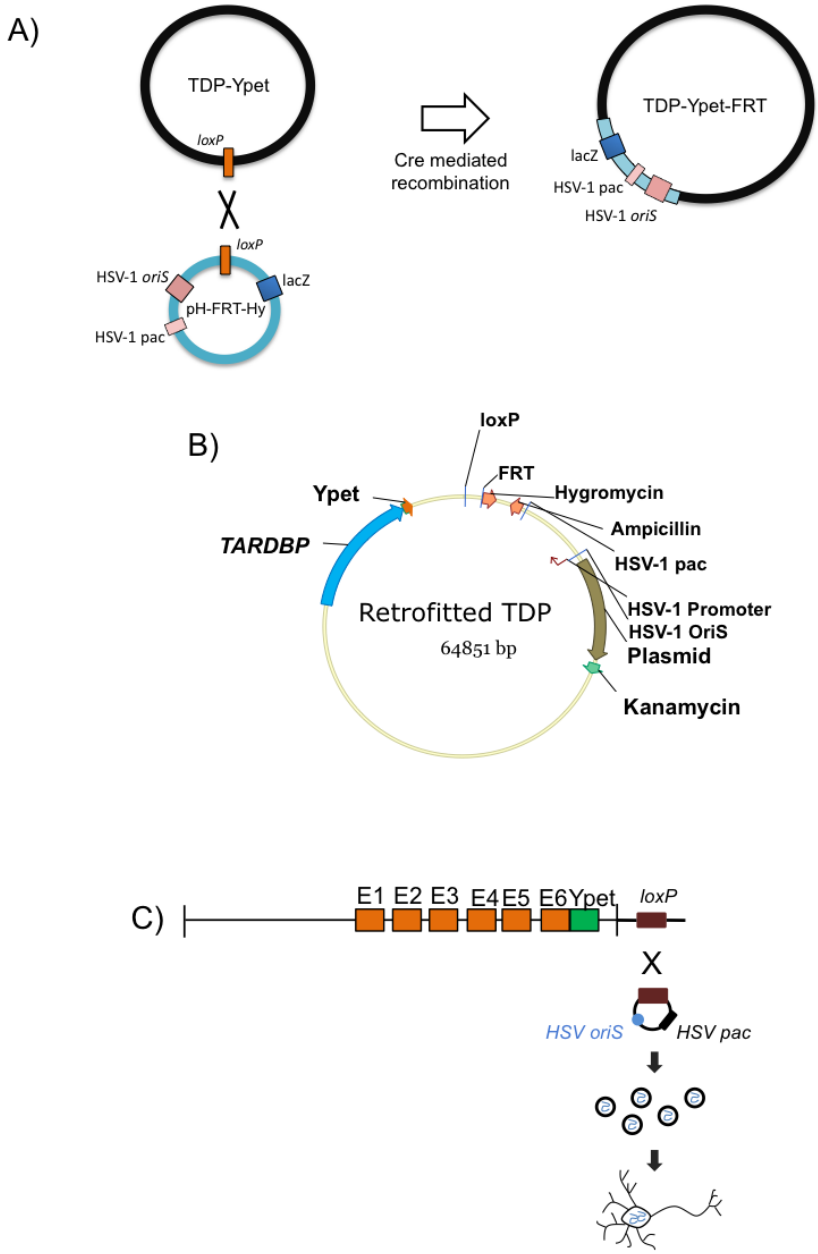

A)
TDP-Ypet
loxP
Cre mediated recombination
TDP-Ypet-FRT
lacZ
HSV-1 pac
HSV-1 oriS
loxP
HSV-1 oriS
lacZ
pH-FRT-Hy
HSV-1 pac
B)
loxP
FRT
Ypet
Hygromycin
Ampicillin
TARDBP
HSV-1 pac
Retrofitted TDP
64851 bp
HSV-1 Promoter
HSV-1 OriS
Plasmid
Kanamycin
C)
E1 E2 E3 E4 E5 E6 Ypet
loxP
X
HSV oriS
HSV pac

Figure 5.8. TDP-43 vectors are packaged in infectious HSV-1 amplicons. A) Schematic representation of the Cre/lox recombination used to retrofit the TDP-43 vectors with pH-FRT-HY plasmid, which carries the HSV-1 elements HSV-1 pac and HSV-1 *oriS*. B) Illustration of the retrofitted TDP-43 vectors shows location of the HSV-1 cassettes in the sequence of the vector. C) Overview of HSV-1 amplicons packaging and neuronal transduction.

5.3.2. Optimization of HSV-1 amplicons infectivity and retention in iPSC-derived motor neurons

In order to determine the minimum amount of HSV-1 amplicon necessary to transduce and express the TDP-43 vectors in iPSC-derived motor neurons, we first packaged a GFP-expressing plasmid in HSV-1 amplicons and used it to assess the infectivity of terminally differentiated motor neurons. Several multiplicities of infection (MOI – viral particles/cell ratio) can be used depending on cell infectivity and amplicon stock titer. For optimization purposes, we used MOI=1, MOI=5 and MOI=10 (Figure 5.9). Motor neurons were transduced on weeks 5 and 6 of differentiation (only week 6 shown), and expression of the GFP plasmid was monitored every 24 hours for one week. No differences in expression were observed between transductions performed on week 5 and week 6, and I chose to transduce the motor neurons with TDP-43 vectors on week 6 due to the advanced maturation state of the motor neurons. While MOI=10 showed highest infectivity and expression of the GFP plasmid, HSV-1 carrying TDP-43 vectors could only be used at MOI=1 due to the low titer obtained by packaging TDP-43 vectors (Figure 5.9).

These results confirm iPSC-derived motor neurons can be transduced by HSV-1 amplicons and that they retain long-term expression of the delivered plasmids. After optimization of the conditions necessary for delivery and retention of HSV-1 amplicons to iPSC-derived motor neurons, the genomic TDP-43 vectors were delivered to the motor neurons and expression was analyzed.

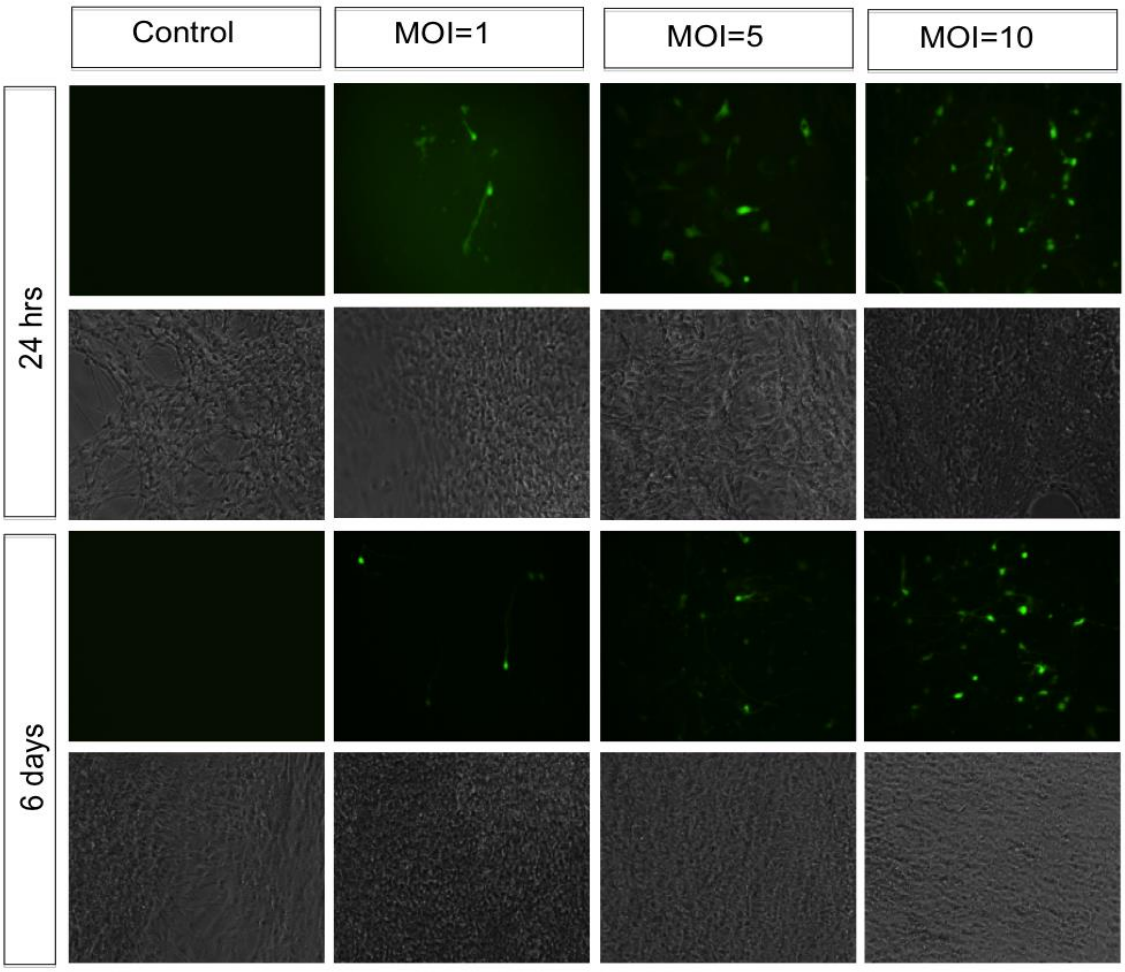

Control
MOI=1
MOI=5
MOI=10
24 hrs
6 days

Figure 5.9. **Optimization of HSV-1 transduction in iPSC-derived motor neurons**. A GFP-expressing plasmid was packaged in HSV-1 amplicons at different multiplicities of infectivity (MOI). MOI=1, 5 and 10 are used in order to determine optimal transduction efficiency. Images are taken 24 hours and 6 days after transduction. The optimal efficiency was determined by estimating the condition with the highest proportion of transduced cells to dead cells.

5.3.3. Genomic TDP-43 vectors were successfully expressed in iPSC-derived motor neurons by HSV-1 amplicons

The HSV-1 amplicons carrying TDP-Ypet, TDP-M337V and TDP-A382T were used to transduce the terminally differentiated iPSC derived motor neurons. The HSV-1 amplicons carrying the TDP-43 vectors, GFP plasmid and the pH-FRT-Hy plasmid were successfully delivered to iPSCs derived motor neurons on week 6 at MOI=1. The GFP plasmid delivered by HSV-1 amplicons was used as positive control and the pH-FRT-Hy was used as negative control for immunostaining (Figure 5.10). Expression was detected by immunostaining against GFP on week 8 (Figure 5.10).

Immunoblotting showed low expression of TDP-Ypet, TDP-M337V and TDP-A382T in iPSC-derived motor neurons (Figure 5.11.A). No differences were observed in protein levels of endogenous TDP-43 between untransduced and transduced motor neurons (Figure 5.11.B). Interestingly, the appearance of a lower molecular weight TDP-43 product at 35 kDa was also detected by western blotting, which appeared to increase in intensity in cells transduced with TDP-M337V (Figure 5.11.C).

These results demonstrate that constructs carrying the entire genomic locus of TDP-43 can be delivered to iPSC-derived motor neurons by HSV-1 amplicons. Since the three vectors carrying TDP-Ypet, TDP-M337V and TDP-A382T showed similar expression

levels of exogenous TDP-43 as assessed by immunocytochemistry, we next investigated whether the presence of TDP-43 mutations induces pathological modifications in TDP-43 subcellular localization in motor neurons.

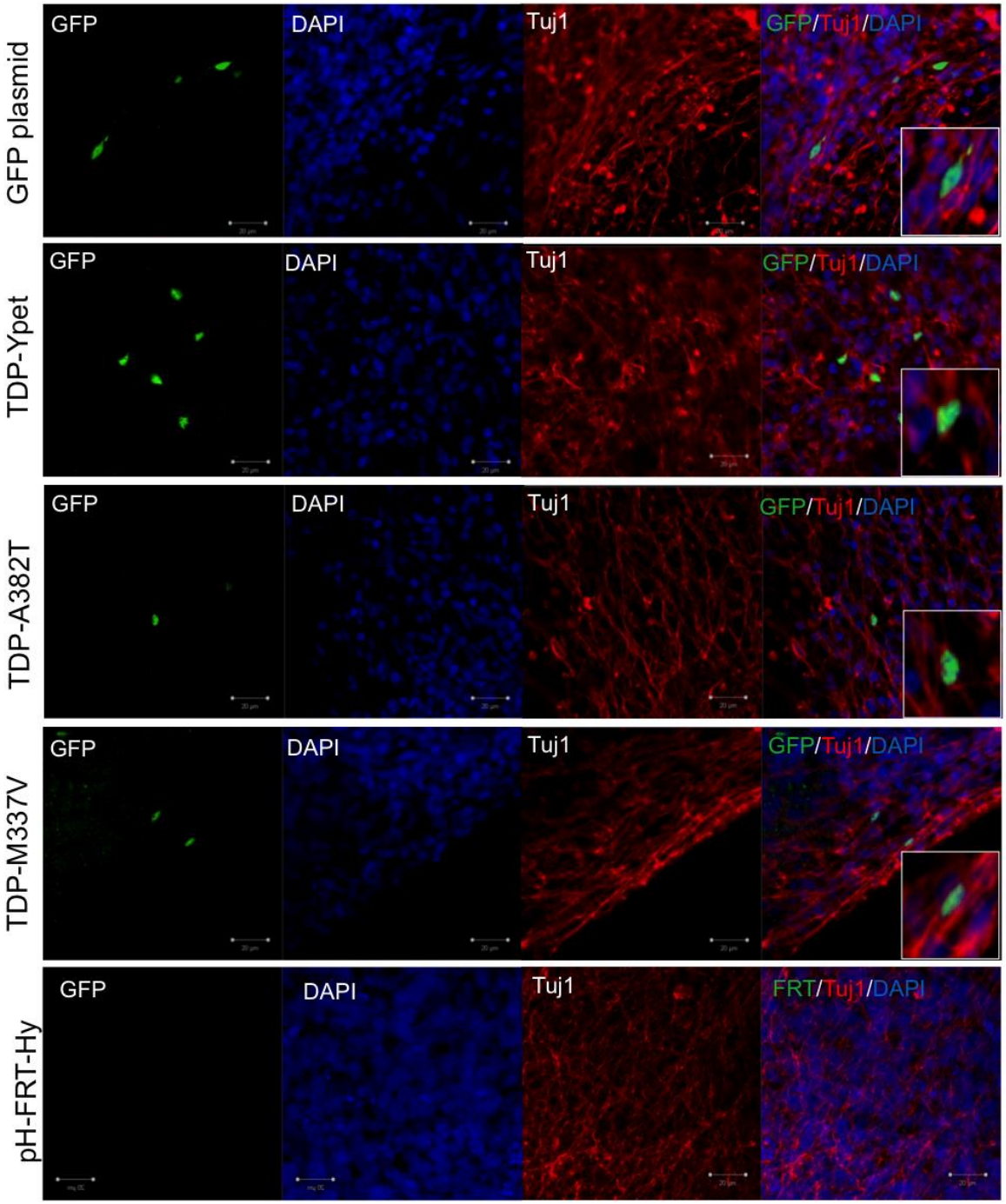


Figure 5.10. HSV-1 amplicons carrying TDP-43 vectors are successfully transduced in iPSC-derived motor neurons. TDP-Ypet, TDP-M337V and TDP-A382T were delivered to iPSC derived motor neurons on day 52 by HSV-1 amplicons (MOI=1). Expression was detected 10 days following transduction by immunostaining for GFP and Tuj1. HSV-1 amplicons carrying a GFP plasmid is used as a positive control and pH-FRT-HY as negative control. Scale bar: 70 µm.

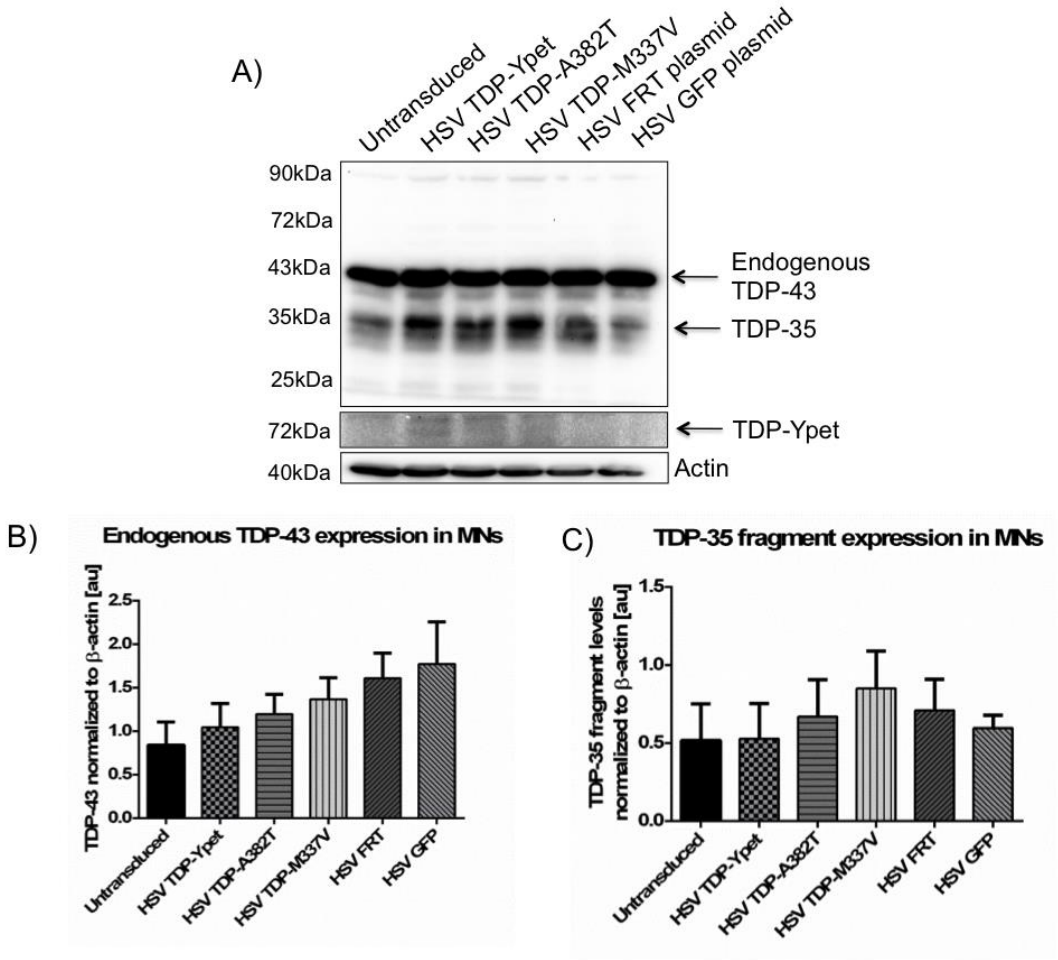

A)
Untransduced
HSV TDP-Ypet
HSV TDP-A382T
HSV TDP-M337V
HSV FRT plasmid
HSV GFP plasmid
90kDa
72kDa
43kDa
35kDa
25kDa
72kDa
40kDa
Endogenous TDP-43
TDP-35
TDP-Ypet
Actin
B)
Endogenous TDP-43 expression in MNs
TDP-43 normalized to β-actin [au]
2.5
2.0
1.5
1.0
0.5
0.0
Untransduced
HSV TDP-Ypet
HSV TDP-A382T
HSV TDP-M337V
HSV FRT
HSV GFP
C)
TDP-35 fragment expression in MNs
TDP-35 fragment levels normalized to β-actin [au]
1.5
1.0
0.5
0.0
Untransduced
HSV TDP-Ypet
HSV TDP-A382T
HSV TDP-M337V
HSV FRT
HSV GFP

Figure 5.11. TDP-43 vectors are expressed in iPSC-derived motor neurons after HSV-1 transduction. A) Immunoblotting for TDP-43 shows high expression of endogenous TDP-43. B) Quantification of band intensity shows similar levels of expression of endogenous TDP-43 between untransduced and transduced motor neurons. C) A cleaved fragment of TDP-43 detected at 35 kDa has similar expression levels in all transduced iPSC-derived motor neurons.

5.4. TDP-43 cytoplasmic mislocalization is detected in iPSC-derived motor neurons following oxidative stress

5.4.1. High oxidative stress induces TDP-43 cytoplasmic mislocalization in healthy motor neurons

There is strong evidence that oxidative stress injury plays a major role in the pathogenesis of motor neuron disease and the effects of oxidative stress on postmitotic neurons are most likely cumulative over the course of years (Barber & Shaw, 2010). ALS patients carrying TDP-43 mutations tolerate these mutations for decades without signs of pathology or motor symptoms, suggesting that the effect of the mutations may be mild, but cumulated with other factors over several decades leads to pathology and disease onset. Since our vectors express TDP-43 at physiological levels under its native promoter, we aimed to model the disease *in vitro* by applying external oxidative stress and analyzing whether mutations enhance toxicity in motor neurons.

To investigate the effects of oxidative stress on subcellular localization of TDP-43 in iPSC-derived motor neurons, untransduced motor neurons were first treated with several concentrations of H_2O_2 for 24 hours. Immunostaining for TDP-43 and Tuj1 was used to determine localization of TDP-43 in the neuronal culture. Endogenous TDP-43 subcellular localization was analyzed following treatment with 0 μM, 50 μM, 250 μM and 500 μM H_2O_2 for 24 hours (Figure 5.12.A). Cytoplasmic mislocalization of endogenous TDP-43 was

observed following treatment with 250 μM and 500 μM H_2O_2 (Figure 5.12.A). Subcellular fractionation was performed on the H_2O_2-treated neuronal culture and illustrative immunoblots suggest increases in cytoplasmic TDP-43 with increasing concentration of H_2O_2 (Figure 5.12.B). Immunoblotting also shows the appearance of a cleaved product of TDP-43 at 35 kDa in the presence of H_2O_2-induced stress (Figure 5.12.B).

5.4.2. High oxidative stress induces TDP-43 cytoplasmic mislocalization in healthy motor neurons carrying TDP-43 mutations

To investigate the effects of H_2O_2 on subcellular localization of mutated TDP-43 in iPSC derived motor neurons, fully differentiated motor neurons were transduced with HSV-1 amplicons carrying TDP-Ypet, TDP-M337V and TDP-A382T on week 6. On week 8, 50 μM, 100 μM, 250 μM H_2O_2 and 500 μM H_2O_2 were added to the medium and cells were fixed after 24 hours for analysis. To specifically investigate the subcellular localization of mutated TDP-43, we used immunostaining for GFP (Figure 5.13). We detected punctae of TDP-Ypet, TDP-M337V and TDP-A382T in the cytoplasm of some motor neurons, but the majority of the cells displayed physiological nuclear TDP-43 (Figure 5.13). Due to the presence of dense neurospheres on the plates and low transduction efficiency, quantification of the cells expressing nuclear or cytoplasmic TDP-43 was not possible.

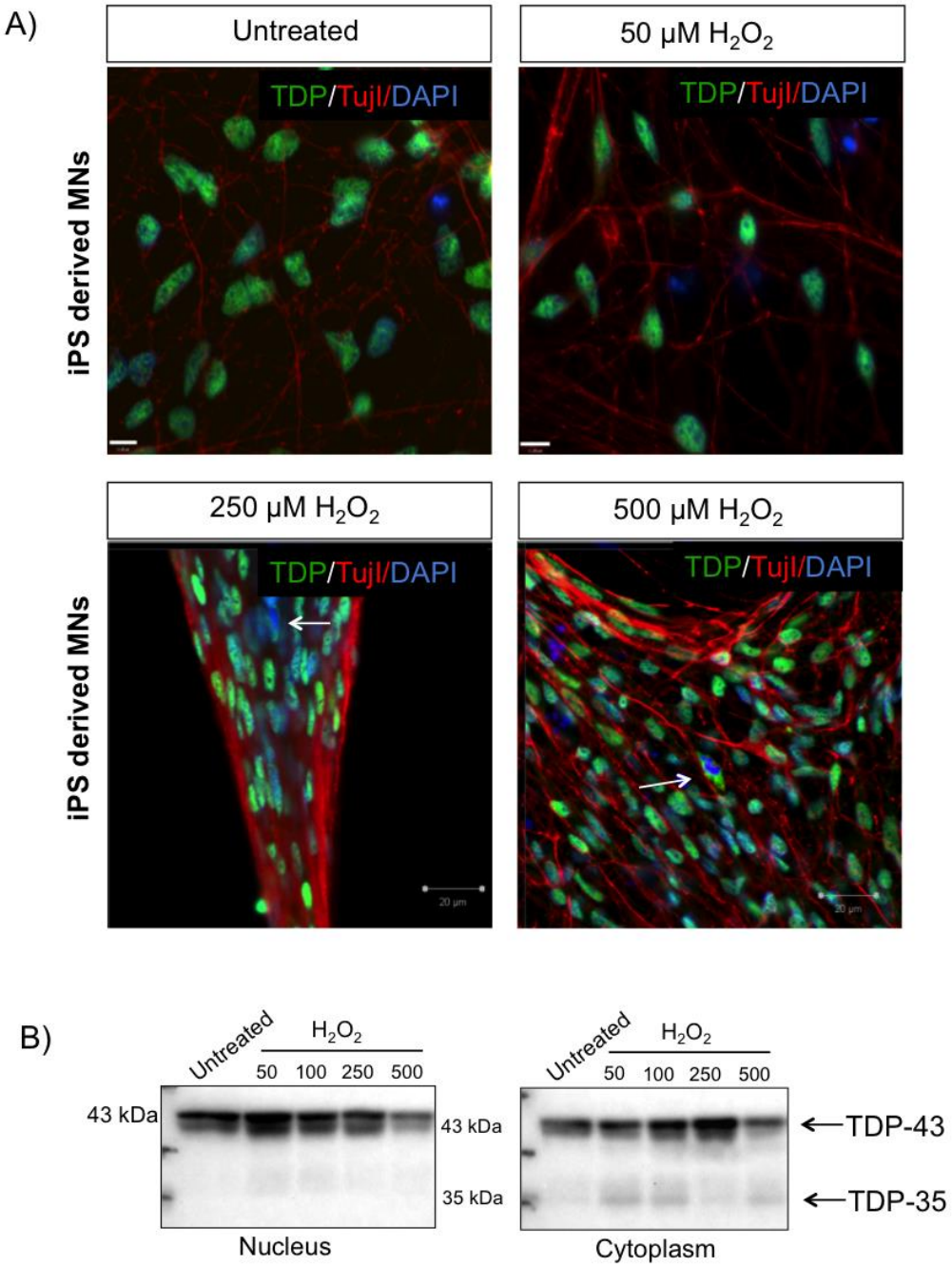


Figure 5.12. Oxidative stress induces endogenous TDP-43 cytoplasmic mislocalization in iPSC derived motor neurons. A) Immunostaining for TDP-43 shows nuclear localization of TDP-43 when iPSC-derived motor neurons are treated with 50 μm H_2O_2 and some neurons show TDP-43 cytoplasmic mislocalization at 250 μm H_2O_2 and 500 μm H_2O_2. B) Immunoblotting shows that oxidative stress triggers the appearance of a fragment of TDP-43 detected at 35 kDa.

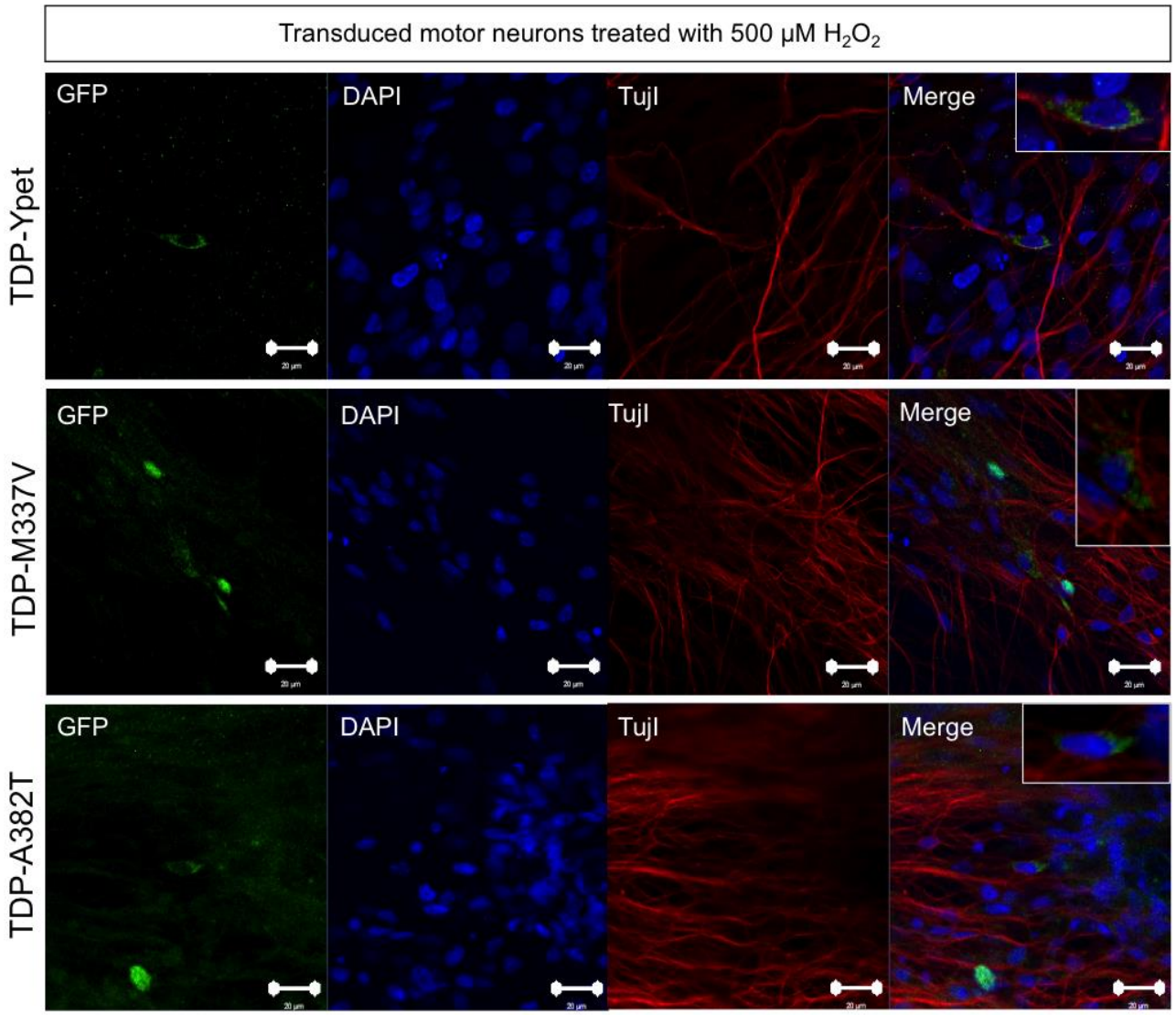


Figure 5.13. TDP-Ypet, TDP-M337V and TDP-A382T form cytoplasmic punctae in iPSC-derived motor neurons in the presence of high oxidative stress. Immunostaining for GFP on day 68 of differentiation, after 24 hours of treatment with 500 μm H_2O_2 shows the formation of cytoplasmic TDP-43 punctae in iPSC-derived motor neurons (HFF1). Scale bar: 20 μm.

5.5. M337V and A382T mutations do not affect neuronal survival

To evaluate the effects of TDP-43 mutations on susceptibility to cell death, iPSC-derived motor neurons were transduced with HSV-1 carrying TDP-43 vectors on week 6 and cell death was assessed two weeks later. Transduced motor neurons were also treated with 500 μM H_2O_2 to ensure detection of otherwise undetectable mildly toxic effects of TDP-43 mutations.

Two weeks following transduction of iPSC-derived motor neurons with TDP-43 vectors as HSV-1 amplicons, the motor neurons were treated with 500 μM H_2O_2 for 24 hours and immunostained against cleaved caspase-3 (Figure 5.14.A). Cell counts showed no significant differences in the number of cells positive for cleaved caspase-3 between the transduced and untransduced motor neurons (Figure 5.14.B). We see a variable effect of oxidative stress on cell death and we did not detect significant differences between TDP-Ypet and TDP-43 mutations.

These results indicate that at low expression levels mutations in TDP-43 do not affect susceptibility to cell death in motor neurons. However, the effects of the mutations may be diminished due to the low transduction efficiency as well as other factors discussed in Chapter 6.

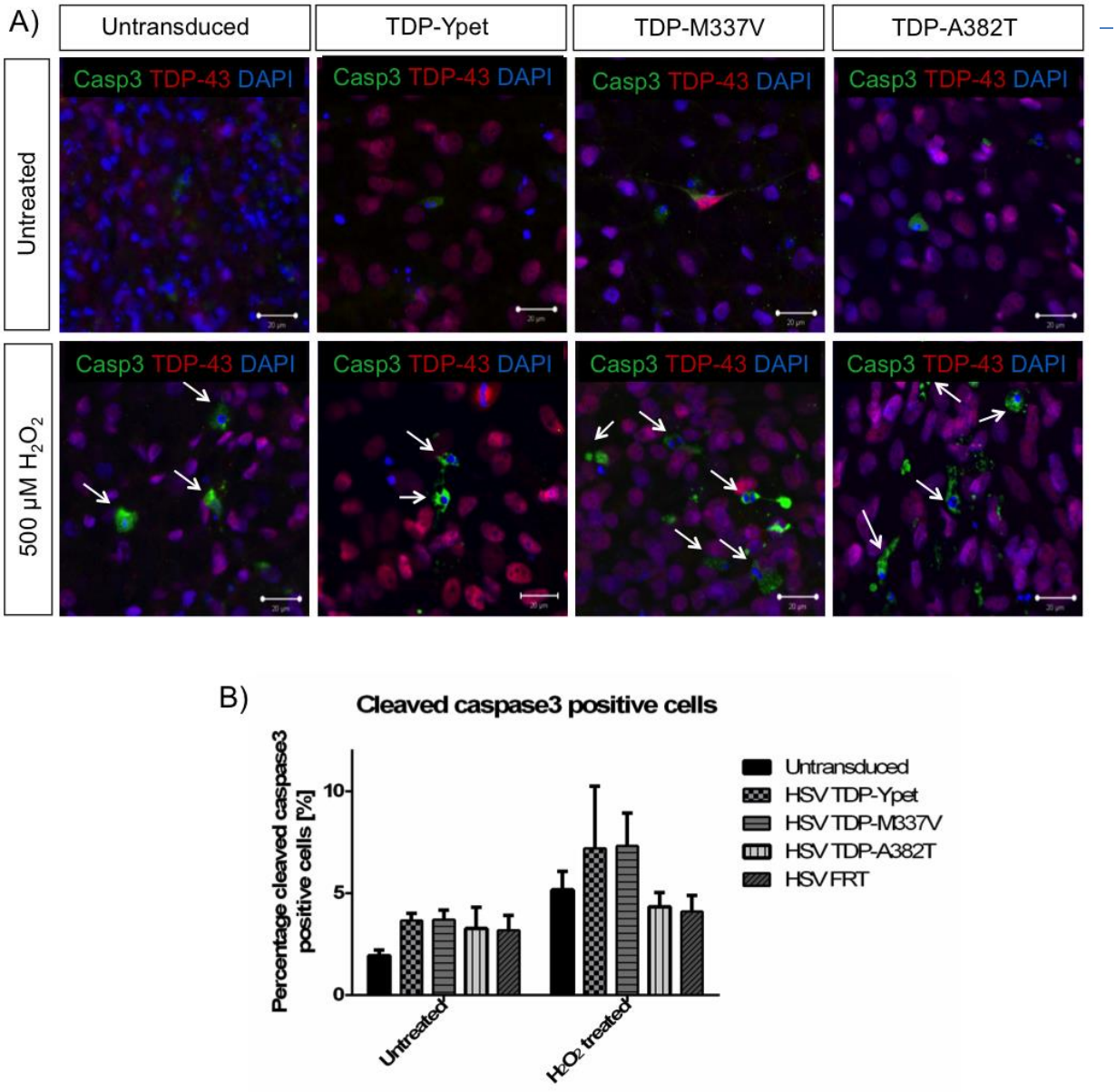


Figure 5.14. TDP-43 mutations do not affect survival of iPSC-derived motor neurons. A) Immunostaining for cleaved caspase-3 apoptotic marker in iPSC-derived motor neurons transduced with TDP-Ypet, TDP-M337V or TDP-A382T that were untreated (top row) or treated with 500 µm H_2O_2 (bottom row); B) Cell counts of cleaved caspase-3 positive cells show no significant differences in the number of apoptotic cells between untransduced, TDP-Ypet, TDP-M337V and TDP-A382T transduced cells (ANOVA). Scale bar: 20 µm.

5.6. ALS patient iPSCs carrying C9orf72 expansions are successfully differentiated to motor neurons

5.6.1. Generation of iPSCs from ALS patients fibroblasts carrying the C9orf72 hexanucleotide repeats using the Sendai virus

Several studies have shown that production of iPS cells from elderly patients diagnosed with familial forms of ALS could be achieved efficiently and that the generated iPSCs possess a genetic signature similar to that of an embryonic stem cell (Bilican et al, 2012; Dimos et al, 2008; Egawa et al, 2012).

We obtained primary skin cells by biopsy from two ALS patients carrying the pathogenic hexanucleotide repeats in C9orf72. The first patient presented with prevalent dementia symptoms and the second showed predominantly motor symptoms. Fibroblasts from these two patients were reprogrammed to a pluripotent state by a novel technique using the Sendai (SeVdp-iPS) vectors by Dr. Sally Cowley, Jane Vowles and Cathy Browne at the Oxford Stem Cell Facility according to a recently established protocol (Nishimura et al, 2011a). Three iPS lines were obtained for each patient and one line of each was used for motor neuron differentiation.

5.6.2. C9orf72 iPSCs can be differentiated to motor neurons

One iPSC line from each patient carrying C9orf72 expansions was differentiated to motor neurons following the previously described protocol (Figure 5.1). The patient lines, C9_Turke and C9_7245 were differentiated in parallel with NHDF1 iPSC control line.

Cellular morphology was assessed throughout the differentiation protocol to ensure correct attachment of EBs to Geltrex-coated plates, formation of neural rosettes, neurospheres and extension of neural structures in the final stages (Figure 5.15).

At the end of the differentiation protocol, the assessment of motor neuron differentiation efficiency was done by immunostaining. We found that both ALS patient derived lines, C9_Turke and C9_7245 successfully differentiated to motor neurons positive for Islet-1/Tuj1 at similar efficiencies to NHDF1 (Figure 5.16). The presence of the hexanucleotide repeats in C9orf72 iPSCs did not seem to influence differentiation efficiency to motor neurons.

After confirming the efficient differentiation of C9orf72 patient derived iPSCs to motor neurons, we investigated the contribution of TDP-43 pathology to the disease caused by C9orf72 pathological expansions.

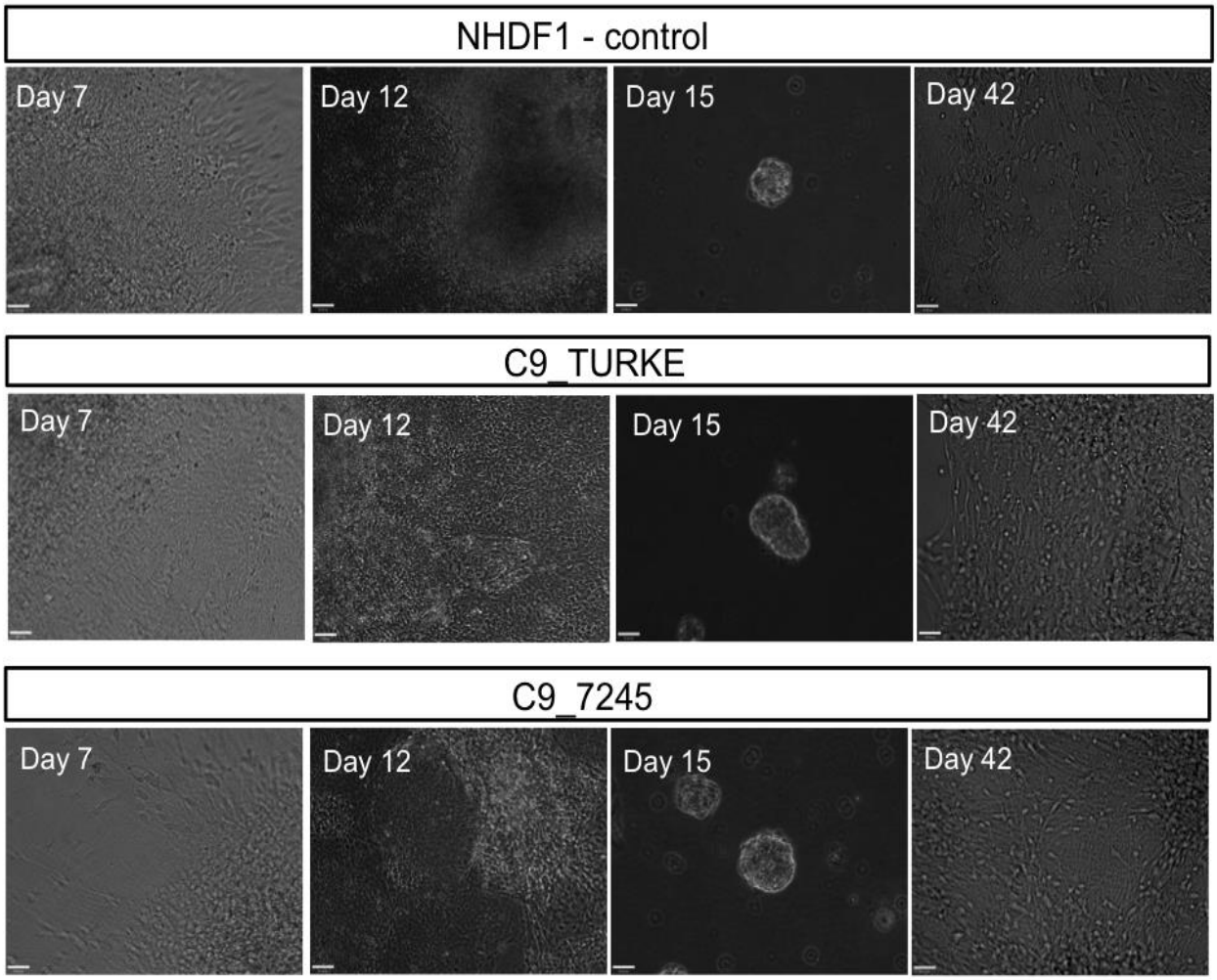


Figure 5.15. C9orf72 iPSCs can be differentiated to motor neurons. Bright field images show cellular morphology typical of motor neuron differentiation in NHDF1 (control) and 2 iPS lines from 2 different ALS patients carrying C9orf72 pathogenic expansions (C9_Turke and C9_7245). Images show attachment of the EBs to the Geltrex coated plates on day 7, formation of neural rosettes and neural tube-like structures after exposure to 0.1 µM RA on day 12, formation of neurospheres in the presence of 100 ng/ml SHH on day 15, and extension of axons and dendrites in the final stage of differentiation on day 42. Scale bars: 20 µm (days 7, 12 and 42), 70 µm (day 15).

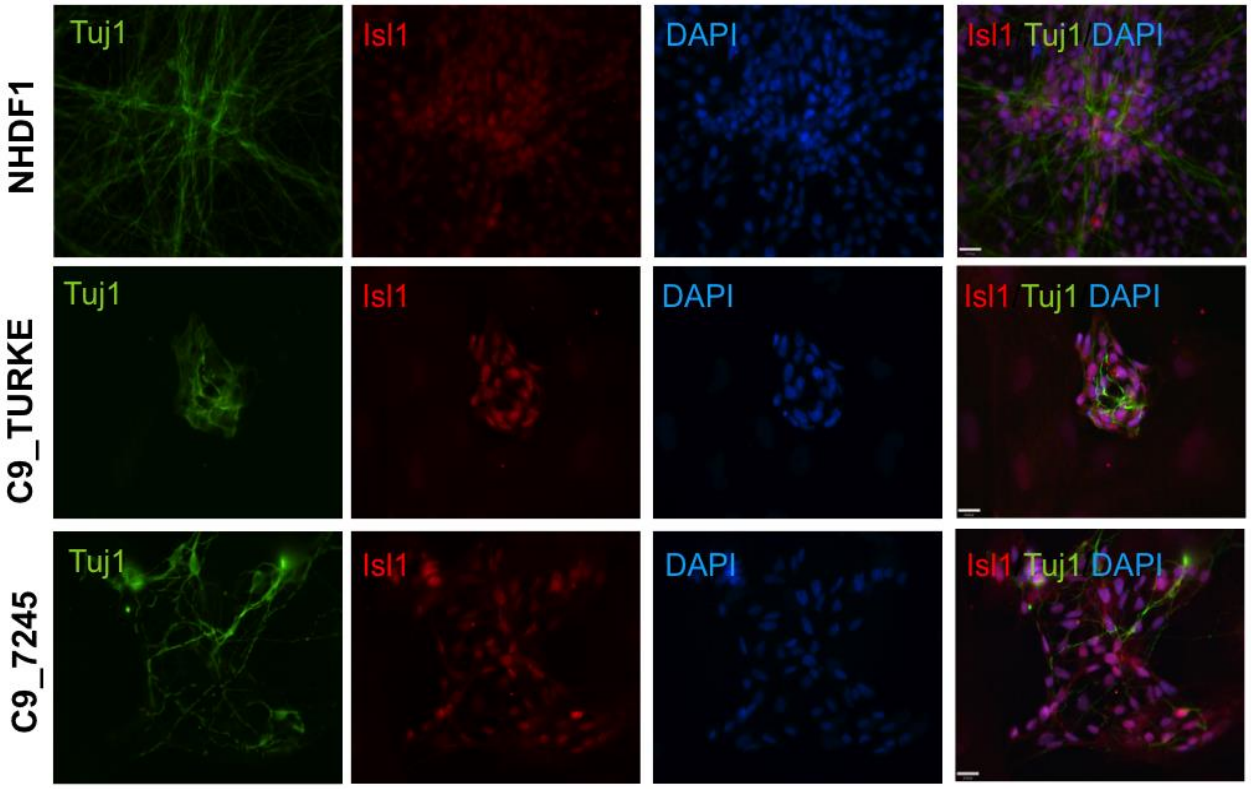


Figure 5.16. C9orf72 iPSC-derived motor neurons express characteristic motor neuron markers. Immunostaining shows a high percentage of Tuj1 positive neurons co-expressing the motor neuron marker Islet-1 (Isl1) in the neuronal population obtained by differentiation of two C9orf72 iPSC lines, C9_Turke and C9_7245. Scale bar: 20 µm.

5.7. Preliminary results suggest C9orf72 motor neurons display functional dysregulations

5.7.1. TDP-43 pathology is not present in the C9orf72 motor neurons

Alterations in C9orf72 have been previously found to correlate well with high levels of protein aggregations found in the cytoplasm that contain the protein TDP-43 and

neuropathology demonstrated that TDP-43 aggregation remained a core feature of C9orf72 related ALS cases (King et al, 2012).

We investigated subcellular localization of endogenous TDP-43 in the C9orf72 iPSC derived motor neurons to determine whether TDP-43 pathology associated with the two lines of C9orf72 cases. The fully differentiated motor neurons were fixed and immunostained for TDP-43 and Tuj1 (Figure 5.17.A). Under basal conditions, we did not detect aberrant translocation of endogenous TDP-43 to the cytoplasm in the C9orf72 motor neurons (Figure 5.17.A).

These preliminary results show that TDP-43 pathology is not present in the motor neurons derived from C9orf72 iPSCs of 2 ALS patients. We next analyzed physiological modifications in the C9orf72 motor neurons, focusing on ER Ca^{2+} homeostasis.

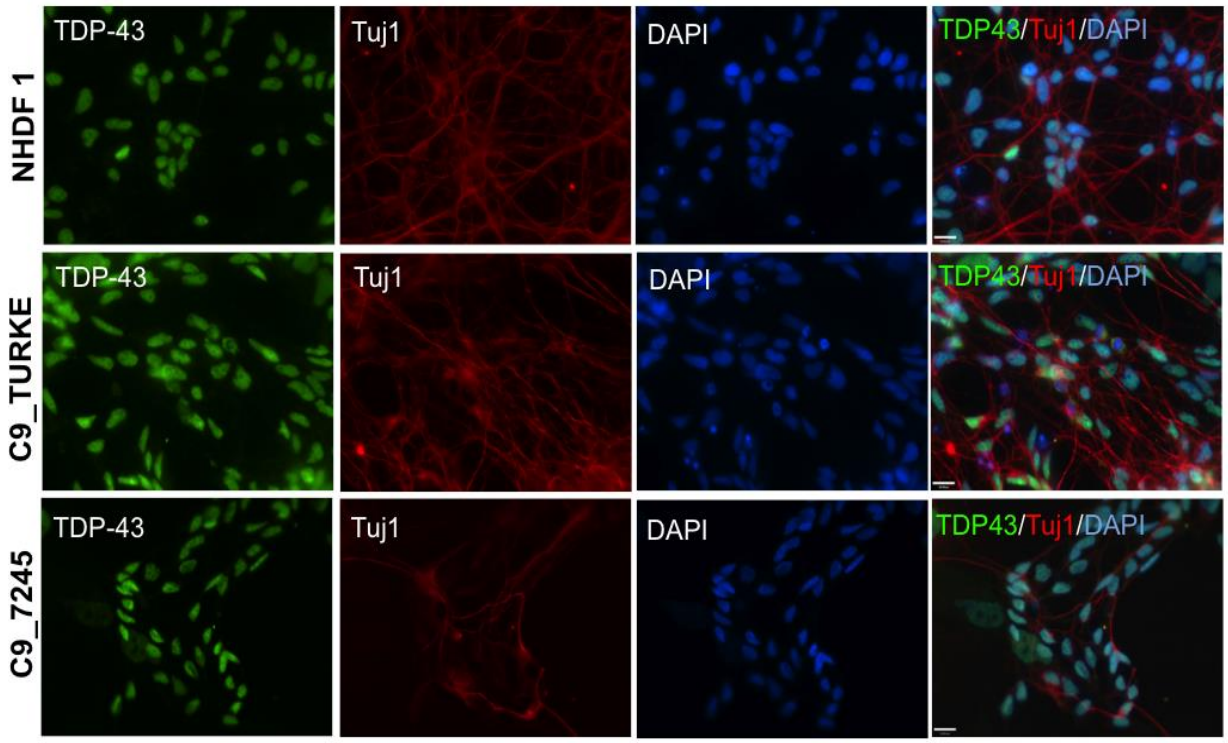


Figure 5.17. **C9orf72 iPSC derived motor neurons do not show TDP-43 pathological cytoplasmic mislocalization.** Immunostaining for TDP-43 and Tuj1 in C9_Turke and C9_7245 motor neurons shows physiological nuclear localization of endogenous TDP-43. Scale bar: 20 µm.

5.7.2. ER Ca^2 signalling is impaired in a C9orf72 patient line differentiated to motor neurons

Although a direct link between calcium signalling and C9orf72 expansions has not yet been established, calcium dysregulation is a major player in the pathogenesis of ALS. We therefore aimed to investigate whether C9orf72 expansions influence Ca^{2+} homeostasis in iPSC derived motor neurons.

In order to investigate Ca^{2+} signalling, I analyzed levels of ER Ca^{2+} stores and total intracellular stores. For the analysis of ER Ca^{2+} stores content, I imaged fully differentiated motor neurons from 8 separate cultures of one single differentiation for each cell line (NHDF1, C9_Turke, C9_7245). The motor neurons were incubated with the Ca^{2+} binding dye Fluo-4 AM for 30 minutes and the medium was then replaced with Ca^{2+} free medium for recordings. The recordings were performed using pharmacological stimulation, as described in Chapter 4 for HEK293 clonal cell lines. In the absence of a fluorescent motor neuron reporter, recordings were only made in cells displaying a clear neuronal morphology.

To assess total ER Ca^{2+} stores content, 10 μM thapsigargin (TG) was applied to the motor neurons and the peak increase in fluorescence intensity resulting from ER Ca^{2+} depletion into the cytoplasm was measured (Figure 5.17.A). We detected significantly higher levels of ER Ca^{2+} content in the C9_7245 motor neurons, which showed an increase in fluorescence of $\Delta F/F_0$=1.30±0.09 (mean±SEM), compared to NHDF1 which had an increase in fluorescence of $\Delta F/F_0$=0.88±0.08 (p<0.01, ANOVA). A trend for increased ER Ca^{2+} content was also detected in C9_Turke motor neurons, which showed $\Delta F/F_0$=0.99±0.08 (Figure 5.18.B).

Total intracellular Ca^{2+} stores were assessed by pharmacological stimulation of Ca^{2+} depletion from all organelles induced by ionomycin. Measurement of total intracellular Ca^{2+} stores was achieved by addition of 1 μM of ionomycin one to two minutes after recovery of intracellular Ca^{2+} balance from TG application (Figure 5.18.A). We found that overall intracellular Ca^{2+} levels were higher in C9_7245, which had a $\Delta F/F_0$=2.46±0.3 (mean±SEM), compared to NHDF1 which exhibited $\Delta F/F_0$=1.60±0.3 (p<0.01, ANOVA) (Figure 5.18.C). The motor neurons derived from C9_Turke patient line showed a trend towards high intracellular levels with $\Delta F/F_0$=2.09±0.3, but did not reach significance levels (Figure 5.18.C).

Calcium release from the ER was analyzed by carbachol stimulation, as described in Chapter 4. Recordings were only made in cells that did not exhibit spontaneous Ca^{2+} activity. Eight different cultures from each cell line were loaded with Fluo-4AM for 30 minutes and recording was performed under continuous perfusion of physiological Ca^{2+} free medium with 50 μM carbachol. The highest peak resulting from the carbachol specific increase in fluorescence was measured to determine the ER Ca^{2+} release amplitude. Results showed significantly decreased amplitude of ER Ca^{2+} release in C9_7245 motor neurons, which showed $\Delta F/F_0$=0.44±0.2 (mean±SEM), compared to NHDF1 $\Delta F/F_0$=0.96±0.1 (p<0.05, ANOVA) (Figure 5.18.D). The motor neurons derived from C9_Turke ALS patient line showed similar ER Ca^{2+} release amplitude to NHDF1, with $\Delta F/F_0$=0.96±0.1 (Figure 5.18.D).

These preliminary results performed on one single differentiation of the C9orf72 iPSCs suggest a potential Ca^{2+} signalling dysregulation in the motor neurons carrying pathological C9orf72 expansions. In contrast to the findings in HEK293 carrying TDP-43

mutations, the C9orf72 expansions tend to associate with intracellular Ca^{2+} overload, specifically in the ER, while TDP-43 mutations associate with reduced ER Ca^{2+} content.

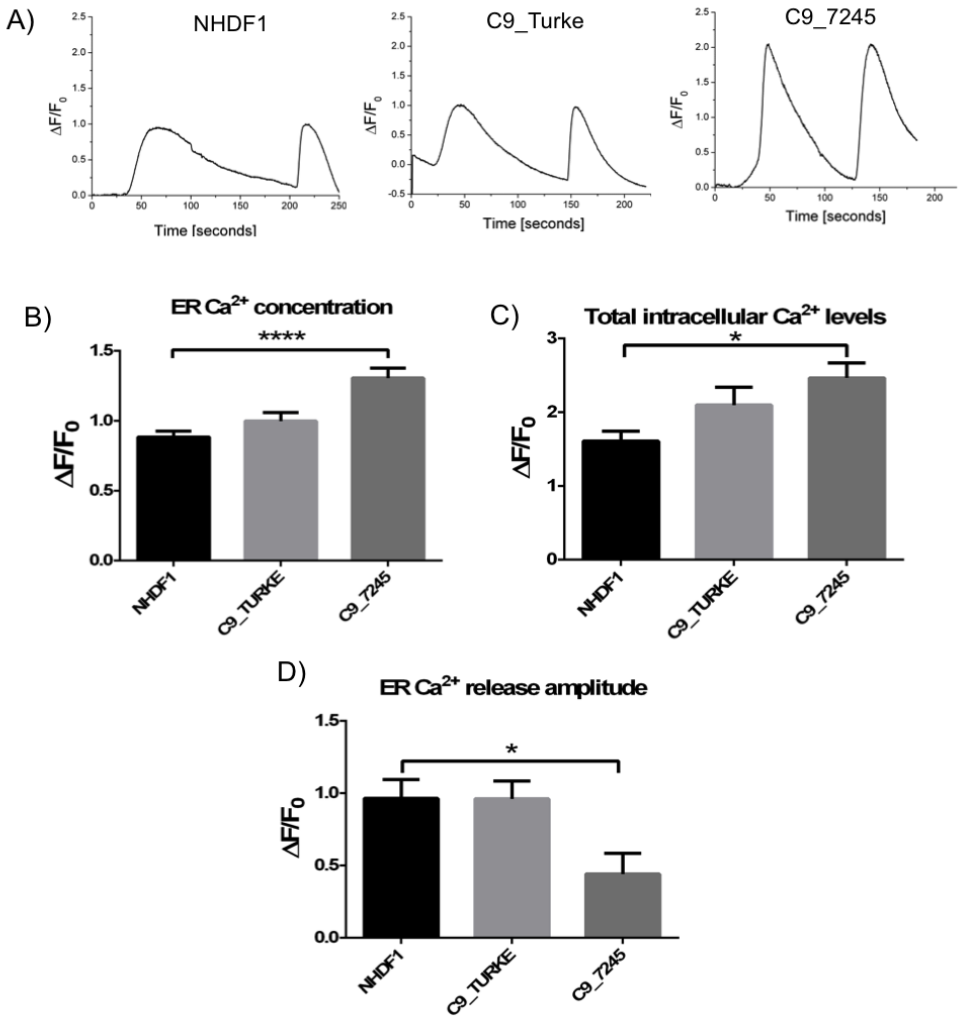


Figure 5.18. High ER calcium concentration and high intracellular calcium are detected in motor neurons derived from C9_7245 iPSCs. A) Representative fluorescent traces detected on stimulation with 10 µM TG (first peak) and 1 µM ionomycin (second peak) in NHDF1, C9_Turke and C9_7245 motor neurons after loading with Fluo-4 AM calcium binding dye in Ca^{2+}-free HBSS medium. B) Amplitude of the first calcium peak elicited in response to TG stimulation was measured after background subtraction and normalization using ImageJ software and it shows average values for NHDF1 $\Delta F/F_0$=0.88±0.08 (mean±SEM), C9_Turke $\Delta F/F_0$=0.99±0.08 and C9_7245 $\Delta F/F_0$=1.30±0.09. The increase in fluorescence in C9_7245 on TG stimulation was significantly higher than NHDF1 (***p<0.01, ANOVA). C) Total intracellular Ca^{2+} levels were assessed by measuring the height of the Ca^{2+} peak resulting from ionomycin stimulation and C9_7245 had significantly elevated total intracellular Ca^{2+}, exhibiting an average increase in fluorescence $\Delta F/F_0$=2.46±0.3 (mean±SEM), compared to NHDF1 $\Delta F/F_0$=1.60±0.3 and C9_Turke $\Delta F/F_0$=2.09±0.3 (***p<0.01, ANOVA). D) ER Ca^{2+} release measured as the height of the highest Ca^{2+} peak recorded during 4 minutes of continuous exposure to 50 µM carbachol. C9_7245 shows significantly reduced ER Ca^{2+} release, with $\Delta F/F_0$=0.44±0.2, compared to NHDF1 $\Delta F/F_0$=0.96±0.1 and C9_Turke $\Delta F/F_0$=0.96±0.1 (*p<0.05, ANOVA).

5.7.3. Downregulation of Bcl-2 and upregulation of GRP78/BiP and p62 were detected in C9orf72 motor neurons

Detection of ER Ca^{2+} signalling dysregulation associated with C9orf72 expansions lead to the investigation of proteins associated with ER stress and common mediators of ER Ca^{2+} regulation.

The antiapoptotic protein Bcl-2, which is an important player in modulating ER Ca^{2+} release through IP_3R, was found to be significantly downregulated in motor neurons derived from C9_7245 iPSC patient line compared to NHDF1 ($p<0.05$, ANOVA) (Figure 5.19.A). A trend for decreased Bcl-2 levels was also detected in C9_Turke iPSC derived motor neurons.

Next, we investigated levels of sequestosome-1/p62 and GRP/BiP proteins. In addition to its frequent association with aggregates in C9orf72 patient cases, p62 is also a marker of the unfolded protein response (UPR) and ER stress. We found elevated levels of p62 in motor neurons derived from both C9orf72 iPSC patient lines, with C9_7245 showing the highest p62 levels (Figure 5.19.B). Furthermore, we found significantly elevated levels of GRP78/BiP protein in C9_7245 motor neurons compared to NHDF1 motor neurons (Figure 5.19.C) ($p<0.05$, ANOVA).

These preliminary results suggest an association between C9orf72 expansions and reduced levels of the antiapoptotic protein Bcl-2 in parallel with upregulation of ER stress markers GRP78/BiP and p62.

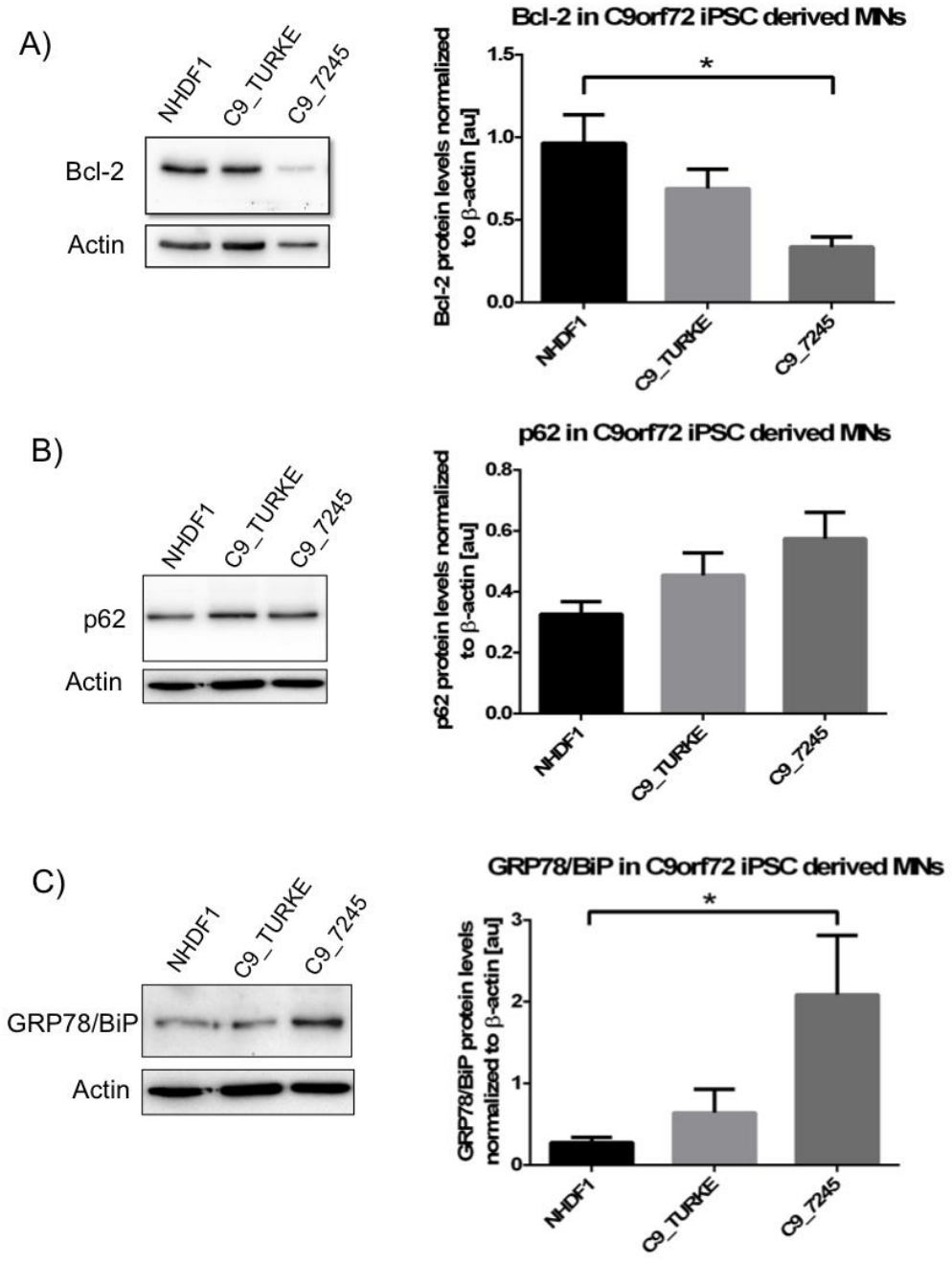


Figure 5.19. C9_7245 motor neurons show downregulation of Bcl-2 and elevation of ER stress markers p62 and GRP78/BiP. A) Immunoblotting on NHDF1, C9_Turke and C9_7245 motor neurons shows reduction in Bcl-2 levels in C9_7245 (*p<0.05, ANOVA) compared to NHDF1 motor neurons. B) Immunoblotting for p62 shows a trend for increased levels of p62 in both lines of C9orf72 derived motor neurons. C) Immunoblotting shows significantly increased protein levels of GRP78/BiP stress markers in C9_7245 motor neurons (*p<0.05, ANOVA).

5.8. Conclusions

In this chapter, stem cell technology was used to generate iPSCs from the fibroblasts of healthy and C9orf72 ALS patients and these cells were differentiated to motor neurons for functional investigations.

I obtained thoroughly characterized iPSCs from the Oxford Stem Cell Facility and successfully directed their differentiation to motor neurons according to a previously established protocol (Hu & Zhang, 2009). Several modifications have been made in order to increase efficiency and reduce cell death.

Analysis of gene and protein expression showed specific expression of motor neuron genes throughout the differentiation protocol. Using RT-PCR, I observed increasing levels of Nkx6, Pax6, Olig2 and ChAT, demonstrating the specificity of the differentiated cells.

In addition to assessment of motor neuron-specific molecular markers, I also investigated functional aspects of the motor neurons and demonstrated the ability of iPSC derived motor neurons to produce spontaneous Ca^{2+} transients and respond to exogenous stimulation of Ca^{2+} channels. Spontaneous oscillations in intracellular Ca^{2+} under resting conditions have been previously shown in ES derived motor neurons and their characteristics are generally consistent with the firing of action potentials (Boulting et al, 2011; Karumbayaram et al, 2009). I also observed that networks of cells appeared synchronized between several cells in vicinity to one another, suggesting a functional network was produced between the differentiated motor neurons, similar to previous *in vivo* observations during the development of the spinal cord (Hanson & Landmesser, 2003). The increases in cytosolic Ca^{2+} as a response to KCl and kainate exposure showed that the cells have ionotropic glutamate receptors and voltage-gated Ca^{2+} channels.

Having confirmed the motor neuron differentiation protocol, I investigated the effects of TDP-43 mutations in healthy motor neurons. The delivery of TDP-43 vectors to fully differentiated motor neurons was successfully achieved by HSV-1 amplicons, which have been previously used to efficiently transduce many different cell types including post mitotic cells.

Under basal conditions, cytoplasmic mislocalization was not detected in the iPSC-derived motor neurons transduced with TDP-43 vectors. Functional assays on the transduced motor neurons showed that TDP-43 cytoplasmic mislocalization could be induced by oxidative stress, but TDP-43 mutations do not potentiate the effect and do not induce apoptosis. High levels of the 35 kDa C-terminal fragment of TDP-43 (TDP-35) were detected in both untransduced and HSV-1 transduced iPSC-derived motor neurons, without significant increases in the presence of the mutations. Previous studies showed that caspase mediated cleavage of TDP-43 generates C-terminal fragments of 35kDa and 27kDa in cultured neuronal cells, which are prone to cytoplasmic aggregation (Suzuki et al, 2011).

Induced pluripotent stem cells were derived at the Oxford Stem Cell Facility from fibroblasts of ALS patients carrying the newly discovered C9orf72 pathogenic expansions and I differentiated them to motor neurons using the described protocol. The patient-derived iPSC could be successfully differentiated to mature motor neurons, at similar efficiencies to the control lines NHDF1 and HFF1, demonstrating that the presence of pathogenic hexanucleotide repeats in C9orf72 does not affect motor neuron specification.

Motor neurons derived from C9orf72 ALS patient iPSCs were examined for TDP-43 pathology, but no cytoplasmic mislocalization of TDP-43 was detected. It has recently been established that TDP-43 aggregation is a main feature of ALS cases carrying C9orf72

expansions and neuropathology has shown that TDP-43 positive neuronal cytoplasmic inclusions are present in the frontal and temporal lobe of ALS patients (King et al, 2012).

Although we did not detect TDP-43 pathology in the *C9orf72* iPSC derived motor neurons, we detected increased levels of ER stress markers GRP78/BiP and p62 in the C9_7245 motor neurons, which are derived from fibroblasts of the patient showing a more severe motor phenotype than C9_Turke. The C9orf72-associated cases also show cerebral pathology characterized by abundant cytoplasmic and intranuclear inclusions positive for ubiquitin and sequestosome-1/p62 (Bieniek et al, 2012; Troakes et al, 2012). We can hypothesize that disturbances in normal RNA processing caused by the expansions in *C9orf72* may lead to erroneously assembled proteins, which increase aggregate formation and result in high ER stress.

Abnormal ER Ca^{2+} homeostasis was detected in the motor neurons displaying increased ER stress. Preliminary experiments suggested ER Ca^{2+} overload in motor neurons differentiated from a *C9orf72* patient iPSC line, accompanied by reduced levels of the antiapoptotic protein Bcl-2. Taken together, these results suggest that disruption of Ca^{2+} homeostasis may be an early event in ALS pathogenesis and together with ER stress may play a key role in Bcl-2 mediated cell death of affected motor neurons.

In summary, this chapter describes the generation of iPSCs from healthy and ALS patients fibroblasts and their differentiation to functional motor neurons. TDP-43 pathology was only detected in human motor neurons following high oxidative stress and TDP-43 mutations did not have an effect on cell survival. Preliminary experiments have shown that iPSCs derived from ALS patients with C9orf72 pathogenic expansions can be successfully differentiated to mature motor neurons. The C9orf72 iPSC-derived motor neurons showed dysfunction in Ca^{2+} homeostasis and high ER stress correlating with decreased Bcl-2 protein

levels. Further investigations in several different iPSC lines will be necessary to confirm the initial findings in the C9orf72 motor neurons.

CHAPTER 6

General discussion and future directions

The lack of physiologically-relevant models for ALS has hampered the advancement of research and understanding of the processes underlying motor neuron pathology. In the first part of this study, the molecular mechanisms of TDP-43 mutations are investigated in cellular models obtained by site-specific genomic integration of full-length genomic *TARDBP* constructs with ALS-associated mutations. In the second part of this study, iPSC technology is used to generate motor neurons from the fibroblasts of healthy volunteers and ALS patients carrying the novel *C9orf72* pathogenic expansions and pathogenic modifications are investigated.

A novel full-length genomic *TARDBP* BAC construct was engineered that carried the upstream regulatory sequences of the endogenous promoter along with intronic and exonic sequences of the *TARDBP* gene. Since TDP-43 function has been shown to vary with protein expression levels, our genomic constructs override the difficulties previously encountered with cDNA constructs which overexpress TDP-43 and lead to high toxicity followed by premature cell death (Barmada et al, 2010).

Even though TDP-43 is a predominantly nuclear protein, it is synthesized in the cytoplasm and it is capable of shuttling between the nuclear and cytoplasmic compartments (Ayala et al, 2008; Winton et al, 2008). In order to facilitate the visualization of the protein expressed by the vectors, a Ypet fluorescent tag was fused to the C-terminus of TDP-43. The C-terminus was chosen because C-terminal cleavage products were found in the cytoplasmic inclusions in FTLD and ALS (Neumann et al, 2006) and the C-terminal fragments were previously shown to have a high aggregation propensity (Yang et al, 2010). Furthermore, most mutations associated with ALS are located in the C-terminal domain of TDP-43, indicating a strong link between this domain and pathological mechanisms (Daoud et al, 2009; Pesiridis et al, 2009). Three mutations were chosen to be engineered in exon 6 according to their previously reported level of pathogenicity: A382T, M337V and Y374X. However, the Y374X mutation was not pursued in functional investigations because of difficulties in discriminating between TDP-43 carrying the Y374X mutation and endogenous TDP-43 as the Ypet fused C-terminus was truncated.

6.1. TDP-43 pathology in stable human cell lines

Functional assays on site-specific BAC HEK293 clonal cells revealed that two ALS-specific mutations, A382T and M337V, increased TDP-43 cytoplasmic mislocalization. Cytoplasmic inclusions of phosphorylated, polyubiquinated TDP-43 represent the defining feature of FTLD-TDP and ALS (Neumann et al, 2006; Pesiridis et al, 2009), but the contribution of pathological TDP-43 mislocalization to neurodegeneration remains unknown.

It has previously been established in cellular and transgenic overexpression models of TDP-43 that increased levels of either wild-type or mutant TDP-43 in the cytoplasm correlate with high toxicity and cell death (Barmada et al, 2010; Lagier-Tourenne et al, 2010; Wegorzewska & Baloh, 2011), but this is the first report of pathology in a physiological cell model.

In our cellular model, the expression level of exogenous TDP-43 was significantly lower than the endogenous level of TDP-43. At relatively low expression levels, TDP-43 mutations were able to induce a detectable phenotype even in the presence of compensatory endogenous TDP-43, which indicates a potential toxic gain of function mechanism.

In a recent study, TDP-43 protein was shown to autoregulate its synthesis by binding to its 3' untranslated region of its own mRNA in a negative feedback look (Ayala et al, 2011). This was proposed as a potential mechanism for the pathogenic formation of TDP-43 cytoplasmic aggregations. An initiating insult may trap TDP-43 in the cytoplasm leading to a reduction in 3' UTR splicing and to the subsequent generation of an elevated pool of stable TDP-43 mRNA in the cytoplasm (Polymenidou et al, 2011). The elevated TDP-43 expression in the cytoplasm that I observed in the TDP-M337V transfected cells could follow a similar mechanism of action.

Autophagy and ER stress were not associated with the differences in cell survival and cytoplasmic mislocalization of TDP-43 in the mutation-bearing cells. TDP-43 has been recently shown to be involved in the regulation of autophagy by regulating ATG7 mRNA (Bose et al, 2011). ATG7 is essential in macroautophagy and its mRNA is downregulated upon TDP-43 knockdown (Bose et al, 2011), which in turn leads to an elevation in sequestosome-1/p62 marker of the unfolded protein response (UPR). In our model, there were no differences in protein levels of autophagy and ER stress markers, suggesting that the

mutations induce pathology through a different mechanism and the physiological effects I detect are specific consequences of TDP-43 mutations and do not represent measurements of cellular stress effects.

When ER stress was induced by thapsigargin (TG), increased frequency of cytoplasmic TDP-43 punctae was detected in cells carrying the M337V mutation. Similar TDP-43 cytoplasmic punctae have been previously reported and were associated with stress granules, and their frequency in cells carrying TDP-43 ALS-specific mutations could be increased by oxidative stress (McDonald et al, 2011). Nuclear punctae were also formed in the presence of ER stress in TDP-A382T and TDP-Ypet. Similar nuclear punctae were also previously reported in FTLD-U pathology and ALS, where TDP-43 exhibited a characteristic 'cat eye' morphology in the nucleus and was also considered to be mislocalized (Neumann et al, 2006) and associated with mutations in the gene encoding progranulin (*PRGN*) (Neumann et al, 2006) and the valosin containing protein (VCP) (Sampathu et al, 2006).

ER stress induced by TG significantly increased cytoplasmic mislocalization of TDP-Ypet and TDP-A382T, which could partially recapitulate the phenotype observed in TDP-M337V. Treatment with TG did not affect the already high cytoplasmic levels of TDP-M337V. Since TG acts by inhibition of the Ca^{2+}-ATPase pump on the ER, we hypothesized that ER Ca^{2+} signalling may mediate the pathological effects observed in TDP-M337V and investigated differences in ER Ca^{2+} dynamics.

The Ca^{2+} signalling findings in this study showed that TDP-43 mutations impair ER Ca^{2+} regulation. Decreased and delayed Ca^{2+} release from the ER was detected in cells carrying TDP-M337V and TDP-A382T, which correlated with low ER Ca^{2+} content. Depletion of ER Ca^{2+} has been previously shown to potently inhibit signal mediated nuclear transport through the nuclear envelope (Greber & Gerace, 1995). Such a mechanism may trap

TDP-43 in the cytoplasm in M337V mutation carrying cells, where it may gain a toxic function and contribute to cell death. Disturbances in intraluminal ER Ca^{2+} concentration lead to the perturbation of intracellular Ca^{2+} homeostasis, which may have an impact on mitochondrial functioning, cell death and protein trafficking (Berridge et al, 2000). Many physiological processes are mediated by Ca^{2+} oscillations originating from the ER, with information being encoded by the frequency as well as the amplitude of Ca^{2+} spikes (Berridge et al, 2000). Any dysregulation of the complex patterns of Ca^{2+} oscillations will be transmitted downstream to Ca^{2+}-sensitive phosphatases and kinases, which are involved in the regulation of apoptosis.

Upregulation of the antiapoptotic protein Bcl-2 was detected in cells carrying the A382T and M337V mutations. There is an increasing body of evidence showing that modulation of ER Ca^{2+} levels is an essential mechanism by which Bcl-2 regulates the susceptibility of cells to apoptosis (Nakamura et al, 2000; Orrenius et al, 2003; Scorrano et al, 2003) and overexpression of Bcl-2 in cell culture reduces TG-induced efflux of ER Ca^{2+}, interfering with Ca^{2+} signaling (Lam et al, 1994).

One of the mechanisms previously proposed for the antiapoptotic action of Bcl-2 is by interacting with the IP_3 receptor on the ER membrane, thereby blocking the release of Ca^{2+} into the cytosol (Rong et al, 2008). Even though increases in cytosolic Ca^{2+} have commonly been associated with the apoptotic signal transduction pathway, depletion of ER Ca^{2+} pool may also contribute to cell death (Lam et al, 1994).

Furthermore, Bcl-2 has been recently identified as an mRNA target of TDP-43, which directly regulates its alternative splicing (Tollervey et al, 2011). A homologue of Bcl-2, Bcl-X, exists in two isoforms generated by alternative splicing and its large form, Bcl-X_L, protects cells against death, whereas the short form, Bcl-X_S, promotes cell death by inhibiting

Bcl-2 or Bcl-X_L function (Li et al, 2002). The presence of elevated levels of Bcl-2 under normal conditions in TDP-M337V cells suggests an activation of an anti-apoptotic pathway, possibly due to stress inflicted by the M337V mutation, and the subsequent elevation in Bcl-X_S after ER stress leads to cell death by the inhibitory action of Bcl-X_S on the anti-apoptotic Bcl-2.

To investigate whether Bcl-2 is an upstream regulator of Ca^{2+} signalling in this cellular model, I used siRNA knockdown of Bcl-2 to evaluate its effects on ER Ca^{2+} oscillations. Knockdown of Bcl-2 restored amplitude of Ca^{2+} signaling in TDP-M337V cells, but was not sufficient to restore Ca^{2+} signalling in cells carrying the less pathogenic mutation, A382T. While there was less ER Ca^{2+} detected in TDP-A382T, the signalling patterns were not as severely altered as those seen in TDP-M337V. This suggests that in this cellular model Bcl-2 is implicated primarily in the regulation of ER Ca^{2+} release and less so in regulating the overall ER Ca^{2+} levels, which were left unaffected by Bcl-2 knockdown. There may be additional compensatory mechanisms that mediate A382T pathology, which may explain why Bcl-2 knockdown was unable to restore Ca^{2+} signalling in cells carrying TDP-A382T.

To determine the involvement of Bcl-2 in other phenotypes associated with TDP-43 mutations, future experiments should focus on evaluating TDP-43 subcellular localization after Bcl-2 knockdown and whether this phenotype is rescued when Bcl-2 levels are lowered. Also, immunoprecipitation and quantitative PCR (qPCR) assays can be used to determine the nature of the interaction between TDP-43 and Bcl-2. The hypothesis of a direct TDP-43-Bcl-2 interaction is supported by a recent study that revealed increased levels of TDP-43 in the rough ER in spinal motor neurons of sporadic ALS patients when compared to healthy controls using immunogold electron microscopy (Sasaki et al, 2010). The study also reported

that the increase in co-localization of TDP-43 with ER correlated with nuclear depletion in ALS motor neurons (Sasaki et al, 2010).

However, in this study I found Ca^{2+} dysregulation in ~50% of TDP-M337V cells, while cytoplasmic mislocalization of TDP-43 was detected in only ~3% of TDP-M337V cells. My results indicate that the interaction between TDP-43 and Bcl-2 is more likely to occur at the nuclear level. An important consideration when formulating such a hypothesis is the nucleo-cytoplasmic shuttling property of TDP-43 (Ayala et al, 2008; Winton et al, 2008). Cell counts were performed on fixed cells which represent the localization of TDP-43 at one specific timepoint, while calcium imaging was recorded live for an extended period of time and the physiological effects may be the reflection of TDP-43 activity in either the nuclear or cytoplasmic compartment. Even though present at low levels in the cytoplasm, mutated TDP-43 could have a higher physiological impact on Ca^{2+} homeostasis when in the cytoplasm compared to wild-type TDP-Ypet, suggested also by the significantly increased Bcl-2 levels in the mutation-bearing cells. If higher expression of exogenous TDP-43 could be achieved as to allow increased Ypet fluorescence and detection of the subcellular localization of TDP-43 in live cells, Ca^{2+} signalling could be performed in cells expressing either nuclear or cytoplasmic TDP-43. Such an experiment could pinpoint whether the pathogenic effects on Ca^{2+} regulation are the consequence of cytoplasmic TDP-43 or nuclear TDP-43. For this purpose, a strongly driven cDNA construct of TDP-Ypet and A382T or M337V mutations could be used which would allow visualization of the subcellular localization of the transgene and calcium recordings could be performed specifically in cells with cytoplasmic TDP-43.

The molecular findings described here may underlie the different severity of the clinical symptoms seen in patients carrying the M337V or A382T mutation. The A382T mutation has been described as a less pathogenic mutation, commonly encountered in ALS

and FTLD in homozygous state, whereas heterozygous M337V mutations are associated with severe disease (Mosca et al, 2012). In our model, M337V was sufficient to induce cytoplasmic mislocalization of TDP-43, cytoplasmic TDP-43 punctae and Bcl-2 mediated Ca^{2+} dysregulation, while A382T required oxidative stress to induce TDP-43 cytoplasmic translocation, and ER stress to form TDP-43 cytoplasmic punctae.

6.2. TDP-43 pathology in iPSC-derived motor neurons

One major drawback in the studies of motor neuron disease has been the lack of relevant cell culture models and our inability to directly study human motor neurons from patients who carry the specific genetic background conferring disease susceptibility. The breakthrough discovery that somatic cells can be reprogrammed to a pluripotent state and the recent development of efficient neuronal differentiation protocols brought many opportunities to study neurodegenerative diseases directly in the affected neurons from the patients carrying those specific disorders (Takahashi et al, 2007b; Yu et al, 2007a).

There have been several published protocols for motor neuron differentiation from iPSCs or embryonic stem cells and the protocol by Hu and Zhang was chosen due its previously reported high differentiation efficiency (~50%) (Dimos et al, 2008; Hu & Zhang, 2009; Li et al, 2005). The differentiation efficiency I obtained was significantly lower and was estimated at only ~12% Islet-1-positive cells in the fully differentiated population. Such discrepancies could result from the individual propensity of each iPSC line for motor neuron specification. Recent studies have revealed significant quantitative differences between the propensities of each iPSC line for terminal motor neuron differentiation, which are the result

of intrinsic characteristics of each line (Boulting et al, 2011). This may explain the low propensity of NHDF2 cell line to differentiate to motor neurons, as this iPSC line consistently generated fewer motor neurons than HFF1 and Df19.9 iPSC lines and was consequently not used for functional assays.

For investigating the effects of TDP-43 mutations on iPSC-derived motor neurons, the TDP-43 vectors were delivered to fully differentiated healthy motor neurons by Herpes Simplex Virus Type 1 (HSV-1) amplicons. Viral vectors are more efficient than most other gene delivery vehicles because of their high transduction efficiency. Furthermore, recombinant HSV-1 vectors have broad limits for packaging large transgenes, which is an essential aspect when using genomic loci (Wade-Martins et al, 2001).

The transduction efficiency of HSV-1 viral particles with TDP-43 vectors in iPSC-derived motor neurons was estimated at ~10%. Even though I found that using a high multiplicity of infection (MOI) increased transduction efficiency, low titers of the viral preparations and high cytotoxicity were limiting factors in choosing the optimal MOI. Following packaging in Vero 2-2 cells, low titers were consistently obtained. To increase the yield and eliminate toxic cellular debris, I filtered and concentrated the HSV-1 amplicons by ultracentrifugation on a sucrose cushion. Cytotoxicity was then assessed in motor neuron cultures by examining survival rates after several MOIs were used. Due to high cytotoxicity, I found that only MOI=1 could be reliably used without significant cell death.

In iPSC-derived motor neurons, endogenous levels of TDP-43 were not affected by HSV-1 transductions with TDP-43 mutations. Considering the previously reported self-regulatory loop of TDP-43 (Ayala et al, 2011; Polymenidou et al, 2011), protein levels of TDP-43 were expected to fluctuate in the presence of exogenous TDP-43. Autoregulation may have occurred, but it may have been undetectable for immunoblotting due to low

transduction efficiency. The alternative hypothesis based on these results is that endogenous TDP-43 may have downregulated exogenous TDP-43, which is consistent with the findings in Chapter 4 in the clonal cell lines where we see no alternations in endogenous TDP-43 levels in the presence of TDP-Ypet, TDP-M337V or TDP-A382T.

A 35 kDa C-terminal fragment of TDP-43 was detected in iPSC-derived motor neurons, which was not seen in HEK293 cells. Cleaved products of TDP-43 have been consistently reported in the motor neurons of ALS and FTLD patients and they were previously shown to be prone to aggregation (Neumann et al, 2006; Yang et al, 2010). Their absence from HEK293 cells indicates there may be different regulatory mechanisms specific to motor neurons that regulate the cleavage of TDP-43 and that may contribute to the specific vulnerability of motor neurons to TDP-43 proteinopathies.

In healthy iPSC-derived motor neurons transduced with HSV-1 amplicons carrying TDP-43 vectors we detected cytoplasmic re-localization of TDP-43 when exposed to H_2O_2-induced oxidative stress. Injury by free radical species is a major cause of age-related progressive neuronal degeneration seen in many neurodegenerative diseases. Excitotoxicity from the surrounding glia is believed to play a major role in motor neuron death in ALS. Consistent with our findings, a recent study using patient specific iPSC-derived motor neurons from an ALS patient carrying the M337V mutation showed that TDP-43 was distributed in both nucleus and cytoplasm in patient iPSC-derived motor neurons and in healthy control iPSC derived motor neurons (Egawa et al, 2012).

In line with our findings, the same study did not detect increased cell death in the patient-derived motor neurons at basal levels (Egawa et al, 2012). However, they reported that in the presence of oxidative stress, iPSC-derived motor neurons with the M337V mutation had a higher susceptibility to cell death compared to control iPSC-derived motor

neurons (Egawa et al, 2012). In our study, we did not detect differences in cell survival under basal or oxidative stress conditions and we speculate that this may be due to low transduction efficiencies and low expression levels of TDP-Ypet, TDP-M337V and TDP-A382T.

An optimal control for our experiments would consist of iPSC-derived motor neurons obtained from reprogramming the fibroblasts of ALS patients carrying M337V or A382T mutations. A comparison of phenotypes between healthy motor neurons transduced with TDP-43 vectors and motor neurons derived from TDP-43 patient fibroblasts would be a key experiment to pinpoint the exact mechanisms of disease that are exclusively triggered by pathogenic TDP-43. Even though it may be the case that mutations do not induce TDP-43 mislocalization or directly affect motor neuron survival, there are several aspects that need to be considered before formulating a conclusion in our cellular model. For instance, transduction efficiency was very low and in addition to that, expression of exogenous TDP-43 was also relatively low. Expression could not be detected by live fluorescence and could only be detected using immuncytochemistry against GFP. Consequently, the effects of low-expressing mutations from 10% of the cells may not be obvious when assessing the entire cellular population.

There are several other important issues that need to be addressed in interpreting the results from iPSC-derived motor neurons in the study of neurodegeneration. An important consideration is that patients live with TDP-43 mutations for decades before symptoms and pathology occur and an immediate effect is perhaps not expected when mutations are delivered at a late stage during differentiation. Moreover, one of the drawbacks in the cultures of iPSC-derived neurons is that the age of the neurons cannot be determined and the cells are at different stages of differentiation in the same culture, often contaminated by early progenitors. The age of the cells is an essential factor in the study of neurodegenerative

disorders, as pathology only occurs as a result of the mechanisms involved in the aging process and other unknown environmental triggers.

Further progress in optimizing viral delivery of BAC constructs to neurons might make it possible to recapitulate findings from patient iPSC-derived motor neurons and will provide a tool for analyzing functional effects of genetic mutations without interference from an uncontrolled disease-specific genetic background of patient iPSC-derived motor neurons.

6.3. C9orf72 iPSC-derived motor neurons

The recent discovery of the pathogenic $(GGGGCC)_n$ hexanucleotide repeats in C9orf72 accounting for 40% of fALS cases has been a major breakthrough (DeJesus-Hernandez et al, 2011). The motor neurons obtained by iPSC derivation of *C9orf72* fibroblasts have the advantage of carrying ALS-specific genetic profile and display characteristic neurodegenerative traits. Once reprogrammed, the iPSCs from ALS patients were differentiated to human motor neurons to investigate the molecular mechanisms of the novel *C9orf72* expansions.

Interestingly, the clinical symptoms of the two patients correlated with the phenotypes I detected in their iPSC-derived motor neurons. The C9_Turke iPSCs were derived from an ALS patient who predominantly exhibited a form of cognitive impairment and fewer motor symptoms. In contrast, the C9_7245 iPSCs were obtained from a patient who presented typical ALS motor symptoms.

In contrast to the findings in HEK293 cells carrying TDP-43 mutations, Ca^{2+} imaging studies in C9orf72 iPSC-derived motor neurons revealed high intracellular Ca^{2+} contents. While HEK293 cells carrying TDP-43 mutations exhibited reduced ER Ca^{2+} contents, the

iPSC-derived motor neurons with *C9orf72* expansions showed significantly higher ER Ca^{2+} contents compared to healthy iPSC-derived motor neurons. Nonetheless, in line with the HEK293 experiments, the correlation between Bcl-2 and ER Ca^{2+} levels was consistent throughout these two different cellular models, showing an inversely proportional relationship.

Increases in intracellular Ca^{2+} in motor neurons have been previously shown to trigger cell death *in vivo* in a rat model of ALS (Corona & Tapia, 2007). Motor neurons were shown to be specifically vulnerable to Ca^{2+} overload as a result of low Ca^{2+} buffering capacity and high input of glutamatergic stimulation (Carriedo et al, 2000; Siklós et al, 1996). Oxidative stress was shown to reduce the activity of the glial glutamate transporter, thereby contributing to excitotoxicity and Ca^{2+} dysregulation in motor neurons (Trotti et al, 1999). Furthermore, the antiapoptotic protein Bcl-2 is known to play a major role in protecting motor neurons from apoptotic cell death and reduced levels suggest motor neurons from the *C9orf72* patient line may be more prone to apoptotic signals (Farlie et al, 1995).

The deficits in ER Ca^{2+} signalling detected in the motor neurons derived from C9_7245 iPSCs were also accompanied by high levels of GRP78/BiP and p62, which indicate high ER stress. It has previously been shown that *C9orf72*-associated cases exhibit pathology that is characterized by abundant cytoplasmic and intranuclear inclusions immunopositive for ubiquitin and sequestosome-1/p62 (Bieniek et al, 2012; Cooper-Knock et al, 2012; Troakes et al, 2012), which is in line with our observations in *C9orf72* iPSC-derived motor neurons. ER stress markers have also been previously reported to be elevated in postmortem motor neurons of ALS (Atkin et al, 2008; Ilieva et al, 2007) and ER stress was hypothesized to contribute to the deficits in Ca^{2+} buffering in motor neurons (Grosskreutz et al, 2010).

The data presented here on C9orf72 iPSC-derived motor neurons are novel and further work will be required to confirm these findings. An exciting link appears to be emerging between *C9orf72* expansions and Bcl-2 mediated dysfunction of ER Ca^{2+}.

6.4. General iPSC discussion

The iPSC technology offers an unprecedented opportunity to recapitulate both normal and pathologic human tissue formation, enabling disease investigation and drug development. In addition to ALS and SMA iPSCs, induced pluripotent stem cells have also been successfully generated from patients with a variety of genetic diseases, including Parkinson's disease, Huntington's disease, Down syndrome, diabetes type 1, Duchenne muscular atrophy (Park et al, 2008). However, many challenges still remain to be overcome before iPSC technology can efficiently contribute to the treatment of diseases.

One of the greatest challenges is to reliably differentiate iPSC into a homogeneous population of the desired cell type. Current differentiation protocols for motor neurons generate a heterogeneous population of neurons, glia and other unidentified cells. A widely used method for motor neuron enrichment in differentiating cultures was developed in 2002 (Wichterle et al, 2002). Using an HB9 promoter driven GFP, motor neurons can be transduced with lentiviruses carrying the HB9:GFP plasmid and cell sorting for cells expressing the fluorescent reporter can be performed by fluorescence activated cell sorting (FACS) (Boulting et al, 2011; Dimos et al, 2008; Wichterle et al, 2002). Although this process enriches the motor neuron population, it remains to be established whether normal functionality of motor neurons can be restored following FACS to reliably perform functional

assays. Such enriched pure populations of motor neurons are extremely useful tools for applications such as drug screening for toxicity and efficacy.

Another challenge to be overcome by iPS technology in regenerative medicine is the safety of transplants after using viral reprogramming methods. Transgene silencing is not consistently achieved and the reactivation of retroviruses can lead to malignant transformations and potential teratoma formation (Jaenisch & Young, 2008; Muller et al, 2009; Okita et al, 2007). Newer methods are being developed for safer delivery of the necessary reprogramming factors by miRNAs (Anokye-Danso et al, 2011) and Sendai virus (Nishimura et al, 2011b).

Several groups have highlighted the importance of non-cell autonomous effects when attempting to study a specific iPSC-derived cell-type *in vitro*, outside of its environmental context. For instance, genotypically mutant glia cells carrying the G93A mutation in SOD1 have been previously shown to have a direct, toxic effect on motor neuron survival (Di Giorgio et al, 2007). It was also recently shown *in vivo* that overexpression of the M337V mutation in TDP-43 in astrocytes induces loss of spinal motor neurons through progressive paralysis (Tong et al, 2013). It is therefore important for *in vitro* experiments to consider the contributions of more than one cell-type to the phenotype and explore interactions between several types of cells that would normally interact *in vivo*.

The iPSC technology has opened a wide breadth of possibilities for investigating disease pathogenesis and it represents a fast advancing field of research, which will answer many questions about diseases previously difficult to study.

6.5. Final conclusions

In these studies, I investigated the effects of TDP-43 mutations in cellular models to elucidate the molecular mechanisms of TDP-43 pathology, which is at the core of ALS pathogenesis. I generated a novel genomic construct carrying the entire human *TARDBP* locus, which was tagged with a fluorescent Ypet tag and engineered three disease-associated mutations, A382T, M337V and Y374X. I showed that the M337V and A382T mutations increase cytoplasmic mislocalization of TDP-43 in stably expressing cells, which was potentiated by oxidative stress, and the M337V induced spontaneous formation of cytoplasmic TDP-43 punctae. Calcium signalling was found to be impaired in TDP-M337V and TDP-A382T, which could be rescued by Bcl-2 knockdown.

In healthy iPSC-derived motor neurons, TDP-43 mutations did not induce significant cell death or cytoplasmic mislocalization. Preliminary results in ALS patient iPSC-derived motor neurons carrying C9orf72 pathogenic expansions showed impairments in Bcl-2 mediated Ca^{2+} signalling along with intracellular overload of Ca^{2+} and elevated levels of ER stress markers.

Both human cellular models used in these studies highlight the importance of Ca^{2+} dysregulation in ALS. While TDP-43 mutations reduced ER Ca^{2+} signalling and ER Ca^{2+} content, *C9orf72* expansions increased ER Ca^{2+} content and overall intracellular Ca^{2+} levels. In both studies, the effects observed in Ca^{2+} contents correlated with expression levels of the antiapoptotic protein Bcl-2. Our experiments showed that Bcl-2 primarily mediates ER Ca^{2+} release in HEK293 cells while in iPSC-derived motor neurons it primarily regulates ER Ca^{2+} levels and additional factors may be involved in regulating ER Ca^{2+} release. This is a novel

finding which identifies Bcl-2 mediated Ca^{2+} dysregulation as an important player in the phenotype of ALS.

There are many challenges in understanding TDP-43 pathology and they are largely related to the complexity of its functions and the vast number of mRNAs it regulates which are involved in many essential cellular pathways. Much still remains to be discovered, but given the recent progress in understanding neurodegenerative diseases and the development of essential biological tools, such as iPS technology, we are significantly closer to advancing the knowledge on TDP-43 proteinopathies and to translating this knowledge into better diagnosis and treatments of these diseases.

Bibliography

Aasen T, Raya A, Barrero M, Garreta E, Consiglio A, Gonzalez F, Vassena R, Bilic J, Pekarik V, Tiscornia G, Edel M, Boue S, Belmonte J (2008) Efficient and rapid generation of induced pluripotent stem cells from human keratinocytes. *Nature Biotechnology* **26:** 1276-1284

Abhinav K, Stanton B, Johnston C, Hardstaff J, Orrell RW, Howard R, Clarke J, Sakel M, Ampong MA, Shaw CE, Leigh PN, Al-Chalabi A (2007) Amyotrophic lateral sclerosis in South-East England: a population-based study. The South-East England register for amyotrophic lateral sclerosis (SEALS Registry). *Neuroepidemiology* **29:** 44-48

Al-Sarraj S, King A, Troakes C, Smith B, Maekawa S, Bodi I, Rogelj B, Al-Chalabi A, Hortobagyi T, Shaw C (2011) p62 positive, TDP-43 negative, neuronal cytoplasmic and intranuclear inclusions in the cerebellum and hippocampus define the pathology of C9orf72-linked FTLD and MND/ALS. *Acta Neuropathologica* **122:** 691-702

Alegre-Abarrategui J, Christian H, Lufino MM, Mutihac R, Venda LL, Ansorge O, Wade-Martins R (2009) LRRK2 regulates autophagic activity and localizes to specific membrane microdomains in a novel human genomic reporter cellular model. *Hum Mol Genet* **18:** 4022-4034

Amador-Ortiz C, Lin W, Ahmed Z, Personett D, Davies P, Dara R, Graff-Radford N, Hutton M, Dickson D (2007) TDP-43 immunoreactivity in hippocampal sclerosis and Alzheimer's disease. *Annals of Neurology* **61:** 435-445

Andersen PM, Al-Chalabi A (2011) Clinical genetics of amyotrophic lateral sclerosis: what do we really know? *Nat Rev Neurol* **7:** 603-615

Annis MG, Yethon JA, Leber B, Andrews DW (2004) There is more to life and death than mitochondria: Bcl-2 proteins at the endoplasmic reticulum. *Bba-Mol Cell Res* **1644:** 115-123

Anokye-Danso F, Trivedi C, Juhr D, Gupta M, Cui Z, Tian Y, Zhang Y, Yang W, Gruber P, Epstein J, Morrisey E (2011) Highly Efficient miRNA-Mediated Reprogramming of Mouse and Human Somatic Cells to Pluripotency. *Cell Stem Cell* **8:** 376-388

Arai T, Hasegawa M, Akiyama H, Ikeda K, Nonaka T, Mori H, Mann D, Tsuchiya K, Yoshida M, Hashizume Y, Oda T (2006) TDP-43 is a component of ubiquitin-positive tau-negative inclusions in frontotemporal lobar degeneration and amyotrophic lateral sclerosis. *Biochem Biophys Res Commun* **351:** 602-611

Ash PE, Bieniek KF, Gendron TF, Caulfield T, Lin WL, Dejesus-Hernandez M, van Blitterswijk MM, Jansen-West K, Paul JW, 3rd, Rademakers R, Boylan KB, Dickson DW, Petrucelli L (2013) Unconventional Translation of C9ORF72 GGGGCC Expansion Generates Insoluble Polypeptides Specific to c9FTD/ALS. *Neuron* **77:** 639-646

Atkin JD, Farg MA, Walker AK, McLean C, Tomas D, Horne MK (2008) Endoplasmic reticulum stress and induction of the unfolded protein response in human sporadic amyotrophic lateral sclerosis. *Neurobiol Dis* **30:** 400-407

Ayala YM, De Conti L, Avendaño-Vázquez SE, Dhir A, Romano M, D'Ambrogio A, Tollervey J, Ule J, Baralle M, Buratti E, Baralle FE (2011) TDP-43 regulates its mRNA levels through a negative feedback loop. *EMBO J* **30:** 277-288

Ayala YM, Pantano S, D'Ambrogio A, Buratti E, Brindisi A, Marchetti C, Romano M, Baralle FE (2005) Human, Drosophila, and C.elegans TDP43: nucleic acid binding properties and splicing regulatory function. *J Mol Biol* **348:** 575-588

Ayala YM, Zago P, D'Ambrogio A, Xu YF, Petrucelli L, Buratti E, Baralle FE (2008) Structural determinants of the cellular localization and shuttling of TDP-43. *Journal of Cell Science* **121:** 3778-3785

Barber SC, Shaw PJ (2010) Oxidative stress in ALS: key role in motor neuron injury and therapeutic target. *Free Radic Biol Med* **48:** 629-641

Barmada SJ, Skibinski G, Korb E, Rao EJ, Wu JY, Finkbeiner S (2010) Cytoplasmic mislocalization of TDP-43 is toxic to neurons and enhanced by a mutation associated with familial amyotrophic lateral sclerosis. *The Journal of neuroscience : the official journal of the Society for Neuroscience* **30:** 639-649

Baumer D, Hilton D, Paine SM, Turner MR, Lowe J, Talbot K, Ansorge O (2010) Juvenile ALS with basophilic inclusions is a FUS proteinopathy with FUS mutations. *Neurology* **75:**611-618

Beckman JS, Carson M, Smith CD, Koppenol WH (1993) ALS, SOD and peroxynitrite. *Nature* **364:** 584

Beleza-Meireles A, Al-Chalabi A (2009) Genetic studies of amyotrophic lateral sclerosis: controversies and perspectives. *Amyotroph Lateral Scler* **10:** 1-14

Berridge MJ, Lipp P, Bootman MD (2000) The versatility and universality of calcium signalling. *Nat Rev Mol Cell Biol* **1:** 11-21

Bertolotti A, Zhang Y, Hendershot LM, Harding HP, Ron D (2000) Dynamic interaction of BiP and ER stress transducers in the unfolded-protein response. *Nat Cell Biol* **2:** 326-332

Bieniek KF, Murray ME, Rutherford NJ, Castanedes-Casey M, Dejesus-Hernandez M, Liesinger AM, Baker MC, Boylan KB, Rademakers R, Dickson DW (2012) Tau pathology in frontotemporal lobar degeneration with C9ORF72 hexanucleotide repeat expansion. *Acta Neuropathol*

Bilican B, Serio A, Barmada SJ, Nishimura AL, Sullivan GJ, Carrasco M, Phatnani HP, Puddifoot CA, Story D, Fletcher J, Park IH, Friedman BA, Daley GQ, Wyllie DJ, Hardingham GE, Wilmut I, Finkbeiner S, Maniatis T, Shaw CE, Chandran S (2012) Mutant induced pluripotent stem cell lines recapitulate aspects of TDP-43 proteinopathies and reveal cell-specific vulnerability. *Proc Natl Acad Sci U S A* **109:** 5803-5808

Borghero G, Floris G, Cannas A, Marrosu MG, Murru MR, Costantino E, Parish LD, Pugliatti M, Ticca A, Traynor BJ, Calvo A, Cammarosano S, Moglia C, Cistaro A, Brunetti M, Restagno G, Chiò A (2011) A patient carrying a homozygous p.A382T TARDBP missense mutation shows a syndrome including ALS, extrapyramidal symptoms, and FTD. *Neurobiol Aging* **32:** 2327.e2321-2325

Bosco DA, Morfini G, Karabacak NM, Song Y, Gros-Louis F, Pasinelli P, Goolsby H, Fontaine BA, Lemay N, McKenna-Yasek D, Frosch MP, Agar JN, Julien JP, Brady ST, Brown RH (2010) Wild-type and mutant SOD1 share an aberrant conformation and a common pathogenic pathway in ALS. *Nat Neurosci* **13:** 1396-1403

Bose J, Huang C, Shen C (2011) Regulation of Autophagy by Neuropathological Protein TDP-43. *Journal of Biological Chemistry* **286:** 44441-44448

Bose JK, Wang IF, Hung L, Tarn WY, Shen CK (2008) TDP-43 overexpression enhances exon 7 inclusion during the survival of motor neuron pre-mRNA splicing. *J Biol Chem* **283:** 28852-28859

Boulting GL, Kiskinis E, Croft GF, Amoroso MW, Oakley DH, Wainger BJ, Williams DJ, Kahler DJ, Yamaki M, Davidow L, Rodolfa CT, Dimos JT, Mikkilineni S, MacDermott AB,

Woolf CJ, Henderson CE, Wichterle H, Eggan K (2011) A functionally characterized test set of human induced pluripotent stem cells. *Nat Biotechnol* **29:** 279-286

Brooks BR (1994) El Escorial World Federation of Neurology criteria for the diagnosis of amyotrophic lateral sclerosis. Subcommittee on Motor Neuron Diseases/Amyotrophic Lateral Sclerosis of the World Federation of Neurology Research Group on Neuromuscular Diseases and the El Escorial "Clinical limits of amyotrophic lateral sclerosis" workshop contributors. *J Neurol Sci* **124 Suppl:** 96-107

Brooks BR, Miller RG, Swash M, Munsat TL, Diseases WFoNRGoMN (2000) El Escorial revisited: revised criteria for the diagnosis of amyotrophic lateral sclerosis. *Amyotroph Lateral Scler Other Motor Neuron Disord* **1:** 293-299

Brostrom CO, Brostrom MA (1990) Calcium-dependent regulation of protein synthesis in intact mammalian cells. *Annu Rev Physiol* **52:** 577-590

Buratti E, Baralle FE (2001) Characterization and functional implications of the RNA binding properties of nuclear factor TDP-43, a novel splicing regulator of CFTR exon 9. *J Biol Chem* **276:** 36337-36343

Buratti E, Brindisi A, Giombi M, Tisminetzky S, Ayala YM, Baralle FE (2005) TDP-43 binds heterogeneous nuclear ribonucleoprotein A/B through its C-terminal tail: an important region for the inhibition of cystic fibrosis transmembrane conductance regulator exon 9 splicing. *J Biol Chem* **280:** 37572-37584

Buratti E, De Conti L, Stuani C, Romano M, Baralle M, Baralle F (2010) Nuclear factor TDP-43 can affect selected microRNA levels. *FEBS J* **277:** 2268-2281

Buratti E, Dork T, Zuccato E, Pagani F, Romano M, Baralle FE (2001) Nuclear factor TDP-43 and SR proteins promote in vitro and in vivo CFTR exon 9 skipping. *EMBO J* **20:** 1774-1784

Byrne S, Walsh C, Lynch C, Bede P, Elamin M, Kenna K, McLaughlin R, Hardiman O (2011) Rate of familial amyotrophic lateral sclerosis: a systematic review and meta-analysis. *J Neurol Neurosurg Psychiatry* **82:** 623-627

Calfon M, Zeng H, Urano F, Till JH, Hubbard SR, Harding HP, Clark SG, Ron D (2002) IRE1 couples endoplasmic reticulum load to secretory capacity by processing the XBP-1 mRNA. *Nature* **415:** 92-96

Cannas A, Borghero G, Floris GL, Solla P, Chiò A, Traynor BJ, Calvo A, Restagno G, Majounie E, Costantino E, Piras V, Lavra L, Pani C, Orofino G, Di Stefano F, Tacconi P, Mascia MM, Muroni A, Murru MR, Tranquilli S, Corongiu D, Rolesu M, Cuccu S, Marrosu F, Marrosu MG (2013) The p.A382T TARDBP gene mutation in Sardinian patients affected by Parkinson's disease and other degenerative parkinsonisms. *Neurogenetics* **14:** 161-166

Carriedo SG, Sensi SL, Yin HZ, Weiss JH (2000) AMPA exposures induce mitochondrial Ca(2+) overload and ROS generation in spinal motor neurons in vitro. *J Neurosci* **20:** 240-250

Chen YZ, Bennett CL, Huynh HM, Blair IP, Puls I, Irobi J, Dierick I, Abel A, Kennerson ML, Rabin BA, Nicholson GA, Auer-Grumbach M, Wagner K, De Jonghe P, Griffin JW, Fischbeck KH, Timmerman V, Cornblath DR, Chance PF (2004) DNA/RNA helicase gene mutations in a form of juvenile amyotrophic lateral sclerosis (ALS4). *Am J Hum Genet* **74:** 1128-1135

Chow CY, Landers JE, Bergren SK, Sapp PC, Grant AE, Jones JM, Everett L, Lenk GM, McKenna-Yasek DM, Weisman LS, Figlewicz D, Brown RH, Meisler MH (2009) Deleterious variants of FIG4, a phosphoinositide phosphatase, in patients with ALS. *Am J Hum Genet* **84:** 85-88

Cleveland DW, Rothstein JD (2001) From Charcot to Lou Gehrig: deciphering selective motor neuron death in ALS. *Nat Rev Neurosci* **2:** 806-819

Colombrita C, Zennaro E, Fallini C, Weber M, Sommacal A, Buratti E, Silani V, Ratti A (2009) TDP-43 is recruited to stress granules in conditions of oxidative insult. *J Neurochem* **111:** 1051-1061

Cooper-Knock J, Hewitt C, Highley J, Brockington A, Milano A, Man S, Martindale J, Hartley J, Walsh T, Gelsthorpe C, Baxter L, Forster G, Fox M, Bury J, Mok K, McDermott C, Traynor B, Kirby J, Wharton S, Ince P, Hardy J, Shaw P (2012) Clinico-pathological features in amyotrophic lateral sclerosis with expansions in C9ORF72. *Brain* **135:** 751-764

Corbett EF, Michalak M (2000) Calcium, a signaling molecule in the endoplasmic reticulum? *Trends Biochem Sci* **25:** 307-311

Corona JC, Tapia R (2007) Ca2+-permeable AMPA receptors and intracellular Ca2+ determine motoneuron vulnerability in rat spinal cord in vivo. *Neuropharmacology* **52:** 1219-1228

D'Ambrogio A, Buratti E, Stuani C, Guarnaccia C, Romano M, Ayala YM, Baralle FE (2009) Functional mapping of the interaction between TDP-43 and hnRNP A2 in vivo. *Nucleic Acids Res* **37:** 4116-4126

Daoud H, Valdmanis PN, Kabashi E, Dion P, Dupre N, Camu W, Meininger V, Rouleau GA (2009) Contribution of TARDBP mutations to sporadic amyotrophic lateral sclerosis. *J Med Genet* **46:** 112-114

DeJesus-Hernandez M, Mackenzie IR, Boeve BF, Boxer AL, Baker M, Rutherford NJ, Nicholson AM, Finch NA, Flynn H, Adamson J, Kouri N, Wojtas A, Sengdy P, Hsiung GY, Karydas A, Seeley WW, Josephs KA, Coppola G, Geschwind DH, Wszolek ZK, Feldman H, Knopman DS, Petersen RC, Miller BL, Dickson DW, Boylan KB, Graff-Radford NR, Rademakers R (2011) Expanded GGGGCC hexanucleotide repeat in noncoding region of C9ORF72 causes chromosome 9p-linked FTD and ALS. *Neuron* **72:** 245-256

Deng HX, Chen W, Hong ST, Boycott KM, Gorrie GH, Siddique N, Yang Y, Fecto F, Shi Y, Zhai H, Jiang H, Hirano M, Rampersaud E, Jansen GH, Donkervoort S, Bigio EH, Brooks BR, Ajroud K, Sufit RL, Haines JL, Mugnaini E, Pericak-Vance MA, Siddique T (2011) Mutations in UBQLN2 cause dominant X-linked juvenile and adult-onset ALS and ALS/dementia. *Nature* **477:** 211-215

Dewey CM, Cenik B, Sephton CF, Dries DR, Mayer P, Good SK, Johnson BA, Herz J, Yu G (2011) TDP-43 is directed to stress granules by sorbitol, a novel physiological osmotic and oxidative stressor. *Mol Cell Biol* **31:** 1098-1108

Di Giorgio F, Carrasco M, Siao M, Maniatis T, Eggan K (2007) Non-cell autonomous effect of glia on motor neurons in an embryonic stem cell-based ALS model. *Nature Neuroscience* **10:** 608-614

Dimos JT, Rodolfa KT, Niakan KK, Weisenthal LM, Mitsumoto H, Chung W, Croft GF, Saphier G, Leibel R, Goland R, Wichterle H, Henderson CE, Eggan K (2008) Induced pluripotent stem cells generated from patients with ALS can be differentiated into motor neurons. *Science* **321:** 1218-1221

Dormann D, Rodde R, Edbauer D, Bentmann E, Fischer I, Hruscha A, Than ME, Mackenzie IR, Capell A, Schmid B, Neumann M, Haass C (2010) ALS-associated fused in sarcoma (FUS) mutations disrupt Transportin-mediated nuclear import. *EMBO J* **29:** 2841-2857

Ebert A, Yu J, Rose F, Mattis V, Lorson C, Thomson J, Svendsen C (2009) Induced pluripotent stem cells from a spinal muscular atrophy patient. *Nature* **457:** 277-U271

Egawa N, Kitaoka S, Tsukita K, Naitoh M, Takahashi K, Yamamoto T, Adachi F, Kondo T, Okita K, Asaka I, Aoi T, Watanabe A, Yamada Y, Morizane A, Takahashi J, Ayaki T, Ito H, Yoshikawa K, Yamawaki S, Suzuki S, Watanabe D, Hioki H, Kaneko T, Makioka K, Okamoto K, Takuma H, Tamaoka A, Hasegawa K, Nonaka T, Hasegawa M, Kawata A, Yoshida M, Nakahata T, Takahashi R, Marchetto MC, Gage FH, Yamanaka S, Inoue H (2012) Drug screening for ALS using patient-specific induced pluripotent stem cells. *Sci Transl Med* **4:** 145ra104

Elden AC, Kim HJ, Hart MP, Chen-Plotkin AS, Johnson BS, Fang X, Armakola M, Geser F, Greene R, Lu MM, Padmanabhan A, Clay-Falcone D, McCluskey L, Elman L, Juhr D, Gruber PJ, Rüb U, Auburger G, Trojanowski JQ, Lee VM, Van Deerlin VM, Bonini NM, Gitler AD (2010) Ataxin-2 intermediate-length polyglutamine expansions are associated with increased risk for ALS. *Nature* **466:** 1069-1075

Ericson J, Thor S, Edlund T, Jessell TM, Yamada T (1992) Early stages of motor neuron differentiation revealed by expression of homeobox gene Islet-1. *Science* **256:** 1555-1560

Farlie PG, Dringen R, Rees SM, Kannourakis G, Bernard O (1995) bcl-2 transgene expression can protect neurons against developmental and induced cell death. *Proc Natl Acad Sci U S A* **92:** 4397-4401

Ferraiuolo L, Kirby J, Grierson AJ, Sendtner M, Shaw PJ (2011) Molecular pathways of motor neuron injury in amyotrophic lateral sclerosis. *Nat Rev Neurol* **7:** 616-630

Ferrante RJ, Browne SE, Shinobu LA, Bowling AC, Baik MJ, MacGarvey U, Kowall NW, Brown RH, Beal MF (1997) Evidence of increased oxidative damage in both sporadic and familial amyotrophic lateral sclerosis. *J Neurochem* **69:** 2064-2074

Fiesel FC, Voigt A, Weber SS, Van den Haute C, Waldenmaier A, Gorner K, Walter M, Anderson ML, Kern JV, Rasse TM, Schmidt T, Springer W, Kirchner R, Bonin M, Neumann M, Baekelandt V, Alunni-Fabbroni M, Schulz JB, Kahle PJ (2009) Knockdown of transactive response DNA-binding protein (TDP-43) downregulates histone deacetylase 6. *EMBO J*

Foyouzi-Youssefi R, Arnaudeau S, Borner C, Kelley WL, Tschopp J, Lew DP, Demaurex N, Krause KH (2000) Bcl-2 decreases the free Ca2+ concentration within the endoplasmic reticulum. *Proc Natl Acad Sci U S A* **97:** 5723-5728

Freibaum BD, Chitta RK, High AA, Taylor JP (2010) Global analysis of TDP-43 interacting proteins reveals strong association with RNA splicing and translation machinery. *J Proteome Res* **9:** 1104-1120

Geser F, Brandmeir NJ, Kwong LK, Martinez-Lage M, Elman L, McCluskey L, Xie SX, Lee VM, Trojanowski JQ (2008) Evidence of multisystem disorder in whole-brain map of pathological TDP-43 in amyotrophic lateral sclerosis. *Arch Neurol* **65:** 636-641

Gijselinck I, Van Langenhove T, van der Zee J, Sleegers K, Philtjens S, Kleinberger G, Janssens J, Bettens K, Van Cauwenberghe C, Pereson S, Engelborghs S, Sieben A, De Jonghe P, Vandenberghe R, Santens P, De Bleecker J, Maes G, Baumer V, Dillen L, Joris G, Cuijt I, Corsmit E, Elinck E, Van Dongen J, Vermeulen S, Van den Broeck M, Vaerenberg C, Mattheijssens M, Peeters K, Robberecht W, Cras P, Martin JJ, De Deyn PP, Cruts M, Van Broeckhoven C (2012) A C9orf72 promoter repeat expansion in a Flanders-Belgian cohort with disorders of the frontotemporal lobar degeneration-amyotrophic lateral sclerosis spectrum: a gene identification study. *Lancet Neurol* **11:** 54-65

Gitcho MA, Baloh RH, Chakraverty S, Mayo K, Norton JB, Levitch D, Hatanpaa KJ, White CL, 3rd, Bigio EH, Caselli R, Baker M, Al-Lozi MT, Morris JC, Pestronk A, Rademakers R, Goate AM, Cairns NJ (2008) TDP-43 A315T mutation in familial motor neuron disease. *Ann Neurol* **63:** 535-538

Gitler A, Shorter J (2011) RNA-binding proteins with prion-like domains in ALS and FTLD-U. *Molecular Biology of the Cell* **22**

Greber UF, Gerace L (1995) Depletion of calcium from the lumen of endoplasmic reticulum reversibly inhibits passive diffusion and signal-mediated transport into the nucleus. *J Cell Biol* **128:** 5-14

Greenway MJ, Andersen PM, Russ C, Ennis S, Cashman S, Donaghy C, Patterson V, Swingler R, Kieran D, Prehn J, Morrison KE, Green A, Acharya KR, Brown RH, Hardiman O (2006) ANG mutations segregate with familial and 'sporadic' amyotrophic lateral sclerosis. *Nat Genet* **38:** 411-413

Grosskreutz J, Van Den Bosch L, Keller BU (2010) Calcium dysregulation in amyotrophic lateral sclerosis. *Cell Calcium* **47:** 165-174

Gunnarsson LG, Dahlbom K, Strandman E (1991) Motor neuron disease and dementia reported among 13 members of a single family. *Acta Neurol Scand* **84:** 429-433

Gurdon J (1962) Developmental capacity of nuclei taken from intestinal epithelium cells of feeding tadpoles. *Journal of Embryology and Experimental Morphology* **10:** 622-624

Gurney ME, Pu H, Chiu AY, Dal Canto MC, Polchow CY, Alexander DD, Caliendo J, Hentati A, Kwon YW, Deng HX (1994) Motor neuron degeneration in mice that express a human Cu,Zn superoxide dismutase mutation. *Science* **264:** 1772-1775

Hadano S, Hand CK, Osuga H, Yanagisawa Y, Otomo A, Devon RS, Miyamoto N, Showguchi-Miyata J, Okada Y, Singaraja R, Figlewicz DA, Kwiatkowski T, Hosler BA, Sagie T, Skaug J, Nasir J, Brown RH, Scherer SW, Rouleau GA, Hayden MR, Ikeda JE (2001) A gene encoding a putative GTPase regulator is mutated in familial amyotrophic lateral sclerosis 2. *Nat Genet* **29:** 166-173

Hajnoczky G, Davies E, Madesh M (2003) Calcium signaling and apoptosis. *Biochem Biophys Res Commun* **304:** 445-454

Hand CK, Khoris J, Salachas F, Gros-Louis F, Lopes AA, Mayeux-Portas V, Brewer CG, Brown RH, Meininger V, Camu W, Rouleau GA (2002) A novel locus for familial amyotrophic lateral sclerosis, on chromosome 18q. *Am J Hum Genet* **70:** 251-256

Hanson MG, Landmesser LT (2003) Characterization of the circuits that generate spontaneous episodes of activity in the early embryonic mouse spinal cord. *J Neurosci* **23:** 587-600

Hasegawa M, Arai T, Nonaka T, Kametani F, Yoshida M, Hashizume Y, Beach TG, Buratti E, Baralle F, Morita M, Nakano I, Oda T, Tsuchiya K, Akiyama H (2008) Phosphorylated TDP-43 in frontotemporal lobar degeneration and amyotrophic lateral sclerosis. *Ann Neurol* **64:** 60-70

Hodges JR, Davies RR, Xuereb JH, Casey B, Broe M, Bak TH, Kril JJ, Halliday GM (2004) Clinicopathological correlates in frontotemporal dementia. *Ann Neurol* **56:** 399-406

Hu B, Weick J, Yu J, Ma L, Zhang X, Thomson J, Zhang S (2010) Neural differentiation of human induced pluripotent stem cells follows developmental principles but with variable potency. *Proceedings of the National Academy of Sciences of the United States of America* **107:** 4335-4340

Hu BY, Zhang SC (2009) Differentiation of spinal motor neurons from pluripotent human stem cells. *Nat Protoc* **4:** 1295-1304

Huangfu D, Osafune K, Maehr R, Guo W, Eijkelenboom A, Chen S, Muhlestein W, Melton D (2008) Induction of pluripotent stem cells from primary human fibroblasts with only Oct4 and Sox2. *Nature Biotechnology* **26:** 1269-1275

Igaz LM, Kwong LK, Xu Y, Truax AC, Uryu K, Neumann M, Clark CM, Elman LB, Miller BL, Grossman M, McCluskey LF, Trojanowski JQ, Lee VM (2008) Enrichment of C-terminal fragments in TAR DNA-binding protein-43 cytoplasmic inclusions in brain but not in spinal cord of frontotemporal lobar degeneration and amyotrophic lateral sclerosis. *Am J Pathol* **173:** 182-194

Ilieva EV, Ayala V, Jove M, Dalfo E, Cacabelos D, Povedano M, Bellmunt MJ, Ferrer I, Pamplona R, Portero-Otin M (2007) Oxidative and endoplasmic reticulum stress interplay in sporadic amyotrophic lateral sclerosis. *Brain* **130:** 3111-3123

Irwin DJ, McMillan CT, Brettschneider J, Libon DJ, Powers J, Rascovsky K, Toledo JB, Boller A, Bekisz J, Chandrasekaran K, Wood EM, Shaw LM, Woo JH, Cook PA, Wolk DA, Arnold SE, Van Deerlin VM, McCluskey LF, Elman L, Lee VM, Trojanowski JQ, Grossman M (2012) Cognitive decline and reduced survival in C9orf72 expansion frontotemporal degeneration and amyotrophic lateral sclerosis. *J Neurol Neurosurg Psychiatry*

Jaenisch R, Young R (2008) Stem cells, the molecular circuitry of pluripotency and nuclear reprogramming. *Cell* **132:** 567-582

Johnson BS, Snead D, Lee JJ, McCaffery JM, Shorter J, Gitler AD (2009) TDP-43 is intrinsically aggregation-prone, and amyotrophic lateral sclerosis-linked mutations accelerate aggregation and increase toxicity. *J Biol Chem* **284:** 20329-20339

Johnson JO, Mandrioli J, Benatar M, Abramzon Y, Van Deerlin VM, Trojanowski JQ, Gibbs JR, Brunetti M, Gronka S, Wuu J, Ding J, McCluskey L, Martinez-Lage M, Falcone D, Hernandez DG, Arepalli S, Chong S, Schymick JC, Rothstein J, Landi F, Wang YD, Calvo A, Mora G, Sabatelli M, Monsurrò MR, Battistini S, Salvi F, Spataro R, Sola P, Borghero G, Galassi G, Scholz SW, Taylor JP, Restagno G, Chiò A, Traynor BJ, Consortium I (2010) Exome sequencing reveals VCP mutations as a cause of familial ALS. *Neuron* **68:** 857-864

Julien JP, Côté F, Collard JF (1995) Mice overexpressing the human neurofilament heavy gene as a model of ALS. *Neurobiol Aging* **16:** 487-490; discussion 490-482

Kabashi E, Lin L, Tradewell ML, Dion PA, Bercier V, Bourgouin P, Rochefort D, Bel Hadj S, Durham HD, Vande Velde C, Rouleau GA, Drapeau P (2009) Gain and loss of function of ALS-related mutations of TARDBP (TDP-43) cause motor deficits in vivo. *Hum Mol Genet*

Kabashi E, Valdmanis PN, Dion P, Spiegelman D, McConkey BJ, Vande Velde C, Bouchard JP, Lacomblez L, Pochigaeva K, Salachas F, Pradat PF, Camu W, Meininger V, Dupre N,

Rouleau GA (2008) TARDBP mutations in individuals with sporadic and familial amyotrophic lateral sclerosis. *Nat Genet* **40:** 572-574

Karumbayaram S, Kelly TK, Paucar AA, Roe AJ, Umbach JA, Charles A, Goldman SA, Kornblum HI, Wiedau-Pazos M (2009) Human embryonic stem cell-derived motor neurons expressing SOD1 mutants exhibit typical signs of motor neuron degeneration linked to ALS. *Dis Model Mech* **2:** 189-195

Kim SH, Zhan L, Hanson KA, Tibbetts RS (2012) High-content RNAi screening identifies the Type 1 inositol triphosphate receptor as a modifier of TDP-43 localization and neurotoxicity. *Hum Mol Genet*

King A, Al-Sarraj S, Troakes C, Smith BN, Maekawa S, Iovino M, Spillantini MG, Shaw CE (2012) Mixed tau, TDP-43 and p62 pathology in FTLD associated with a C9ORF72 repeat expansion and p.Ala239Thr MAPT (tau) variant. *Acta Neuropathol*

Koyanagi M, Takahashi J, Arakawa Y, Doi D, Fukuda H, Hayashi H, Narumiya S, Hashimoto N (2008) Inhibition of the Rho/ROCK pathway reduces apoptosis during transplantation of embryonic stem cell-derived neural precursors. *J Neurosci Res* **86:** 270-280

Krencik R, Zhang SC (2011) Directed differentiation of functional astroglial subtypes from human pluripotent stem cells. *Nat Protoc* **6:** 1710-1717

Kress M, Riedl B, Reeh PW (1995) Effects of oxygen radicals on nociceptive afferents in the rat skin in vitro. *Pain* **62:** 87-94

Kwiatkowski TJ, Bosco DA, Leclerc AL, Tamrazian E, Vanderburg CR, Russ C, Davis A, Gilchrist J, Kasarskis EJ, Munsat T, Valdmanis P, Rouleau GA, Hosler BA, Cortelli P, de Jong PJ, Yoshinaga Y, Haines JL, Pericak-Vance MA, Yan J, Ticozzi N, Siddique T, McKenna-Yasek D, Sapp PC, Horvitz HR, Landers JE, Brown RH (2009) Mutations in the FUS/TLS gene on chromosome 16 cause familial amyotrophic lateral sclerosis. *Science* **323:** 1205-1208

Lagier-Tourenne C, Polymenidou M, Cleveland DW (2010) TDP-43 and FUS/TLS: emerging roles in RNA processing and neurodegeneration. *Hum Mol Genet* **19:** R46-64

Lam M, Dubyak G, Chen L, Nunez G, Miesfeld RL, Distelhorst CW (1994) Evidence that BCL-2 represses apoptosis by regulating endoplasmic reticulum-associated Ca2+ fluxes. *Proc Natl Acad Sci U S A* **91:** 6569-6573

Lander ES, Linton LM, Birren B, Nusbaum C, Zody MC, Baldwin J, Devon K, Dewar K, Doyle M, FitzHugh W, Funke R, Gage D, Harris K, Heaford A, Howland J, Kann L, Lehoczky J, LeVine R, McEwan P, McKernan K, Meldrim J, Mesirov JP, Miranda C, Morris W, Naylor J, Raymond C, Rosetti M, Santos R, Sheridan A, Sougnez C, Stange-Thomann N, Stojanovic N, Subramanian A, Wyman D, Rogers J, Sulston J, Ainscough R, Beck S, Bentley D, Burton J, Clee C, Carter N, Coulson A, Deadman R, Deloukas P, Dunham A, Dunham I, Durbin R, French L, Grafham D, Gregory S, Hubbard T, Humphray S, Hunt A, Jones M, Lloyd C, McMurray A, Matthews L, Mercer S, Milne S, Mullikin JC, Mungall A, Plumb R, Ross M, Shownkeen R, Sims S, Waterston RH, Wilson RK, Hillier LW, McPherson JD, Marra MA, Mardis ER, Fulton LA, Chinwalla AT, Pepin KH, Gish WR, Chissoe SL, Wendl MC, Delehaunty KD, Miner TL, Delehaunty A, Kramer JB, Cook LL, Fulton RS, Johnson DL, Minx PJ, Clifton SW, Hawkins T, Branscomb E, Predki P, Richardson P, Wenning S, Slezak T, Doggett N, Cheng JF, Olsen A, Lucas S, Elkin C, Uberbacher E, Frazier M, Gibbs RA, Muzny DM, Scherer SE, Bouck JB, Sodergren EJ, Worley KC, Rives CM, Gorrell JH, Metzker ML, Naylor SL, Kucherlapati RS, Nelson DL, Weinstock GM, Sakaki Y, Fujiyama A, Hattori M, Yada T, Toyoda A, Itoh T, Kawagoe C, Watanabe H, Totoki Y, Taylor T, Weissenbach J, Heilig R, Saurin W, Artiguenave F, Brottier P, Bruls T, Pelletier E, Robert C, Wincker P, Smith DR, Doucette-Stamm L, Rubenfield M, Weinstock K, Lee HM, Dubois J, Rosenthal A, Platzer M, Nyakatura G, Taudien S, Rump A, Yang H, Yu J, Wang J, Huang G, Gu J, Hood L, Rowen L, Madan A, Qin S, Davis RW, Federspiel NA, Abola AP, Proctor MJ, Myers RM, Schmutz J, Dickson M, Grimwood J, Cox DR, Olson MV, Kaul R, Shimizu N, Kawasaki K, Minoshima S, Evans GA, Athanasiou M, Schultz R, Roe BA, Chen F, Pan H, Ramser J, Lehrach H, Reinhardt R, McCombie WR, de la Bastide M, Dedhia N, Blöcker H, Hornischer K, Nordsiek G, Agarwala R, Aravind L, Bailey JA, Bateman A, Batzoglou S, Birney E, Bork P, Brown DG, Burge CB, Cerutti L, Chen HC, Church D, Clamp M, Copley RR, Doerks T, Eddy SR, Eichler EE, Furey TS, Galagan J, Gilbert JG, Harmon C, Hayashizaki Y, Haussler D, Hermjakob H, Hokamp K, Jang W, Johnson LS, Jones TA, Kasif S, Kaspryzk A, Kennedy S, Kent WJ, Kitts P, Koonin EV, Korf I, Kulp D, Lancet D, Lowe TM, McLysaght A, Mikkelsen T, Moran JV, Mulder N, Pollara VJ, Ponting CP, Schuler G, Schultz J, Slater G, Smit AF, Stupka E, Szustakowski J, Thierry-Mieg D, Thierry-Mieg J, Wagner L, Wallis J, Wheeler R, Williams A, Wolf YI, Wolfe KH, Yang SP, Yeh RF, Collins F, Guyer MS, Peterson J, Felsenfeld A, Wetterstrand KA, Patrinos A, Morgan MJ, de Jong P, Catanese JJ, Osoegawa K, Shizuya H, Choi S, Chen YJ, Szustakowki J, Consortium IHGS (2001) Initial sequencing and analysis of the human genome. *Nature* **409:** 860-921

Leigh PN, Whitwell H, Garofalo O, Buller J, Swash M, Martin JE, Gallo JM, Weller RO, Anderton BH (1991) Ubiquitin-immunoreactive intraneuronal inclusions in amyotrophic lateral sclerosis. Morphology, distribution, and specificity. *Brain* **114 (Pt 2):** 775-788

Li C, Fox CJ, Master SR, Bindokas VP, Chodosh LA, Thompson CB (2002) Bcl-X(L) affects Ca(2+) homeostasis by altering expression of inositol 1,4,5-trisphosphate receptors. *Proc Natl Acad Sci U S A* **99:** 9830-9835

Li C, Jackson RM (2002) Reactive species mechanisms of cellular hypoxia-reoxygenation injury. *Am J Physiol Cell Physiol* **282:** C227-241

Li XJ, Du ZW, Zarnowska ED, Pankratz M, Hansen LO, Pearce RA, Zhang SC (2005) Specification of motoneurons from human embryonic stem cells. *Nat Biotechnol* **23:** 215-221

Lin W, Dickson D (2008) Ultrastructural localization of TDP-43 in filamentous neuronal inclusions in various neurodegenerative diseases. *Acta Neuropathologica* **116:** 205-213

Ling S-C, Albuquerque CP, Han JS, Lagier-Tourenne C, Tokunaga S, Zhou H, Cleveland DW (2010) ALS-associated mutations in TDP-43 increase its stability and promote TDP-43 complexes with FUS/TLS. *Proceedings of the National Academy of Sciences of the United States of America* **107:** 13318-13323

Loh Y, Agarwal S, Park I, Urbach A, Huo H, Heffner G, Kim K, Miller J, Ng K, Daley G (2009) Generation of induced pluripotent stem cells from human blood. *Blood* **113:** 5476-5479

Lomen-Hoerth C, Anderson T, Miller B (2002) The overlap of amyotrophic lateral sclerosis and frontotemporal dementia. *Neurology* **59:** 1077-1079

Lufino MM, Popplestone AR, Cowley SA, Edser PA, James WS, Wade-Martins R (2011) Episomal transgene expression in pluripotent stem cells. *Methods Mol Biol* **767:** 369-387

Mackenzie IR, Bigio EH, Ince PG, Geser F, Neumann M, Cairns NJ, Kwong LK, Forman MS, Ravits J, Stewart H, Eisen A, McClusky L, Kretzschmar HA, Monoranu CM, Highley JR, Kirby J, Siddique T, Shaw PJ, Lee VM, Trojanowski JQ (2007) Pathological TDP-43 distinguishes sporadic amyotrophic lateral sclerosis from amyotrophic lateral sclerosis with SOD1 mutations. *Ann Neurol* **61:** 427-434

Majounie E, Renton AE, Mok K, Dopper EG, Waite A, Rollinson S, Chio A, Restagno G, Nicolaou N, Simon-Sanchez J, van Swieten JC, Abramzon Y, Johnson JO, Sendtner M, Pamphlett R, Orrell RW, Mead S, Sidle KC, Houlden H, Rohrer JD, Morrison KE, Pall H, Talbot K, Ansorge O, Hernandez DG, Arepalli S, Sabatelli M, Mora G, Corbo M, Giannini F, Calvo A, Englund E, Borghero G, Floris GL, Remes AM, Laaksovirta H, McCluskey L, Trojanowski JQ, Van Deerlin VM, Schellenberg GD, Nalls MA, Drory VE, Lu CS, Yeh TH, Ishiura H, Takahashi Y, Tsuji S, Le Ber I, Brice A, Drepper C, Williams N, Kirby J, Shaw P, Hardy J, Tienari PJ, Heutink P, Morris HR, Pickering-Brown S, Traynor BJ (2012) Frequency of the C9orf72 hexanucleotide repeat expansion in patients with amyotrophic lateral sclerosis and frontotemporal dementia: a cross-sectional study. *Lancet Neurol* **11:** 323-330

Maruyama H, Morino H, Ito H, Izumi Y, Kato H, Watanabe Y, Kinoshita Y, Kamada M, Nodera H, Suzuki H, Komure O, Matsuura S, Kobatake K, Morimoto N, Abe K, Suzuki N, Aoki M, Kawata A, Hirai T, Kato T, Ogasawara K, Hirano A, Takumi T, Kusaka H, Hagiwara K, Kaji R, Kawakami H (2010) Mutations of optineurin in amyotrophic lateral sclerosis. *Nature* **465:** 223-226

McDonald KK, Aulas A, Destroismaisons L, Pickles S, Beleac E, Camu W, Rouleau GA, Vande Velde C (2011) TAR DNA-binding protein 43 (TDP-43) regulates stress granule dynamics via differential regulation of G3BP and TIA-1. *Hum Mol Genet* **20:** 1400-1410

McKhann GM, Albert MS, Grossman M, Miller B, Dickson D, Trojanowski JQ, Disease WGoFDaPs (2001) Clinical and pathological diagnosis of frontotemporal dementia: report of the Work Group on Frontotemporal Dementia and Pick's Disease. *Arch Neurol* **58:** 1803-1809

Mercado PA, Ayala YM, Romano M, Buratti E, Baralle FE (2005) Depletion of TDP 43 overrides the need for exonic and intronic splicing enhancers in the human apoA-II gene. *Nucleic Acids Res* **33:** 6000-6010

Michaelis E, Dremina E, Sharov V, Kumar K, Zaidi A, Schoneich C (2004) Antiapoptotic protein Bcl-2 interacts with and destabilizes the sarco/endoplasmic reticulum CA-ATPase (SERCA). *Neurobiology of Aging* **25:** S411-S411

Miller RG, Mitchell JD, Lyon M, Moore DH (2003) Riluzole for amyotrophic lateral sclerosis (ALS)/motor neuron disease (MND). *Amyotroph Lateral Scler Other Motor Neuron Disord* **4:** 191-206

Mori K, Weng SM, Arzberger T, May S, Rentzsch K, Kremmer E, Schmid B, Kretzschmar HA, Cruts M, Van Broeckhoven C, Haass C, Edbauer D (2013) The C9orf72 GGGGCC Repeat Is Translated into Aggregating Dipeptide-Repeat Proteins in FTLD/ALS. *Science*

Mosca L, Lunetta C, Tarlarini C, Avemaria F, Maestri E, Melazzini M, Corbo M, Penco S (2012) Wide phenotypic spectrum of the TARDBP gene: homozygosity of A382T mutation in a patient presenting with amyotrophic lateral sclerosis, Parkinson's disease, and frontotemporal lobar degeneration, and in neurologically healthy subject. *Neurobiol Aging* **33:** 1846.e1841-1844

Muller L, Daley G, Williams D (2009) Upping the Ante: Recent Advances in Direct Reprogramming. *Molecular Therapy* **17:** 947-953

Nagai M, Re DB, Nagata T, Chalazonitis A, Jessell TM, Wichterle H, Przedborski S (2007) Astrocytes expressing ALS-linked mutated SOD1 release factors selectively toxic to motor neurons. *Nat Neurosci* **10:** 615-622

Nakamura K, Bossy-Wetzel E, Burns K, Fadel MP, Lozyk M, Goping IS, Opas M, Bleackley RC, Green DR, Michalak M (2000) Changes in endoplasmic reticulum luminal environment affect cell sensitivity to apoptosis. *J Cell Biol* **150:** 731-740

Neumann M, Sampathu DM, Kwong LK, Truax AC, Micsenyi MC, Chou TT, Bruce J, Schuck T, Grossman M, Clark CM, McCluskey LF, Miller BL, Masliah E, Mackenzie IR, Feldman H, Feiden W, Kretzschmar HA, Trojanowski JQ, Lee VM (2006) Ubiquitinated TDP-43 in frontotemporal lobar degeneration and amyotrophic lateral sclerosis. *Science* **314:** 130-133

Nishimoto Y, Ito D, Yagi T, Nihei Y, Tsunoda Y, Suzuki N (2010) Characterization of alternative isoforms and inclusion body of the TAR DNA-binding protein-43. *J Biol Chem* **285:** 608-619

Nishimura AL, Mitne-Neto M, Silva HC, Richieri-Costa A, Middleton S, Cascio D, Kok F, Oliveira JR, Gillingwater T, Webb J, Skehel P, Zatz M (2004) A mutation in the vesicle-trafficking protein VAPB causes late-onset spinal muscular atrophy and amyotrophic lateral sclerosis. *Am J Hum Genet* **75:** 822-831

Nishimura K, Sano M, Ohtaka M, Furuta B, Umemura Y, Nakajima Y, Ikehara Y, Kobayashi T, Segawa H, Takayasu S, Sato H, Motomura K, Uchida E, Kanayasu-Toyoda T, Asashima M, Nakauchi H, Yamaguchi T, Nakanishi M (2011a) Development of defective and persistent Sendai virus vector: a unique gene delivery/expression system ideal for cell reprogramming. *J Biol Chem* **286:** 4760-4771

Nishimura K, Sano M, Ohtaka M, Furuta B, Umemura Y, Nakajima Y, Ikehara Y, Kobayashi T, Segawa H, Takayasu S, Sato H, Motomura K, Uchida E, Kanayasu-Toyoda T, Asashima M, Nakauchi H, Yamaguchi T, Nakanishia M (2011b) Development of Defective and Persistent Sendai Virus Vector A UNIQUE GENE DELIVERY/EXPRESSION SYSTEM IDEAL FOR CELL REPROGRAMMING. *Journal of Biological Chemistry* **286:** 4760-4771

Oakes SA, Opferman JT, Pozzan T, Korsmeyer SJ, Scorrano L (2003) Regulation of endoplasmic reticulum Ca2+ dynamics by proapoptotic BCL-2 family members. *Biochem Pharmacol* **66:** 1335-1340

Oda Y (1999) Choline acetyltransferase: the structure, distribution and pathologic changes in the central nervous system. *Pathol Int* **49:** 921-937

Okita K, Ichisaka T, Yamanaka S (2007) Generation of germline-competent induced pluripotent stem cells. *Nature* **448:** 313-U311

Orlacchio A, Babalini C, Borreca A, Patrono C, Massa R, Basaran S, Munhoz RP, Rogaeva EA, St George-Hyslop PH, Bernardi G, Kawarai T (2010) SPATACSIN mutations cause autosomal recessive juvenile amyotrophic lateral sclerosis. *Brain* **133:** 591-598

Orrenius S, Zhivotovsky B, Nicotera P (2003) Regulation of cell death: the calcium-apoptosis link. *Nat Rev Mol Cell Biol* **4:** 552-565

Ou SH, Wu F, Harrich D, Garcia-Martinez LF, Gaynor RB (1995) Cloning and characterization of a novel cellular protein, TDP-43, that binds to human immunodeficiency virus type 1 TAR DNA sequence motifs. *J Virol* **69:** 3584-3596

Palmer AE, Jin C, Reed JC, Tsien RY (2004) Bcl-2-mediated alterations in endoplasmic reticulum Ca2+ analyzed with an improved genetically encoded fluorescent sensor. *Proc Natl Acad Sci U S A* **101:** 17404-17409

Park I, Arora N, Huo H, Maherali N, Ahfeldt T, Shimamura A, Lensch M, Cowan C, Hochedlinger K, Daley G (2008) Disease-specific induced pluripotent stem cells. *Cell* **134:** 877-886

Paschen W, Mengesdorf T (2005) Endoplasmic reticulum stress response and neurodegeneration. *Cell Calcium* **38:** 409-415

Peruzzi PP, Lawler SE, Senior SL, Dmitrieva N, Edser PA, Gianni D, Chiocca EA, Wade-Martins R (2009) Physiological transgene regulation and functional complementation of a neurological disease gene deficiency in neurons. *Mol Ther* **17:** 1517-1526

Pesiridis GS, Lee VM, Trojanowski JQ (2009) Mutations in TDP-43 link glycine-rich domain functions to amyotrophic lateral sclerosis. *Hum Mol Genet* **18:** R156-162

Pinton P, Ferrari D, Magalhaes P, Schulze-Osthoff K, Di Virgilio F, Pozzan T, Rizzuto R (2000) Reduced loading of intracellular Ca(2+) stores and downregulation of capacitative Ca(2+) influx in Bcl-2-overexpressing cells. *J Cell Biol* **148:** 857-862

Polymenidou M, Lagier-Tourenne C, Hutt KR, Huelga SC, Moran J, Liang TY, Ling SC, Sun E, Wancewicz E, Mazur C, Kordasiewicz H, Sedaghat Y, Donohue JP, Shiue L, Bennett CF,

Yeo GW, Cleveland DW (2011) Long pre-mRNA depletion and RNA missplicing contribute to neuronal vulnerability from loss of TDP-43. *Nat Neurosci*

Purkiss JR, Willars GB (1996) Ionomycin induced changes in intracellular free calcium in SH-SY5Y human neuroblastoma cells: sources of calcium and effects on [3H]-noradrenaline release. *Cell Calcium* **20:** 21-29

Ravits J, Appel S, Baloh RH, Barohn R, Rix Brooks B, Elman L, Floeter MK, Henderson C, Lomen-Hoerth C, Macklis JD, McCluskey L, Mitsumoto H, Przedborski S, Rothstein J, Trojanowski JQ, van den Berg LH, Ringel S (2013) Deciphering amyotrophic lateral sclerosis: What phenotype, neuropathology and genetics are telling us about pathogenesis. *Amyotroph Lateral Scler Frontotemporal Degener* **14 Suppl 1:** 5-18

Renton AE, Majounie E, Waite A, Simon-Sanchez J, Rollinson S, Gibbs JR, Schymick JC, Laaksovirta H, van Swieten JC, Myllykangas L, Kalimo H, Paetau A, Abramzon Y, Remes AM, Kaganovich A, Scholz SW, Duckworth J, Ding J, Harmer DW, Hernandez DG, Johnson JO, Mok K, Ryten M, Trabzuni D, Guerreiro RJ, Orrell RW, Neal J, Murray A, Pearson J, Jansen IE, Sondervan D, Seelaar H, Blake D, Young K, Halliwell N, Callister JB, Toulson G, Richardson A, Gerhard A, Snowden J, Mann D, Neary D, Nalls MA, Peuralinna T, Jansson L, Isoviita VM, Kaivorinne AL, Holtta-Vuori M, Ikonen E, Sulkava R, Benatar M, Wuu J, Chio A, Restagno G, Borghero G, Sabatelli M, Heckerman D, Rogaeva E, Zinman L, Rothstein JD, Sendtner M, Drepper C, Eichler EE, Alkan C, Abdullaev Z, Pack SD, Dutra A, Pak E, Hardy J, Singleton A, Williams NM, Heutink P, Pickering-Brown S, Morris HR, Tienari PJ, Traynor BJ (2011) A hexanucleotide repeat expansion in C9ORF72 is the cause of chromosome 9p21-linked ALS-FTD. *Neuron* **72:** 257-268

Ritson GP, Custer SK, Freibaum BD, Guinto JB, Geffel D, Moore J, Tang W, Winton MJ, Neumann M, Trojanowski JQ, Lee VM, Forman MS, Taylor JP (2010) TDP-43 mediates degeneration in a novel Drosophila model of disease caused by mutations in VCP/p97. *J Neurosci* **30:** 7729-7739

Ron D, Walter P (2007) Signal integration in the endoplasmic reticulum unfolded protein response. *Nat Rev Mol Cell Biol* **8:** 519-529

Rong YP, Aromolaran AS, Bultynck G, Zhong F, Li X, McColl K, Matsuyama S, Herlitze S, Roderick HL, Bootman MD, Mignery GA, Parys JB, De Smedt H, Distelhorst CW (2008) Targeting Bcl-2-IP3 receptor interaction to reverse Bcl-2's inhibition of apoptotic calcium signals. *Mol Cell* **31:** 255-265

Rosen DR, Siddique T, Patterson D, Figlewicz DA, Sapp P, Hentati A, Donaldson D, Goto J, O'Regan JP, Deng HX, et al. (1993) Mutations in Cu/Zn superoxide dismutase gene are associated with familial amyotrophic lateral sclerosis. *Nature* **362:** 59-62

Saeki Y, Fraefel C, Ichikawa T, Breakefield X, Chiocca E (2001) Improved helper virus-free packaging system for HSV amplicon vectors using an ICP27-deleted, oversized HSV-1 DNA in a bacterial artificial chromosome. *Molecular Therapy* **3:** 591-601

Sambrook JF (1990) The involvement of calcium in transport of secretory proteins from the endoplasmic reticulum. *Cell* **61:** 197-199

Sampathu DM, Neumann M, Kwong LK, Chou TT, Micsenyi M, Truax A, Bruce J, Grossman M, Trojanowski JQ, Lee VM (2006) Pathological heterogeneity of frontotemporal lobar degeneration with ubiquitin-positive inclusions delineated by ubiquitin immunohistochemistry and novel monoclonal antibodies. *Am J Pathol* **169:** 1343-1352

Sapp PC, Hosler BA, McKenna-Yasek D, Chin W, Gann A, Genise H, Gorenstein J, Huang M, Sailer W, Scheffler M, Valesky M, Haines JL, Pericak-Vance M, Siddique T, Horvitz HR, Brown RH (2003) Identification of two novel loci for dominantly inherited familial amyotrophic lateral sclerosis. *Am J Hum Genet* **73:** 397-403

Sasaki S, Takeda T, Shibata N, Kobayashi M (2010) Alterations in subcellular localization of TDP-43 immunoreactivity in the anterior horns in sporadic amyotrophic lateral sclerosis. *Neurosci Lett* **478:** 72-76

Saxena S, Cabuy E, Caroni P (2009) A role for motoneuron subtype-selective ER stress in disease manifestations of FALS mice. *Nat Neurosci* **12:** 627-636

Schröder M (2008) Endoplasmic reticulum stress responses. *Cell Mol Life Sci* **65:** 862-894

Schwab C, Arai T, Hasegawa M, Yu S, McGeer P (2008) Colocalization of Transactivation-Responsive DNA-Binding Protein 43 and Huntingtin in Inclusions of Huntington Disease. *Journal of Neuropathology and Experimental Neurology* **67:** 1159-1165

Scorrano L, Oakes SA, Opferman JT, Cheng EH, Sorcinelli MD, Pozzan T, Korsmeyer SJ (2003) BAX and BAK regulation of endoplasmic reticulum Ca2+: a control point for apoptosis. *Science* **300:** 135-139

Senior SL, Wade-Martins R (2005) Herpes simplex virus type 1 amplicon vectors for the infectious delivery and expression of genomic DNA loci. *Curr Opin Mol Ther* **7:** 337-345

Serio A, Bilican B, Barmada S, Ando D, Zhao C, Siller R, Burr K, Haghi G, Story D, Nishimura A, Carrasco M, Phatnani H, Shum C, Wilmut I, Maniatis T, Shaw C, Finkbeiner

S, Chandran S (2013) Astrocyte pathology and the absence of non-cell autonomy in an induced pluripotent stem cell model of TDP-43 proteinopathy. *Proceedings of the National Academy of Sciences of the United States of America* **110:** 4697-4702

Shan X, Chiang PM, Price DL, Wong PC (2010) Altered distributions of Gemini of coiled bodies and mitochondria in motor neurons of TDP-43 transgenic mice. *Proc Natl Acad Sci U S A* **107:** 16325-16330

Shaw PJ, Ince PG, Falkous G, Mantle D (1995) Oxidative damage to protein in sporadic motor neuron disease spinal cord. *Ann Neurol* **38:** 691-695

Shen J, Chen X, Hendershot L, Prywes R (2002) ER stress regulation of ATF6 localization by dissociation of BiP/GRP78 binding and unmasking of Golgi localization signals. *Dev Cell* **3:** 99-111

Siklós L, Engelhardt J, Harati Y, Smith RG, Joó F, Appel SH (1996) Ultrastructural evidence for altered calcium in motor nerve terminals in amyotropic lateral sclerosis. *Ann Neurol* **39:** 203-216

Sreedharan J, Blair IP, Tripathi VB, Hu X, Vance C, Rogelj B, Ackerley S, Durnall JC, Williams KL, Buratti E, Baralle F, de Belleroche J, Mitchell JD, Leigh PN, Al-Chalabi A, Miller CC, Nicholson G, Shaw CE (2008) TDP-43 mutations in familial and sporadic amyotrophic lateral sclerosis. *Science* **319:** 1668-1672

Stallings NR, Puttaparthi K, Luther CM, Burns DK, Elliott JL (2010) Progressive motor weakness in transgenic mice expressing human TDP-43. *Neurobiol Dis* **40:** 404-414

Sternberg N, Hamilton D (1981) Bacteriophage P1 site-specific recombination. I. Recombination between loxP sites. *J Mol Biol* **150:** 467-486

Strong MJ, Volkening K, Hammond R, Yang W, Strong W, Leystra-Lantz C, Shoesmith C (2007) TDP43 is a human low molecular weight neurofilament (hNFL) mRNA-binding protein. *Molecular and cellular neurosciences* **35:** 320-327

Strong MJ, Yang W, Strong WL, Leystra-Lantz C, Jaffe H, Pant HC (2006) Tau protein hyperphosphorylation in sporadic ALS with cognitive impairment. *Neurology* **66:** 1770-1771

Suzuki H, Lee K, Matsuoka M (2011) TDP-43-induced death is associated with altered regulation of BIM and Bcl-xL and attenuated by caspase-mediated TDP-43 cleavage. *J Biol Chem* **286:** 13171-13183

Takahashi K, Okita K, Nakagawa M, Yamanaka S (2007a) Induction of pluripotent stem cells from fibroblast cultures. *Nat Protoc* **2:** 3081-3089

Takahashi K, Tanabe K, Ohnuki M, Narita M, Ichisaka T, Tomoda K, Yamanaka S (2007b) Induction of pluripotent stem cells from adult human fibroblasts by defined factors. *Cell* **131:** 861-872

Takahashi K, Yamanaka S (2006) Induction of pluripotent stem cells from mouse embryonic and adult fibroblast cultures by defined factors. *Cell* **126:** 663-676

Talbot K (2009) Another gene for ALS: mutations in sporadic cases and the rare variant hypothesis. *Neurology* **73:** 1172-1173

Tollervey JR, Curk T, Rogelj B, Briese M, Cereda M, Kayikci M, Konig J, Hortobagyi T, Nishimura AL, Zupunski V, Patani R, Chandran S, Rot G, Zupan B, Shaw CE, Ule J (2011) Characterizing the RNA targets and position-dependent splicing regulation by TDP-43. *Nat Neurosci* **14:**452-458

Tong J, Huang C, Bi F, Wu Q, Huang B, Liu X, Li F, Zhou H, Xia XG (2013) Expression of ALS-linked TDP-43 mutant in astrocytes causes non-cell-autonomous motor neuron death in rats. *EMBO J* **32:**1917-1926

Tradewell ML, Cooper LA, Minotti S, Durham HD (2011) Calcium dysregulation, mitochondrial pathology and protein aggregation in a culture model of amyotrophic lateral sclerosis: mechanistic relationship and differential sensitivity to intervention. *Neurobiol Dis* **42:** 265-275

Tradewell ML, Durham HD (2010) Calpastatin reduces toxicity of SOD1G93A in a culture model of amyotrophic lateral sclerosis. *Neuroreport* **21:** 976-979

Troakes C, Maekawa S, Wijesekera L, Rogelj B, Siklos L, Bell C, Smith B, Newhouse S, Vance C, Johnson L, Hortobagyi T, Shatunov A, Al-Chalabi A, Leigh N, Shaw CE, King A, Al-Sarraj S (2012) An MND/ALS phenotype associated with C9orf72 repeat expansion: abundant p62-positive, TDP-43-negative inclusions in cerebral cortex, hippocampus and cerebellum but without associated cognitive decline. *Neuropathology* **32:** 505-514

Trojanowski JQ, Lee VM (2000) "Fatal attractions" of proteins. A comprehensive hypothetical mechanism underlying Alzheimer's disease and other neurodegenerative disorders. *Ann N Y Acad Sci* **924:** 62-67

Trotti D, Rolfs A, Danbolt NC, Brown RH, Hediger MA (1999) SOD1 mutants linked to amyotrophic lateral sclerosis selectively inactivate a glial glutamate transporter. *Nat Neurosci* **2:** 427-433

Tsai KJ, Yang CH, Fang YH, Cho KH, Chien WL, Wang WT, Wu TW, Lin CP, Fu WM, Shen CK (2010) Elevated expression of TDP-43 in the forebrain of mice is sufficient to cause neurological and pathological phenotypes mimicking FTLD-U. *J Exp Med* **207:** 1661-1673

van der Zee J, Gijselinck I, Dillen L, Van Langenhove T, Theuns J, Engelborghs S, Philtjens S, Vandenbulcke M, Sleegers K, Sieben A, Baumer V, Maes G, Corsmit E, Borroni B, Padovani A, Archetti S, Perneczky R, Diehl-Schmid J, de Mendonca A, Miltenberger-Miltenyi G, Pereira S, Pimentel J, Nacmias B, Bagnoli S, Sorbi S, Graff C, Chiang HH, Westerlund M, Sanchez-Valle R, Llado A, Gelpi E, Santana I, Almeida MR, Santiago B, Frisoni G, Zanetti O, Bonvicini C, Synofzik M, Maetzler W, Vom Hagen JM, Schols L, Heneka MT, Jessen F, Matej R, Parobkova E, Kovacs GG, Strobel T, Sarafov S, Tournev I, Jordanova A, Danek A, Arzberger T, Fabrizi GM, Testi S, Salmon E, Santens P, Martin JJ, Cras P, Vandenberghe R, De Deyn PP, Cruts M, Van Broeckhoven C, van der Zee J, Gijselinck I, Dillen L, Van Langenhove T, Theuns J, Philtjens S, Sleegers K, Baumer V, Maes G, Corsmit E, Cruts M, Van Broeckhoven C, van der Zee J, Gijselinck I, Dillen L, Van Langenhove T, Philtjens S, Theuns J, Sleegers K, Baumer V, Maes G, Cruts M, Van Broeckhoven C, Engelborghs S, De Deyn PP, Cras P, Engelborghs S, De Deyn PP, Vandenbulcke M, Vandenbulcke M, Borroni B, Padovani A, Archetti S, Perneczky R, Diehl-Schmid J, Synofzik M, Maetzler W, Muller Vom Hagen J, Schols L, Synofzik M, Maetzler W, Muller Vom Hagen J, Schols L, Heneka MT, Jessen F, Ramirez A, Kurzwelly D, Sachtleben C, Mairer W, de Mendonca A, Miltenberger-Miltenyi G, Pereira S, Firmo C, Pimentel J, Sanchez-Valle R, Llado A, Antonell A, Molinuevo J, Gelpi E, Graff C, Chiang HH, Westerlund M, Graff C, Kinhult Stahlbom A, Thonberg H, Nennesmo I, Borjesson-Hanson A, Nacmias B, Bagnoli S, Sorbi S, Bessi V, Piaceri I, Santana I, Santiago B, Santana I, Helena Ribeiro M, Rosario Almeida M, Oliveira C, Massano J, Garret C, Pires P, Frisoni G, Zanetti O, Bonvicini C, Sarafov S, Tournev I, Jordanova A, Tournev I, Kovacs GG, Strobel T, Heneka MT, Jessen F, Ramirez A, Kurzwelly D, Sachtleben C, Mairer W, Jessen F, Matej R, Parobkova E, Danel A, Arzberger T, Maria Fabrizi G, Testi S, Ferrari S, Cavallaro T, Salmon E, Santens P, Cras P, European Early-Onset Dementia C (2013) A Pan-European Study of the C9orf72 Repeat Associated with FTLD: Geographic Prevalence, Genomic Instability, and Intermediate Repeats. *Human mutation* **34:** 363-373

van Es MA, Diekstra FP, Veldink JH, Baas F, Bourque PR, Schelhaas HJ, Strengman E, Hennekam EA, Lindhout D, Ophoff RA, van den Berg LH (2009a) A case of ALS-FTD in a large FALS pedigree with a K17I ANG mutation. *Neurology* **72:** 287-288

van Es MA, Veldink JH, Saris CG, Blauw HM, van Vught PW, Birve A, Lemmens R, Schelhaas HJ, Groen EJ, Huisman MH, van der Kooi AJ, de Visser M, Dahlberg C, Estrada K, Rivadeneira F, Hofman A, Zwarts MJ, van Doormaal PT, Rujescu D, Strengman E,

Giegling I, Muglia P, Tomik B, Slowik A, Uitterlinden AG, Hendrich C, Waibel S, Meyer T, Ludolph AC, Glass JD, Purcell S, Cichon S, Nöthen MM, Wichmann HE, Schreiber S, Vermeulen SH, Kiemeney LA, Wokke JH, Cronin S, McLaughlin RL, Hardiman O, Fumoto K, Pasterkamp RJ, Meininger V, Melki J, Leigh PN, Shaw CE, Landers JE, Al-Chalabi A, Brown RH, Robberecht W, Andersen PM, Ophoff RA, van den Berg LH (2009b) Genome-wide association study identifies 19p13.3 (UNC13A) and 9p21.2 as susceptibility loci for sporadic amyotrophic lateral sclerosis. *Nat Genet* **41:** 1083-1087

Vance C, Rogelj B, Hortobágyi T, De Vos KJ, Nishimura AL, Sreedharan J, Hu X, Smith B, Ruddy D, Wright P, Ganesalingam J, Williams KL, Tripathi V, Al-Saraj S, Al-Chalabi A, Leigh PN, Blair IP, Nicholson G, de Belleroche J, Gallo JM, Miller CC, Shaw CE (2009) Mutations in FUS, an RNA processing protein, cause familial amyotrophic lateral sclerosis type 6. *Science* **323:** 1208-1211

Venter JC, Adams MD, Myers EW, Li PW, Mural RJ, Sutton GG, Smith HO, Yandell M, Evans CA, Holt RA, Gocayne JD, Amanatides P, Ballew RM, Huson DH, Wortman JR, Zhang Q, Kodira CD, Zheng XH, Chen L, Skupski M, Subramanian G, Thomas PD, Zhang J, Gabor Miklos GL, Nelson C, Broder S, Clark AG, Nadeau J, McKusick VA, Zinder N, Levine AJ, Roberts RJ, Simon M, Slayman C, Hunkapiller M, Bolanos R, Delcher A, Dew I, Fasulo D, Flanigan M, Florea L, Halpern A, Hannenhalli S, Kravitz S, Levy S, Mobarry C, Reinert K, Remington K, Abu-Threideh J, Beasley E, Biddick K, Bonazzi V, Brandon R, Cargill M, Chandramouliswaran I, Charlab R, Chaturvedi K, Deng Z, Di Francesco V, Dunn P, Eilbeck K, Evangelista C, Gabrielian AE, Gan W, Ge W, Gong F, Gu Z, Guan P, Heiman TJ, Higgins ME, Ji RR, Ke Z, Ketchum KA, Lai Z, Lei Y, Li Z, Li J, Liang Y, Lin X, Lu F, Merkulov GV, Milshina N, Moore HM, Naik AK, Narayan VA, Neelam B, Nusskern D, Rusch DB, Salzberg S, Shao W, Shue B, Sun J, Wang Z, Wang A, Wang X, Wang J, Wei M, Wides R, Xiao C, Yan C, Yao A, Ye J, Zhan M, Zhang W, Zhang H, Zhao Q, Zheng L, Zhong F, Zhong W, Zhu S, Zhao S, Gilbert D, Baumhueter S, Spier G, Carter C, Cravchik A, Woodage T, Ali F, An H, Awe A, Baldwin D, Baden H, Barnstead M, Barrow I, Beeson K, Busam D, Carver A, Center A, Cheng ML, Curry L, Danaher S, Davenport L, Desilets R, Dietz S, Dodson K, Doup L, Ferriera S, Garg N, Gluecksmann A, Hart B, Haynes J, Haynes C, Heiner C, Hladun S, Hostin D, Houck J, Howland T, Ibegwam C, Johnson J, Kalush F, Kline L, Koduru S, Love A, Mann F, May D, McCawley S, McIntosh T, McMullen I, Moy M, Moy L, Murphy B, Nelson K, Pfannkoch C, Pratts E, Puri V, Qureshi H, Reardon M, Rodriguez R, Rogers YH, Romblad D, Ruhfel B, Scott R, Sitter C, Smallwood M, Stewart E, Strong R, Suh E, Thomas R, Tint NN, Tse S, Vech C, Wang G, Wetter J, Williams S, Williams M, Windsor S, Winn-Deen E, Wolfe K, Zaveri J, Zaveri K, Abril JF, Guigó R, Campbell MJ, Sjolander KV, Karlak B, Kejariwal A, Mi H, Lazareva B, Hatton T, Narechania A, Diemer K, Muruganujan A, Guo N, Sato S, Bafna V, Istrail S, Lippert R, Schwartz R, Walenz B, Yooseph S, Allen D, Basu A, Baxendale J, Blick L, Caminha M, Carnes-Stine J, Caulk P, Chiang YH, Coyne M, Dahlke C, Mays A, Dombroski M, Donnelly M, Ely D, Esparham S, Fosler C, Gire H, Glanowski S, Glasser K, Glodek A, Gorokhov M, Graham K, Gropman B, Harris M, Heil J, Henderson S, Hoover J, Jennings D, Jordan C, Jordan J, Kasha J, Kagan L, Kraft C, Levitsky A, Lewis M, Liu X, Lopez J, Ma D, Majoros W, McDaniel J, Murphy S, Newman M, Nguyen T, Nguyen N, Nodell M, Pan S, Peck J, Peterson M, Rowe W, Sanders R, Scott J, Simpson M, Smith T, Sprague A, Stockwell T,

Turner R, Venter E, Wang M, Wen M, Wu D, Wu M, Xia A, Zandieh A, Zhu X (2001) The sequence of the human genome. *Science* **291:** 1304-1351

Vignais PV (2002) The superoxide-generating NADPH oxidase: structural aspects and activation mechanism. *Cell Mol Life Sci* **59:** 1428-1459

Voigt A, Herholz D, Fiesel FC, Kaur K, Müller D, Karsten P, Weber SS, Kahle PJ, Marquardt T, Schulz JB (2010) TDP-43-mediated neuron loss in vivo requires RNA-binding activity. *PLoS One* **5:** e12247

Wade-Martins R, Saeki Y, Chiocca EA (2003) Infectious delivery of a 135-kb LDLR genomic locus leads to regulated complementation of low-density lipoprotein receptor deficiency in human cells. *Mol Ther* **7:** 604-612

Wade-Martins R, Smith ER, Tyminski E, Chiocca EA, Saeki Y (2001) An infectious transfer and expression system for genomic DNA loci in human and mouse cells. *Nat Biotechnol* **19:** 1067-1070

Wakayama T, Perry A, Zuccotti M, Johnson K, Yanagimachi R (1998) Full-term development of mice from enucleated oocytes injected with cumulus cell nuclei. *Nature* **394:** 369-374

Waldron RT, Rozengurt E (2000) Oxidative stress induces protein kinase D activation in intact cells. Involvement of Src and dependence on protein kinase C. *J Biol Chem* **275:** 17114-17121

Wang H-Y, Wang IF, Bose J, Shen CKJ (2004) Structural diversity and functional implications of the eukaryotic TDP gene family. *Genomics* **83:** 130-139

Wang IF, Wu LS, Shen CK (2008) TDP-43: an emerging new player in neurodegenerative diseases. *Trends Mol Med* **14:** 479-485

Wang L, Popko B, Roos RP (2011) The unfolded protein response in familial amyotrophic lateral sclerosis. *Hum Mol Genet* **20:** 1008-1015

Wegorzewska I, Baloh RH (2011) TDP-43-based animal models of neurodegeneration: new insights into ALS pathology and pathophysiology. *Neurodegener Dis* **8:** 262-274

Wegorzewska I, Bell S, Cairns NJ, Miller TM, Baloh RH (2009) TDP-43 mutant transgenic mice develop features of ALS and frontotemporal lobar degeneration. *Proc Natl Acad Sci U S A* **106:** 18809-18814

Wichterle H, Lieberam I, Porter JA, Jessell TM (2002) Directed differentiation of embryonic stem cells into motor neurons. *Cell* **110:** 385-397

Wiedau-Pazos M, Goto JJ, Rabizadeh S, Gralla EB, Roe JA, Lee MK, Valentine JS, Bredesen DE (1996) Altered reactivity of superoxide dismutase in familial amyotrophic lateral sclerosis. *Science* **271:** 515-518

Wilmut I, Schnieke A, McWhir J, Kind A, Campbell K (1997) Viable offspring derived from fetal and adult mammalian cells. *Nature* **385:** 810-813

Wils H, Kleinberger G, Janssens J, Pereson S, Joris G, Cuijt I, Smits V, Ceuterick-de Groote C, Van Broeckhoven C, Kumar-Singh S (2010) TDP-43 transgenic mice develop spastic paralysis and neuronal inclusions characteristic of ALS and frontotemporal lobar degeneration. *Proc Natl Acad Sci U S A* **107:** 3858-3863

Winton MJ, Igaz LM, Wong MM, Kwong LK, Trojanowski JQ, Lee VMY (2008) Disturbance of nuclear and cytoplasmic TAR DNA-binding protein (TDP-43) induces disease-like redistribution, sequestration, and aggregate formation. *The Journal of biological chemistry* **283:** 13302-13309

Xu YF, Gendron TF, Zhang YJ, Lin WL, D'Alton S, Sheng H, Casey MC, Tong J, Knight J, Yu X, Rademakers R, Boylan K, Hutton M, McGowan E, Dickson DW, Lewis J, Petrucelli L (2010) Wild-type human TDP-43 expression causes TDP-43 phosphorylation, mitochondrial aggregation, motor deficits, and early mortality in transgenic mice. *J Neurosci* **30:** 10851-10859

Xu YF, Zhang YJ, Lin WL, Cao X, Stetler C, Dickson DW, Lewis J, Petrucelli L (2011) Expression of mutant TDP-43 induces neuronal dysfunction in transgenic mice. *Mol Neurodegener* **6:** 73

Yang C, Tan W, Whittle C, Qiu L, Cao L, Akbarian S, Xu Z (2010) The C-Terminal TDP-43 Fragments Have a High Aggregation Propensity and Harm Neurons by a Dominant-Negative Mechanism. *PLoS One* **5:** e15878

Yoshida H, Matsui T, Yamamoto A, Okada T, Mori K (2001) XBP1 mRNA is induced by ATF6 and spliced by IRE1 in response to ER stress to produce a highly active transcription factor. *Cell* **107:** 881-891

Yu J (2009) Human induced pluripotent stem cells free of vector and transgene sequences (vol 324, pg 797, 2009). *Science* **324:** 1266-1266

Yu J, Vodyanik M, Smuga-Otto K, Antosiewicz-Bourget J, Frane J, Tian S, Nie J, Jonsdottir G, Ruotti V, Stewart R, Slukvin I, Thomson J (2007a) Induced pluripotent stem cell lines derived from human somatic cells. *Science* **318:** 1917-1920

Yu J, Vodyanik MA, Smuga-Otto K, Antosiewicz-Bourget J, Frane JL, Tian S, Nie J, Jonsdottir GA, Ruotti V, Stewart R, Slukvin II, Thomson JA (2007b) Induced pluripotent stem cell lines derived from human somatic cells. *Science* **318:** 1917-1920

Zhang L, Valdez JM, Zhang B, Wei L, Chang J, Xin L (2011) ROCK inhibitor Y-27632 suppresses dissociation-induced apoptosis of murine prostate stem/progenitor cells and increases their cloning efficiency. *PLoS One* **6:** e18271

Zhang Y, Muyrers JP, Testa G, Stewart AF (2000) DNA cloning by homologous recombination in Escherichia coli. *Nat Biotechnol* **18:** 1314-1317

Zhang YJ, Gendron TF, Xu YF, Ko LW, Yen SH, Petrucelli L (2010) Phosphorylation regulates proteasomal-mediated degradation and solubility of TAR DNA binding protein-43 C-terminal fragments. *Mol Neurodegener* **5:** 33

Zhou H, Huang C, Chen H, Wang D, Landel CP, Xia PY, Bowser R, Liu YJ, Xia XG (2010) Transgenic rat model of neurodegeneration caused by mutation in the TDP gene. *PLoS Genet* **6:** e1000887

Zhu LP, Yu XD, Ling S, Brown RA, Kuo TH (2000) Mitochondrial Ca(2+)homeostasis in the regulation of apoptotic and necrotic cell deaths. *Cell Calcium* **28:** 107-117